DOKUZ EYLUL UNIVERSITY

GRADUATE SCHOOL OF NATURAL AND APPLIED

SCIENCES

NEW FIBER OPTIC COMPETIBLE CHROMOIONOPHORE/MATRIX COMBINATIONS FOR HCO$_3^-$ ANALYSIS IN REAL GROUNDWATER SAMPLES

by

Sibel AYDOĞDU

March, 2012

İZMİR

NEW FIBER OPTIC COMPETIBLE CHROMOIONOPHORE/MATRIX COMBINATIONS FOR HCO$_3^-$ ANALYSIS IN REAL GROUNDWATER SAMPLES

A Thesis Submitted to the
Graduate School of Natural and Applied Sciences of Dokuz Eylul University in
Partial Fulfillment of the Requirements for the Degree of Doctor of
Chemistry in
Chemistry, Applied Chemistry Program

by
Sibel AYDOĞDU

March, 2012
İZMİR

Ph.D. THESIS EXAMINATION RESULT FORM

We have read the thesis entitled **"NEW FIBER OPTIC COMPETIBLE CHROMOIONOPHORE/MATRIX COMBINATIONS FOR HCO$_3^-$ ANALYSIS IN REAL GROUNDWATER SAMPLES"** completed by **SIBEL AYDOGDU** under supervision of **PROFESSOR KADRIYE ERTEKIN** and we certify that in our opinion it is fully adequate, in scope and in quality, as a thesis for the degree of Doctor of Chemistry.

Prof. Dr. Kadriye ERTEKİN

Supervisor

Prof. Dr. Gültekin TARCAN

Thesis Committee Member

Prof. Dr. M. Yavuz Ergün

Thesis Committee Member

Prof. Dr. Mehmet ASLANOĞLU

Examining Committee Member

Doç. Dr. Özlem ÖTER

Examining Committee Member

Prof.Dr. Mustafa SABUNCU

Director

Graduate School of Natural and Applied Sciences

ACKNOWLEDGEMENTS

NEW FIBER OPTIC COMPETIBLE CHROMOIONOPHORE/MATRIX COMBINATIONS FOR BICARBONATE ANALYSIS IN REAL GROUNDWATER SAMPLES

ABSTRACT

Dissolved and gaseous carbon dioxide is an important parameter in water samples, industrial, biochemical and medical applications. Mostly, correct analysis of gaseous and dissolved carbon dioxide is difficult due to the matrix effects. Here we intended to investigate new approaches for optical analysis of dissolved carbon dioxide in groundwater samples. Our investigations focused on newly synthesized choromoionphores or their combination with new matrix materials. We performed their spectral chacterization in transperent polymers and tested their compatibility to solid state optics.

In this work, the ion pair form of pH indicator dye, 8-hydroxypyrene-1,3,6-trisulfonicacidtrisodiumsalt was used for the gaseous carbon dioxide detection. Poly (methyl methacrylate) and ethyl cellulose were used as polymeric materials. Sensing slides were fabricated by electrospinning technique. In this sensor design, the response time, reversibility, linear concentration range and repeatability characteristics also have been studied. Similarly newly synthesized dyes MY9 and MY10 were characterized by spectroscopic ways in thin film or nanofiber form in the ethyl cellulose and poly (methyl methacrylate) polymers. Acidity constant and quantum yield calculations of the employed dyes were performed in the conventional solvents and/or in the solid matrices. Their fluorescence based response to dissolved carbon dioxide was examined both in thin film and nanofiber form. Their cross sensitivities to anions, metal cations were tested.

The indicator dyes MY2, MY4 and MY5 were spectroscopically chacterized and offered for emission based analysis of bicarbonate anion. Acidity constant values of three indicator dyes were calculated and cross sensitivities to other cations and anions were also tested and evaluated.

Bicarbonate analysis in groundwater samples was performed by spectrophotometric and volumetric (indicator and potentiometric) methods. Obtained results were compared with proposed method.

Keywords: Dissolved carbon dioxide, optical chemical sensors, ethyl cellulose, poly (methyl methacrylate) and fiber optic chemical sensor.

GERÇEK YERALTI SUYU ÖRNEKLERİNDE BİKARBONAT ANALİZİ İÇİN FİBER OPTİK UYUMLU KROMOİYONOFOR/MATRİKS KOMBİNASYONLARI

ÖZ

Çözünmüş ve gaz haldeki karbon dioksit su örnekleri, endüstriyel, biyokimyasal ve medikal uygulamalar için önemli bir parametredir. Genellikle gaz ve çözünmüş karbon dioksitin doğru tayini matriks etkileri nedeniyle zordur. Bu çalışmada yeraltı suyu örneklerinde çözünmüş karbon dioksitin optik analizi için yeni yaklaşımlar araştırıldı. Çalışmalarımız yeni sentezlenmiş kromoiyonoforlar veya onların yeni matriks materyalleri ile kombinasyonları üzerine odaklanmıştır. Bu kromoiyonoforların spektral karekterizasyonu şeffaf polimerlerde yapılmış ve katı haldeki optiklere uyumluluğu test edilmiştir.

Bu çalışmada, pH indikatörü olan 8-hidroksipiren–1,3,6-trisülfonik asidin iyon çifti karbon dioksit gazı tayininde kulanıldı. Polimer olarak etil selüloz ve polimetil metakrilat kullanılmıştır. Sensör yüzeyleri elektro eğirme yöntemi kullanılarak üretildi. Tüm sensör tasarımlarında, sensör yanıtı, rejenere edilebilirliği, doğrusal çalışma aralığı ve tekrarlanabilirlik özellikleri belirlendi.

Benzer şekilde, yeni sentezlenen MY9 ve MY10 etil selüloz ve polimetil metakrilat polimerlerinde nanofiber formunda veya ince film fazında spektroskopik çalışmalarla karakterize edilmiştir. İndikatör boyaların asitlik sabiti hesaplamaları ve kuantum verimi bilinen çözücülerde ve/veya kullanılan katı matrikslerde gerçekleştirilmiştir. İndikatörlerin ince film ve nanofiber formunda çözünmüş karbon dioksite floresans esaslı yanıtları incelenmiştir. İndikatör kompozisyonunun anyonlara ve metal katyonlarına karşı duyarlılıkları incelenmiştir.

MY2, MY4 ve MY5 boyaları spektroskopik olarak karakterize edilmiş ve bikarbonat iyonunun spektrofotometrik analizi için önerilmiştir. Boyar maddelerin

asitlik sabitleri ve metal katyonlarına ve anyonlara olan yanıtları da test edilip değerlendirilmiştir.

Yeraltı suyu örneklerinde bikarbonat analizi spektrofotometrik ve volumetrik (indikatör ve potansiyometrik) metodla gerçekleştirilmiştir. Bu metotlardan elde edilen sonuçlar önerilen metot ile karşılaştırılmıştır.

Anahtar Kelimeler: Çözünmüş karbon dioksit, optik kimyasal sensör, etil selüloz, polimetil metakrilat, fiber optik kimyasal sensör.

CONTENTS

CHAPTER FIVE- HPTS BASED OPTICAL CO_2 SENSING WITH IONIC LIQUID DOPED ELECTROSPUN NANOFIBERS..**68**

CHAPTER SIX- SPECTRAL CHARACTERIZATION AND DISSOLVED CO_2 SENSING WITH UTILIZED INDICATOR DYES OF MY9 and MY10..**85**

CHAPTER SEVEN- EMISSION BASED BICARBONATE SENSING WITH ELECTROSPUN NANOFIBERS

xi

CHAPTER ONE
GASEOUS AND DISSOLVED CARBON DIOXIDE

1.1 Introduction

The concentration of CO_2, the most potent greenhouse gas, after water vapour, in the atmosphere has increased by more than 30 % from the pre-industrial era which increase the average temperature of the earth and result in dramatic changes in climate and the ecosystem. Developed countries are committed to an overall reduction of about 5.2 % of all greenhouse gas emissions in the period 2008–2012 compared to 1990 according to Kyoto Protocol. Therefore, the reduce of CO_2 emissions and the continuous and accurate monitoring of CO_2 levels in atmosphere and surface waters such as coastal oceans, deep oceans, estuaries, rivers and groundwater reservoirs has a vital importance on global climate and ecosystem and is an exigency for governments. Also the detection of dissolved and gaseous CO_2 is an important feature in industrial applications, in chemical, biochemical, medicine and clinical analysis such as blood gas monitoring, breathe gas analysis, respiration, photosynthesis etc.

The dissolved CO_2 level in surface waters or oceans can also be concluded as an indicator of atmospheric CO_2 levels. In this thesis we intended to develop an optical chemical sensor for measurement of dissolved CO_2 content of groundwater samples. Prior to discussions regarding optical chemical CO_2 sensing we will introduce general approachs in gaseous or dissolved CO_2 measurement.

1.2 Measurement of CO_2

The present CO_2 sensing techniques are based on infrared (IR) absorptiometry, electrochemical Severinghouse electrode and optical chemical sensors. Among them the IR absorptiometry is intensively used for gas phase CO_2 measurement.

The CO_2 molecule's asymmetric and polyatomic nature causes it to strongly absorb light in the infrared (IR) part of the spectrum. The concentration of CO_2 in a gas mixture can be measured comparing the IR light passing through the CO_2 containing sample, and the blank. The light intensity is reduced as it passes through the sample in proportion to the concentration of CO_2 present. In order to clarify the IR based sensing approach vibration modes of carbon dioxide molecule is shown below.
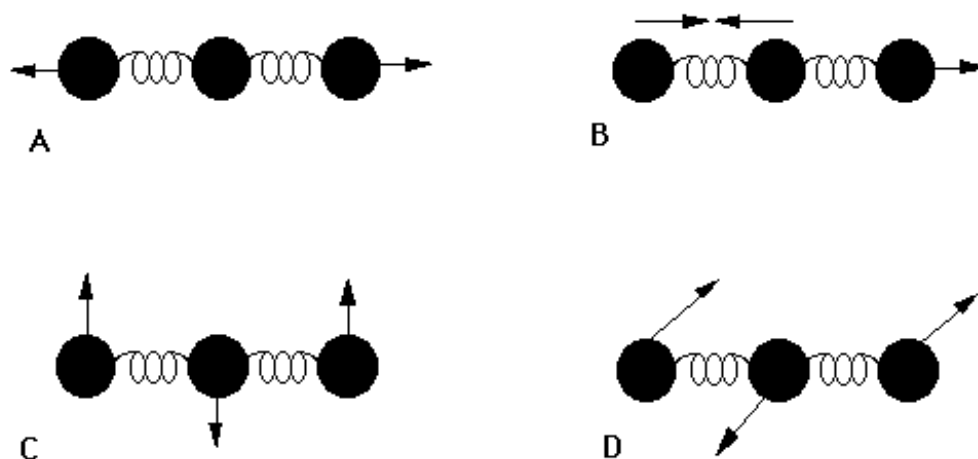
Figure 1.1 CO_2 molecule vibrations (taken from http://www.wag.caltech.edu/home/jang/genchem/infrared.htm).

Some of these vibrational modes, shown in the Figure 1.1 are responsible for the absorption of IR light by CO_2 molecules. The arrows indicate the directions of motion. Vibrations labeled A and B represent the stretching of the chemical bonds, one in a symmetric (A) fashion, in which both C=O bonds lengthen and contract together (in-phase), and the other in an asymmetric (B) fashion, in which one bond shortens while the other lengthens. The asymmetric stretch (B) is infrared *active* because there is a change in the molecular dipole moment during this vibration. Infrared radiation at 2349 cm^{-1} excites this particular vibration. The symmetric stretch is not infrared active, and so this vibration is not observed in the infrared spectrum of CO_2. The two equal-energy bending vibrations in CO_2 (C and D in Fig. 1.1) are identical except that one bending mode is in the plane of the paper, and one is out of the plane. Infrared radiation at 667 cm^{-1} excites these vibrations (http://www.wag.caltech.edu/home/jang/genchem/infrared.htm).

Because the IR spectrum of each molecule is unique, it can serve as a signature to identify the molecule. This feature, have made infrared spectroscopy a reliable method in sensing of gaseous CO_2.

The "essentials" of nearly all IR gas analyzers are (a) a source of IR radiation with an emission spectrum that includes the absorption bands of the gases to be measured; (b) a sample cell fitted with windows "possessing" suitable transmission properties; (c) an optical or gas filter to limit the wavelength range measured by the detector; (d) a means, either physical in the form of a rotating chopper disk or electronic circuit, to modulate the IR radiation from the source; and (e) a detector, based on either a thermal or photonic mechanism,c to convert the IR radiation into an electrical signal (Jaffe, 2008).

However, in spite of the sensitiveness of the IR absorptiometry sensor, it is subject to strong interference from water vapour and is an expensive, bulky and not particularly robust system.

Another well known approach in CO_2 sensing is the Severinghaus electrode. Severinghaus CO_2 sensor consists of a bicarbonate solution filled glass electrode covered by a thin CO_2 permeable membrane. The membrane is impermeable to water and other electrolytes. The sensor functions on principle that in an aqueous solution, CO_2 forms carbonic acid, which is then dissociates into a bicarbonate anion and a proton (Dieckmann & Buchholz, 1999). The proton-induced pH change in electrolyte solution can be measured by the pH probe. The change in pH is monitored by the pH electrode. Although it can be used to measure dissolved CO_2, the Severinghaus type CO_2 electrode has a long response time (typically 5 /15 min) and suffers from the same drawbacks of the pH electrode upon which it is based (Ge, Kostov & Rao, 2003).

However, it has a number of disadvantages. Severinghouse electrode is markedly affected from electromagnetic disturbances, from interferent asidic and basic gases

and from osmotic pressure in the sample. It is bulky, quite expensive and prone to electrical and chemical interference.

A CO_2 sensor principle that slightly differs from Severinghaus concept was presented by Varlan and Sansen (1997). The concept is based on conductivity change as a result of the reaction of carbon dioxide and bicarbonate solution inside a cavity covered with a gas permeable membrane. This kind of sensors can measure CO_2 concentrations between 0 and 11 kPa with a very fast response time. The advantage with this kind of sensors is that the use of a separate reference electrode is not required. Unfortunately, however, keeping the cavities clean is a major concern.

1.3 Dissolved CO_2 Equilibria in Groundwater Samples

In addition to being a component of the atmosphere, carbon dioxide also dissolves in the water of the oceans and in groundwater. At room temperature, the solubility of carbon dioxide is about 90 cm^3 of CO_2 per 100 mL of water. CO_2 can dissolve in groundwater, referred to as solubility trapping. This mechanism can increase the acidity of groundwater and affect the solubilities of other minerals composing the host rock and caprock matrix. It should be noted that pressure is a very important variable in the solubility of CO_2.

Calculation of concentrations of CO_2 related species requires the realistic representations of the thermodynamic properties (density, fugacity, enthalpy, viscosity) of water, separate phase CO_2 (gas and supercritical phases), and aqueous mixtures of CO_2 over the range of temperatures and pressures foreseen in a given geologic environment. In addition, capillary pressure and relative permeability must be evaluated. Subsequently, an adequate representation of the solubility of CO_2 as a function of temperature and pressure needs to be included. However in this thesis we focused on dissolved CO_2 measurements at atmospheric pressure and room temperature. The excess CO_2 dissolved under high pressure conditions leaves the groundwater when the sample was brought to surface.

1.4 Disssolved CO_2 in Surface Waters

In aqueous solution, carbon dioxide exists in many forms. First, it simply dissolves. Then, equilibrium is established between the dissolved CO_2 and H_2CO_3, carbonic acid as shown below.

The chemical equilibria are (a) and (b) are as follows

$$CO_2 \text{ (g)} \leftrightarrow CO_2 \text{ (aq)} \qquad \text{(a)}$$

$$CO_2 \text{ (aq)} + H_2O \leftrightarrow H_2CO_3 \qquad \text{(b)}$$
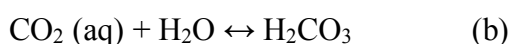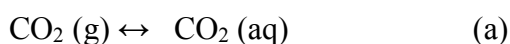
The equilibrium concentration of $[H_2CO_3]$, $[HCO_3^-]$ and $[CO_3^{2-}]$ are quantified by the dissociation or acidity constants:

$$H_2CO_3 \leftrightarrow H^+ + HCO_3^- \qquad K_1 = \frac{[H^+][HCO_3^-]}{[H_2CO_3]} \qquad \text{(Eq. 1.1)}$$

and

$$HCO_3^- \leftrightarrow H^+ + CO_3^{2-} \qquad K_2 = \frac{[H^+][CO_3^{2-}]}{[HCO_3^-]} \qquad \text{(Eq. 1.2)}$$

$$H_2O \leftrightarrow H^+ + OH^-$$
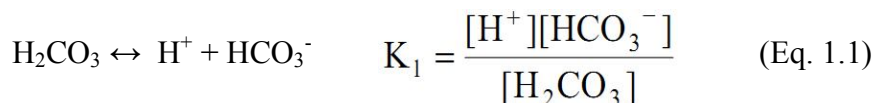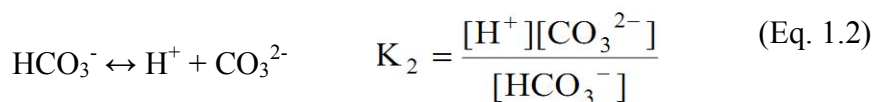
The mass equilibrium is shown in Eq. 1.3

$C_{H2CO3} = [H_2CO_3] + [HCO_3^-] + [CO_3^{2-}]$ where the analytical concentration of H_2CO_3 is C_{H2CO3} and acidity constants are K_{a1} and K_{a2}, respectively. When the equations were arranged $[HCO_3^-]$ and $[CO_3^{2-}]$ can be calculated as follows.

$$Ka_1 Ka_2 = \left(\frac{[H^+]^2 [CO_3^{2-}]}{[H_2CO_3]} \right) \qquad \text{(Eq. 1.4)}$$

$$[HCO_3^-] = K_{a1} \frac{[H_2CO_3]}{[H^+]} \qquad [CO_3^{2-}] = K_{a1}K_{a2} \frac{[H_2CO_3]}{[H^+]^2} \qquad \text{(Eq. 1.5)}$$

$$C_{H2CO3} = \left([H_2CO_3] + K_{a1} \frac{[H_2CO_3]}{[H^+]} + K_{a1}K_{a2} \frac{[H_2CO_3]}{[H^+]^2}\right) \qquad \text{(Eq. 1.6)}$$

$$C_{H2CO3} = [H_2CO_3]\left(1 + \frac{K_{a1}}{[H^+]} + \frac{K_{a1}K_{a2}}{[H^+]^2}\right) \qquad \text{(Eq. 1.7)}$$

$$[H_2CO_3] = \left(C_{H_2CO_3} \frac{[H^+]^2}{[H^+]^2 + K_{a1}[H^+] + K_{a1}K_{a2}}\right) \qquad \text{(Eq. 1.8)}$$

The α functions, indicating pH dependent carbonic acid (H$_2$CO$_3$) related species were derived below.

$$\frac{[H^+]^2}{[H^+]^2 + K_{a1}[H^+] + K_{a1}K_{a2}} = \alpha_{H_2CO_3} \qquad \text{(Eq. 1.9)}$$

$$[H_2CO_3] = C_{H_2CO_3}\alpha_{H_2CO_3} \qquad \text{(Eq. 1.10)}$$

The α_{H2CO3} is a H$_2$CO$_3$ related value; and is equals to

$$\alpha_{H_2CO_3} = \frac{[H_2CO_3]}{C_{H_2CO_3}} \qquad \text{(Eq. 1.11)}$$

Similar arrangements can also be performed for [HCO$_3^-$] calculations.

$$[H_2CO_3] = \frac{[H^+][HCO_3^-]}{K_{a1}} \qquad [CO_3^{2-}] = K_{a2} \frac{[HCO_3^-]}{[H^+]} \qquad \text{(Eq. 1.12)}$$

$$C_{H_2CO_3} = \frac{[H^+][HCO_3^-]}{K_{a1}} + [HCO_3^-] + K_{a2}\frac{[HCO_3^-]}{[H^+]} \qquad \text{(Eq. 1.13)}$$

$$C_{H_2CO_3} = [HCO_3^-]\left(\frac{[H^+]^2 + K_{a1}[H^+] + K_{a1}K_{a2}}{K_{a1}[H^+]}\right) \qquad \text{(Eq. 1.14)}$$

$$[HCO_3^-] = C_{H_2CO_3}\frac{K_{a1}[H^+]}{[H^+]^2 + K_{a1}[H^+] + K_{a1}K_{a2}} \qquad \text{(Eq. 1.15)}$$

Similarly the function for HCO_3^- is as follows.

$$\frac{K_{a1}[H^+]}{[H^+]^2 + K_{a1}[H^+] + K_{a1}K_{a2}} = \alpha_{HCO_3^-} \qquad \text{(Eq. 1.16)}$$

$$[HCO_3^-] = C_{HCO_3^-}\alpha_{HCO_3^-} \qquad \text{(Eq. 1.17)}$$

When the similar arrangements were performed for $[CO_3^{2-}]$ the equilibrium concentration of CO_3^{2-} can be calculated as follows.

$$[CO_3^{2-}] = C_{H_2CO_3}\frac{K_{a1}K_{a2}}{[H^+]^2 + K_{a1}[H^+] + K_{a1}K_{a2}} = C_{H_2CO_3}\alpha_{CO_3^{2-}} \qquad \text{(Eq. 1.18)}$$

pH dependencies of H_2CO_3/HCO_3^- and CO_3^{2-} species show in Fig. 1.2.
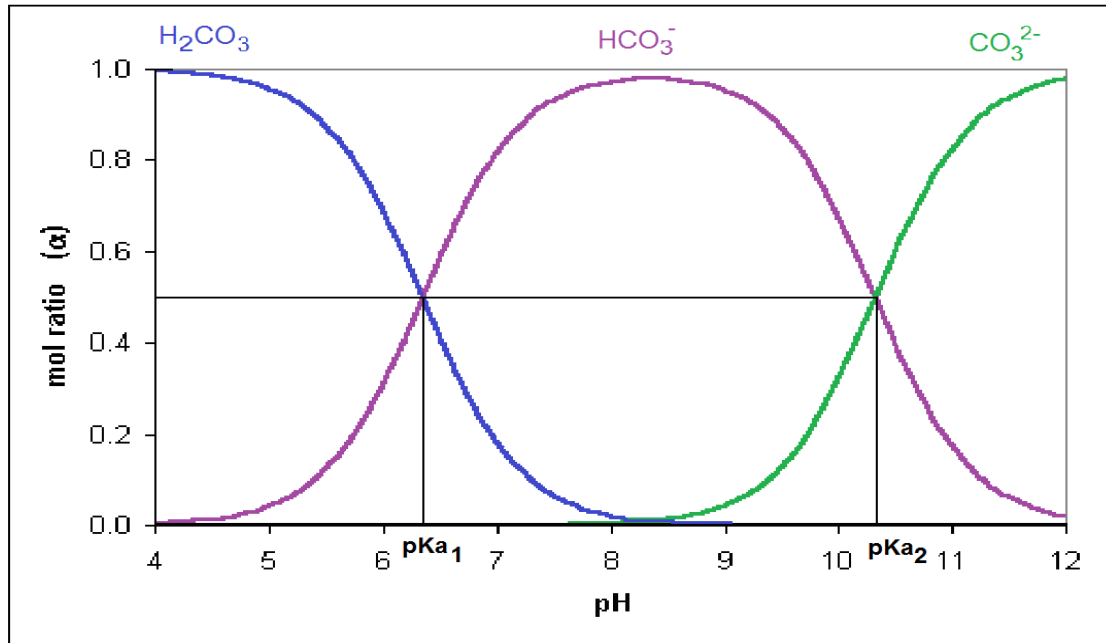
Figure 1.2 pH dependencies of H_2CO_3/HCO_3^- and CO_3^{2-} species in terms of α function.

The equations for α function of $H_2CO_3/ HCO_3^-/ CO_3^{2-}$ can be summarized as follows.

$$\alpha_{H_2CO_3} = \frac{\left[H^+\right]^2}{\left[H^+\right]^2 + \left[H^+\right]K_{a1} + K_{a1}K_{a2}} = \frac{\left[H_2CO_3\right]}{totCO_2(aq)}$$

$$\alpha_{HCO_3^-} = \frac{\left[H^+\right]K_{a1}}{\left[H^+\right]^2 + \left[H^+\right]K_{a1} + K_{a1}K_{a2}} = \frac{\left[HCO_3^-\right]}{totCO_2(aq)} \qquad \text{(Eq. 1.19)}$$

$$\alpha_{CO_3^{2-}} = \frac{K_{a1}K_{a2}}{\left[H^+\right]^2 + \left[H^+\right]K_{a1} + K_{a1}K_{a2}} = \frac{\left[CO_3^{2-}\right]}{totCO_2(aq)}$$

1.5 pH Calculations in a Dissolved Carbon Dioxide (H_2CO_3) Solution

For a solution of dissolved CO_2 solution (H_2CO_3) the following equations can be written. Numerical pH value of such a solution can be calculated following given equations.

$H_2CO_3 \leftrightarrow \ H^+ + HCO_3^-$

$HCO_3^- \ \leftrightarrow H^+ + CO_3^{2-}$

$H_2O \leftrightarrow \ H^+ + OH^-$
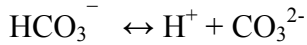
The charge balance equaiton and following steps show the way for pH calculation.

$[H^+] = [HCO_3^-] + 2\,[CO_3^{2-}] + [OH^-]$ (Eq. 1.20)

$$\left[HCO_3^-\right] = C_{H_2CO_3}\,\alpha_{HCO_3^-} = C_{H_2CO_3}\,\frac{K_{a1}\left[H^+\right]}{\left[H^+\right]^2 + \left[H^+\right]K_{a1} + K_{a1}K_{a2}}$$ (Eq. 1.21)

$$\left[CO_3^{2-}\right] = C_{H_2CO_3}\,\frac{K_{a1}K_{a2}}{\left[H^+\right]^2 + \left[H^+\right]K_{a1} + K_{a1}K_{a2}}$$ (Eq. 1.22)

$$\left[OH^-\right] = \frac{Kw}{\left[H^+\right]}$$ (Eq. 1.23)

$$\left[H^+\right] = C_{H_2CO_3}\left(\frac{K_{a1}\left[H^+\right] + 2K_{a1}K_{a2}}{\left[H^+\right]^2 + \left[H^+\right]K_{a1} + K_{a1}K_{a2}}\right) + \frac{Kw}{\left[H^+\right]}$$ (Eq. 1.24)

The equation 1.24 is a quadratic equation and should be simplified,

$$\left[H^+\right] = C_{H_2CO_3}\left(\frac{K_{a1}\left[H^+\right] + 2K_{a1}K_{a2}}{\left[H^+\right]^2 + \left[H^+\right]K_{a1} + K_{a1}K_{a2}}\right)$$ (Eq. 1.25)

The equation eq. 1.22 is still a third order equation and should be simplified once more considering

$[H^+] \approx [HCO_3^-]$ and $[HCO_3^-] \gg 2\,[CO_3^{2-}]$

Therefore the equation eq. 1.22 becomes,

$$C_{H_2CO_3} \frac{K_{a1}[H^+]}{[H^+]^2+[H^+]K_{a1}+K_{a1}K_{a2}} \rangle\rangle 2C_{H_2CO_3} \frac{K_{a1}K_{a2}}{[H^+]^2+[H^+]K_{a1}+K_{a1}K_{a2}} \quad \text{(Eq.1.26)}$$

When the acidity constant of K_{a2} considered as

$[H^+] \gg 2 K_{a2}$ and the assumption shown in eq. 1.27 was accepted the pH can be calculated as follows (Eq. 1.28)

$$\frac{2K_{a2}}{[H^+]} < 10^{-2} \qquad \text{(Eq. 1.27)}$$

$$[H^+] = \sqrt{K_{a1}C_{H_2CO_3}} \qquad \text{(Eq. 1.28)}$$

1.6 Titrimetric Method for Analysis of Dissolved CO₂

When dissolved in water, free CO_2 reacts with Na_2CO_3 or $NaOH$ to form $NaHCO_3$. Additionally, due to the given equilibrium constants of silisic and phosphoric acid may yield the anions of $HSiO_3^-$ and $H_2PO_4^-$ and these species may interfere in quantitative analysis of dissolved CO_2.

$H_2CO_3 \leftrightarrows H^+ + HCO_3^-$ $pK_{a1}= 6.35$ (First dissociation of carbonic acid)

$HCO_3^- \leftrightarrows H^+ + CO_3^{2-}$ $pK_{a2}= 10.33$

$H_2SiO_3 \leftrightarrows H^+ + HSiO_3^-$ $pK_{a1}= 9.86$ (First dissociation of silisic acid)

$HSiO_3^- \leftrightarrows H^+ + SiO_3^-$ $pK_{a2}= 13.1$

$H_3PO_4 \leftrightarrows H^+ + H_2PO_4^-$ $pK_{a1}= 2.15$

$H_2PO_4^- \leftrightarrows H^+ + HPO_4^{2-}$ $pK_{a2}= 7.20$ (Second dissociation of phosporic acid)

$HPO_4^{2-} \leftrightarrows H^+ + PO_4^{3-}$ $pK_{a3}= 12.35$
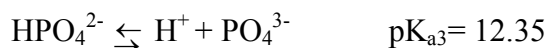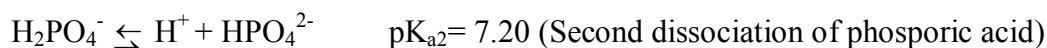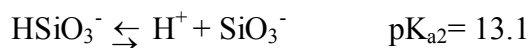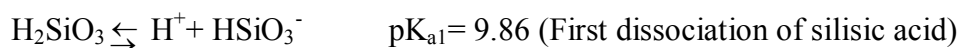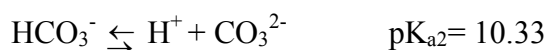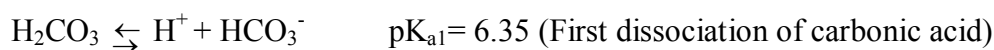
Completion of the reactions is indicated potentiometrically or by the development of the pink color characteristic of phenolphatalein indicator at the equivalence pH of 8.3. A 0.01 M $NaHCO_3$ solution containing phenolphatalein indicator is as suitable colour standard for the end point (Greenberg, Connors, Jenkins, 1980, 268).

1.6.1 Cations and Anions that Quantitatively Disturb the Determination of Dissolved CO_2

Aluminum, chromium, copper and iron are some of the metals with salts that contribute to high results. Ferrous ion should not exceed 1.0 mg/L. Positive errors also are caused by amines, ammonia, borate, nitrite, silicate, phosphate and sulfide. Negative errors can occur by high total dissolved solids, such as those encountered in seawater, or by addition of excees indicator (Greenberg et al., 1980, 268).

1.6.2 Sampling and Storage of Dissolved CO_2 Samples

Even with a careful collection technic, some loss in free CO_2 can be expected in storage and transit. This occurs more frequently when the gas is present in large amounts. Occasionally a sample may show an increase in free CO_2 content on standing. Consequently, one should determine free CO_2 immediately at the point of sampling. Where a field determination is impractical, a bottle for laboratory examination should completely be filled. The sample shoul be kept, until tested, at a temperature lower than that at which the water was collected. The laboratory examination should be made as soon as possible to minimize the effect of CO_2 changes (Greenberg et al., 1980, 268-269).

1.6.3 Apparatus for Titrimetric Analysis

a. Electrometric titrator: Any commercial pH meter or electrically operated titrator that uses a glass electrode and can be read to 0.05 pH unit can be used. Instrument should be standardized and calibrated according to the manufacturer's instructions. Special attention should be paid to temperature compensation and

electrode care. If automatic temperature compensation can not be provided, titration can be performed at $25 \pm 2^{\circ} C$.

b. Titration vessel: The size and form depends on the electrodes and the sample size. There should be a free space above the sample as small as practicable, but allow room for titrant and full immersion of the indicating portions of electrodes. For conventional-sized electrodes 200 mL beaker can be used. With a miniature combination glass-reference electrode 125 mL or 250 mL Erlenmeyer flask with a two-hole stopper can be used.

c. Magnetic stirrer

d. Pipets, volumetric

e. Flasks, volumetric

f. Burets, borosilicate glass

g. Polyolefin bottle (Greenberg et al., 1980, 251).

1.6.4 Reagents for Titrimetric Analysis

a. Carbon dioxide free water: Prepare all stock and standard solutions and dilution water for the standardization procedure with distilled or deionized water that has been freshly boiled for 15 min and cooled to room temperature. The final pH of the water should be ≥ 6.0 and its conductivity should be ± 2 μmhos/cm.

b. Potassium hydrogen phthalate solution, approximately 0.05N: Crush 15 to 20 a primary standard $KHC_8H_4O_4$ to about 100 mesh and dry at $120^{\circ} C$ for 2 hr. Cool in a dessicator. Weigh 10.0 ± 0.5 g (to the nearest mg), transfer to a 1 L volumetric flask, and dilute to 1000 mL.

c. Standard sodium hydroxide titrant, 0.1N: Dissolve 11 g NaOH in 10 mL distilled water, cool and filters through a Gooch crucible or hardened filter paper. Dilute 5.45 mL clear filtrate to 1 L with water and store in a polyolefin bottle

protected from atmospheric CO_2 by a soda lime tube or tight cap. Standardize by titrating 40.00 mL $KHC_8H_4O_4$ solution, using a 25 mL buret. Titrate to the inflection point, which should be close to pH 8.7. Calculate normality of NaOH:

$$Normality = \frac{A \times B}{204.2 \times C} \qquad \text{(Eq. 1.29)}$$

Where:

A= g $KHC_8H_4O_4$ weighed into 1 L flask,

B= mL $KHC_8H_4O_4$ solution taken for titration and

C= mL NaOH solution used.

Use the measured normality in further calculations or adjust to 0.1000N; 1 mL= 5.00 mg $CaCO_3$.

d. Standard sodium hydroxide titrant, 0.02N: Dilute 200 mL 0.1N NaOH to 1000 mL and store in a polyolefin bottle protected from atmospheric CO_2 by a soda lime tube or tight cap.

e. Hydrogen peroxide, H_2O_2, 30 %.

f. Methyl orange indicator solution.

g. Phenolphthalein indicator solution.

h. Sodium thiosulfate, 0.1N: Dissolve 25 g $Na_2S_2O_35H_2O$ and dilute to 1000 mL with distilled water (Greenberg et al., 1980, 251-252).

1.6.5 Procedure for Titrimetric Analysis

a. Color change: Select sample size and normality of titrant. Adjust sample to room temperature, if necessary, and with a pipet discharge sample into an erlenmeyer flask, while keeping pipet tip near flask bottom. If free residual chlorine is present add 0.05 mL (1 drop) 0.1N $Na_2S_2O_3$ solution, or destroy with ultraviolet radiation.

Add 0.1 mL (2 drops) indicator solution and titrate over a white surface to a persistent color change characteristic of the equivalence point (Greenberg et al., 1980, 252).

b. Potentiometric titration curve: Rinse electrodes and titration vessel with distilled water and drain. Select sample size and normality of titrant. Adjust sample to room temperature, if necessary, and with a pipet discharge sample while keeping pipet tip near the titration vessel bottom.

Measure sample pH. Add standard alkali in increments of 0.5 mL or less. After each addition, mix thoroughly but gently with a magnetic stirrer. Avoid splashing. Record pH when a constant reading is obtained. Continue adding titrant and measure pH until pH 9.0 is reached. Construct the titration curve by plotting observed pH values versus cumulative milliliters titrant added. A smooth curve showing one or more inflections should be obtained. A ragged or erratic curve may indicate that equilibrium was not reached between successive alkali additions. Determine acidity relative to a particular pH from the curve.

c. Potentiometric titration to pH 3.7 or 8.3: Prepare sample and titration assembly as specified in b. Titrate to preselected end point pH without recording intermediate pH values. As the end point is approached make smaller additions of alkali and be sure that pH equilibrium is reached before making the next addition (Greenberg et al., 1980, 252).

1.6.6 Calculations

$$mg\ CO_2 / L = \frac{A \times N \times 44.000}{mL\ sample}$$
(Eq. 1.30)

Where,

A= mL titrant and

N= normality of NaOH (Greenberg et al., 1980, 268).

1.6.7 Precision and Accurarcy of Titrimetric Analysis

Precision and accurarcy of the titrimetric method are on the order of ± 10 % of the known CO_2 concentration (Greenberg et al., 1980, 268).

1.7 Optical Chemical Sensing of Gaseous and Dissolved CO_2

The principle of optical CO_2 sensing is mainly based on monitoring the color, absorption, transmittance, refractive index, fluorescence or another optical property of an indicator dye which is sensitive to the pH changes in its environment. The pH change is mainly caused by the dissociation of H_2CO_3, where the concentration of H_2CO_3 is in thermodynamic equilibrium with the CO_2 concentration of the medium (Wolfbeis, Kovács, Goswami & Klainer, 1998).

The whole sensing chemistry, namely the dye and a suitable buffer system, is separated from the probe by a polymeric, CO_2 permeable but ion-impermeable membrane which excludes proton exchange, with the environment.

Optical CO_2 sensors based on the absorbance or fluorescence changes of pH indicators have several attractive features, including electrical isolation, reduced noise interference, the possibility of miniaturization, and remote sensing.

In the following chapter general optical chemical sensing approach will be explained into detail in terms of definition, advantages, and classification, structure and sensor parameters. Later, literature information regarding optical chemical CO_2 and dissolved CO_2 sensors will be given. In this thesis we intended to investigate fiber optic competible choromoionophore/matrix combinations. For this reason in next chapters fiber optics will be explained into detail.

CHAPTER TWO
OPTICAL CHEMICAL SENSING APPROACH

2.1 Definition of an Optical Chemical Sensor

Simply, an optical chemical sensor is a device that measures a physical quantity or the concentration of a chemical or biochemical species and converts it into a signal which can be read by an observer or by an instrument. The most widely used basic measuring techniques in optical chemical sensors are optical absorption and luminescence, but sensors based on other optical parameters, such as refractive index and dispersion, have also been developed. However, sometimes the term "sensor" is being used to refer to a cation or anion-selective molecular probe or a pH indicator (Janata, 1990).

Different definitions of sensors can be seen in the literature and the discussion about the charecteristics and the requirements of sensors is still going on. The following definition is given by an IUPAC commission on sensors.

"A chemical sensor is a device that transforms chemical information ranging from the concentration of a spesific sample component to total composition analysis into analytical usefull signal. The chemical information mentioned above may originate from a chemical reaction of the analyte or from a physical property of the system investigated. A chemical sensor is an essential component of an analyser. In addition to the sensor, the analyser may contain that perform the following functions: sampling, sample transport, signal processing, data processing."

Sensors are normally designed to operate under well defined conditions for specified analytes in certain sample. Therefore, it is not always necessary that a sensor responds specifically to a certain analyte. Under attentively controlled operating conditions, the analyte signal may be independent of other sample

components, thus allowing the determination of the analyte without any major preliminary treatment of the sample.

Otherwise unspecific but satisfactory reproducible sensors may be used in series for multicomponent analysis. Such systems for multicomponent analysis are called sensor arrays (Hulanicki, Glab & Ingman, 1991).

2.2 Structure of Optical Chemical Sensor

According to IUPAC "An optical chemical sensor contains two basic functional units: a receptor part and a transducer part. Some sensors may include a separator which is for example a membrane. In the receptor part of a sensor the chemical information is transformed into form of energy which may be measured by the transducer. The transducer part is a device capable of transforming the energy carring the chemical information about the sample into o useful analytical signal. The transducer as such does not show selectivity." (Hulanicki, Glab & Ingman, 1991).

2.3 Classification of Sensors

Optical properties which have been utilized in an optical chemical sensor can be listed as follows (Hulanicki, Glab & Ingman, 1991):

a) Absorbance, measured in a transparent medium, caused by the absorptivity of the analyte itself or by a reaction with some suitable indicator.

b) Reflectance is measured in non-transparent media, usually using an immobilized indicator.

c) Luminescence, based on the measurement of the intensity of light emitted by a chemical reaction in the receptor system.

d) Fluorescence, measured as the positive emission effect caused by irradiation. Also, selective quenching of fluorescence may be the basis of such devices.

e) Refractive index, measured as the result of a change in solution composition. This may include also a surface plasmon resonance effect.

f) Optothermal effect, based on a measurement of the thermal effect caused by light absorption.

g) Light scattering, based on effects caused by particles of definite size present in the sample (Hulanicki, Glab & Ingman, 1991).

Optical sensors have shortly been named optrodes (optical electrodes) or optodes. An optode or optrode is an optical sensor device that optically measures a specific substance usually with the aid of a chemical transducer.

Sensors have also been classified according to the application to detect or determine a given analyte. Examples are sensors for pH, for metal ions or for determing oxygen, carbon dioxide or other gases (Hulanicki, Glab & Ingman, 1991).

2.4 Validity of Sensors

The development of sensors is still at an embryonic stage and major problems still need to be solved. The characterization of a newly constructed sensor involves the testing of several parameters before the detection limit, limit of quantification; linearity of response etc. can be calculated (Camara, Perez-Conde, Moreno-Bondi & Rivas, 1995, 165-193).

Response Time; in some sensors this parameter is a function of the analyte concentration. Thus, the response time is not constant over the whole calibration curve. This is quite frequent in pH sensors whose response time at near neutral pH may be higher than at acid or basic pH. The alternative methods proposed for preparing calibration curves are measuring at a fixed time before the equilibrium is reached, measuring at equilibrium or measuring the variation in the slope (change in

analytical signal versus time) with concentration. To minimize the delay in response, probes should be designed with low analyte mass transport times. Sensor Reversibility; is the most desirable characteristic because it allows indefinite sensor use and therefore continuous monitoring of the analyte.

Precision; is the reproducibility of the method as shown by the agreement of independent measurements under defined conditions. The lack of specific reversible reactions makes it necessary to use disposable probes or big reservoirs (which allow several determinations), or to regenerate the probe after use. All these problems, combined with the inherent irreproducibility of sensor construction, result in considerable irreproducibility of sensor measurements (Camara, Perez-Conde, Moreno-Bondi & Rivas, 1995, 165-193).

Bias; is a systematic error inherent in a method or caused by other factors that affect the result. An example of possible bias is the measurement of pH by a reflectance or luminescence sensor in samples of different ionic strength or viscosity. It is important to evaluate all these possible errors before the measurement and to ensure that the solutions for calibration are prepared in matrices similar to those of the samples to be tested.

Cross-Sensitivity; is caused by the presence in the sample of substances that may affect the sensitivity of the sensor response to the analyte of interest (Camara, Perez-Conde, Moreno-Bondi & Rivas, 1995, 165-193).

Sensor Lifetime; in many cases immobilized reagents suffer degradation due to the action of light, temperature or solutions used for regeneration. This degradation often occurs very slowly, so the sensor can be used for many measurements, although it has to be recalibrated after a certain number of analyses. To overcome bleaching or other kinds of reagent deterioration, the device focussing the light from the lamp has a shutter to avoid illumination of the sensor for longer periods than are strictly necessary and thus to preserve the active phase of the sensor.

Reproducibility; two measures of reproducibility can be used. One is the variation in the readings of an individual sensor at different times, the other the reproducibility among different sensors. The latter is estimated by comparing the response of many sensors to the same set of calibrants. Irreproducibility among sensors is a major problem because the immobilization of reagents at different times under the same conditions results in probes with different analytical characteristics. This problem becomes more serious if the solid supports, especially resins, used for immobilization are from different batches (Camara, Perez-Conde, Moreno-Bondi & Rivas, 1995, 165-193).

2.5 Advantages and Disadvantages of Optical Sensors

The following features of optical sensors are considered to be advantageous over currently existed other ones (Wolfbeis, 1991);

1) They do not require a reference signal. In practice, however, a reference detector for compensating intensity drifts of the light source is sometimes required.

2) Electric and magnetic fields do not interfere with optical signals.

3) Most optical sensor spots are cheap and simple, and the reagent phase can be easily exchanged.

Especially for fiber optic sensors it can be stated that (Wolfbeis, 1991);

1) The ease of miniaturization allows the development of very small, light and flexible sensors.

2) Low-loss optical fibers allow transmittance of optical signals over wide distances and remote sensing in hazardous or inaccessible environments.

3) Distributed multiplexed sensing is possible.

Optical sensors may exhibit one or more of the following disadvantages;

1) Ambient light can interfere.

2) Sensors with indicator phases are likely to have limited long-term stability because of photobleaching or wash-out.

3) Sensors with immobilized pH indicators as well as chelating reagents have limited dynamic ranges as compared to electrodes since the respective association equilibria obey the mass action law.

4) Response time is determined by the mass transfer of the analyte into the indicator phase.

5) In the water analysis it is often mandatory to control the pH and to correct the signal for pH effects.

2.6 Optical Fiber Basics

The alternative use of optical fibers in various applications has rapidly grown, especially in last two decades. Optical fibers can be used as auxiliary agent in design of sensors to measure temperature, pressure and other physical quantities. The optical fibers, which are a component of the communication industry, provide an ideal media for the transport of optical information. They are particularly important for remote sensing.

An optical fiber is composed of three parts; the core, the cladding, and the coating or buffer. The basic structure of an optical fiber is shown in Figure 2.1. The core is a cylindrical rod of dielectric material and is generally made of glass. Light propagates mainly along the core of the fiber (Jones, 1998).
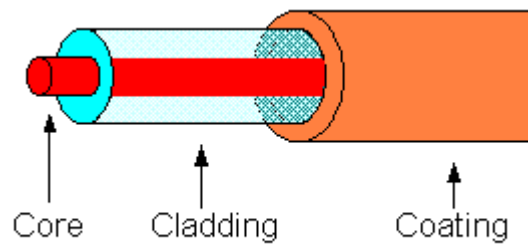
Figure 2.1 Basic parts of an optical fiber.

The cladding layer is made up of a dielectric material with a less index of refraction then that of the core. The cladding is generally made up of glass or plastic material. The cladding executes such functions as decreasing loss of light from core into the surrounding air, decreasing scattering loss at the surface of the core, protecting the fiber from absorbing the surface contaminants and adding mechanical strength (Jones, 1998).

The outer layer; coating or buffer is a layer of material used to protect an optical fiber from physical damage. The material exploited as coating is mainly a type of plastic, is elastic in nature and prevents abrasions.

The light-guiding principle along the fiber is based on the "total internal reflection". The angle at which total internal reflection occurs is called the critical angle of incidence. At any angle of incidence, greater than the critical angle, light is totally reflected back into the glass medium (see Figure 2.2). The critical angle of incidence is determined by using Snell's Law. Optical fiber is an example of electromagnetic surface waveguide (Jones, 1998).
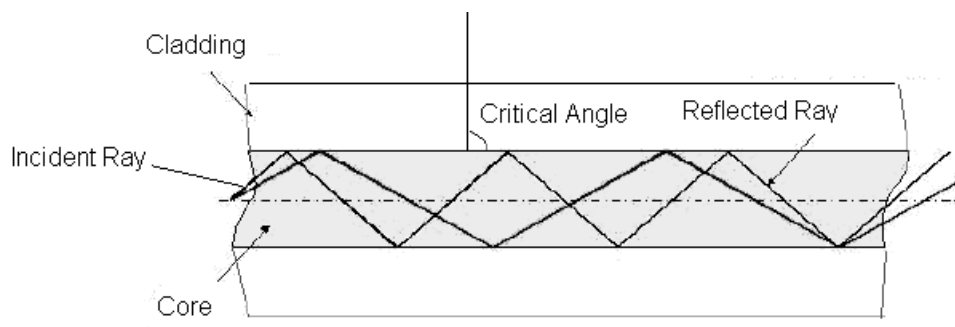
Figure 2.2 Total internal reflections in an optical fiber.

Numerical aperture (NA) is a critical performance specification for multimode fibers. It is defines the "cone of acceptance" and is a measure of the light gathering capacity of optical fiber (See Figure 2.3). It indicates the maximum angle at which a particular fiber can accept the light that will be transmitted through it. The higher an optical fiber's NA, the larger the cone of light that can be coupled into its core (taken from (http://www.ofsoptics.com/resources/Understanding-Fiber-Optics-Numerical-Aperture.pdf).

Theoretical NA may be expressed by the equation $NA = (n_1^2 - n_2^2)^{1/2}$, where n_1 is the refractive index of the core and n_2 is the refractive index of the cladding. The refractive index of a material is defined as the ratio of the speed of light in a vacuum to the speed of light in that particular material (taken from http://www.ofsoptics.com/resources/Understanding-Fiber-Optics-Numerical-Aperture.pdf).
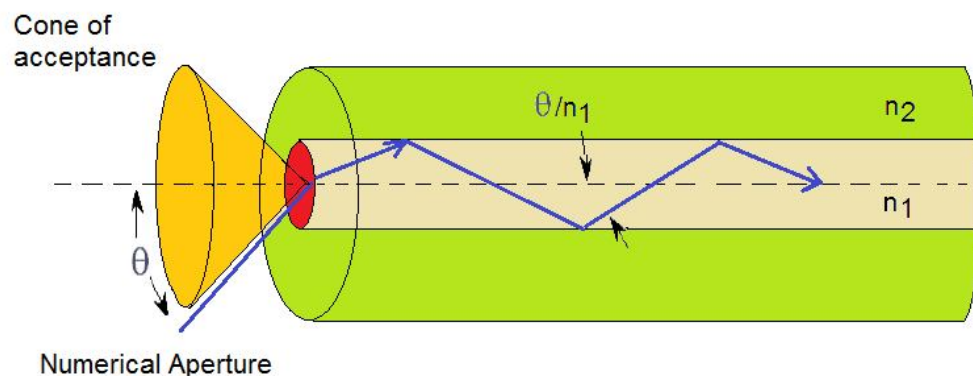
Figure 2.3 Schematic representation of cone of acceptance and numerical aperture (taken from http://www.ofsoptics.com/resources/Understanding-Fiber-Optics-Numerical-Aperture.pdf).

Optical fibers are divided into two groups called single mode and multimode. In classifying the index of refraction profile, we differentiate between step index and gradient index. Step index fibers have a constant index profile over the whole cross section. Gradient index fibers have a nonlinear, rotationally symmetric index profile, which falls off from the center of the fiber outwards (Jenny,2000). Figure 2.4, Figure 2.5 and Figure 2.6 shows the different types of fibers.

Figure 2.4 Schematic representation of
single mode step index fiber.
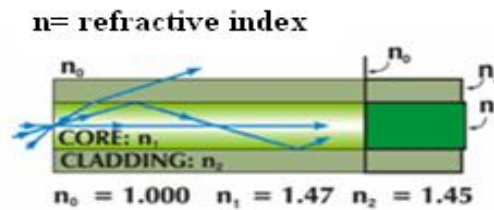
Figure 2.5 Schematic representation of multimode
step index fiber.
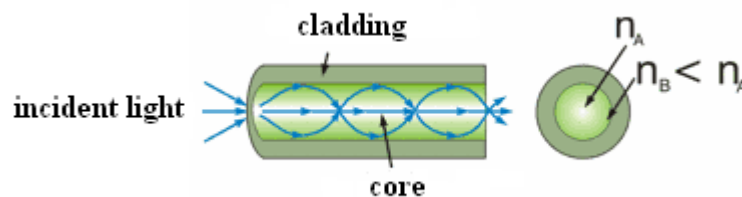
Figure 2.6 Schematic representation of multimode graded index fiber.

Graded-index multimode fibers have a large NA. This is a major advantage of the product: it enables them to be used with relatively low-cost optical components and light sources such as light-emitting diodes (LEDs) and Vertical Cavity Surface Emitting Lasers (VCSELs). LEDs and VCSELs, which have large spot sizes, can be easily coupled to multimode fibers. In contrast, single-mode fibers, which have a small NA, typically use narrow width lasers as power sources and carry only one mode of light straight through a very narrow core. Transmitter alignment and tolerances must be very precise to couple the small beam of light into the tiny core of a single-mode fiber. This drives up the cost of single-mode components (http://www.ofsoptics.com/resources/Understanding-Fiber-Optics-Numerical-Aperture.pdf).

Multimode fibers allow more modes of light to be transmitted, resulting in greater pulse spreading, or dispersion, and less bandwidth. Consequently, these easily-connectorized, high-NA graded-index multimode fibers are ideal for short-distance (up to several kilometers) data communications applications such as local area networks. For graded-index multimode fiber used in data communications, the standard NAs are 0.20 for 50/125 μm fiber and 0.275 for 62.5/125 μm fiber (http://www.ofsoptics.com/resources/Understanding-Fiber-Optics-Numerical-Aperture.pdf).

Fiber optics extensively utilized in design of optical chemical sensors. The sensing agent can be immobilized on to tip of a fiber optic. In this case this is called extrinsic design where the fiber is simply used to carry the light to the sensing takes place. In this case, the fiber just acts as a light transfer agent getting the light to the sensing location.

Based on the operating principle or modulation and demodulation process, a fiber optic sensor can be classified as an intensity, a phase, a frequency, or a polarization sensor. All these parameters may be subject to change due to external perturbations. Thus, by detecting these parameters and their changes, the external perturbations can be sensed (Yu & Shizhuo, 2002).

Based on the application, a fiber optic sensor can be classified as follows:
• Physical sensors: Used to measure physical properties like temperature, stress, etc.

• Chemical sensors: Used for pH, gas analysis, spectroscopic studies, etc.

• Bio-medical sensors: Used in bio-medical applications like measurement of blood flow, glucose content etc) (Fidanboylu & Efendioğlu, 2009).

In extrinsic designs the sensing agent is usually immobilized on glass, cellulose or polyester support materials and attached to the fiber optics. In intirinsic ones the sensing agent is in contact with the fiber optic material. In both cases the sensing

agent is excited with proper light. In all cases optical compatibilitiy of the support/matrix material with fiber optics is quite important. Another parameter is the optical transperency range of the fiber material. In Table 2.1 transmission charecteristics of different types of optical fibers were shown.

Table 2.1 Fibers and their transmission characteristic.

Material	Type	Transmission wavelength	Nominal diameter
Plastic	Single, bundles	500-900 nm	>600 µm
Silica	Single, bundles	600-1800 nm	>150 µm
Quartz	Single, bundles	200-1800 nm	200 µm-3 mm
Florine doped Fibers	Single	220-IR Reg.	> 300 µm

In most of the sensor designs bifurcated optic fiber has been intensively used. Schematic structure of a bifurcated optical fiber is given in Figure 2.7.

Figure 2.7 Schematic structure of a bifurcated optical fiber.

2.6.1 Fiber Optic Sensor Principles

Schematic structure of an optical fiber sensor system is shown in Figure 2.8. It consists of a light source (Laser, LED, Laser diode etc), optical fiber, sensing or modulator element (which transduces the measurand to an optical

signal), an optical detector and processing electronics (luck in amplifier, oscilloscope, optical spectrum analyzer etc).
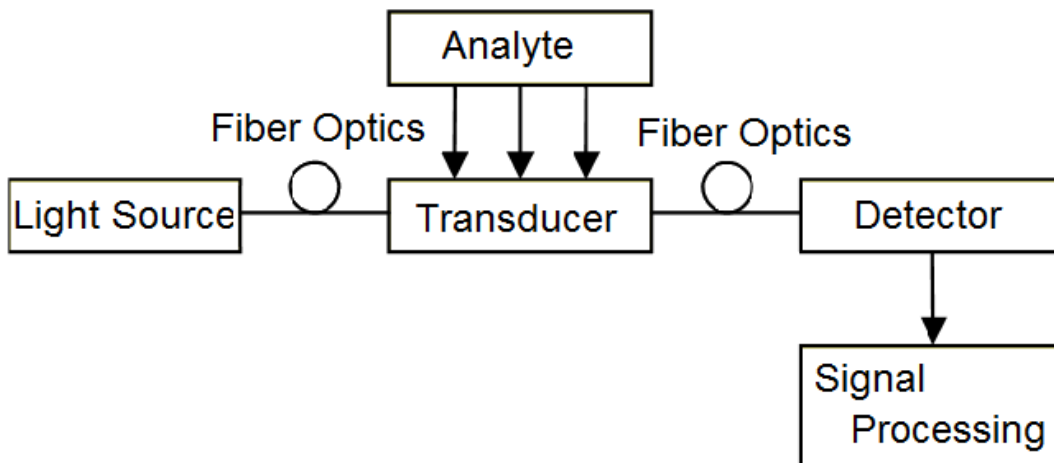
Figure 2.8 Basic components of an optical fiber sensor system.

✓ The main advantages of FOCS over other kinds of sensors can be summarized as follows (Camara, Perez-Conde, Moreno-Bondi & Rivas, 1995, 165-193):

They allow in situ determination and real-time analyte monitoring;

They are easy to miniaturize because optical fibers have very small diameters;

They are fairly flexible: optical fibers can be bent within certain limits without damage;

They can be used in hazardous places and locations of difficult access because of the ability of optical fibers to transmit optical signals over long distances (between 10 m and 10000 m);

Multielement analysis is possible using various fibers and a single central unit;

They normally permit non-destructive analysis;

Optical fibers can carry more information than electrical cables;

Probes are often easy and inexpensive to build.

✓ They also have the following disadvantages:

The number or reversible reactions is very limited, so in many cases probes have to be regenerated after use;

Commercial accessories for optical fibers are not standard items;

The properties of the indicator may vary when it is immobilized;

They usually have lower dynamic ranges than electrodes;

In some cases the concentration of the immobilized indicator is unknown and two optodes prepared similarly can have different analytical characteristics;

The sensor life-time is limited (Camara, Perez-Conde, Moreno-Bondi & Rivas, 1995, 165-193).

As mentioned earlier fundamental approachs utilized in optical chemical sensors are absorbance, reflectance luminescence, fluorescence and refractive index. In this thesis, absorbance and luminescence (fluorescence) chareteristics of the sensing composites were extensively studied.

2.7 Theory of Absorption and Fluorescence

2.7.1 Principle of UV/VIS Absorption Spectroscopy

Molecules having proper chromophore groups absorb ultraviolet or visible fraction of light. The absorbance of a solution increases as attenuation of the beam increases. Absorbance is directly proportional to the path length, b, and the concentration, c, of the absorbing species.
Beer's Law states that

$$A = \varepsilon bc \quad (Eq.\ 2.1)$$

where ε is a constant of proportionality, called the molar absorbtivity coefficient. Different molecules absorb radiation of different wavelengths. An absorption

spectrum will show a number of absorption bands corresponding to certain chromophore groups within the molecule. For example, the absorption that is observed in the UV region for the carbonyl group in acetone is of the same wavelength as the absorption from the carbonyl group in diethyl ketone (Baldini, Chester, Homola & Martellucci, 2006). Ultraviolet-visible spectroscopy (UV = 200 - 400 nm, visible = 400 – 800 nm) corresponds to electronic excitations between the energy levels that correspond to the molecular orbital of the systems. In particular, transitions involving π orbital and ion pairs (n = non-bonding) are important and so UV/VIS spectroscopy is of most use for identifying conjugated systems which tend to have stronger absorptions (Wolfbeis, 1991; Göpel, Hesse, Zemel, 1991-1993; Janata, 1989; Seitz, 1991; MacCraith, O'Keeffe, McEvoy, McDonagh, McGilp, O'Kelly et. al., 1994; Wong, Angell, 1977; Skoog, West, Holler, 1994).

2.8 Luminescence

2.8.1 Mechanism of Luminescence

Luminescence means emission of light by electronically excited atoms or molecules. Electronic excitation requires the supply of energy. Various kinds of luminescence, such as electroluminescence, chemiluminescence, thermoluminescence and photoluminescence, are known and called by the source from which energy is derived. In the case of photoluminescence (fluorescence and phosphorescence) the energy is provided by the absorption of infra-red, visible or ultra-violet light. Two models are necessary to describe the interaction of light with matter: In the one light is regarded as a succession of waves, in the other as a collection of particles. The latter was introduced by Planck, who showed that radiant energy can only be absorbed in definite unites or quanta. The energy quantum E, is defined as

$$E = h\,\nu = h\,\frac{c}{\lambda} \qquad \text{(Eq. 2.2)}$$

where ν is the frequency, h is Planck's constant (6.626. 10^{-34} Js), λ the wavelength, and c the constant velocity of light in vacuum (2.998. 10^8 ms^{-1}). The absorption and emission of light is illustrated by Jablonski level diagram, shown in Figure 2.9. According to the Boltzmann distribution, at room temperature the valance electrons are in the lowest vibration level (ν=0) of the ground electronic state. A transition of these electrons from the ground state (level 0 of S_0) to higher energy levels takes place on absorption (a) of light. The Franck-Condon principle states that there is approximately no change in nuclear position and spin orientation, because absorption of light occurs in about 10^{-15}s. Therefore, the electronic transition is represented by a vertical line. Molecules excited to an upper vibrational level of any excited state rapidly lose their excess of vibrational energy by collision with solvent molecules, and falls to the lowest vibrational level. Molecules in the upper excited states (S_2, S_3, ...) relax by internal conversion (IC), radiationless to the lowest excited singlet state (S_1) within 10^{-12} s. Transition from this level to the vibration levels of the ground state can take place by emitting photons (f). A portion of the excited molecules may return to the ground state by other mechanisms, such as electron transfer, collision, intersystemcrossing (ICS), internal conversion or chemical reaction. Fluorescence emission occurs spontaneously, again in accordance with the Franck-Condon principle, if the radiationless transition lifetime is sufficiently long. The radiative lifetime of fluorescence lies between 10^{-9} s for spin allowed transitions ($\pi* \ \pi$) to 10^{-6} for less probable transitions ($\pi^* \ n$). Molecules in the lowest excited state (S_1) can also undergo conversion to the first triplet state (T_1) by intersystem crossing (ISC).This process requires a time of the same order of magnitude as fluorescence radiation lifetime and therefore competes with fluorescence. Although radiative transitions between states of different multiplicity are spin forbidden, these transitions do take place with low probability compared with singlet-singlet, or triplet-triplet transitions. Emission from the first triplet state (T_1) to the ground state is termed phosphorescence, and usually shifted to higher wavelengths than fluorescence. The radiation lifetime for this transition is about 10^{-2} to 10^{+2} s (Lakowicz, 1993; Parker, 1968; Schmidt, 1994).
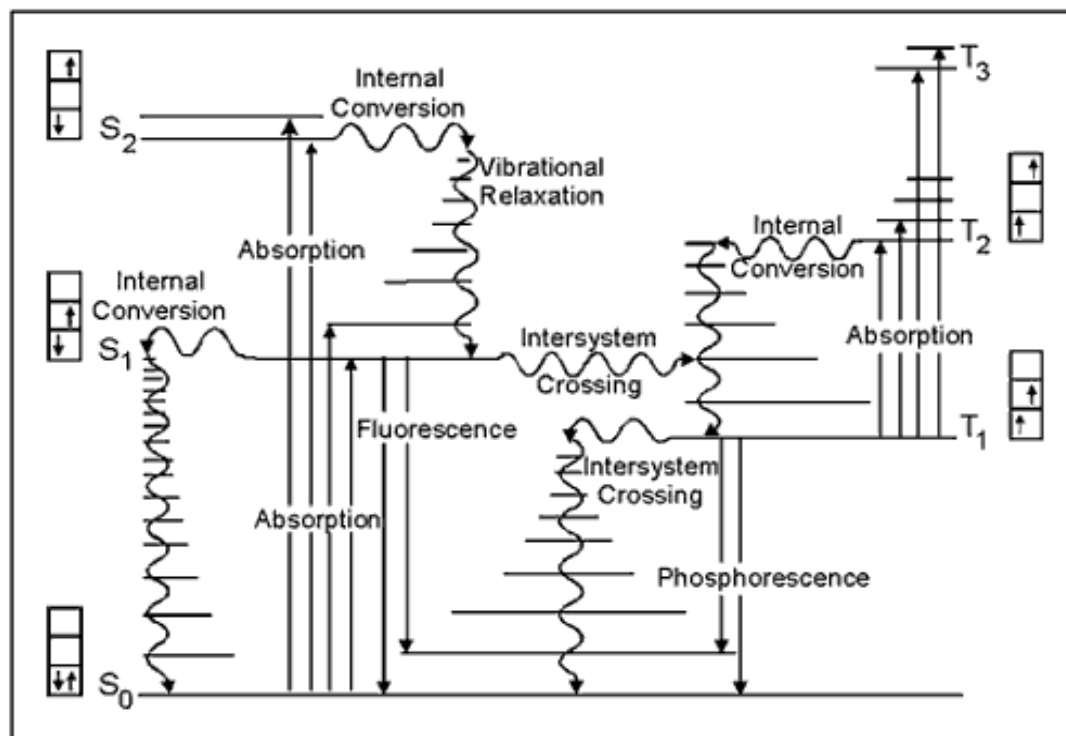
Figure 2.9 The basic concepts of this Jablonski diagram are presented in the Basic Photophysics module. This version emphasizes the spins of electrons in each of the singlet states (paired, i.e., opposite orientation, spins) compared to the triplet states (unpaired, i.e., same orientation, spins) (taken from http://www.photobiology.info/Photochem.html).

2.8.2 Stoke's Shift

The law of Stokes states that the fluorescence and phosphorescence is shifted to higher wavelengths relative to absorption (Stoke's shift). The explanation is provided by the Jablonski diagram. As already mentioned, emission usually occurs form the lowest excited state, but higher excited state are reached by absorption. The radiationless vibrational relaxation (VR) and internal conversion (IC) involves a loss of energy which is reflected in a shift to emission bands of lower energy. Furthermore, molecules generally decay to excited vibrational levels of S_0 (Lakowicz, 1993; Parker, 1968; Schmidt, 1994).

IUPAC definitons of Sokes shift is as follows; Stokes shift **(**IUPAC Compendium of Chemical Terminology); **"**The difference (usually in frequency units) between the spectral positions of the band maxima (or the band origin) of the absorption and

luminescence arising from the same electronic transition. Generally, the luminescence occurring at a longer wavelength than the absorption is stronger than the opposite. The latter may be called an anti-Stokes shift" (http://old.iupac.org/goldbook/S06031.pdf.).

Sometimes the Stoke's shift is given as the difference in nanometers between the peak excitation and emission wavelengths of a fluorescent species.

2.8.3 Quantum Yield

The fluorescence quantum yield Φ_f is the ratio of the number of photons emitted to the number absorbed. The rate constants Γ and knr both depopulate the excited state. The fraction of fluorophores that decay through emission, and hence the quantum yield, is given by

$$\Phi = \frac{\Gamma}{\Gamma + k} \qquad \text{(Eq. 2.3)}$$

The quantum yield can be close to unity if the radiationless decay rate is much smaller than the rate of radiative decay, that is knr $< \Gamma$(Lakowicz, 1999).

2.8.4 Solvatochromism

The excitation and emission spectra of many chromophores are sensitive to the polarity of their surrounding environment. A hypsochromic (or blue) shift of the absorption band, with increasing solvent polarity is called negative solvatochromism. The corresponding bathochromic (or red shift) is entitled positive solvatochromism. Obviously, solvatochromism depends on the solvation of the ground and first excited state of the chromophore. If the ground state is better stabilised by increasing solvent polarity than the excited state, negative solvatochromism is observed. Better stabilisation of the excited molecule relative to that in the ground state, with increasing polarity, leads to positive solvatochromism. The solvent polarity does not only affect the absorption spectra, but also the emission spectra. The mechanism is

illustrated in Figure 2.10. According to the Franck-Condon principle nuclei do not move during the timespan of an electronic transition (10^{-15}s). Therefore, the excited molecule (B) has the same solvation pattern as the molecule in the ground state. Excited molecules have a lifetime in order of about 10^{-8}s. The solvent molecules re-orientate within 10^{-10} s resulting in relaxed excited state, with a solvation shell in equilibrium to this state. From this relaxed excited state (C) light is emitted. By analogy, the orientation of the solvent molecules does not change during the emission (D), due to Franck-Condon principle. Re-orientation of the solvent molecules follows, resulting in an equilibrium ground state (A). The interaction of a molecule with solvent upon excitation and emission, can be described by a change of the molecule´s dipole moment in the ground (μ) and excited state (μ^*). A positive solvatochromism is observed if the dipole moment is increased during excitation, while decreasing dipole moment results in negative solvatochromism (Lakowicz, 1993; Schmidt, 1994; Reichardt, 1988).
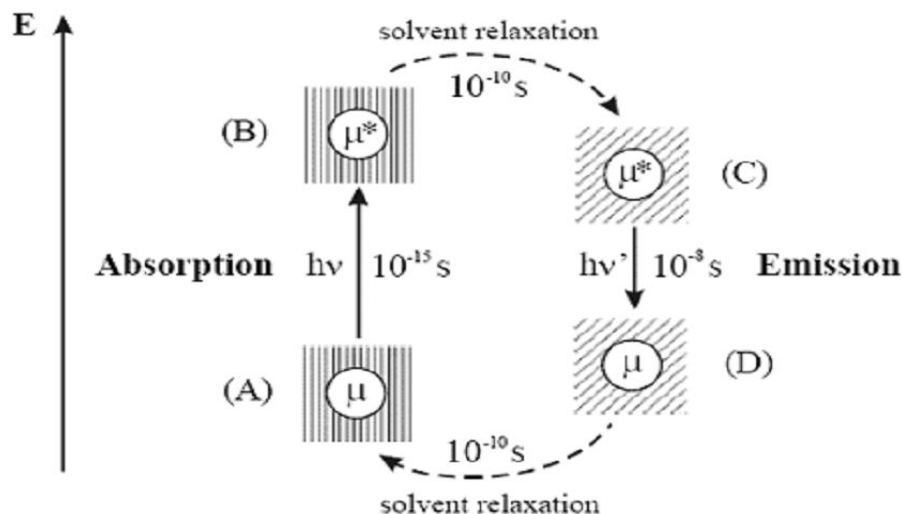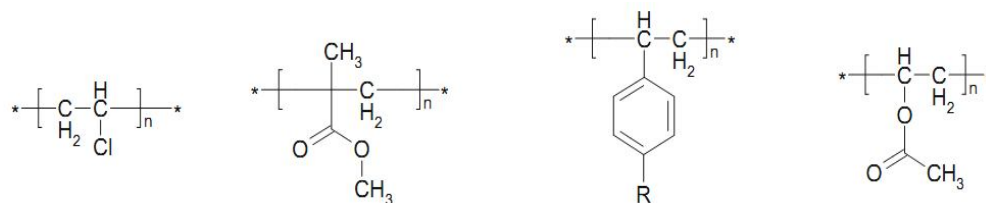

Figure 2.10 Effect of the solvent on the energy of a dipole (μ) upon excitation and emission. Different solvatation shells are illustrated by squares filled with different patterns (taken from Mayr, 1999).

2.9 Matrix Materials and Polymers Utilized in Optical Chemical Sensing

Polymer materials have to provide various requirements to enable optical sensing. First of all, the indicator dye and all additives have to be dissolved properly in the polymer without leaching. The analyte must be able to diffuse fast enough into the polymer and within the polymer. The polymeric material has to be chemically and physically stable in order to achieve good operational lifetime and shelf-life. Furthermore, no crystallization/migration/reorientation of the indicator chemistry in the polymer must occur. The polymer must be stable even at elevated temperatures (e.g. to be resistant to steam heat sterilization). It should be stable against ambient light, chemicals (acid and base vapours, oxidants) and it should be non-toxic and biocompatible (especially when used in biotechnological applications). The polymer should not have any intrinsic color/luminescence, and it should be optically transparent in the spectral range where measurements are being performed. Finally, the material should have good mechanical stability (Mohr, 2006).

2.9.1 Types of Polymers Utilized in Optical Chemical Sensing

Polymers that have a high glassy transition temperature (Tg) like poly (vinyl chloride) (PVC), poly (methyl methacrylate) (PMMA), poly (vinyl acetate) PVAc and poly styrene derivatives are being brittle (See Figure 2.11). Furthermore, the high density/rigidity of the polymer chains (without plasticizers) hinders diffusion of ions and gases in the polymer matrix. They require plasticizers to make them flexible for easier diffusion of analyte. Therefore, plasticizer contents of up to 2:1 may be required (Mohr, 2006). Chemical structures of some common plasticiziers were shown in Figure 2.12 and Figure 2.13.

poly(vinyl chloride)   poly(methyl   polystyrene-   poly(vinyl acetate)
(Tg ~90 °C)   methacrylate)   derivatives   (Tg ~30 °C)
     (Tg ~100 °C)   (Tg 100-140 °C)

Figure 2.11 Chemical structures of some lipophilic polymers (taken from Mohr, 2006).
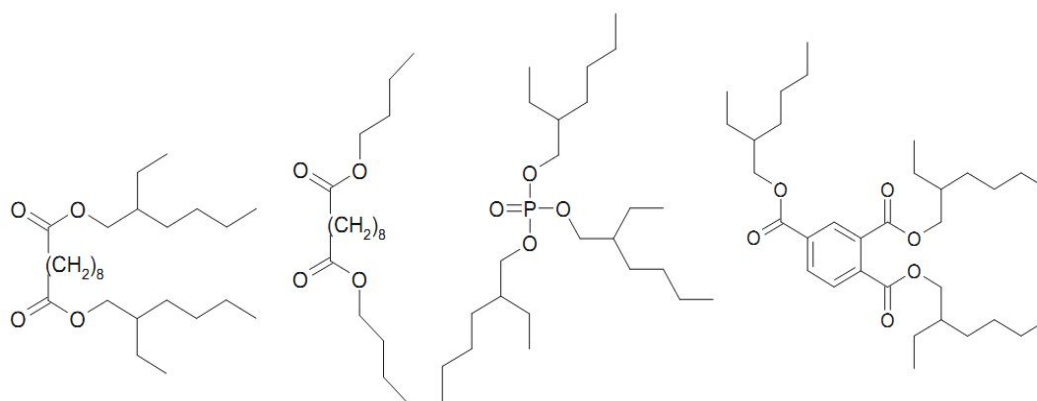
bis(2-ethylhexyl)   dibutyl   tris(2-ethylhexyl)   tris(2-ethylhexyl)
sebacate   sebacate   phosphate   trimellitate

Figure 2.12 Chemical structures of some lipophilic plasticizers (taken from Mohr, 2006).
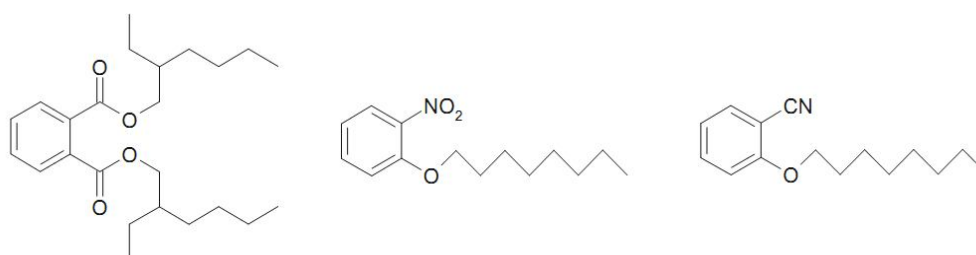
bis(2-ethylhexyl) phthalate   2-nitrophenyloctyl ether   2-cyanophenyloctyl ether

Figure 2.13 Chemical structures of lipophilic and polar plasticizers (taken from Mohr, 2006).

Polymers with low glassy transition do not require plasticizers. However, these compounds are often unpolar (Figure 2.14) and, consequently, they are unsatisfactory solvents for polar ligands, ionophores, dyes and analytes.
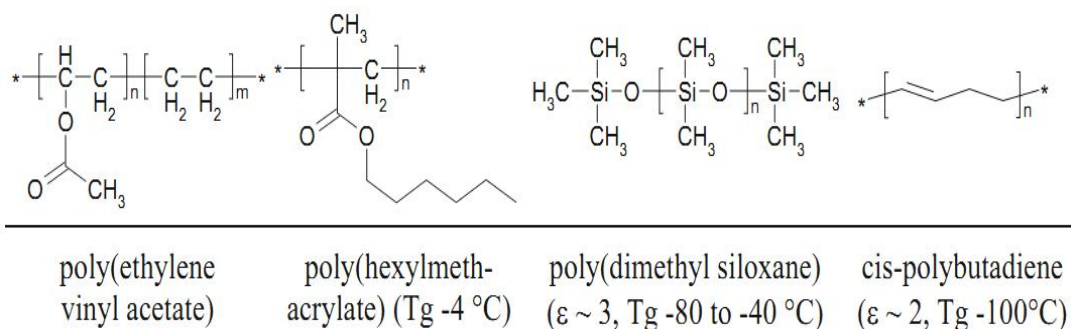
Figure 2.14 Chemical structures of unpolar polymers (taken from Mohr, 2006).

2.9.1.1 Hydrophilic Polymers

Hydrophilic polymers (Figure 2.15) provide a matrix which is comparable to an aqueous environment. Ions can diffuse quite freely, but the possible water uptake (10-1000 %) can cause significant swelling of the polymer. Swelling of the matrix affects the optical properties of the sensors and, consequently, the signal changes. Immobilization of the indicator chemistry usually is achieved via covalent bonding to the polymer.
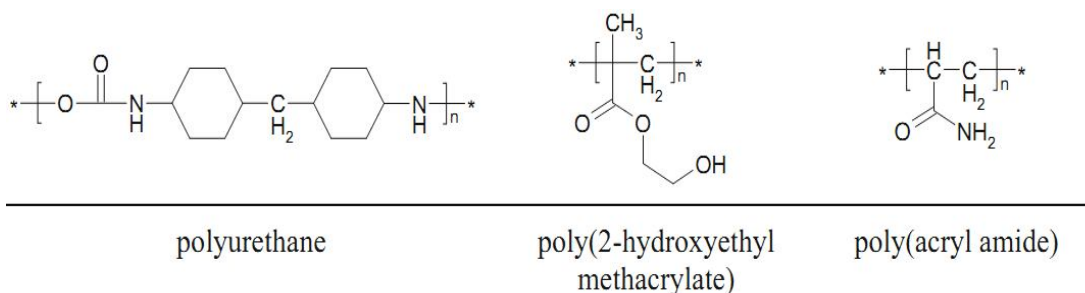
Figure 2.15 Chemical structures of hydrophilic polymers (taken from Mohr, 2006).

2.9.1.2 Charged Polymers (Polyelectrolytes)

Polyelectrolytes (Figure 2.16) exhibit a large amount of dissociable charged groups. They can be used in optical sensor design to bound their counterions; cationic or anionic indicators.
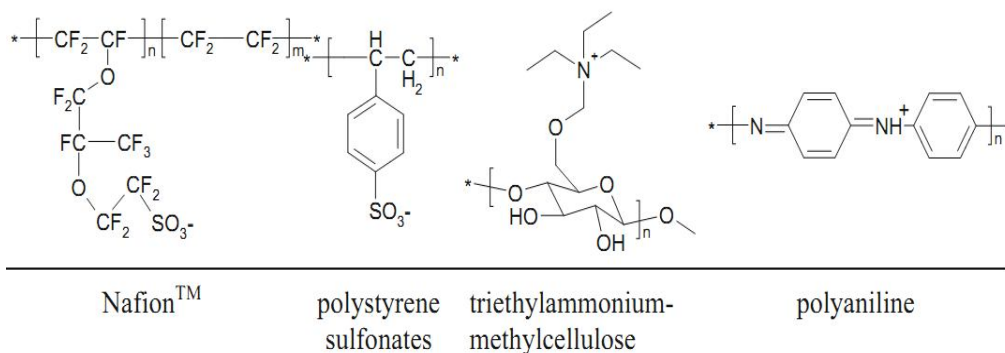
Figure 2.16 Chemical structures of charged polymers (taken from Mohr, 2006).

2.9.1.3 Sol-gel as Matrix Material

Another matrix material for optical chemical sensing purpose is sol-gel material. The sol-gel process itself leads to formation of gels from mixtures of liquid reagents (sols) at ambient temperatures. As its name implies, it contains several steps: the evolution of inorganic networks, formation of colloidal suspension (sol) and gelation of the sol to form a network in a continuos liquid phase (gel). Drying of the obtained gels, even at room temperature, produces glass-like materials called xerogels (xeros + dry). Xerogels are porous, usually transparent and relatively sturdy materials which, when heated at the glass vitrification temperature (ca. 1200° C), turn into the regular glass, identical with classical glasses obtained by melting (Podbielska, Ulatowska-Jarza, Müller, & Eichler, 2006).

The sol-gel process involves the preparation of inorganic matrices via three steps. Components of the sol-gel cocktail are the sol-gel precursor (e.g. tetramethoxysilane), water, a catalyst (acids or bases), the indicator chemistry and a solvent such as ethanol. Mixing these components causes hydrolysis of the ester, silanol-ester condensation, and silanol-silanol condensation of the precursors, (Derinkuyu, 2010).This general reaction scheme can be seen in equations 2.4, 2.5 and 2.6.

$Si(OR)_4 + H_2O \rightarrow Si(OR)_3OH + ROH$ (hydrolysis) (Eq. 2.4)

$Si(OR)_3OH + Si(OR)_4 \rightarrow Si(OR)_3\text{-O-} Si(OR)_3 + ROH$ (condensation) (Eq. 2.5)

$R\text{-Si-OH} + HO\text{-Si-R} \rightarrow R\text{-Si-O-Si-R} + H_2O$ (condensation) (Eq. 2.6)
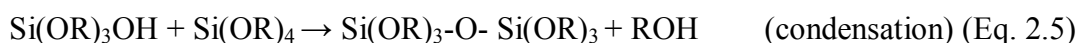
The sol gel matrix materials provide two different advantages for spectroscopic studies; it acts as a diluted and optically transparent moitie like a solution, and also acts as a rigid medium like a solid phase. It is also a competible matrix for bio-technological and clinical applications. The chemical and mechanical stability of the matrix allows, (1) spectral measurements from UV to near IR, (2) ability of giving any desired geometric shape, (3) low temperature studies, without any solubility problems (McKiernan, Yamanaka, Dunn & Zink, 1990; Nakamura, Nasu & Kamiya, 1991). The sol-gel process is influenced by a number of parameters including precursor type, molar water/precursor ratio (R), catalyst type, pH and temperature (Mackenzie, 1994; Sakka 1994). The sol-gel net-work is formed through hydrolysis and condensation reactions. These reactions proceed as long as hydrolysible alkoxy and condensable hydroxyl groups are available (Lev, Tsionsky, Rabinovich, Glezer, Sampath et. al., 1995).

In favourable cases, the immobilization of dye molecules in the solid matrix may reduce intramolecular motions and rearrangements, thus leading to enhanced photostability and fluorescence capability. Entrapment of dye molecules in sol-gel networks allows the investigation of both photophysical and photochemical properties and sensor applications. pH dependent changes in the absorption and emission spectra of certain fluorescent indicators in sol-gel matrices can be followed by optical detection (Ertekin et. al., 2003b).

2.9.1.4 Ionic Liquids as Matrix Materials

Ionic liquids are very new matrix materials for sensor design. Unlike traditional solvents, which can be described as molecular liquids, ionic liquids are composed of ions (see Figure 2.17 for the structures of the commonly used ionic liquids). Their unique properties such as nonvolatility, non-flammability, and excellent chemical and thermal stability have made them an environmentally attractive alternative to conventional organic solvents. Ionic liquids have low melting points (<100° C) and remain as liquids within a broad temperature window (<300° C).

One of the most special properties for ionic liquids is their high polarity. On the normalized polarity scale (ENT) setting tetramethylsilane at 0.0 and water at 1.0, the polarity of common ionic liquids normally falls in the range of 0.6–0.7, similar to that of lower alcohols and formamide (Rantwijk, Lau & Sheldon, 2003). A correlation between the decreases in both the chain length of the alkyl substituents on the imidazolium ring of the cation and the anion size with an increase in polarity can be observed (Carmichael & Seddon, 2000). The polarity values of ionic liquids are sometimes sensitive to the temperature and the presence of water (Baker, Baker & Bright, 2002). Because of the high polarity, ionic liquids present an ideal reaction melieu for chemical and biochemical reactions due to their ability to dissolve a wide range of different substances including polar and nonpolar organic, inorganic, and polymeric compounds.

Despite of their high polarity, most of ionic liquids are hydrophobic and can dissolve up to 1 % of water, and the presence of water may affect the physical properties of the ionic liquids (Seddon, Stark & Torres, 2000). However, the solubility of water in ionic liquids varies unpredictably (Rantwijk et. al., 2003). For example, although 1-butyl-3-methylimidazolium tetrafluoroborate ([BMIm][BF$_4$]), 1-butyl-3-methylimidazolium hexafluorophosphate ([BMIm][PF$_6$]), and 1-butyl-3-methyl-imidazolium-bis-(trifluoromethylsulphonyl) imide ([BMIm][Tf$_2$N]) are similar on Reichardt's polarity scale, the former one is completely water-miscible while the latter two are only slightly soluble in water (Park & Kazlauskas, 2003).

Ionic liquids are generally immiscible with many organic solvents especially when the latter are nonpolar, such as hexane; whereas some may be miscible with polar solvents like dichloromethane and tetrahydrofuran (Park & Kazlauskas, 2003). The immiscibility of ionic liquids with either water or organic solvents has made them feasible to be used to form two-phase systems.

Compared to typical organic solvents, ionic liquids are much more viscous (35–500 cP viscosity for commonly used ionic liquids versus 0.6 cP for toluene and 0.9 cP for water at 25° C) (Park & Kazlauskas, 2003; Brennecke & Maginn, 2001). The

viscosity of an ionic liquid represents its tendency to form hydrogen bonding and the strength of its van der Waals interactions, and can be lowered by increasing the temperature or by adding some organic co-solvents. Normally, an ionic liquid with longer alkyl chains on the cation and a larger anion size presents a higher viscosity.

One obvious advantage of using ionic liquids over the use of normal organic solvents is that the physical and chemical properties of the ionic liquids, including their polarity, hydrophobicity, viscosity, and solvent miscibility, can be finely tuned by altering the cation, anion, and attached substituents. This is important, because by manipulating the solvent properties, one is allowed to design an ionic liquid for specific reaction conditions, such as to increase the substrate solubility, to modify the enzyme selectivity, or to tailor the reaction rate.

| Most commonly used cations | 1-alkyl-3-methyl imidazolium | N-alkyl pyridinium | Tetraalkyl-ammonium | Tetraalkyl-phosphonium $(R_{1,2,3,4}=$ alkyl) |

Some possible	water-insoluble	→		water-soluble
Anions	$[PF_6]^-$			$[CH_3CO_2]^-$
	$[(CF_3SO_2)_2N]^-$	$[CF_3SO_3]^-$		$[CH_3CO_2]^-$, $[NO_3]^-$
	$[BR_1R_2R_3R_4]^-$			Br^-, Cl^-, I^-
				$[Al_2Cl_3]^-$, $[AlCl_4]^-$

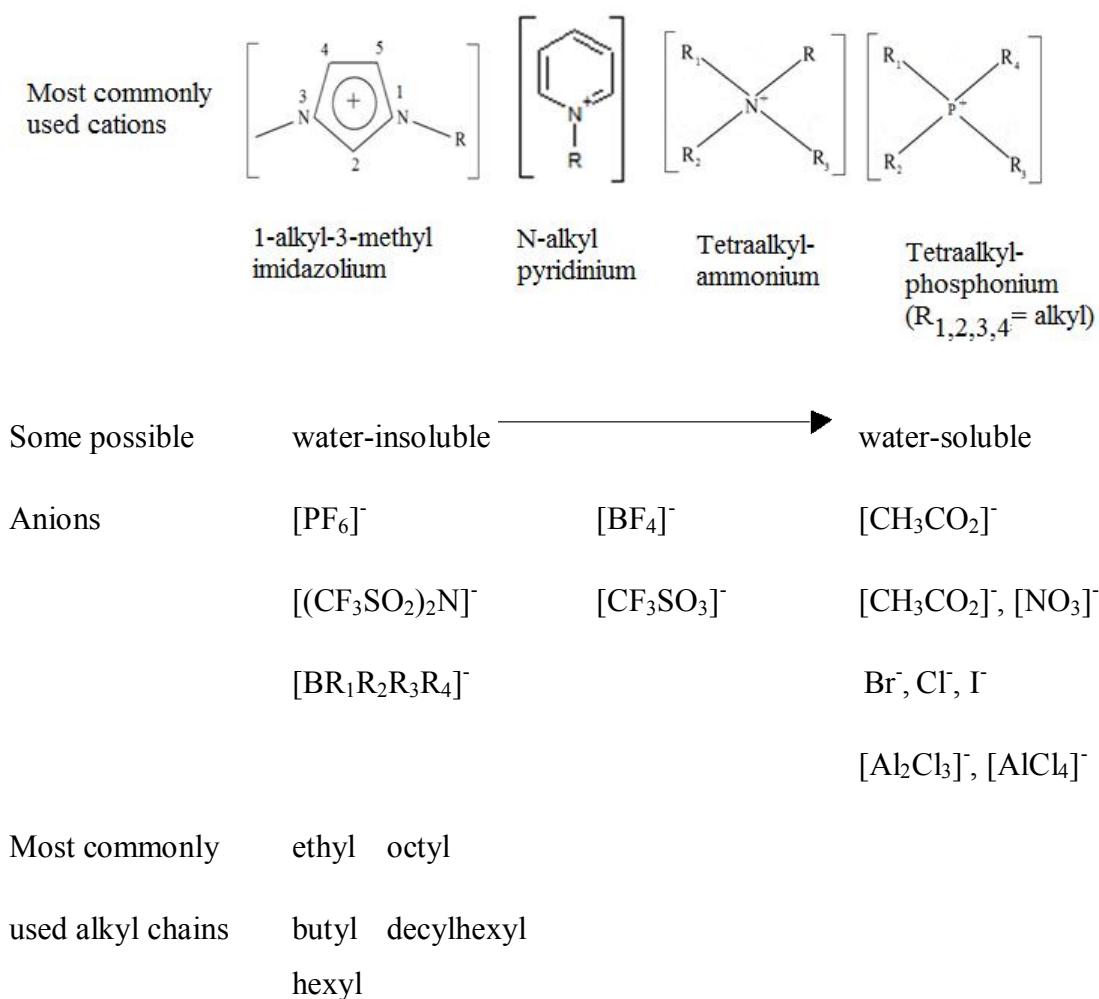| Most commonly used alkyl chains	ethyl	octyl
	butyl	decylhexyl
	hexyl	

Figure 2.17 The building blocks of ionic liquids (taken from Yang & Pan, 2005).

2.9.2.4.1 Usage of Ionic Liquids in the Construction of Sensors. ILs were employed as the sensing materials of quartz crystal microbalance (QCM) sensor for organic vapors, including toluene, methanol, ethanol, 2-propanol, 1-butanol, acetone, acetonitrile, chloroform, tetrahydrofuran, and ethyl acetate (Liang, Yuan, Warmack, Barnes, & Dai, 2002). This application was based on the fact that the viscosity of the IL membrane decreases rapidly because of solubilization of analytes and the change in viscosity varies with the chemical species of the vapors and the types of IL. This results in a frequency shift of the corresponding quartz crystal. The liquid status of ILs at room temperature provided fast diffusion of analytes, so the QCM sensor exhibited a rapid response time (average less than 2 s) to organic vapors with an excellent reversibility. Furthermore, the sensor had a long shelf life because of the zero vapor pressure and stable chemical properties of ILs, which eliminate the possibility of loss of these liquids through vaporization and chemical reaction. This sensor was also applied to determine the solubility of carbon dioxide in a series of imidazolium-based ILs at $25^{o}C$ with CO_2 pressures at or less than 1 bar (Baltus, Culbertson, Dai, Luo, & DePaoli, 2004).

A novel solid-state amperometric O_2-gas sensor based on supported 1-methyl-3-ethyl-imidazolium tetrafluoroborate ($[C_2MIM][BF_4]$) porous polyethylene membrane-coated electrodes has been reported (Wang, Okajima, Kitamura, & Ohsaka, 2004). Compared to solid electrolyte gas sensors and classic Clark-type gas sensors, this proposed O_2-gas sensor possesses the advantages of easy construction and miniaturization, as well as applicability at room temperature. The drawback of this sensor is that it is restricted to detecting O_2 from a dry gas stream, as moisture can be absorbed by the supported $[C_2MIM][BF_4]$ membrane.

It was reported that, when ILs are used in gas sensors, the lower diffusion coefficients of the gaseous analyte in ILs lengthen the response time and limit the attainable steady-state currents (Buzzeo, Hardacre, & Compton, 2004). However, the negligible vapor pressure and robust thermal stability of ILs warrant IL-based gas sensors operating under extreme conditions, such as high temperature and high pressure. Oter, Ertekin, Topkaya & Alp (2006a, 2006b), reported two new and very

stable optical CO_2 sensor prepared by simple doping of water-miscible room temperature ionic liquids, 1-methyl-3-butylimidazolium tetrafluoroborate (RTIL-I) and 1-methyl-3-butylimidazolium bromide (RTIL-II) with pH indicator dyes of 1-hydroxypyrene-3,6,8-trisulfonic acid (HPTS) and bromothymol blue (BTB).

In recent works, ionic liquids intensively used as matrix materials or auxillary agents in polymer based matrices. They enhanced sensor performances and stability with different ways (Aydogdu et. al., 2011; Kacmaz et. al., 2011; Oter, Ertekin & Derinkuyu, 2008; Oter, Ertekin, Topkaya & Alp (2006a, 2006b)).

2.10 Immobilisation of Indicator Chemistry in Polymers

The indicator chemistry is well adapted to aqueous solutions. Most of the known indicator molecules are water-soluble and if dissolved in proper polymers, they can be subject of leaching. In order to make dyes, ionophores and ligands soluble in polymers and to avoid leaching of the components, they have to be made lipophilic with chemical modifications (Figure 2.18) (Mohr, 2002).
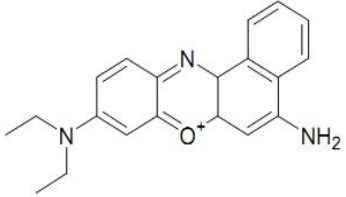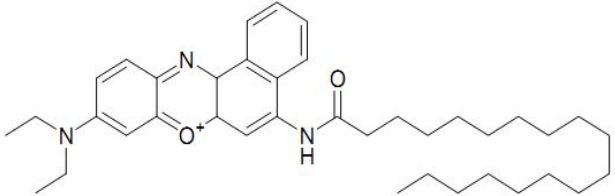

| | Nile Blue

pH indicator (red to blue upon protonation, pK ~11.6)

water-soluble |
| | Octadecyl Nile Blue

pH indicator

polymer/plasticizer-soluble |

Figure 2.18 Nile blue and its lipophilic ion pair form (taken from http://www2.uni-jena.de/~c1moge/Mohr/ASCOS2002.pdf).

Lipophilic molecules can be obtained by introduction of long alkyl chains (Figure 2.19). However, the chemical synthesis involved can be tedious. Therefore, another possibility is to obtain lipophilic compounds by ion-pairing. Ion pairs are mostly

obtained by dissolving both components (water-soluble ionic indicator and water-soluble ionic surfactant of opposite charge) separately in water, pouring both solutions together and filtrating the precipitated product (Mohr, 2002).
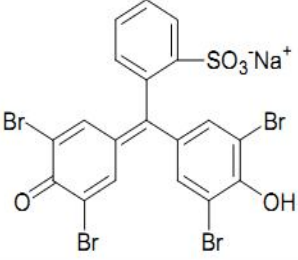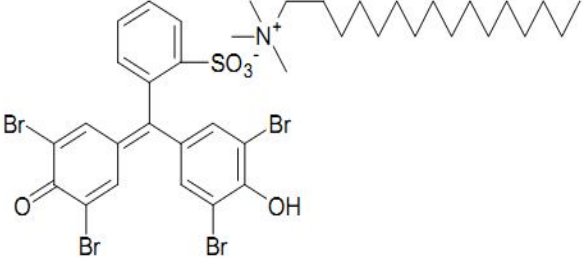
| | Bromophenol Blue

pH indicator (yellow to blue upon deprotonation, pK ~3.8)

water soluble |
| | Hexadecyltrimethylammonium Bromophenol Blue Ion Pair

pH indicator

lipophilic and polymer/plasticizer-soluble |

Figure 2.19 Bromophenol blue and its lipophilic ion pair form (taken from http://www2.uni-jena.de/~c1moge/Mohr/ASCOS2002.pdf).

Indicators can also be made lipophilic by ion-pairing with surfactants. They can be directly immobilised on the polymer by ion-pairing with cationic or anionic polymers (Figure 2.20). Solutions or suspensions of the polymers are usually prepared utilizing aqueous or alcoholic solutions of the dyes (Mohr, 2002).

Figure 2.20 Bromophenol blue immobilized on triethylammoniummethylcellulose and Nafion (taken from http://www2.uni-jena.de/~c1moge/Mohr/ASCOS2002.pdf).

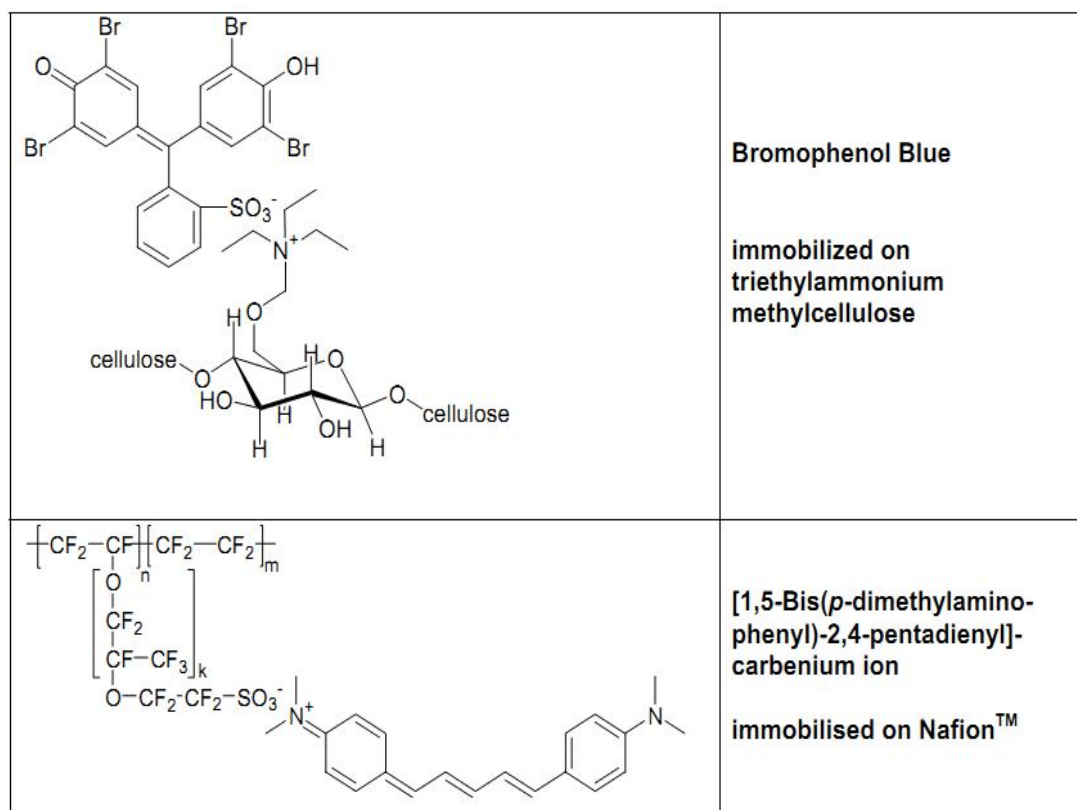Covalent immobilisation of the indicator chemistry to the polymer matrix is probably the most reliable choise among all immobilisation methods. The operational stability and shelf life is superior (no leaching, crystallisation, evaporation of components). However, to obtain indicator chemistry and polymers with functional groups is inevitably linked with significant synthetic effort. Very often, chemical modification of dyes negatively affects their selective and sensitive analyte recognition (Mohr, 2002).

In principal two different ways of immobilisation are possible, namely (a) to bind a reactive dye (e.g. fluorescein succinimidyl ester) to a reactive polymer matrix (e.g. aminocellulose), or (b) to polymerise a reactive dye (e.g. a dye with a methacrylate group) with common monomers (e.g. methyl methacrylate) to give a copolymer. Several indicators are available in a reactive form (primarily for labelling of peptides). These molecules with isothiocyanate groups, sulfonyl chloride groups, vinylsulfonyl groups, or succinimidyl groups (fluorescein isothiocyanate, dabcyl

succinimidyl ester, hydroxypyrene trisulfonyl chloride) can be covalently attached to aminoethylcellulose or amino-PVC. Indicator dyes with amino or hydrazino groups (aminofluorescein, Texas Red hydrazide) can be coupled to carboxy-PVC or carboxymethylcellulose (Figure 2.21) (Mohr, 2002).
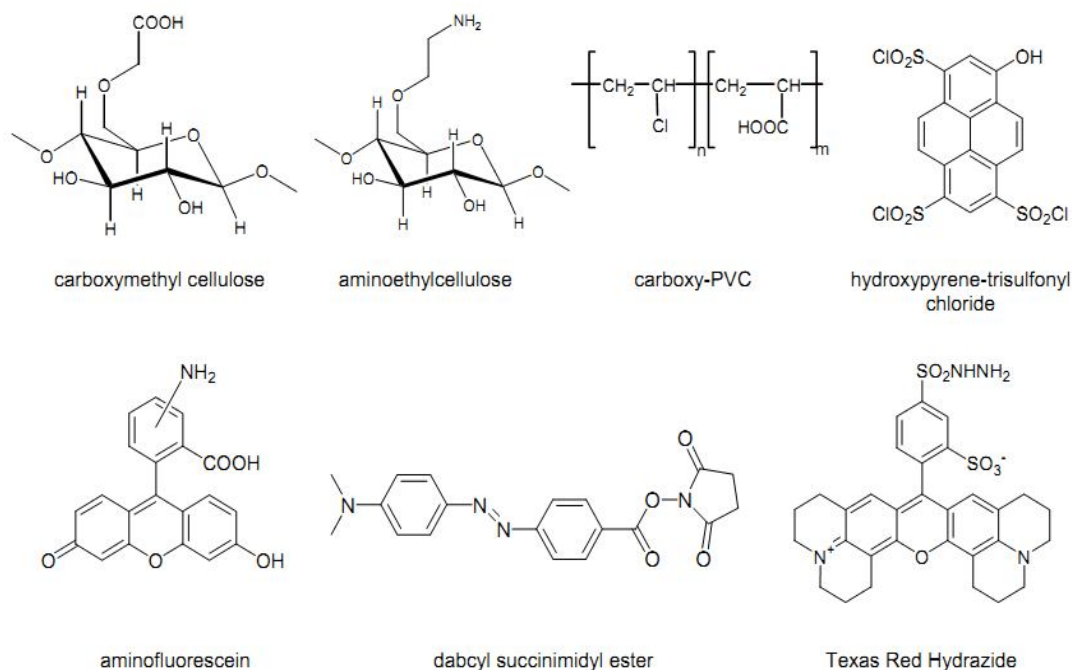

Figure 2.21 Indicators and polymers with functional groups (taken from http://www2.uni-jena.de/~c1moge/Mohr/ASCOS2002.pdf)

CHAPTER THREE
OPTICAL CHEMICAL SENSING OF CARBON DIOXIDE

3.1 Currently Available Optical Chemical Sensing Studies Regarding Carbon Dioxide

As mentioned earlier, the CO_2 molecule's asymmetric and polyatomic nature causes it to strongly absorb light in the infrared (IR) part of the spectrum. The concentration of CO_2 in a gas sample can therefore be measured by IR. However, this approach suffers from humidity. Optical chemical sensing approach has advantages over electrochemical and IR based sensing techniques. They offer several attractive features which include electrical isolation, reduced noise interference, ability of miniaturization and remote sensing. In this chapter studies regarding optical chemical sensing of gaseous and dCO_2 will be discussed.

The measurement of dissolved carbon dioxide (dCO_2) is of importance in many different areas, including in aquatic moieties, agriculture, water treatment and biotechnological studies. There are currently a number of dCO_2 sensors available on the market that employs electrochemical pH detection (Burke, Markey, Nooney, Byrne & McDonagh, 2006). However, such devices are expensive and, in the case of pH electrodes, are not particularly user-friendly, requiring regular renewal for efficient operation.

Optical sensors for dCO_2 facilitate the use of low-cost optoelectronic components (Burke, Markey, Nooney, Byrne & McDonagh, 2006). A variety of CO_2 optodes exploiting colorimetric detection techniques have been reported to date (Mills & Chang, 1994; Mills, Lepre & Wild, 1997, Weigl & Wolfbeis, 1995). In recent years however, the majority of work on optical CO_2 sensors has focused on the use of fluorescence detection techniques, employing the pH-sensitive fluorescent indicator, hydroxypyrenetrisulfonic acid (HPTS). Examples of such sensors include both optical fiber-based and planar devices, exploiting sensing

techniques such as the analysis of fluorescence intensity (Nivens, Schiza & Angel, 2002; Mills & Chang, 1993; Ge, Kostov & Rao, 2003; Muller & Hauser, 1996), fluorescence resonance energy transfer (Neurauter, Klimant & Wolfbeis, 1999; Bultzingslowen, McEvoy, McDonagh & MacCraith, 2003; Chang, Randers-Eichhorn, Lakowicz & Rao, 1998) and dual luminophore referencing (DLR) (Bultzingslowen and et.al, 2002). A number of these sensors have also been applied to the detection of dCO_2 (Nivens, Schiza & Angel, 2002; Muller & Hauser, 1996; Neurauter, Klimant & Wolfbeis, 1999) and, in principle, all of the before mentioned sensing techniques are suitable for this application, given a compatible host matrix. An alternative route for the detection of dCO_2 was also reported recently, namely that of direct spectroscopic measurement using a mid-infrared quantum cascade laser (Schaden, Haberkorn, Frank, Baena & Lendl, 2004). However, the cost and complexity of this device in its current form would appear to preclude its use outside a laboratory environment. With regard to the fluorescence-based dCO_2 optodes presented to date, they have served to demonstrate the high degree of sensitivity that is achievable by exploiting these techniques, yielding micromolar (Nivens, Schiza & Angel, 2002; Ge et. al., 2003; Muller & Hauser, 1996) and even sub-micromolar limits of detection (Neurauter, Klimant & Wolfbeis, 1999). However, the reported systems are not ideally suited to use outside a laboratory environment due to the incorporation of elements such as optical fibers and photomultiplier tubes (Muller & Hauser, 1996; Neurauter, Klimant & Wolfbeis, 1999) into the device, which, despite excellent performance characteristics, detract from the robustness and cost effectiveness of the system. Others rely on bench-top apparatus such as fluorimeters for sensor characterization (Nivens, Schiza & Angel, 2002; Mills & Chang, 1993; Ge et. al., 2003), systems that are obviously intended for use solely in a laboratory-based setting (Burke et. al., 2006).

Recently, the optical chemical CO_2 sensors based on the absorbance or fluorescence change of pH indicator have been developed. Müller & Hauser performed one of the important works on an optode for measurements of low concentrations of dissolved CO_2. The method of lipophilic extraction of ion pairs into

the membrane phase according to Weigl and Wolfbeis was applied to the fluorescent pH indicator hydroxypyrenetrisulfonic acid together with the quaternary ammonium base tetraoctylammonium hydroxide. The membrane solution was applied directly to an acrylic optical fibre of 1 mm diameter. Solutions of $NaHCO_3$ were used as standards and H_2CO_3 concentrations calculated. The dynamic range for the detection of H_2CO_3 was $4 \times 10^{-6} - 1 \times 10^{-2}$ mol l^{-1}. Response times depended on the concentration range and whether the concentration was increased or decreased: $\tau_{90\%}$ was <1 min for increasing H_2CO_3 concentrations in the range $10^{-4} - 10^{-2}$ mol l^{-1}. Recovery times for low concentrations, however, were $\tau_{90\%}$ >6 min. The sensor was found to show an increasing susceptibility to temperature at the low end of the calibration graph for H_2CO_3. The use of a low concentration of base in the membrane resulted in the desired detection limit, but also in a lifetime limited to 1 day. The usefull measuring range was found from 10^{-5} up to 10^{-3} M H_2CO_3 which corresponds to $10^{-3} - 10^{-1}$M $NaHCO_3$ concentration and the response and recovery times were found as 6 and 20 minutes respectively (Müller & Hauser 1996).

Later, Neurauter, Klimant & Wolfbeis (1999) measured dissolved and gaseous CO_2 with ethyl cellulose made sensor films and found the detectable CO_2 level between 0-30 hPa. The cross sensitivity to oxygen was the most crucial factor in this sensors performance. If stored in air and exposed to sunlight the sensors were destroyed within a few days.

Water-dissolved carbon dioxide was quantified with a reservoir type capillary microsensor (Ertekin, Klimant, Neurauter & Wolfbeis, 2003a). A pH indicator in the form of its ion pair with a quaternary ammonium base and a buffer in an ethyl cellulose matrix, all placed at the tip of an optical fiber, served as the sensing chemistry. The dynamic range was between 1 and 20 hPa pCO_2. The response time is 15 s, and the detection limit is 1 hPa pCO_2. The sensitivity of fiber-optic CO_2 sensors utilizing indicator dyes was studied once more. Gastric CO_2 can be monitored with optical fibers of similar design (Baldini et. al., 2003) and the results compare favorably with those obtained with a commercial (non-fiber-optic) instrument. A sol-gel-based optical carbon dioxide sensor that employs dual luminophore internal

referencing and is intended for application in food packaging technology was described (Bultzingslöwen et. al., 2002). A fluorescent pH indicator was immobilized in a hydrophobic organically modified silica matrix, along with cetyltrimethylammonium hydroxide as an internal buffer. Fluorescence is measured in the phase domain by means of the dual luminophore referencing scheme. The resolution is <1 % and the limit of detection is 0.08 % CO_2. Oxygen cross-sensitivity is minimized by immobilizing the reference luminophore in polymer nanobeads.

Amao & Nakamura (2004) designed an optical CO_2 sensor based on the overlay of the CO_2 induced absorbance change of pH indicator dye α-naphtolphtalein with the fluorescence of tetraphenylporphyrin using ethyl cellulose and polystyrene membrane and obtained 53.9 % signal change from 100 % N_2 to 100 % CO_2.

Ertekin & Alp (2006) were proposed emission based simple and fast method for the determination of gaseous and dissolved CO_2. A newly synthesized fluorophore, 4-[(p-N,N-dimethylamino)benzylidene]-2-phenyloxazole-5-one has been used for carbon dioxide sensing together with "carbon dioxide carrier" perfluorochemical (PFC) in ethyl cellulose matrix. The response of the sensor composition to gaseous and dissolved CO_2 has been evaluated in the absence and presence of the PFC. the solubility of CO_2 in fluorocarbons was about 10–20 times as that observed in the parent hydrocarbons or in water.

Lu et. al., (2008) were developed a sensor system suitable for monitoring changes in partial pressure of carbon dioxide (pCO_2) in surface seawater or in the atmosphere. Surface seawater samples are pumped into a PVC tube enclosing an inner Teflon AF tube, which served as a long pathlength gas-permeable liquid-core waveguide for spectrophotometry. The Teflon cell contains a pH-sensitive indicator-buffer solution consisting of bromothymol blue (BTB) and sodium carbonate.The sensor has a response time of 2 min at the 95 % equilibrium value and a measurement precision of 0.26–0.3 7 % in the range 200–800 μatm pCO_2.

Chu & Lo (2008) performed a high-performance fiber-optic carbon dioxide (CO_2) sensor based on hybrid xerogels composed of alkyl and perfluoroalkyl ORMOSILs (organically modified silicates) doped with pH-sensitive fluorescent dye. Sensor exhibited a linear response to CO_2 concentrations in the range 0–30 %. Its limit of detection (LOD) was 0.03 % CO_2; the response time of the sensor was 1.7 s.

Oter et. al., (2008) reported an emission-based ratiometric response of ion pair form of pH sensitive dye to gaseous CO_2 which has been evaluated in ionic liquid (IL) containing ethyl cellulose (EC) matrix. Employed the imidazolium based room temperature ionic liquid (RTIL) as task specific polymer additive in ethyl cellulose to enhance the solubility of CO_2 as well as the stability of the indicator. This sensor exhibited enhanced linear working range between 0 and 100 % pCO_2. The dynamic range was between 0 and 100 % pCO_2. The signal changes were fully reversible and the shelf life of the $EMIMBF_4$ -doped films was extended from 15 to 95 days.

Chu & Lo (2009) measured CO_2 with optical fiber carbon dioxide sensor based on sol–gel matrix doped with silica particles and pH-sensitive fluorescent dye (ion pair form of dye). The sensor has a sensitivity of approximately 26 and exhibits a uniquely linear response for CO_2 concentrations in the range of 0–100 %. The response time of the sensor is 9.8 s when switching from a pure N_2 atmosphere to a pure CO_2 atmosphere and 195.4 s when switching from CO_2 to N_2.

Vargas-Sansalvador et. al., (2009) were developed an optical sensor for gaseous CO_2 based on phosphorescence intensity measurement of the PtOEP complex trapped both in PVCD membranes and in PVCD microparticles due to the displacement of the α-naphtholphthalein acid–base equilibrium. The optical sensor for gaseous CO_2 was based on changes in the phosphorescence intensity of the platinum octaethylporphyrin (PtOEP) complex trapped both on oxygen-insensitive poly (vinylidene chloride-co-vinyl chloride) (PVCD) membranes and PVCD microparticles, due to the displacement of the α-naphtholphthalein acid–base equilibrium with CO_2 concentration. Its detection limit of 0.02 %, the response time (10–90 % maximum signal) is 9 s and the recovery time (90–10 %) is 115 s. The

lifetime of the membranes for CO_2 sensing preserved in a 94 % relative humidity atmosphere and dark conditions is longer than at least 4 months.

Zhang, Li & Li (2010) designed a miniaturized sensor based on infrared absorption for measuring carbon dioxide (CO_2) gas concentration. Sensor response time was 2.5 s and accuracy of the sensor is 0.026 % with a measurement range of 0–3 % for CO_2 gas concentration.

Ali et. al., (2010) designed a nanoparticle based optical sensor for carbon dioxide in concentrations between 0 and 3 %. The sensing scheme was based on the optical interrogation of a 12-µm polystyrene (PS) film containing upconverting nanoparticles (UCNPs; 40–100 nm in size) of the type $NaYF_4$:Yb,Er, and the longwave absorption pH probe bromothymol blue (BTB) in its anionic (blue) form. This was the first optical sensor for CO_2 that is based on the use of UCNPs. Its response time was ~10 s on switching from pure argon gas to 1% CO_2 in argon, the recovery time of the sensing film was ~180 s, and the detection limit was 0.11% of CO_2.

Wencel et. al., (2010) were developed and characterized a fluorescence-based ratiometric sol–gel derived dissolved carbon dioxide (dCO_2) sensor for use in environmental monitoring applications. The sensor developed for this work exploits a pH fluorescent dye ion-paired with cetyl-trimethylammonium bromide, which has been entrapped in a hybrid sol–gel-based matrix derived from n–propyl triethoxysilane along with the liphophilic organic base. Calculated limit of detection for the sensor was 35 ppb. Response time 7 min was measured.The sensor probe was used to monitor dCO_2 levels in a laboratory-based aquatic habitat, and the expected diurnal pattern was clearly visible.

Aydogdu et. al., (2011) were fabricated fluorescence quenching-based optical CO_2 sensors by electrospinning technique. Poly (methyl methacrylate) and ethyl cellulose were used as polymeric materials. A fiber-optic bundle was used for the gas detection. CO_2 sensor based on, the change in the fluorescence signal intensity of ion

pair form of HPTS. The sensor slides showed high sensitivities due to the high surface area-to-volume ratio of the nanofibrous membrane structures.

Table 3.1 gives a comparision of currently available CO_2 sensors in terms of indicator chemistry, matrix materials, response ranges, detection limits and other typical sensor charecteristics.

Table 3.1 Comparision of currently available CO_2 sensor.

Sensitive dye	Matrix material	Storage conditions and lifetime	Dynamic working range	Detection Limit	Ref.
HPTS(TOA)$_4$ ion Pair	Ethyl cellulose and Teflon AF	In refrigerator- Several days	0.05–7 hPa pCO_2	Not mentioned	Neurauter 2000
HPTS ion pair + Ru(dpp)$_3$TMS$_2$)	Ethyl cellulose and black silicone rubber	In the dark, under a CO_2 atmosphere, free of other acidic gases-Not mentioned	0–10 hPa CO_2	Not mentioned	Schröder 2005
BTB$^-$/TOA$^+$) ion pair	1-methyl-3-butylimidazolium tetrafluoroborate (RTIL-I) and 1-methyl-3-butylimidazolium bromide (RTIL-II).	Not mentioned-212 days	1×10^{-6} to 2×10^{-2} mol L−1 [HCO$_3^-$] (in RTIL-I) 0 –80 % CO_2 (in RTIL-I) 0–100 % CO_2 (in RTIL-II)	10^{-6} M [HCO$_3^-$] for dissolved CO_2 1.4 % for gaseous CO_2	Oter 2006a
Thymol blue ion pair + (Ru(dph-bpy)$_3^-$(TMS)$_2$)	Ethyl cellulose	In air and exposed to sunlight-a few days / In sealed bags containing sodium carbonate- 2 months	0–30 hPa pCO_2	0.5 mM (22 ppb) CO_2	Neurauter 1999

Table 3.1 Comparision of currently available CO_2 sensor (continued).

Sensitive dye	Matrix material	Storage conditions and lifetime	Dynamic working range	Detection Limit	Ref.
HPTS(TOA)$_4$ ion pair	Ethyl cellulose	In a desiccator containing sodium carbonate and silica gel-5 days	1–20 hPa pCO_2	1 hPa pCO_2	Ertekin 2003a
HPTS (CTA)$_3$ ion pair	Ethyl cellulose Ethyl cellulose with additive	In a drying chamber at90 $^{\circ}$C- About 6 h In water or in humid air- Over 5 months	1–50 % CO_2 2–100 % CO_2	Not mentioned	Wolfbeis 1998
4-[(p-N,N-dimethylamino) benzylidene]-2-phenyloxazole-5-one	Ethyl cellulose	Not mentioned	3.96×10^{-6}—2.0×10^{-2} mol L−1 [HCO_3^-] 0–80 % CO_2	Not mentioned	Ertekin 2006
α –naphtholphthalein	Poly (trimethylsiliypropyne) - polystyrene	Not mentioned	0–100 % CO_2	Not mentioned	Amao 2005

Table 3.1 Comparision of currently available CO_2 sensor (continued).

Sensitive dye	Matrix material	Storage conditions and lifetime	Dynamic working range	Detection Limit	Ref.
HPTS ion pair + $Ru(dpp)_3^{2+}$	Poly(dimethylsiloxane) (PDMS)	Not mentioned - 4 weeks	Not mentioned	7 µM dissolved CO2	Burke 2006
HPTS ion pair	Polydimethylsiloxane, vinyldimethyl terminated (PS443) and (30/35 %) methyl-hydro- (65 /70 %) dimethylsiloxane	in water and in air - several months	Not mentioned	0.03 % CO_2	Ge 2003
Sudan III	Ormosil/Ethyl cellulose	Not mentioned	0–100 % CO_2	0.06 % CO_2	Bültzingslöwen 2003
Cresol red	Ethyl cellulose	Not mentioned	0–150 h Pa	Not mentioned	Baldini 2003
bromothymol blue (BTB)	Teflon AF 2400	Not mentioned	Not mentioned	200–800 µatm pCO_2	Lu 2008
HPTS(TOA)$_4$ ion Pair	Ethyl cellulose and Poly(methyl methacrylate)	Ambient laboratory conditions - 7 months	0–100 % CO_2	Not mentioned	Aydogdu 2011

CHAPTER FOUR
EXPERIMENTAL STUDIES AND INSTRUMENTATION

All solvents used in this study were of analytical grade and purchased from Merck, Johnson and Mathey, Acros, Fluka and Riedel. Solvents for the spectroscopic studies were used without further purification.

The pH and CO_2 sensitive fluorescent dye, 8-Hydroxypyrene–1,3,6-trisulfonic acid trisodium salt (HPTS) was 98 % purity and from Fluka. Tetrabutylammonium hydroxide for titration (in nonaqueous medium) was standard 0.1 M solution in isopropanol/methanol (0.1 N) from Fluka. The ionic liquid, 1-ethyl-3-methylimidazolium tetrafluoroborate (RTIL) was obtained from Fluka. The plasticizer, dioctylphtalate (DOP) was 99 % from Aldrich. The additive potassium tetrakis (4-chlorophenyl) borate was selectophore, 98 % from Fluka. The sodium bicarbonate in powder form was obtained from Riedel (99-100 %).

The bicarbonate sensitive dyes *N*'-[(*E*)-(2-hydroxyphenyl)methylidene]pyridine-4-carbohydrazide (MY2), *N*'-[(*E*)-(3-hydroxyphenyl)methylidene]pyridine-4-carbohydrazide (MY4), *N*'-[(*E*)-(4-nitrophenyl)methylidene]pyridine-4-carbohydrazide (MY5), *N*'-[(*E*)-(9-methyl-9*H*-carbazol-3-yl)methylidene]pyridine-4-carbohydrazide (MY9) and *N*'-{(1*E*,2*E*)-3-[4-(dimethylamino)phenyl]prop-2-en-1-ylidene}pyridine-4-carbohydrazide (MY10) were supplied from Professor M. Yavuz Ergün and were synthesized in our laboratories.

Diluted solutions of certified reference anion standard solution of Dionex (Fluoride 20 mg/L, Chloride 30mg/L, Nitrite 100mg/L, Bromide 100 mg/L, Nitrate 100mg/L, Phosphate 150 mg/L, Sulfate 150mg/L) and were used for interference tests of anions.

Diluted solutions of certified reference cations standard (CRS) solution of Dionex (Lithium 49.9 mg/L, Sodium 203 mg/L, Potassium 506 mg/L, Magnesium 252 mg/L and Calcium 509 mg/L) were used for interference tests of cations.

The polymer ethyl cellulose was from Organics with an ethoxy content of 48%. Polymethylmethacrylate (PMMA, Mw 120,000) ($-CH_2C-$ (CH_3)) CO_2CH_3)$-$) from Aldrich is used to prepare the solutions that are used as working fluid. Teflon AF (type 1600) was purchased from Du Pont polymers (Switzerland).

The standard metal solutions were prepared from their 0.1 M stock solutions by using the metal salts of $AgNO_3$, $Al(NO_3)_3.9H_2O$, $BaCl_2.2H_2O$, $Co(NO_3)_2.6H_2O$, $Cr(NO_3).9H_2O$, $Cu(NO_3)_2.3H_2O$, $Fe(SO_4).7H_2O$, $Fe(NO_3)_3.9H_2O$, $Hg_2(NO3)_2.2H_2O$, $MnCl_2.4H_2O$, $NaHCO_3$, $NiCl_2.6H_2O$, $Pb(NO_3)_2$, $SnCl_2$, $Zn(NO_3)_2.6H_2O$.

Absorption spectra were recorded using a Shimadzu 1801 UV-Visible spectrophotometer. Steady state fluorescence emission and excitation spectra were measured using Varian Cary Elipse Spectrofluorometer with a Xenon flash lamp as the light source. For fiber optic measurements commecially available fiber optic components and its related software of Varian Cary Elipse Spectrofluorometer were used.

The emission spectra were corrected using a piece of silica ground on both faces held in a triangular cuvette configuration called the diffuser. The pH and CO_2 analysis studies were executed by fiber optical and flow system. The home made flow cell is made up of polytetrafluoroethylene (PTFE).

pH measurements were recorded with an Orion pH meter. All of the experiments were carried out at room temperature; $25\pm1^{o}C$. 8-hydroxypyrene-1,3,6-trisulfonic acid (HPTS) and Quinine sulphate were used as reference standards for fluorescence quantum yield calculations.

In all of the studies ultra pure water of Millipore was used. Cylinders of carbon dioxide, oxygen and nitrogen gases of 99.99 % purity were obtained from Gunes or Karbogaz, Izmir, Turkey. The gas mixtures were prepared with a Sonimix 7000 Gas Diluter instrument.

Electrospinning studies were performed at Dokuz Eylul University department of metallurgical and materials engineering. Top Syringe Pump Top-5300 instrument was used in electrospinning studies. The surface morphology of the fabricated nanofibers was studied using the scanning electron microscope (SEM) instrument (6060-JEOL JSM).

4.1 Construction of Fiber Optic Measurement System

The fiber optical sensor was constructed with the commercial accessories of Varian Cary Eclipse Spectrofluoremeter (Figure 4.1). Eclipse Fiber optic coupler, fluorescence remote read probe (2 meters), Probe tip for solid measurements and Probe tips for liquid measurements (10 mm and 20 mm length tips). This method also allows the remote sensing of the samples. The installation steps are:

• The fiber optic coupler is an accessory that enables the use of a fiber optic probe with Carry Eclipse spectrofluoremeter. After the removal of the sample compartment of the Carry Eclipse, the fiber optic coupler was stabilized to the same position by the help of the screws.

• The fiber optic probe was connected to the coupler accessory by inserting the two connector ends into the two key holds.

• The probe tips were screwed onto the end of the probe. Based on the phase of the sample (solid or liquid), either a solid sample probe tip or a liquid sample probe tip was used.

• To ensure that the fiber optic system will operate at maximum performance, it is necessary to optimize the efficiency with which light passes through the coupling device before the sample measurement. The alignment was done by using the software of the instrument (Derinkuyu, 2010).

Figure 4.1 Varian Cary Eclipse Spectrofluoremeter, fiber optic probe and fiber optical system accessories.

4.2 Combination of the Flow System with Fiber Optics

pH, dissolved or gaseous CO_2 response measurements were carried out with fiber optic probe (2m long) and solid sample tip accessories constructed on the spectrofluorometer. For instrumental control, data acquisition and processing the software package of the spectrofluorometer was used. The tip of the bifurcated fiber optic probe was interfaced with a sensing film in a buffer containing 300 μL flow cell (Figure 4.3). The flow cell was equipped with a four channel Ismatec Reglo Analog peristaltic pump. Analyte solutions or buffers were transported by the peristaltic pump via tygon tubing of 2.06 mm i.d. (Figure 4.2)

Figure 4.2 Ismatec Reglo Analog peristaltic pump.
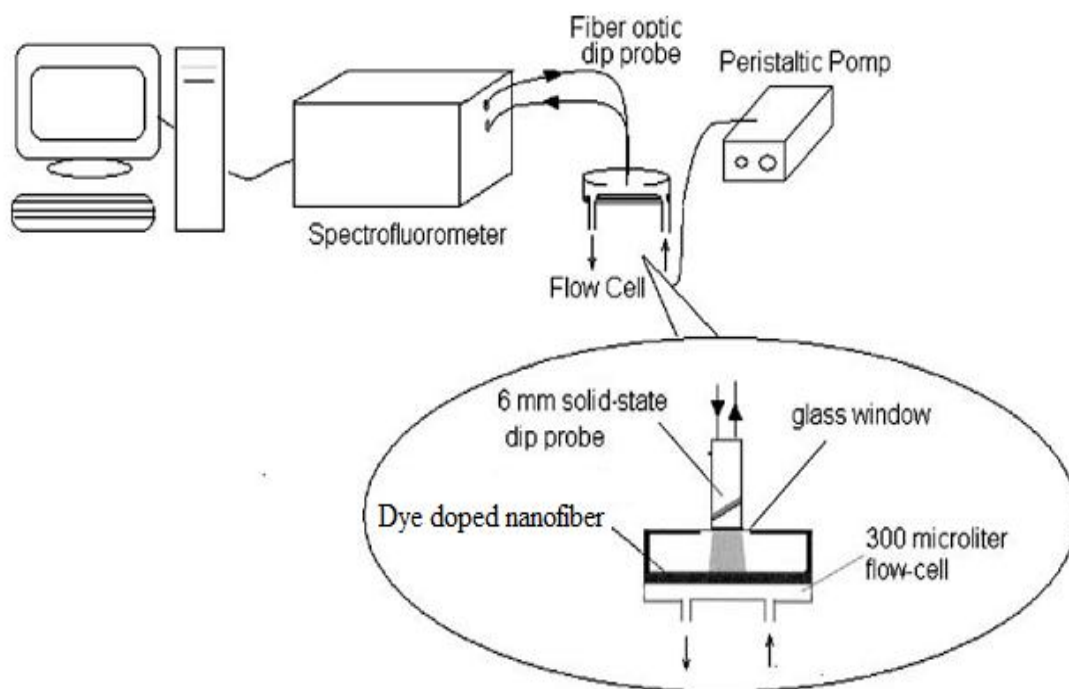
Figure 4.3 Instrumental set-up used for dye-doped thin film and nanofiber evaluation.

4.3 Gas Blender and CO_2 Solutions

Gaseous CO_2 and N_2 were mixed in the concentration range of 0–100 % either in a gas diluter; Sonimix 7000A gas blending system or in a home made gas mixing chamber by controlling the gas flow rates with sensitive flow-meters (Figure 4.4). Gas mixtures were introduced into the sensor agent containing cuvette via a diffuser needle under ambient conditions either directly or after humidification of the gas by bubbling through water at 25° C.

Dissolved CO_2 sloutions were introduced into the flow cell via tubings of the peristaltic pump at a certain flow rate (2 mL/min.).

Figure 4.4 Sonimix 7000 Gases Diluter.

4.4 Synthesis of Ion Pairs

In order to convert the water soluble dye into polymer soluble form, ion pair form of the dye must be synthesized. This method provides the immobilization of the dye into the polymer matrix and prevents the leaching of the dye.

The ion pair between the water soluble dye and the tetraoctylammonium counterion (TOA) was prepared by the following method: The appropriate amounts of the dye and the tetraoctylammonium bromide (TOABr) (834 mg) were dissolved in 30 ml of water containing 1 % sodium carbonate and 30 ml of CH_2Cl_2 respectively, and mixed in a separatory funnel. The ion pair was completely extracted from the aqueous phase into the organic phase. The organic phase was

washed three times with 0.05 M NaOH and separated. After the evaporation of organic solvent under vacuum, the crystalline ion pair was obtained.

4.5 Preparation for Thin Film and Nanofiber

The thin films were prepared by mixing of 240 mg of polymer (PMMA or EC), 192 mg of plasticizer (DOP), 48 mg of IL, 6 mg of dye and in Toluene: DMF (80:20) or DCM: EtOH (25:75) solvent systems. The chemical structures of EC, DOP and PTCPB were shown in Figure 4.6. The resulting mixtures were spread onto a 125 μm polyester support (Mylar TM type) with a spreading device. Thickness of the films was measured using Tencor Alpha Step 500 Prophylometer and found to be 5.11 μm. This result was an average of eight measurements and exhibited a Standard deviation of ±0.081. The films were kept in a desicator in the dark. This way, the photostability of the membrane was ensured and the damage from the ambient air of the laboratory was avoided. For absorbance and steady state fluorescence measurements each sensing film was cut to 1.2 cm width and 2.5 cm length and fixed diagonally into the sample cuvette (Figure 4.5) and the absorption or emission spectra were recorded. For fiber optical and flow system measurements, each sensing film was cut to 1 cm width and 1 cm length and fixed into the flow cell shown in Figure 4.3.
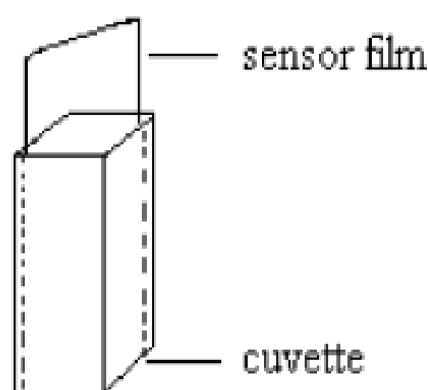
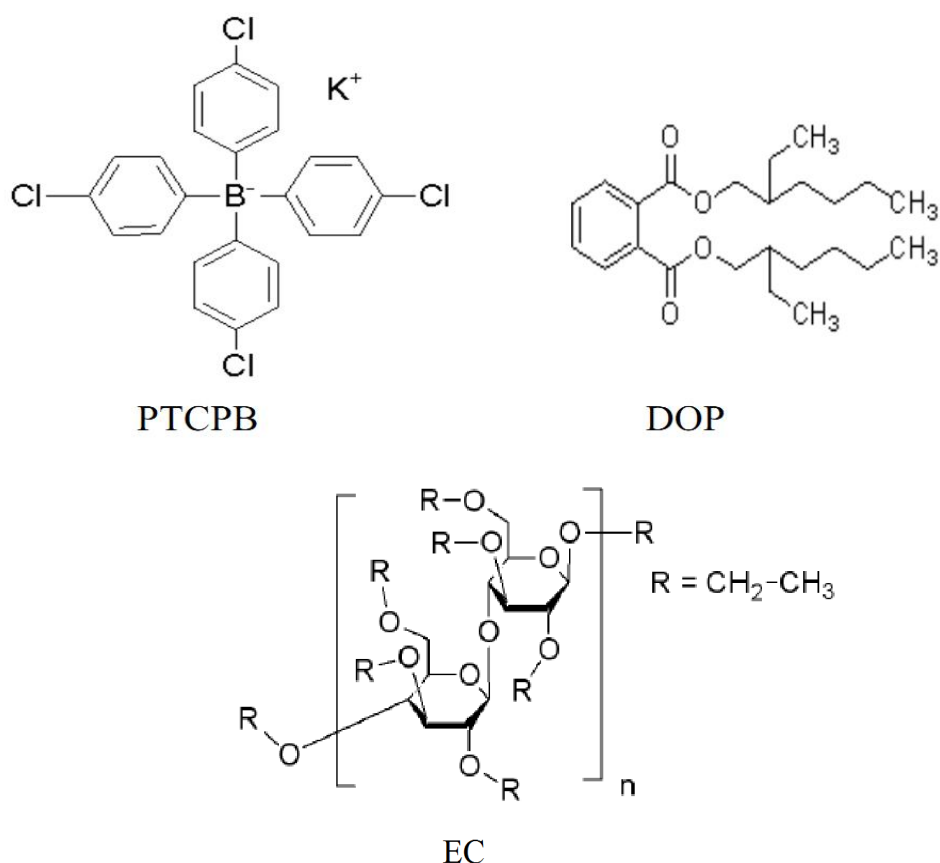Figure 4.5 The placement of the sensor
film in the sample cuvette.

Figure 4.6 Structures of PVC, PTCPB and DOP.

The electrospun nanofibers were prepared employing the same composition for thin films. The homogeneous PMMA or EC solutions were placed in a 1 ml plastic syringe fitted with a metallic needle of 0.4 mm of inner diameter. Electric potential of 20 kV was applied between the needle of the syringe and a substrate in the form of an aluminum foil. The distance between the needle and the electrode was 10 cm. The solution flow rate was maintained at 0.5 mL/h using a syringe pump. The charged polymer solution overcame the surface tension of the liquid and a stream of polymer jet was produced. The solvent evaporated and very fine fibers were completely coated on the clean aluminum foil. The surface morphology of the nano-fibers was studied using SEM instrument. The nano-fibers on aluminum substrate were cut into proper size, fixed in the flow cell and the excitation or emission spectra were recorded.

4.6 Electrospinning Apparatus

Electrospinning apparatus consists of a syringe pump, a high voltage power supply and a collector (See Fig. 4.7). This nonmechanical, electrostatic technique involves the use of a high voltage electrostatic field to charge the surface of a polymer solution droplet, thereby inducing the ejection of a liquid jet through a spinneret.

A typical electrospinning process uses a high voltage source to inject the charge of a certain polarity into a polymer solution, which is then accelerated toward a substrate of opposite polarity. As the electrostatic attraction between the oppositely charged liquid and collector and the electrostatic repulsions between similar charges in the liquid become stronger the leading edge of the solution changes from a rounded meniscus to a cone (Taylor cone). A polymer jet is eventually ejected from the Taylor cone as the electric field strength exceeds the surface tension of the liquid. The polymer jet travels through the atmosphere allowing the solvent to evaporate, thus leading to the deposition of solid polymer fibers on the collector (Sill & Von Recum, 2008; Maleki, 2010).
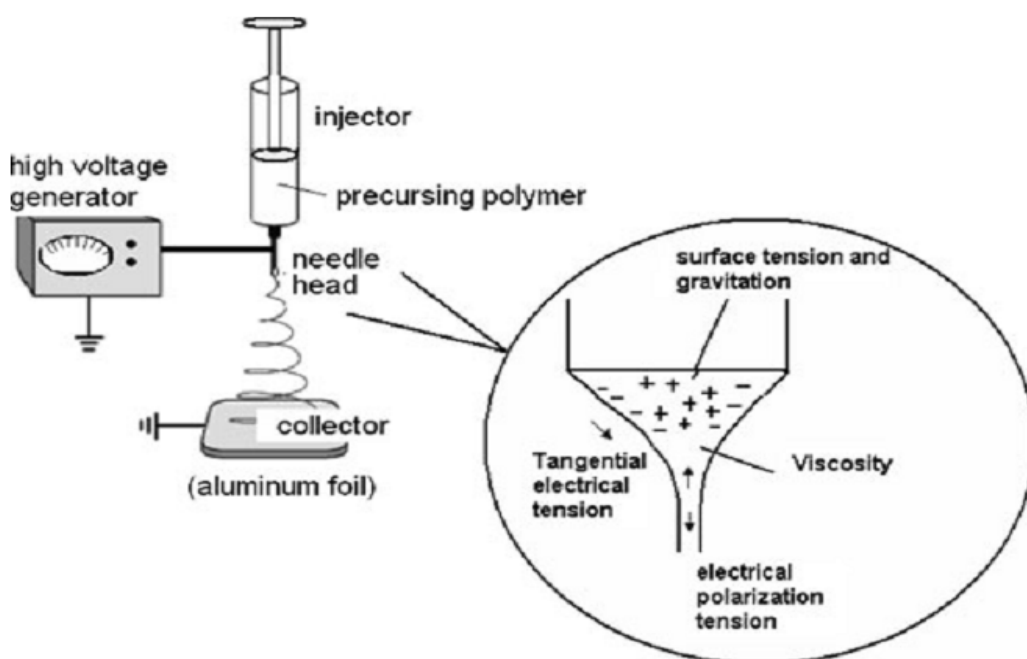
Figure 4.7 Schematic structure of the electrospinning apparatus (was taken from Aydogdu et al, 2011).

4.7 Quantum Yield Calculations

Fluorescence quantum yield values (Φ_F) of the employed dyes were calculated by using the comparative William's method (Williams, Winfield & Miller, 1983). This is a reliable method for recording Φ_F and involves the use of well characterized standard samples with known Φ_F values. Essentially, solutions of the standard and test samples with identical absorbance at the same excitation wavelength can be assumed to be absorbing the same number of photons. Hence, a simple ratio of the integrated fluorescence intensities of the two solutions (recorded under identical conditions) will yield the ratio of the quantum yield values. Since Φ_F for the standard sample is known, it is trivial to calculate the Φ_F for the test sample.

According to this method, the standard samples should be chosen to ensure they absorb at the excitation wavelength of choice for the test sample, and, if possible, emit in a similar region to the test sample. In order to minimise re-absorption effects (Dhami and et al., 1995) absorbances in the 10 mm fluorescence cuvette should never exceed 0.1 at and above the excitation wavelength. Above this level, non-linear effects may be observed due to inner filter effects, and the resulting quantum yield values may be perturbed. This maximum allowable value of the recorded absorbance must be adjusted depending upon the path length of the absorption cuvette being used (for example, 10 mm = 0.1 maximum, 20 mm = 0.2 maximum etc).

In this study, standard 10 mm path length fluorescence and absorption cuvettes were used for running the fluorescence and absorbance measurements. The UV-VIS absorption (absorbance≤0.10 at the excitation wavelength) and corrected fluorescence emission spectra were recorded for three or more solutions with increasing concentrations of the sample and the standard. The integrated fluorescence intensities (that is, the area of the fluorescence spectrum) were calculated from the fully corrected fluorescence spectrum. Graphs of integrated

fluorescence intensity vs absorbance were plotted. The gradient of the plots were later used in the quantum yield calculations according to the following equation.

$$\theta_x = \theta_{st} \left(\frac{Grad_X}{Grad_{ST}} \right) \left(\frac{n_x^2}{n_{ST}^2} \right) \qquad \text{(Eq. 4.1)}$$

Where the subscripts ST and X denote standard and test respectively, Φ is the fluorescence quantum yield, Grad the gradient from the plot of integrated fluorescence intensity vs absorbance and n is the refractive index of the solvent.

4.8 Preparation of the Employed Buffer Solutions

4.8.1 Preparation of 0.005 M Acetic Acid/Acetate Buffer

0.143 mL of acetic acid was dissolved in 950 mL ultra pure water. The solution was titrated to pH 5.0 at the lab temperature of 20° C either with 0.1 M HNO_3 or 0.1 M NaOH as needed. The resulting solution was made up to 1000 mL with ultra pure water in a volumetric flask. The buffer solutions in the range of pH 3.0-7.0 were prepared by the same way by adjusting to the desired pH.

4.8.2 Preparation of 0.005 M $NaH_2PO_4.2H_2O$ and 0.005 M $Na_2HPO_4.12H_2O$ Buffer

0.39 g of $NaH_2PO_4.2H_2O$ was dissolved in 950 mL ultra pure water. The solution was titrated to pH 7.0 at the lab temperature of 20^oC either with 0.1 M HNO_3 or 0.1 M NaOH as needed. The resulting solution was made up to 1000 mL with ultra pure water in a volumetric flask. The buffer solutions in the range of pH 7.0-9.0 were prepared by the same way by adjusting to the desired pH.

0.895 g of $Na_2HPO_4.12H_2O$ was dissolved in 950 mL ultra pure water. The solution was titrated to pH 7.0 at the lab temperature of 20^oC either with 0.1 M HNO_3 or 0.1 M NaOH as needed. The resulting solution was made up to 1000 mL with ultra pure water in a volumetric flask. The buffer solutions in the range of pH 10.0-12.0 were prepared by the same way by adjusting to the desired pH

CHAPTER FIVE

HPTS BASED OPTICAL CO_2 SENSING WITH IONIC LIQUID DOPED ELECTROSPUN NANOFIBERS

5.1 Introduction

In this chapter, utilization of electrospun nanofibrous materials as highly responsive fluorescence quenching-based optical CO_2 sensors has been investigated. Poly (methylmethacrylate) and ethyl cellulose were used as polymeric support materials. Sensing slides were fabricated by electrospinning technique. A fiber-optic bundle was used for the gas detection. CO_2 sensors based on the change in the fluorescence signal intensity of ion pair form of 8-hydroxypyrene-1,3,6-trisulfonic acid (HPTS).

In optical chemical sensors, the sensitivity scales inversely with dimensions. Miniaturization attempts and nanotechnology applications allowed improvements in functionality sensitivity, and response time of the sensors. Consequently, nano-scale structures should be combined with optical chemical sensing approaches.

Here we have successfully combined nano-scale electrospun fiber materials with optical sensing technology for CO_2 detection. Electrospinning, the most convenient way to make a nano-scale continuous polymer, uses a high static voltage to draw the fiber from a liquid polymer. As a jet of charged fluid polymer sprays out the bottom of a needle, an electric field forces the stream to spin, stretching the fiber length wise so its diameter becomes as little as 10 nano-meters. The fiber forms a thin membrane as it hits the electrically conductive substrate below the needle. These electrospun membranes have a unique combination of stretchiness and strength, and are easy to handle, making them suitable for a wide variety of applications. Electrospun nanofibrous membranes can have approximately 1–2 orders of magnitude more surface area than that found in continuous thin films (Reneker & Chun, 1996; Gibson, Schreuder-Gibson & Rivin, 2001). It is expected that this large amount of

functional surface area has the potential to provide unusually high sensitivity and fast response time in sensing applications.

In this study matrix materials of poly (methyl methacrylate) and ethyl cellulose were used together with ionic liquids. Optical nanofibrous membrane chemical sensors were fabricated by electrospinning technique. The ion pair form of HPTS was chosen as the fluorescent indicator because it has large Stokes shift, high quantum yield, strong absorbance, excellent photostability and lifetime. Additionally, similar fluorescence sensing investigation of this material was previously carried out on thin films (Ertekin & Alp, 2006; Oter, Ertekin & Derinkuyu, 2008; Borisov, Ch, Klimant & Wolfbeis, 2007). The electrospun nanofibers were characterized using scanning electron microscopy (SEM) and their average diameter was evaluated.

5.2 Synthesis of Ion Pair

The ion pair between anionic form of the HPTS and the tetraoctylammonium counterion (TOA^+) has the composition (HPTS)/ $(TOA)_3$ and was prepared according to the following literature method (Weigl & Wolfbeis, 1995): 200 mg of the trisodium salt of HPTS and the equivalent amount of TOABr (628 mg) were dissolved in 30 mL of water containing 1% sodium carbonate and 30 mL of CH_2Cl_2, respectively, and were mixed in a separatory funnel. After a few minutes the ion pair was completely extracted from the aqueous phase into the organic phase. The organic phase was washed three times with 0.05 M NaOH and separated. After the evaporation of organic solvent under vacuum, the ion pair was obtained. The ion pair is less subject to leaching from the polymer matrix than the HPTS sodium salt owing to its greater affinity to the EC or PMMA matrices.The schematic structures of the employed ion pair and the ionic liquid were shown in Fig. 5.1.
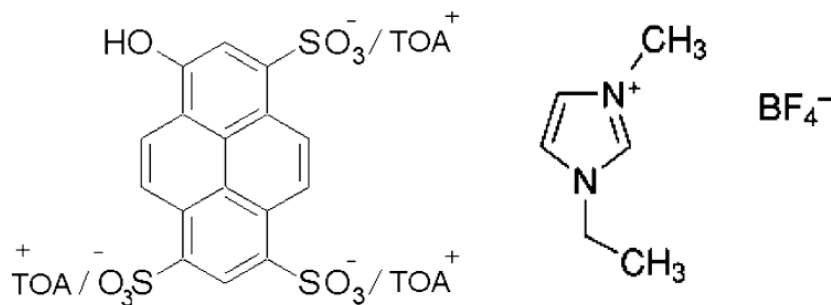
Figure 5.1 The schematic structures of the employed ion pair and the ionic liquid.

5.3 Preparation of Electrospun Nanofibers

Electrospinning was used as a novel fast and simple method to fabricate optical chemical sensing agents. The electrospinning conditions were optimized in order to form nodal-free PMMA or EC based continuous nanofibers by varying the concentrations of, plasticizer, PMMA or EC and RTILs in the solutions. The concentration of RTIL was varied from 5 % up to 50 % w/w, with respect to the PMMA or EC matrices. We find that the presence of the RTILs in the PMMA solutions facilitates the electrospinning of nodal-free nanofibers from the lower polymer concentrations and this behavior is attributed to the high conductivity and proper viscosity of the RTIL doped precursor polymer solutions. The resulting composites were prepared by mixing 240 mg of polymer (PMMA or EC), 192 mg of plasticizer (DOP), 48 mg of RTIL, 6 mg of dye and 200 μl of TOAOH in Toluene:DMF (80:20) or DCM: EtOH (25:75) solvent systems.

The polymer solution was taken in a hypodermic syringe and an electric potential of 20 kV was applied between the needle of the syringe and a substrate in the form of an aluminum foil. The distance between the needle and the electrode was 10 cm while the diameter of the needle was 0.40 mm. The solution flow rate was maintained at 0.5 mL/h using a syringe pump. The charged polymer solution overcame the surface tension of the liquid and a stream of polymer jet was produced. The solvent evaporated and very fine fibers were completely coated on the clean aluminum foil. The surface morphology of the nanofibers was studied using SEM

instrument. The nanofibers on aluminum substrate were cut into proper size, fixed in the flow cell and the excitation or emission spectra were recorded.

5.4 Thin Film Preparation Procedures

The thin films were prepared employing the same composition of nanofibers. The resulting mixtures were spread onto a 125 μm polyester support (Mylar TM type) with a spreading device. Each sensing film was cut to 1.2 cm diameter, fixed in the flow cell, and the excitation or emission spectra were recorded.

5.5 Carbon Dioxide Sensing Studies

Gaseous CO_2 and N_2 were mixed in the concentration range $0 - 100$ % in a gas diluter (Sonimix 7000A gas blending system). The output flow rate of the gas mixture was maintained at 250 mL min−1. Gas mixtures were introduced into the sensor agent-containing flow cell via a diffuser needle under ambient conditions either directly or after humidification of the gas. The humidification of the gaseous was accomplished by bubbling the gas stream through thermostated wash bottles filled with water at 25° C at constant relative humidity level of 100 %.

5.6 RTILs as Polymer Electrolytes

In the electrospinning process, the polymer solution is hanged by its surface tension at the end of the needle. When a sufficiently large electric voltage is applied, the solution at the tip of the needle becomes stretched to form a cone because of coupled effects of the electrostatic repulsion within the charged droplet and attraction to a grounded electrode of opposite polarity. As the strength of the electric field is increased, the charge overcomes the surface tension and at a critical point, fine jet is ejected from the apex of the cone. In order to perform this process, the polymer solution should have a certain electrical conductivity. On the other hand, to achieve true electrical conductivity in polymers one must add compatible electrically conductive additives into the polymer. In this chapter, we have demonstrated that it is

possible to electrospin the EC and PMMA composite fibers in presence of non-volatile room temperature ionic liquid; $EMIMBF_4$. The employed RTIL was chosen as polymer electrolyte due to its high ionic conductivity, high thermal and chemical stability, non-volatile, non-flammable and low toxicity characteristics (Galinski, Lewandowski & Stepniak, 2006).

Apart from ionic conductivity, the IL also enhances photostability of the HPTS in the polymer matrix acting as a sink for acidogenic species from the ambient air of the laboratory (Oter, Ertekin & Alp, 2006b; Oter, Ertekin & Derinkuyu, 2008; Bültzingslöwen et. al., 2002).

The electrospun membranes exhibited good adhesion to the aluminum substrate. The scanning electron microscope (SEM) images of electrospun membranes of the EC and PMMA at various magnifications are shown in Fig. 5.2 and Fig. 5.3. It is observed that the membrane has a 3-D structure with a random fiber orientation that is evenly distributed on the substrate. The diameters of the fibers were between 370 to 527 nm. In addition to these, it can be seen the same figures that the diameters of some nanofibers were smaller than these values. For instance, some nanofibers possess approximately 400 nm.

This type of nano-structure of the electrospun membrane provides higher surface area-to-volume ratio than that known for continuous thin films. Further increase of the surface area-to-volume ratio may be achieved by changing the conditions of the electrospinning process such as solvent composition, viscosity, concentration, temperature, humidity and working distance, which results in either smaller diameter fibers or increased porosity at the fiber surface (Deitzel, Kleinmeyer & Tan, 2001).
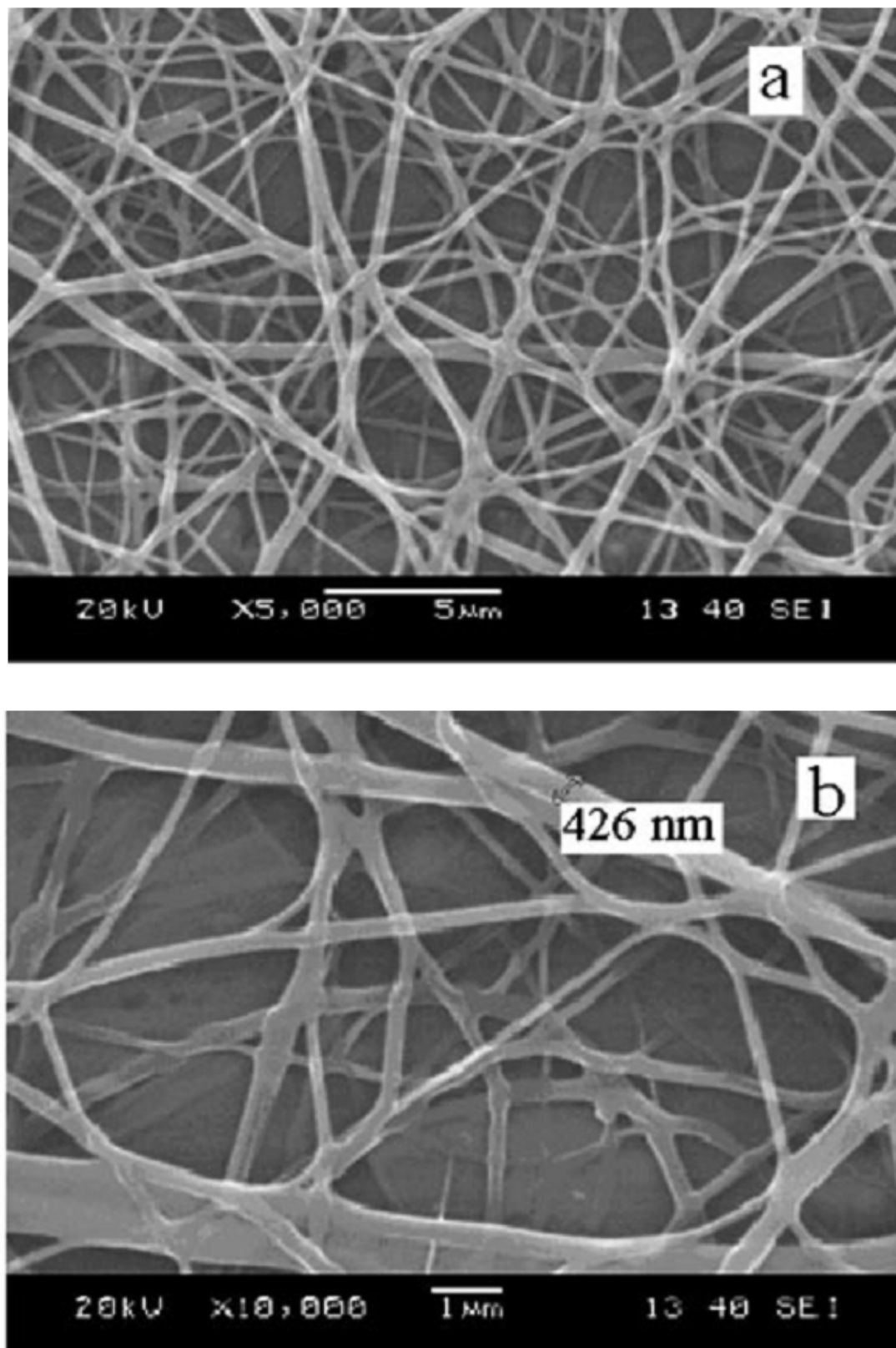
Figure 5.2 SEM images of electrospun membranes a and b; PMMA based nanofibers (×5000 and ×10000).
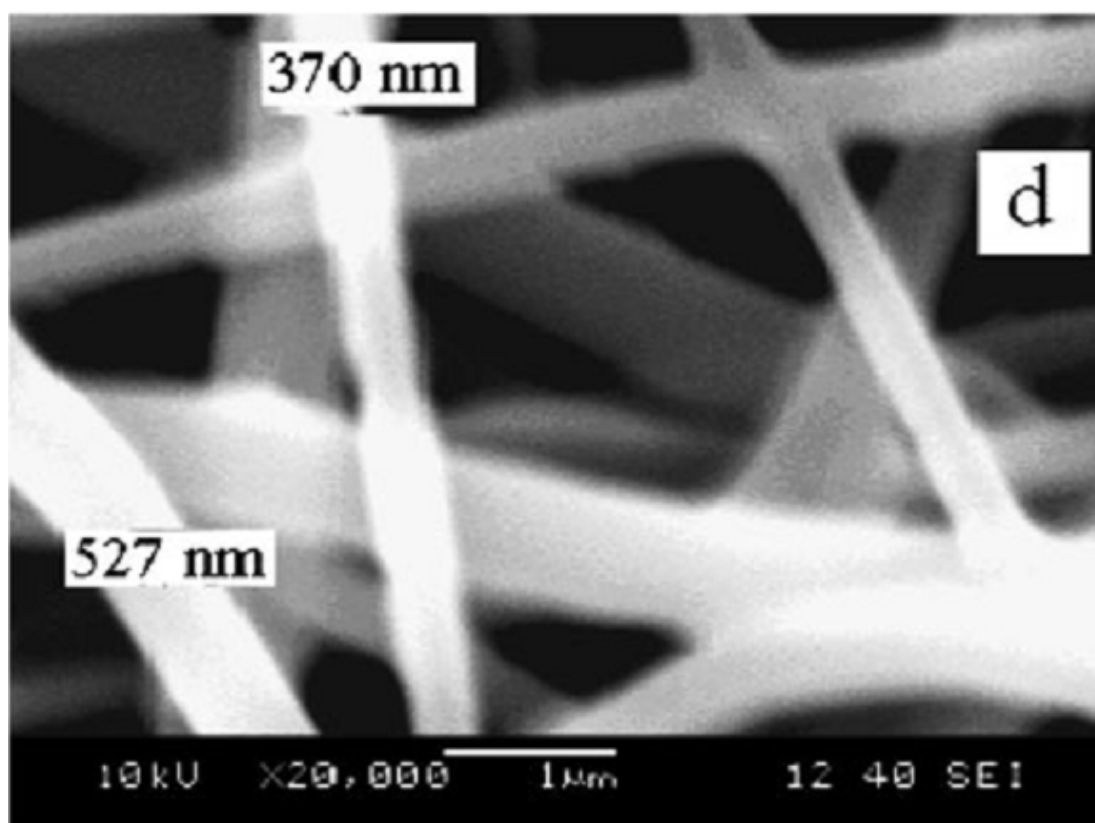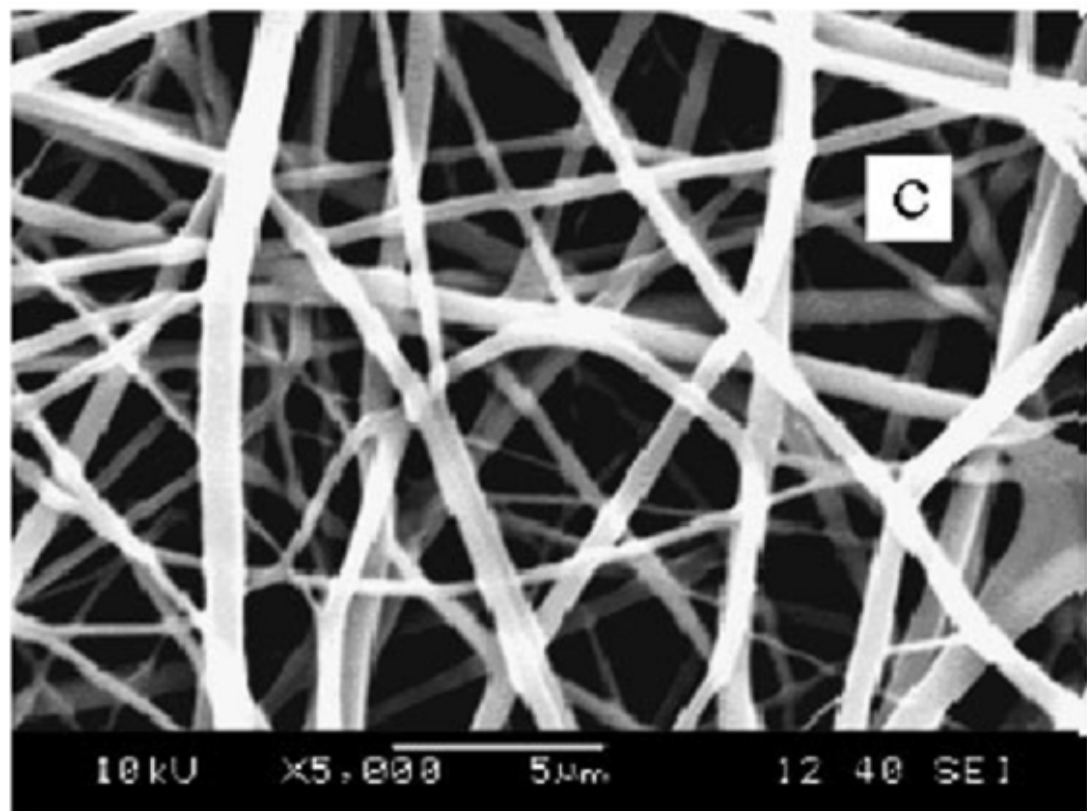
Figure 5.3 SEM images of electrospun membranes c and d EC based nanofibers (×5000 and ×20 000).

5.7 Sensing Mechanism for CO$_2$

In our earlier investigations, ratiometric response of ion pair form of 1-hydroxy-3,6,8-pyrenetrisulfonate (HPTS) to gaseous CO$_2$ was evaluated in ionic liquid doped ethyl cellulose based continuous thin films (Oter, Ertekin & Derinkuyu, 2008). It was found that exposure to carbon dioxide caused reversible and high relative signal changes in fluorescence intensity of HPTS. The employed additive; EMIMBF$_4$ provided enhanced stability, repeatability; wide linear dynamic working range (between 0 and 100 % CO$_2$) and better spectral characteristics allowing ratiometric measurements with more precise data.

In this study, similar experiments with electrospun membranes of PMMA and EC were carried out. Figure 5.4 (I and II) shows the change in fluorescence spectra of electrospun materials as a function of different concentrations of carbon dioxide.

Most of the CO$_2$ sensing films contain the ion pair form of HPTS and the quaternary ammonium base (TOAOH) in a polymer matrix. TOA$^+$OH$^-$ is usually added as a counter ion stabilizing the anionic (deprotonated) form of the HPTS in the lipophilic matrix. In such designs, the sensing scheme is based on two processes, the first being the diffusion of CO$_2$ through the membrane into the sensing region, the second being the reaction of the wet gas with anionic and highly fluorescent HPTS phenolate anion (Ertekin & Alp, 2006; Oter, Ertekin & Derinkuyu, 2008; Borisov, Ch, Klimant & Wolfbeis, 2007; Ertekin, Klimant, Neurauter & Wolfbeis, 2003a). The gaseous carbon dioxide dissolves in the trace amounts of water present in the matrix forming carbonic acid, which interacts with the deprotonated form of the indicator. In these sensors the indicator is functional owing to the water content of the ion pair. In our case two different mechanisms are being effective for carbonic acid formation; the well known water content of the ion pair and the trace amount of water encapsulated in the ionic liquid. Therefore, effective hydration of CO$_2$ and subsequent protolysis decreases the fluorescence intensity of HPTS at 513 nm (See Fig. 5.4 (I and II)) and converts highly fluorescent HPTS anion (Dye$^-$) into the less fluorescent HPTS (Dye) form. The water content of the 1-butyl-3-

methylimidazolium tetrafluoroborate has been reported to be 690 ppm after drying of the liquid for 15 h at 343 K (Jacquemin, Gomes, Husson & Majer, 2006). During experimental studies the water content of the EMIMBF$_4$ was not altered.

Additionally, the [BF4]$^-$ ion of the RTIL also catalyzes bicarbonate formation according to the following mechanism. [EMIM]OH moieties are produced by anion exchange with the present TOAOH in the sensing composition. The ([EMIM]OH) acts as a buffer-like system by neutralization with the hydrated CO_2 or carbonic acid (H_2CO_3). The resulting product is [EMIM]HCO$_3$. Formation of such a buffer-like system tunes the sensitivity of the sensor and enhances the long-term stability of the indicator since its lowly acts as a sink for acidic species (Oter, Ertekin & Derinkuyu, 2008). Therefore the well known hyperbolic response (Neurauter, Klimant & Wolfbeis, 1999; Amao & Nakamura, 2004; Ertekin, Klimant, Neurauter & Wolfbeis, 2003a) of the (HPTS)/(TOA)$_3$ in ethyl cellulose matrix becomes more linear. Another acceptable reason for choosing this material is the remarkable solubility of CO_2 in water- miscible ionic liquids, which is approximately 10–20 times that in conventional solvents, polymer matrices, or water (Blanchard, Hancu, Beckman & Brennecke, 1999; Anthony, Maginn & Brennecke, 2002; Bates, Mayton, Ntai & Davis, 2002).
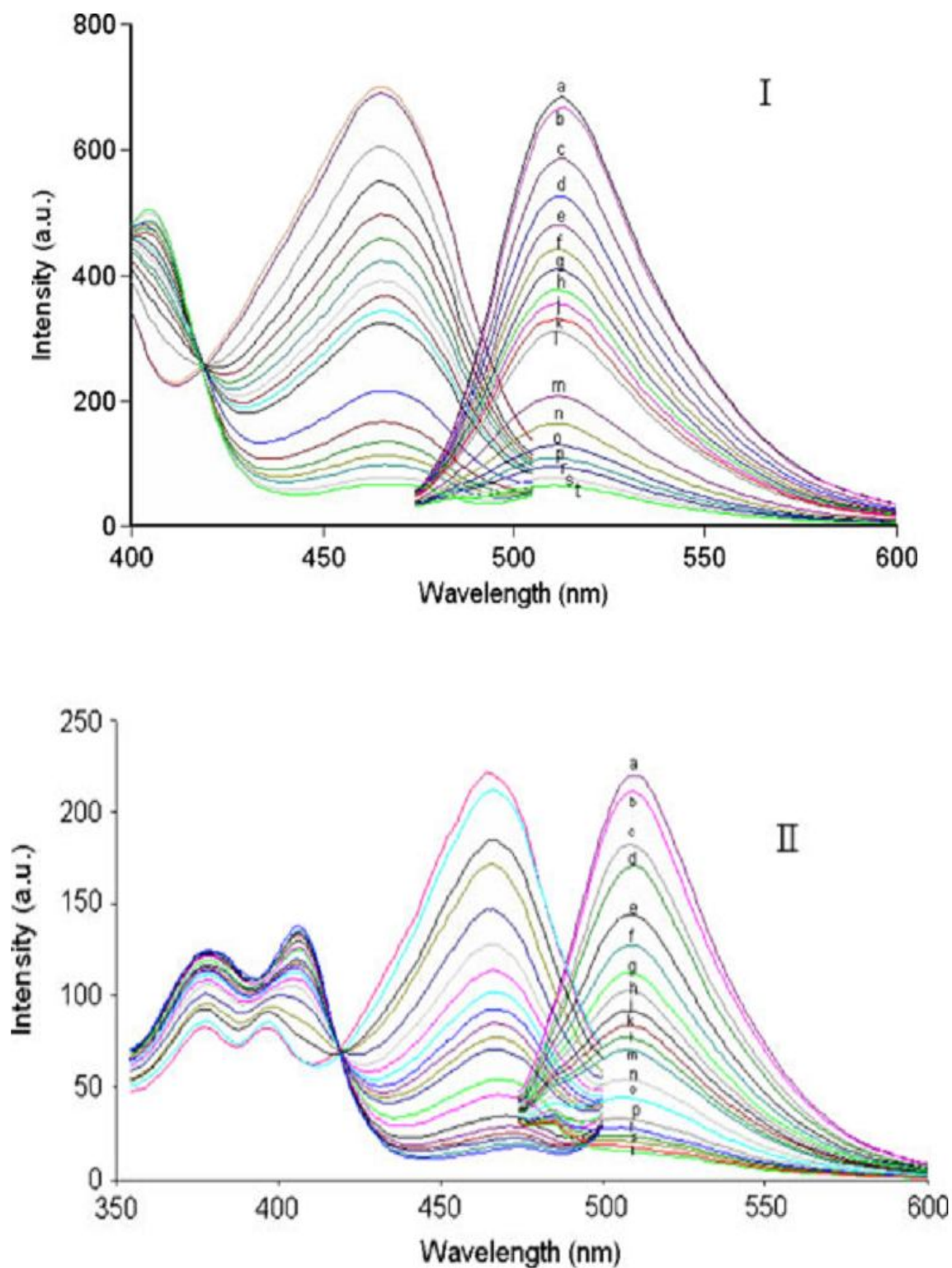
Figure 5.4 Excitation and emission spectra of electrospun fibers I: ion pair form of HPTS in EC, II: in PMMA after exposure to certain concentrations of CO_2 (λ_{max}^{ex} =465 nm, λ_{max}^{em}=513 nm), a: initial b: 1% c: 2% d: 3% e: 4% f: 5% g: 6% h: 7%   j: 8% k: 9% l: 10% m: 20% n: 30%   o: 40% p: 50%   r: 60% s: 80% t: 100% CO_2.

5.8 Emission Based Response of EC and PMMA Nanofibers

The fluorescence spectra related characteristics of the electrospun nanofibers and thin films were shown in Table 5.1.

The EC and PMMA doped HPTS exhibited similar spectral response for CO_2 in thin film form. The acquired spectral data from elecrospun membranes were typical and were very similar with spectral characteristics of both the solution phase and thin film form (See Figs. 5.3 and 5.4). Since the aluminum foil was completely covered with electrospun nanofibers there were no observable scattering effects in the emission spectra.

Table 5.1 The fluorescence spectra related characteristics of electrospun PMMA and EC based nanofibers and thin films.

Indicator dye	Matrix /form	λ_{max}^{em} (nm)	λ_{max}^{ex} (nm)	Stoke's shift (nm)
HPTS/TOAOH	EC /electrospun	513	465	48
HPTS/TOAOH	PMMA/electrospun	510	466	44
HPTS/TOAOH	EC / thin film	513	466	47
HPTS/TOAOH	PMMA/ thin film	510	466	44

In a homogeneous medium, such as in solution, the quantitative measure of fluorescence quenching is described by the Stern-Volmer constant, Ksv,

$$(Io/I) = 1+K_{sv} [Q]$$

In equation, Io and I are the intensities of fluorescence in the absence and in the presence of the quencher, respectively. The equation reveals that I_0/I increases directly proportional to the concentration of the quencher. When all other variables are kept constant, the higher the Ksv, the lower the concentration of quencher required to quench the fluorescence. In a heterogeneous medium, such as in polymer films, a negative deviation from the linear Stern-Volmer equation occurs at high

quencher concentration (Bacon & Demas, 1987; Carraway, Demas, DeGraff & Bacon, 1991).

The data obtained by gathering Stern-Volmer analysis for each electrospun and continuous thin film are shown in Fig. 5.5. For quencher concentrations in the range of 1 to 30 %, linear plots between concentration of quencher and I_0/I are obtained showing an excellent Stern-Volmer relationship.

Stern- Volmer constants (K_{sv}) of the electrospun films, calculated from slopes of the plots were found to be 1.4491 (%−1) and 1.0486 (%−1) for PMMA and EC based nanofibers respectively.

These values are 120 and 24 fold greater than that obtained from the continuous thin film sensor slides of PMMA and EC, respectively (See Table 5.2). Ksv values reveal important practical consequences. The sensitivity of the quenching process is enhanced by controlling the quencher diffusion rate to fluorophores via the nanostructural properties of the sensing films.
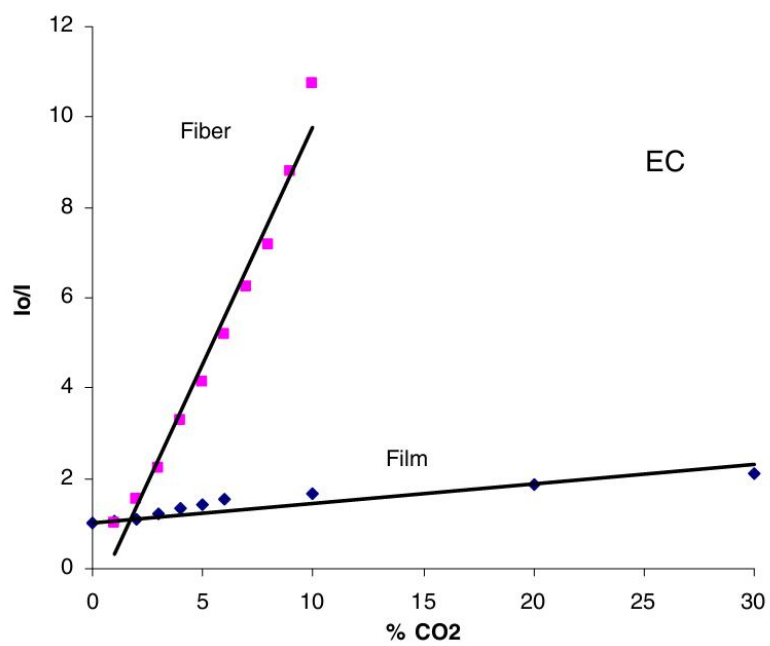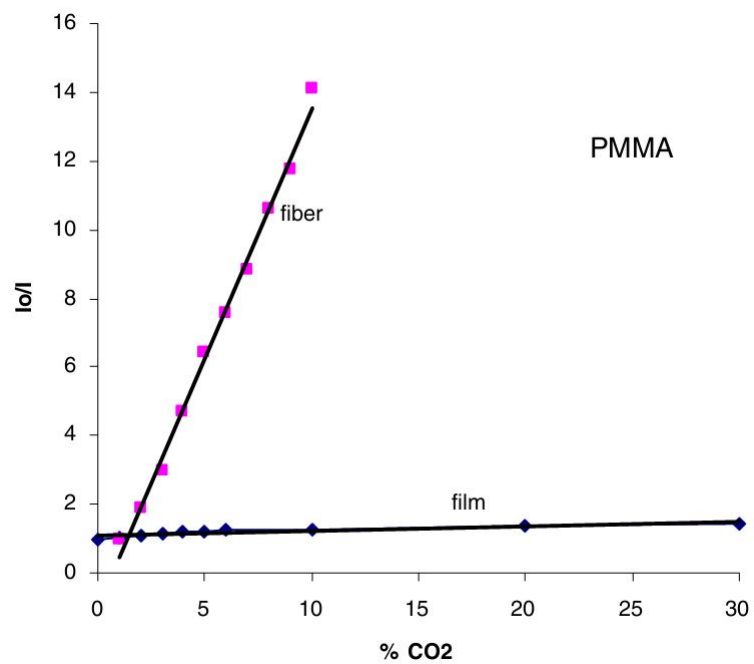
Figure 5.5 Gathered Stern Volmer plots of the electrspun nano-fibers and continuous thin films.

Table 5.2 The Stern Volmer plot related calibration characteristics of PMMA and EC based electrospun nanofibers and thin films.

Indicator Dye	Matrix/form	Con. Range (CO_2 %)	Lineer regression equation	Regression Coefficient (R^2)
HPTS/ TOAOH	EC/ electrospun nanofiber	1-30	y= 1.0486x+0.7322	0.9765
HPTS/ TOAOH	PMMA/electrospun nanofiber	1-30	y= 1.4491x+0.9785	0.9939
HPTS/ TOAOH	EC/ thin film	1-30	y= 0.0437x+1	0.8123
HPTS/ TOAOH	PMMA/ thin film	1-30	y= 0.0121x+1.1007	0.8011

In most of the previous designs, the response of the sensors was hyperbolic, with greater sensitivity at low carbon dioxide concentrations, which is typical of this type of pCO_2 sensors (Amao & Nakamura, 2004; Ertekin, Klimant, Neurauter & Wolfbeis, 2003a).

In this work, the ordinary least-squares OLS regression model was employed for a linear fit of the calibration curves. The response of the sensors was linear, with greater sensitivity at low carbon dioxide concentrations. The linear regression results for both membranes yielded a linear response with coefficients of regression (R^2) of 0.9939 and 0.9765 for PMMA and EC, respectively.

5.9 Response, Recovery and Stability Studies

The tested sensor compositions exhibited large relative signal changes and good sensitivity to gas-phase carbon dioxide. The response and recovery-related data of the sensing cocktails with EC and PMMA based nanofibers were acquired by recording the emission intensity signals during exposure to $0.0 - 10$ % CO_2 and $0 - 60$ % CO_2, respectively (See Fig. 5.6). At each time the reagent phase was regenerated with pure gaseous nitrogen (99.99 %).

The sensor compositions resulted in quite high relative signal changes of approximately 90 % and 95 % in the direction of a decrease in emission intensity at λem max =513 nm. The τ90 response times (the time to achieve 90 % of the overall signal change) in-EC and PMMA were in the range 15–20 s on exposure to 0.0–10 % CO_2. The initial signal intensities for both compositions could be completely recovered after switching in the concentration range 0.0–10 % CO_2. A slight drift was observed after the 2nd cycle. Between the 1st and 10th cycles the level of reproducibility of upper signal levels were 358 ± 4.03 and 734 ± 3.04 (n = 10) for EC and PMMA respectively. The regeneration time was approximately 2 min. The response and recovery time, varying between one and 5 min, includes the equilibration time for the protonation-deprotonation reaction and the dead volume of the gas tubes, rather than the true response time of the sensor slides.

The stability of ion pair form of HPTS in the employed matrix materials was excellent and when stored in the ambient air of the laboratory there was no significant drift in signal intensity after 7 months.
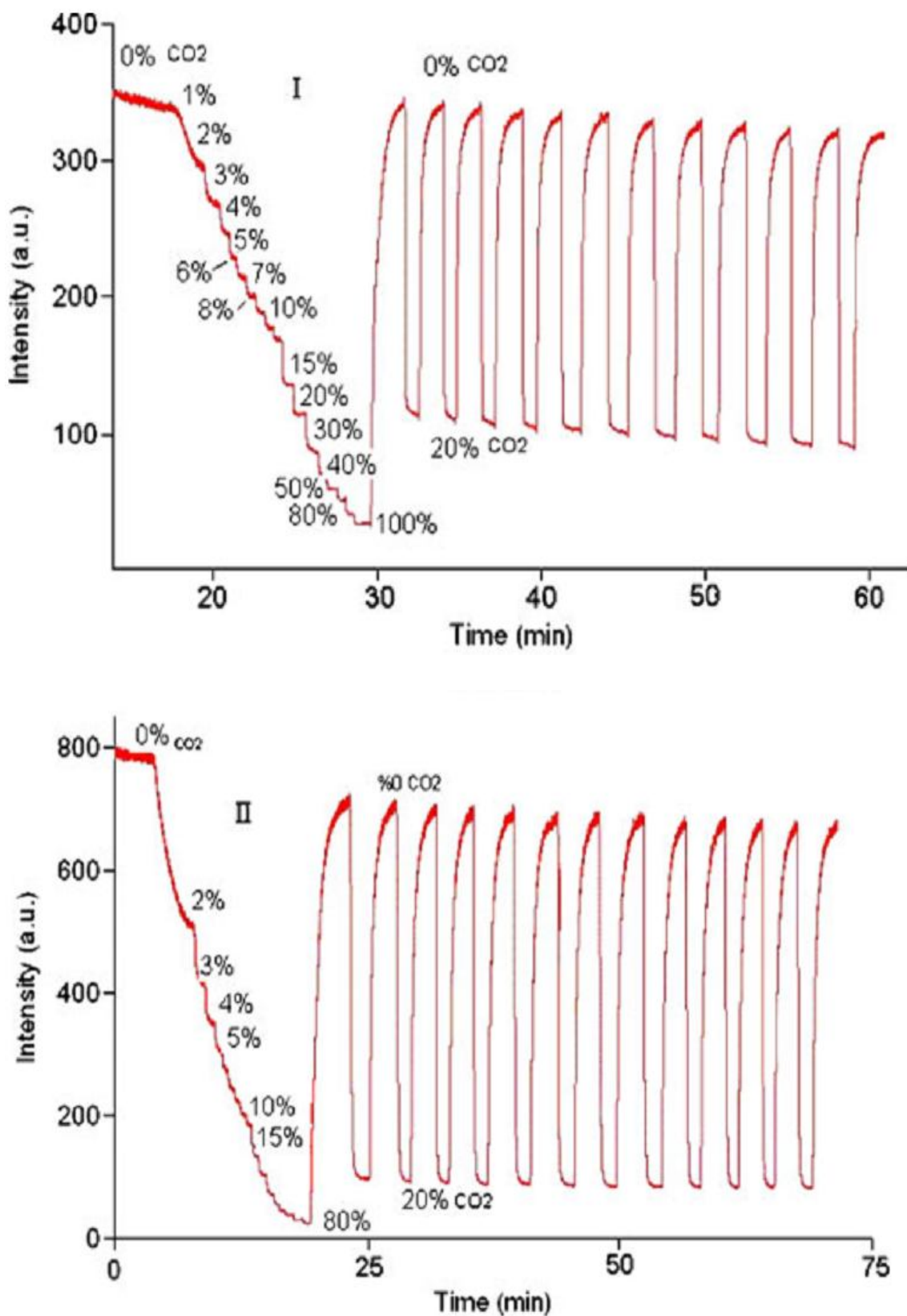
Figure 5.6 Emission based kinetic response of ion pair form of HPTS in I: EC, II: PMMA to gaseous CO_2.

5.10 Conclusions

Electrospinning looks like a promising, simple, and an effective method for fabricating optical chemical sensor devices. This article demonstrates how the sensitivity of micrometer-scale thin film coating on a planar surface can be manipulated by nanometer-scale features on the latter. Electrospun films provide high porosity; large surface area and consequently high gas permeability when compared to continuous thin films. With respect to continuous thin films, electrospun films can offer enhanced sensitivity and reactivity in optical chemical sensing. Further efforts will focus on exploring new sensing materials and polymer compositions, controlling the nano-scale size of the electrospun membranes, and optimizing the sensitivities for the detection of a variety of analytes. The sensor slides showed high sensitivities due to the high surface area-to-volume ratio of the nanofibrous membrane structures.

The preliminary results of Stern-Volmer analysis show that the sensitivities of electrospun nanofibrous membranes to detect CO_2 are 24 to 120 fold higher than those of the thin film based sensors. The response times of the sensing reagents were short and the signal changes were fully reversible. The stability of ion pair form of HPTS in the employed matrix materials was excellent and when stored in the ambient air of the laboratory there was no significant drift in signal intensity after 7 months.

CHAPTER SIX

SPECTRAL CHARACTERIZATION AND DISSOLVED CO_2 SENSING WITH UTILIZED INDICATOR DYES OF MY9 and MY10

In this chapter the newly synthesized fluorophores has been characterized in different solvents and polymer matrices of EC, PMMA and, used for preparation of sensing agent. Sensing performances of the utilized indicators were also tested in thin film and nanofiber form. Indicator dyes were synthesized in our laboratories and characterized with 1H NMR and IR based data by Prof. Dr. Yavuz Ergün.

Synthesis protocols of MY9 and MY10: 1 g of isoniazide (7.29 mmole) and equal amount of aldyhide derivative were mixed in 25 mL of ethyl alcohol. 1 mL of glacial acetic acid was added into the mixture. The mixture was boiled five hours under reflax. The product is filtered and crystallized in EtOH.

Schematic structures of the employed molecules are shown in Figure 6.1. Its possible utilization for optical sensing of dissolved carbon dioxide as well as typical sensor characteristics such as working range; sensitivity and selectivity have been investigated. The interferences of various cations and anions also have been studied. The offered design was also tested for real groundwater samples of Sarikiz, Turkey.

6.1 Structural Identification of MY9 and MY10 Dyes

The molecules MY9 and MY10 were characterized with 1H NMR and IR based data.

MY9: IR (KBr): 3182 (NH), 1646 (C=O), 1599 (C=N) cm^{-1}.

^{1}H-NMR (400 MHz CDCl$_3$): δ 3.85 (s, 3H, N-CH$_3$), 7.25-7.28 (m, 1H, ArH), 7.38-7.41 (m, 2H, ArH), 7.51 (t, 1H, ArH), 7.70-8.20 (m, 5H, pyridine H and ArH), 8.48 (d, 1H, N=CH), 8.75-8.86 (m, 2H, pyridine H), 9.33 (bs, 1H, NH), mp=224 ^{o}C

MY10: IR (KBr): 3302 (NH), 1664 (C=O), 1591 (C=N) cm^{-1}.

^{1}H-NMR (400 MHz CDCl$_3$): δ 3.01 (s, 6H, N-(CH$_3$)$_2$), 6.63-6.70 (m, 2H, ArH), 6.81-6.91 (m, 2H, ArH), 7.32-7.40 (m, 2H, CH=CH), 7.65-7.70 (m, 2H, pyridine H), 7.97-8.01 (m, 1H, N=CH), 8.73-8.80 (m, 2H, pyridine H), 8.92 (bs, 1H, NH), mp=252 ^{o}C.
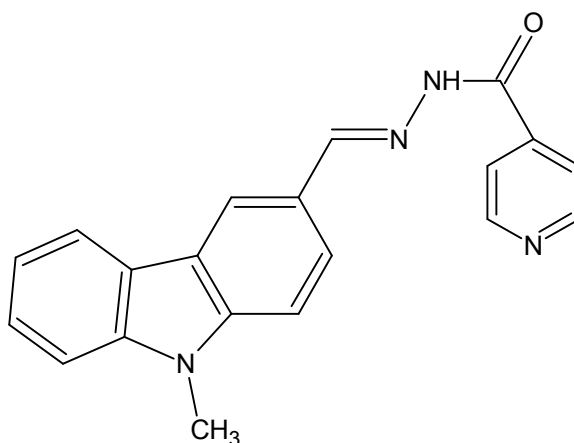
MY-9
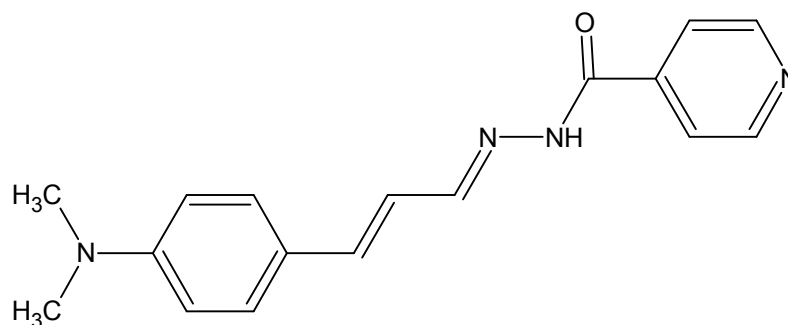
MY-10

Figure 6.1 Schematic structures of the employed molecules, MY9 and MY10.

6.2 Thin Film and Nanofiber Preparation Protocols

The optode membranes were prepared by mixing of 240 mg of polymer (PMMA and EC), 192 mg of plasticizer (DOP), 48 mg of IL, 6 mg of dye and in Toluene: DMF (80:20) or DCM: EtOH (25:75) solvent systems. The nanofibers were prepared employing the same composition explained for the thin films.

The employed polyester support utilized in thin film based studies was optically fully transparent, ion impermeable and exhibited good adhesion to PMMA and EC. Each sensing film was cut to 1.2 cm width and fixed diagonally into the sample cuvette and the excitation and fluorescence emission spectra were recorded. Electrospun nanofibers were produced by electrospinning technique. The nanofibers were collected on an aluminum substrate. The electrospun membranes exhibited good adhesion to the aluminum substrate. The deposited nanofibers were gathered in proper size, fixed in the flow cell and the excitation or emission spectra were recorded. For the flow system experiments, both, the films and nanofibers were cut to proper size and placed into the 300 µL black-Teflon flow cell and interfaced with the fiber tip (6mm diameter). Flow rate of the peristaltic pump was kept at 2.4 mL min-1. The electrospun nanofibers were characterized using scanning electron microscopy (SEM) and their average diameter was evaluated.

6.3 Results and Discussion

6.3.1 Absorption Based Spectral Characterization

For spectral characterization of the MY9 absorption spectra were recorded in the solvents of different polarities and in EC matrix. The gathered absorption spectra are shown in Figure 6.2. The UV-VIS spectroscopy related data (absorption maxima; Abs, and molar extinction coefficient), were shown in Table 6.1. MY9 exhibited efficient absorbance and high molar extinction coefficients around 280-340 nm and 380 nm in all the employed solvents and solid matrices, respectively.

Absorption wavelength of MY9, λ_{max}, in EC is seen to be shifted about 40 nm compared to absorption λ_{max} in THF solution. Red shift of absorption of MY9 may be related to enhanced conjugation in immobilized polymer phase by hindrance of rotational and vibrational motions.
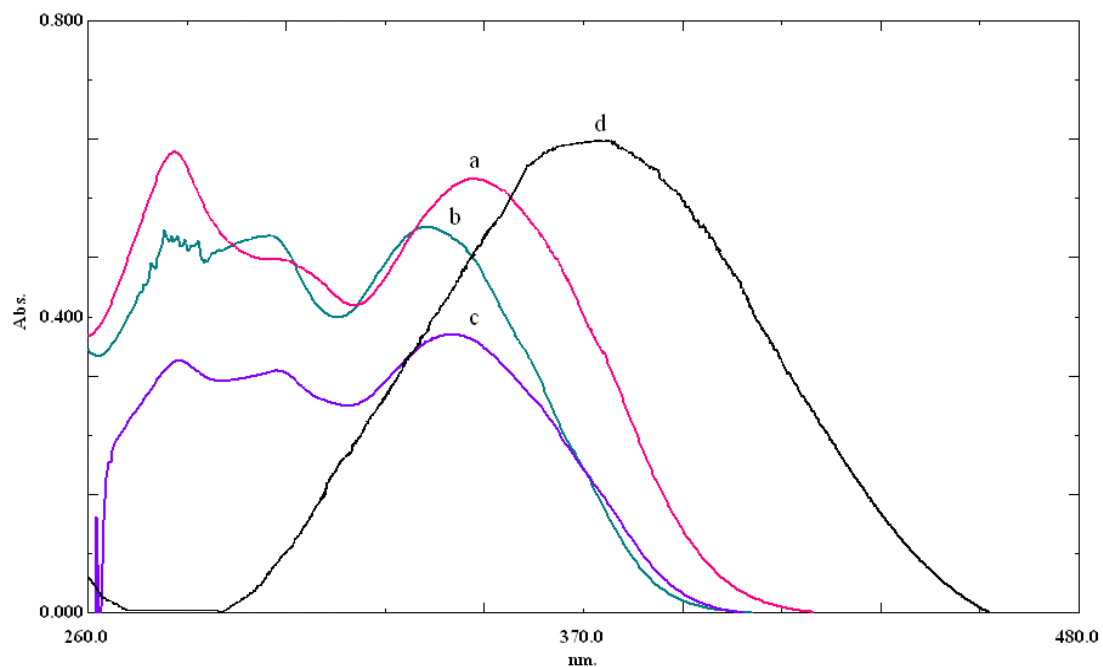
Figure 6.2 Absorption spectra of the MY9 dye in a) EtOH b) THF c) DMF d) EC
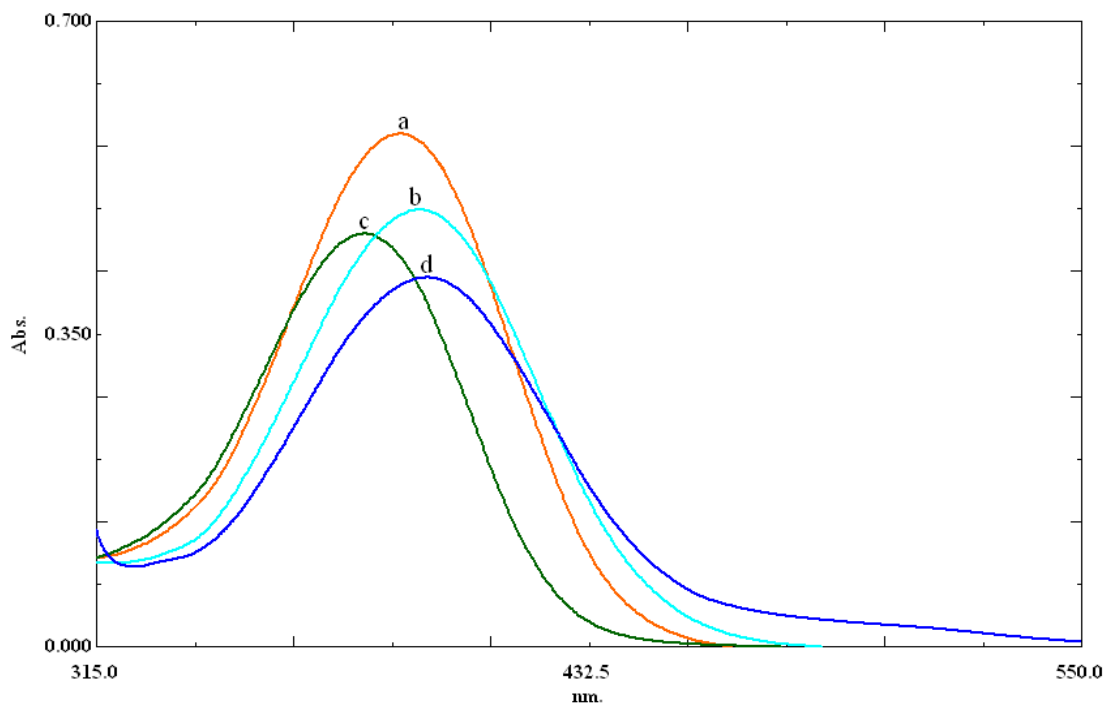
Figure 6.3 Absorption spectra of the MY10 dye in a) DMF b) EtOH c) THF d) EC.

The gathered absorption spectra of MY10 in different moieties were shown in Figure 6.3. Absorption spectra related molar extinction coefficients and maximum absorption wavelengths of the dye in employed solvents and EC are given in Table 6.1. In agreement with Williams, Winfield & Miller (1983), molar extinction coefficients (ε) of MY10 in polymer matrices were increased about 2.5 fold, with respect to the (ε) values observed in the solution phase. These data can be taken as proofs that the MY10 dye absorb better when immobilized in EC matrices.

Table 6.1 UV-Vis spectra related data of MY9 and MY10 in the solvents of EtOH, THF and DMF and in solid matrices of EC.

Compound	Matrix	λ_{abs}^1 (nm)	λ_{abs}^2 (nm)	ε_{max} (L×mol-1× cm-1)	ε_{max} (L×mol-1× cm-1)
MY9	EtOH	279	346	50000	47120
MY9	THF	300	336	51100	52000
MY9	DMF	280	341	34200	37500
MY9	EC	380	--	183700	--
MY10	EtOH	392	--	39120	--
MY10	THF	379	--	37040	--
MY10	DMF	387	--	46160	--
MY10	EC	395	--	109700	--

6.3.2 Spectral Evaluation, Fluorescence Quantum Yield Calculations and Interpretation of Emission Spectra

The excitation-emission spectra and the related data of the dyes are shown in Fig. 6.4, Fig. 6.5 and Table 6.2, respectively. In all of the employed matrices the Stoke's shift values, $\Delta\lambda_{ST}$ (the difference between excitation and emission maximum), calculated from the spectral data are quietly high. Especially in solid matrices the enhanced Stoke's were observed when immobilized in EC the MY9 exhibited a $\Delta\lambda_{ST}$ of 120 nm.
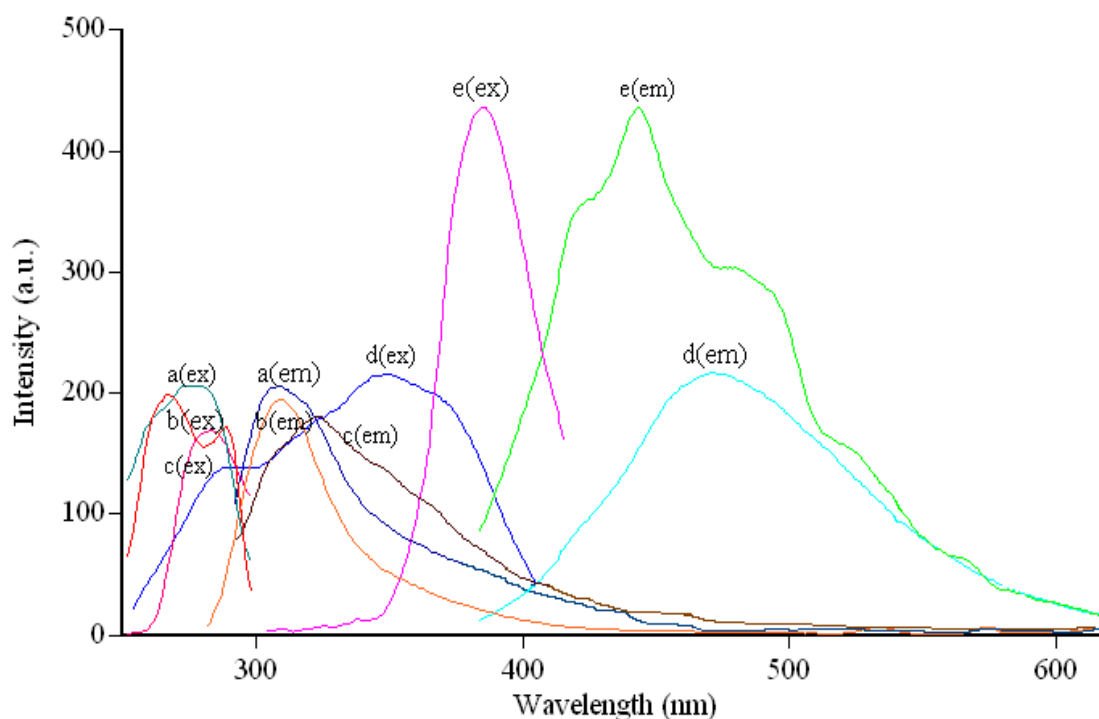
Figure 6.4 Excitation and corrected emission spectra of the MY9 dye in a) EtOH b) THF c) DMF d) EC e) PMMA.
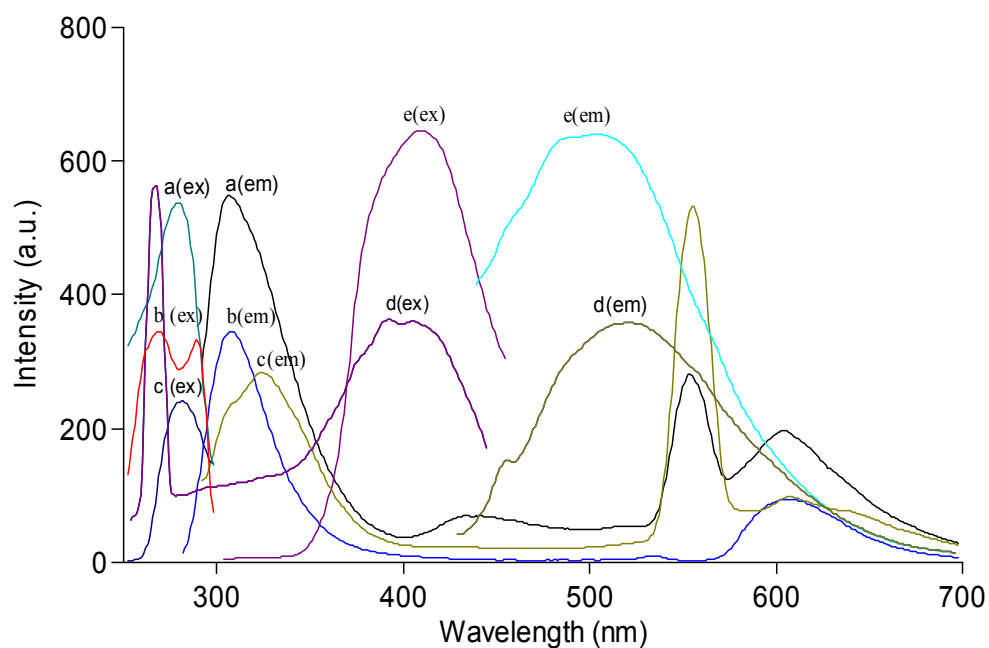
Figure 6.5 Excitation and corrected emission spectra of the MY10 dye in a) EtOH b) THF c) DMF d) EC e) PMMA.

In all of the employed matrices, Stoke's shift values were high enough and extended from 30 to 100 nm for both, MY9 and MY10 dyes, respectively. Stoke's shift is an important parameter for fluorescence and optical sensor studies because the high Stoke's shift value allows the emitted fluorescence photons to be easily distinguished from the excitation photons. Stoke's shift exceeding 30 nm is recommended for easy visualization and sensitive detection with fiber optics. The Stoke's shifts of MY9 and MY10 which are 120 nm and 45 nm in EC matrix, respectively, permit the usage of dyes in together with solid-state optic components such as LEDs or fiber optics.

Today commercially available fiber optics allows measurements in the UV-VIS (200-800 nm) or VIS/NIR wavelength range (350-2000 nm). From this point of view the chosen dyes are available for use together with fiber optics.

Table 6.2 Spectral characterization of MY9 and MY10 dyes. λ_{max}^{em} : maximum emission wavelength in nm; λ_{max}^{ex} : maximum excitation wavelength in nm; $\Delta\lambda_{ST}$: Stoke's shift and Φ_F : Quantum yield.

Compound	Matrix	λ_{max}^{ex}	λ_{max}^{em}	$\Delta\lambda_{ST}$ (Stoke's shift)	Φ_F Quantum yield
MY9	EtOH	280	310	30	3.59×10^{-2} in EtOH
MY9	DMF	280	330	50	
MY9	THF	270	310	40	
MY9	PMMA	385	445	60	0.5534 in EC
MY9	EC	400	520	120	
MY10	EtOH	280	310	30	3.93×10^{-2} in ETOH
MY10	THF	270	310	40	
MY10	DMF	280	320	40	
MY10	PMMA	410	500	90	0.4651 in EC
MY10	EC	320	365	45	

Fluorescence quantum yield values (Φ_F) of the MY9 and MY10 were calculated employing the comparative William's method (Williams, Winfield, Miller, 1983), which involves the use of well-characterized standards with known Φ_F values. For this purpose, the UV-Vis absorbance and corrected emission spectra of different concentrations of reference standard Quinine Sulphate (λ_{ex} = 350 nm, quantum yield (Φ_F) = 0.546 in H_2SO_4) and the employed molecules were recorded, and, the integrated fluorescence intensities were plotted versus corresponding absorbances (See Figure 6.6 and 6.7). In quantum yield calculations

very diluted solutions yielding the absorption values of 0.02, 0.04, 0.06, 0.08, 0.10 and 0.12 to avoid self-quenching effect.
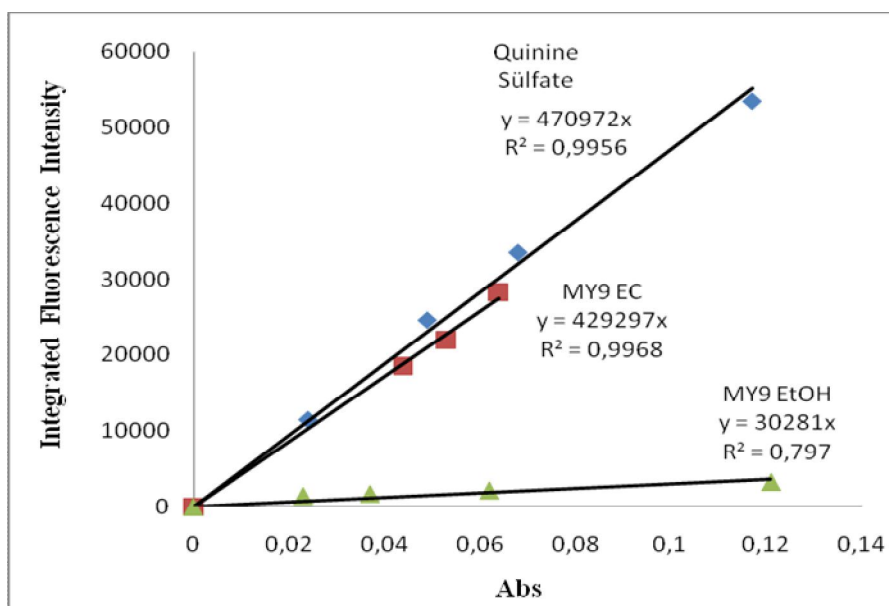
Figure 6.6 The integrated fluorescence intensities vs absorbance for the reference standard; quinine sulphate in H_2SO_4, MY9 dye in EC and EtOH matrices.
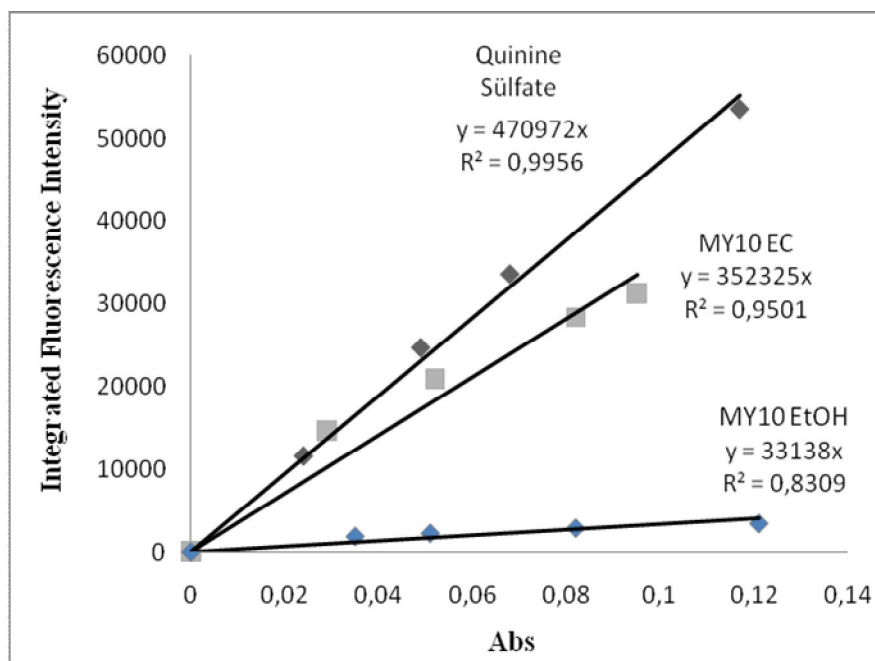
Figure 6.7 The integrated fluorescence intensities vs absorbance for the reference standard; quinine sulphate in H_2SO_4, MY10 dye in EC and EtOH matrices.

The data regarding quantum yields are shown in Table 6.2. Fluorescence quantum yield of MY9 in EC, $\Phi_F = 0.5534$, has increased about 15-fold, with respect to Φ_F of MY9 in EtOH. Similarly for MY10 fluorescence quantum yield in EC matrix, $\Phi_F = 0.4651$, has increased about 12-fold, with repect to $\Phi_F = 3.93 \times 10^{-2}$ in EtOH. These data can be taken as proofs that the dye molecule MY9 fluoresces better in immobilized EC matrix.

The comparatively small Φ_F values reported in ethanol can be attributed to the internal charge transfer (ICT) state by rotation of the central N–N bond and a following radiationless deactivation. The enhancement observed in fluorescence emission quantum yield of MY9 and MY10 in solid matrices can be explained in the same way. By immobilization the rotation around central N–N bonds were hindered and structural rigidity was provided which enhances the brightness of the fluorophore.

6.3.3 pH Dependent Response of MY9 and MY10 Dye

Most of the optical CO_2 sensor designs utilize indicator dyes with pKa values between 7.4 and 10.0. For this reason the number of the fluorescent pH indicators for carbon dioxide sensing is rather limited. The knowledge of acidity constants (pKa) of indicator dye is of fundamental importance in order to provide information on chemical reactivity range of the dyes. For this reason, the absorption and emission based pH response of MY9 and MY10 were investigated in EtOH and PMMA, respectively. pH measurements were performed with commercially available pH electrodes for non-aqueous media.

pH dependent spectral response of the indicators were tested exploiting 10^{-3}M solutions of nonaqueous $HClO_4$ and tetrabutylammonium hydroxide (TBAOH). The ethanolic solutions of indicator dyes were titrated with $HClO_4$ and TBAOH.

Figure 6.8 and Figure 6.9 reveals the absorption based pH dependent responses of the MY9 dye in EtOH. MY9 dye exhibited a decreasing response upon exposure to

solutions between pH 7.12-4.50. There was no significant relative signal change in the acidic region of pH scale (See Figure 6.8). The absorption maximum of the MY9 dye increases as the pH varies from neutral (pH=7.35) to alkaline region (pH=11.50). Related absorption based sigmoidal response was shown in Figure 6.9.
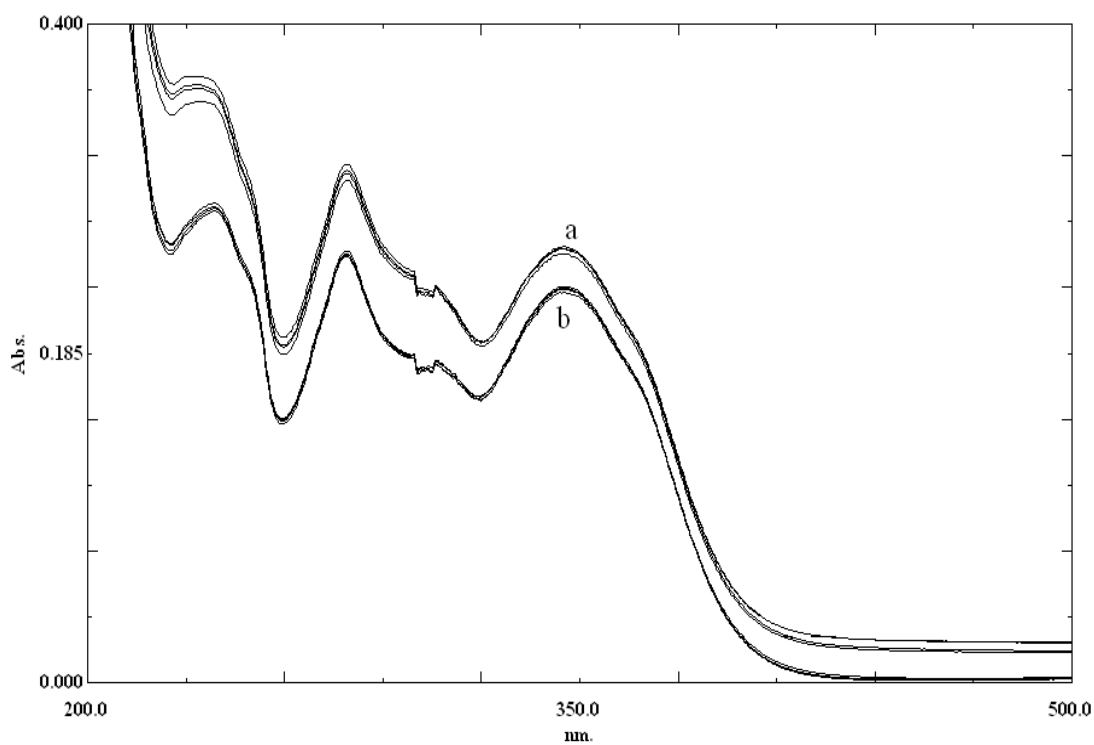
Figure 6.8 Absorption spectra of MY9 in EtOH after addition of acid solutions in the pH range of 7.12-4.50. pH: a) 7.12, 7.00, 6.20, 5.40 b) 4.70, 4.18, 3.90, 3.4.
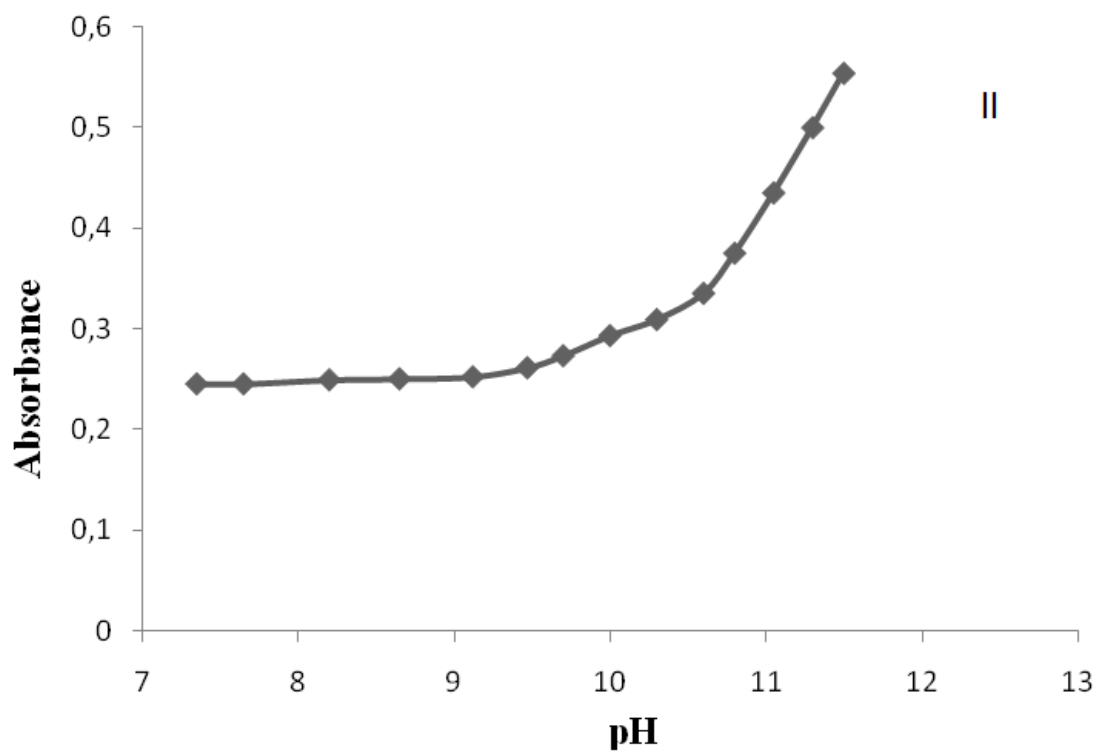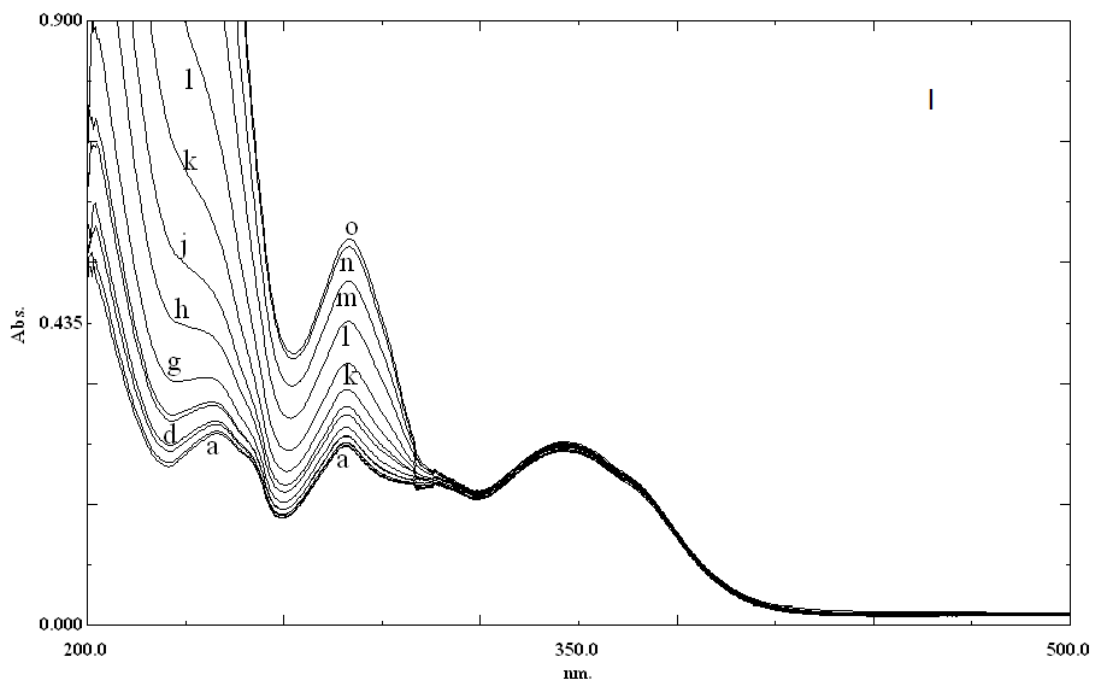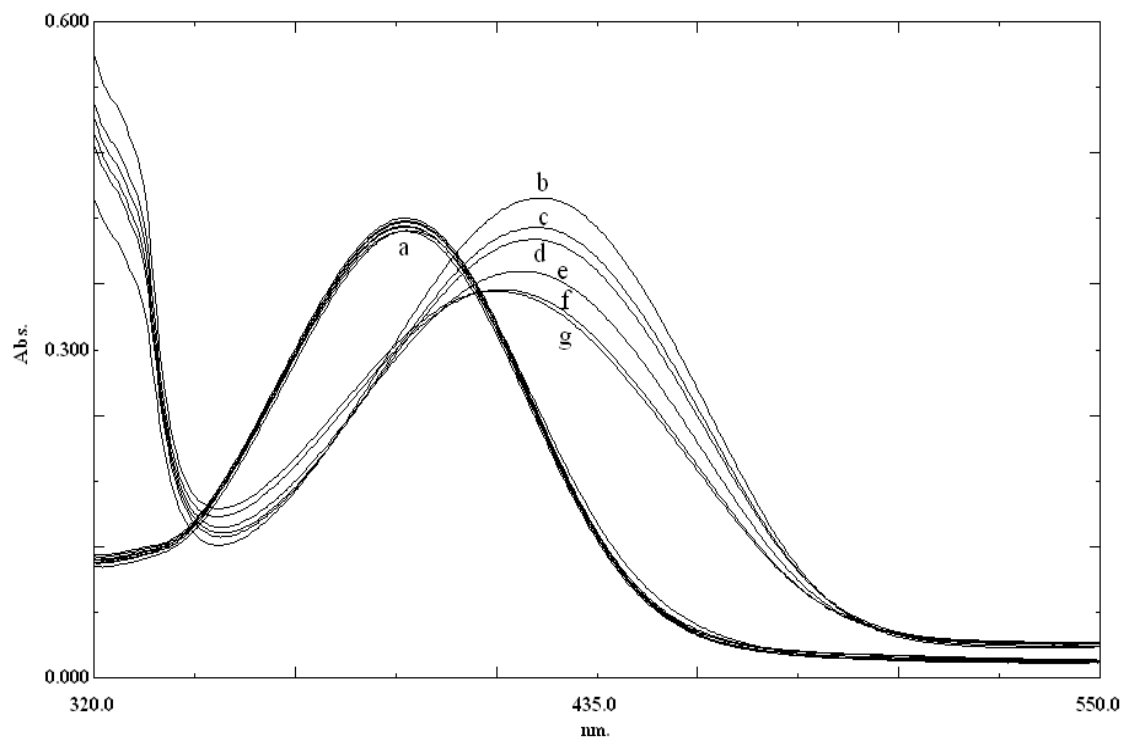
Figure 6.9 I: Absorption spectra of MY9 in EtOH after addition of base solutions in the pH range of 7.35-11.50. pH: a) 7.35 b) 7.65 c) 8.20 d) 8.65 e) 9.12 f) 9.47 g) 9.77 h) 10.00 j) 10.30 k) 10.60 l) 10.90 m) 11.05 n) 11.30 o) 11.50.

II: Absorption based sigmoidal response of MY9 to pH.

Figure 6.10 and 6.11 reveals the absorption based response of MY10 dye for pH range of 7.80 - 6.10 and 5.8-10.08, respectively.

Figure 6.10 Absorption spectra of MY10 in EtOH after addition of acid solutions in the pH range of 7.80 - 6.10. pH: a) 7.80, 7.35, 6.90 b)7.10 c) 6.90 d) 6.80 e) 6.70 f) 6.50 g) 6.10.
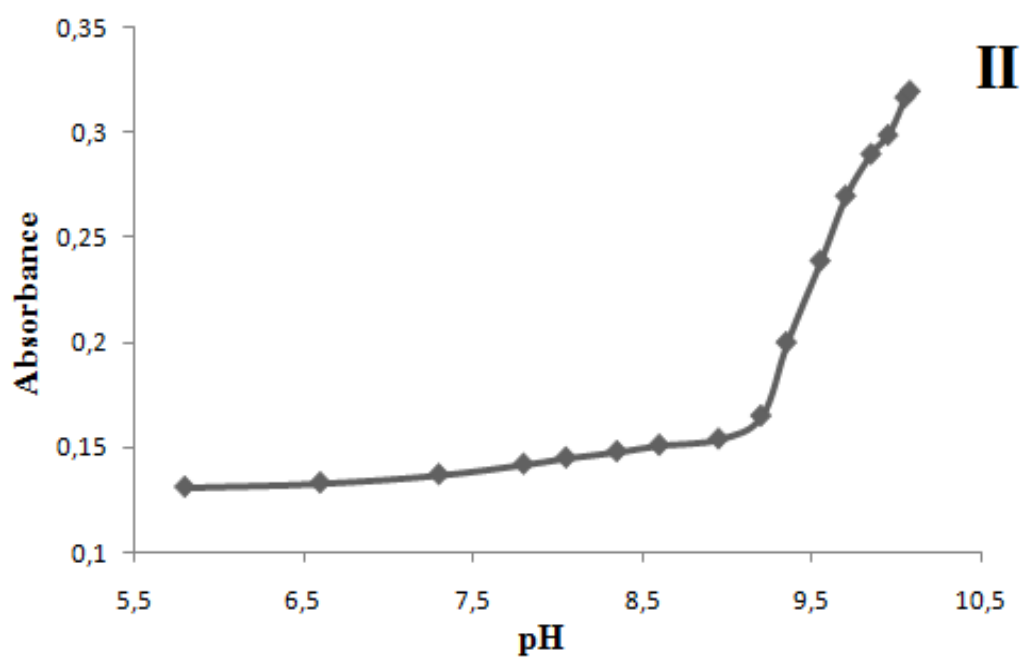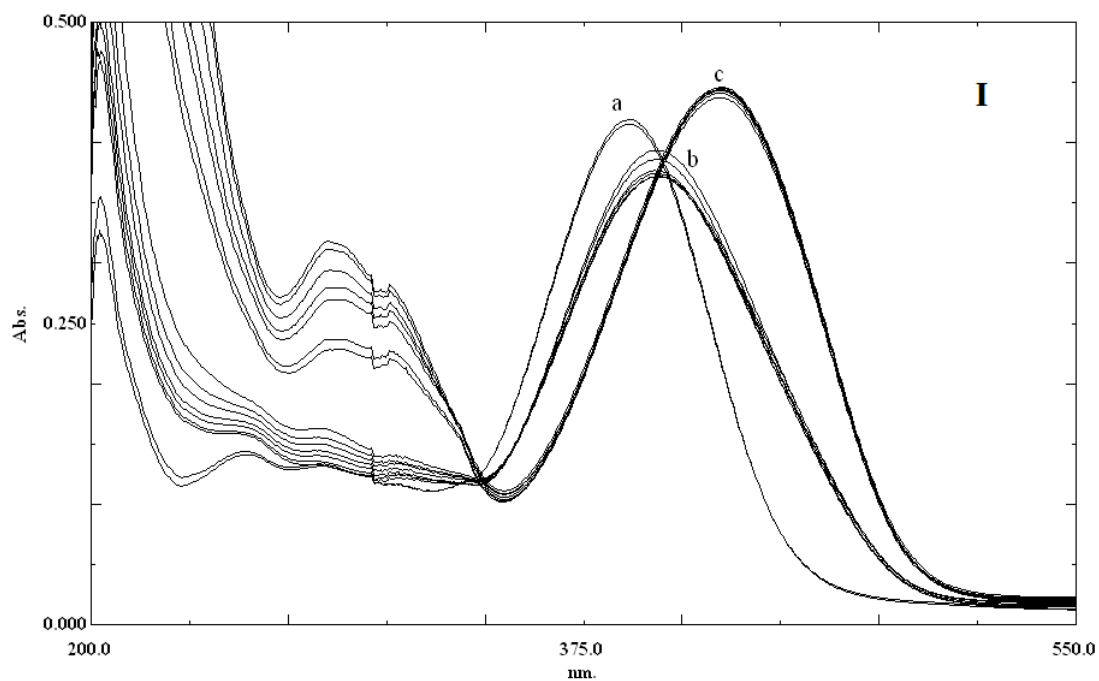
Figure 6.11 I: Absorption spectra of MY10 in EtOH after addition of basic solutions in the pH range of 5.8-10.08. pH: a)5.80; 6.60   b) 7.30; 7.80; 8.05; 8.35; 8.60; 8.95; 9.20   c) 9.35; 9.55; 9.70;9.85;9.95; 10.05;10.08.

II: Absorption based sigmoidal response of MY10 to pH.

The MY10 dye exhibited an interesting absorption based response to pH at different ranges of pH scale. In acidic moieties λ_{max} abs was measured as 390 nm, near neutral region the maximum absorption wavelength was shifted to 410 nm. At more basic pH values the λ_{max} shifted to 437 nm. The observed spectral shifts to longer wavelength can be attributed to protonation-deprotonation of different sites of molecule at different pH values. The MY9 and MY10 dyes contain available positions for protonation (See Fig. 6.12).
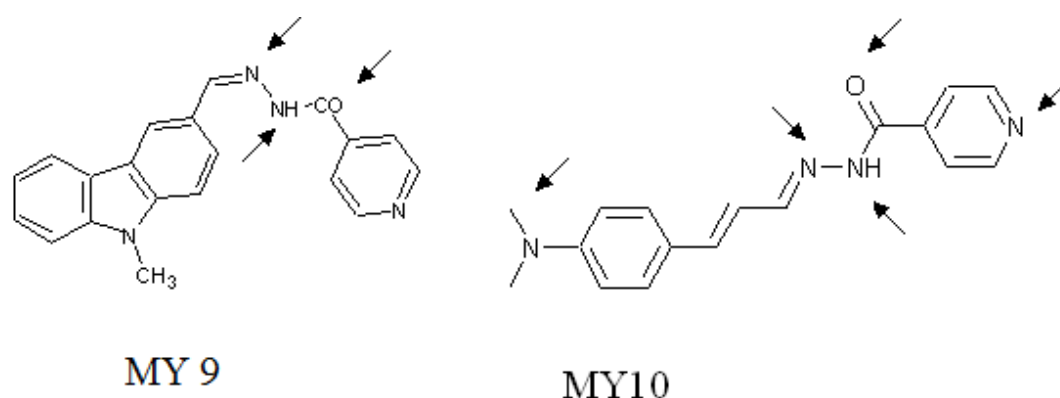
Figure 6.12 Potential active sites for protonation.

The pKa values of the utilized dyes were calculated via following equation;

$$pKa = pH + \log [(Aa-Ax) / (Ax-Ab)]$$

where Aa and Ab are the absorbance intensities of the acidic and basic forms and Ax is the intensity at a pH near to the midpoint (Werner & Wolfbeis, 1993). The pKa values were found to be 10.5 and 9.4 for MY9 and MY10 in ethanol, respectively. Since the emloyed dyes are nonsoluble in water, it is nearly impossible to assess their acid-base characteristics in known water-solvent systems and a known pH scale. It is a well known fact that, the pH scale in nonaqueous media is governed by the autoprotolysis or autodissociation constant of the solvent. Autoprotolysis constant of ethanol is approximately is 10^{-19}. In our case ethanol will govern the pH scale and the measured pKa values in EtOH falls to the neutral region of the pH scale.

6.3.4 pKa Calculations of MY9 and MY10 in PMMA Matrix

Dissociation constants (pKa) of MY9 and MY10 dyes were investigated from the excitation/emission based measurements in polymethyl methyl-methacrylate (PMMA) matrix. Here we utilized the immobilized dyes in buffered solutions. In our opinion these measurements are more informative than that of the pKa calculations performed in EtOH. The relative signal change of emission spectra of the MY9 and MY10 was monitored after addition of certain concentrations of buffered acid solutions at different pH ranges. MY9 in PMMA exhibited a decrease in signal intensity after exposure to different concentrations of acid solutions in the pH range of 7.00 to 11.00. Figure 6.13 and Figure 6.14 shows pH induced emission based spectral response of the MY9 in the pH range of 7.00-4.00 and 7.00-11.00, respectively.
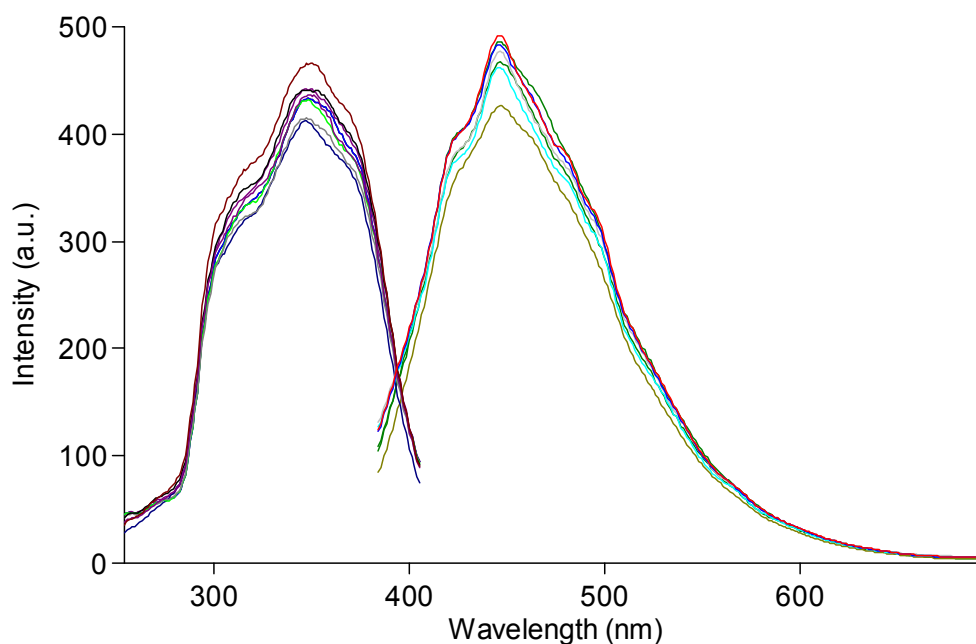
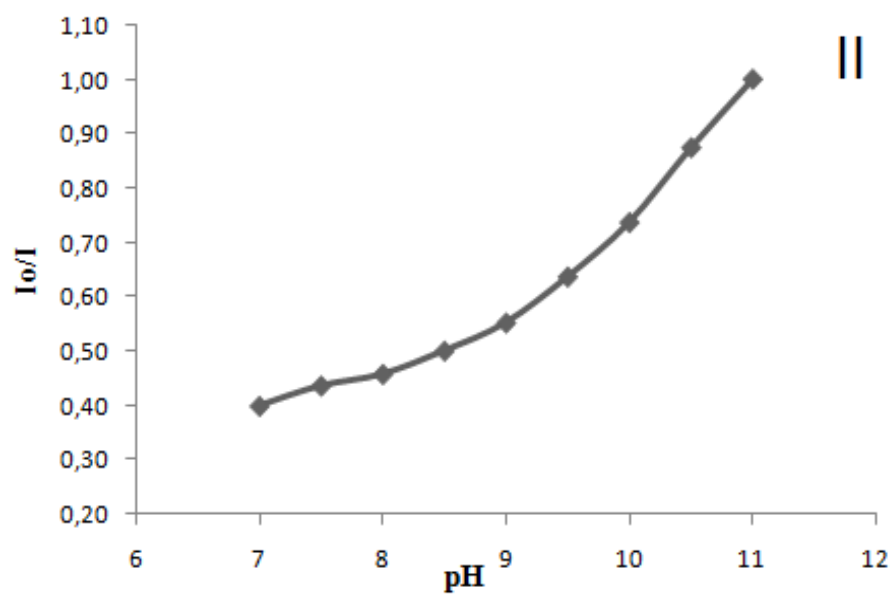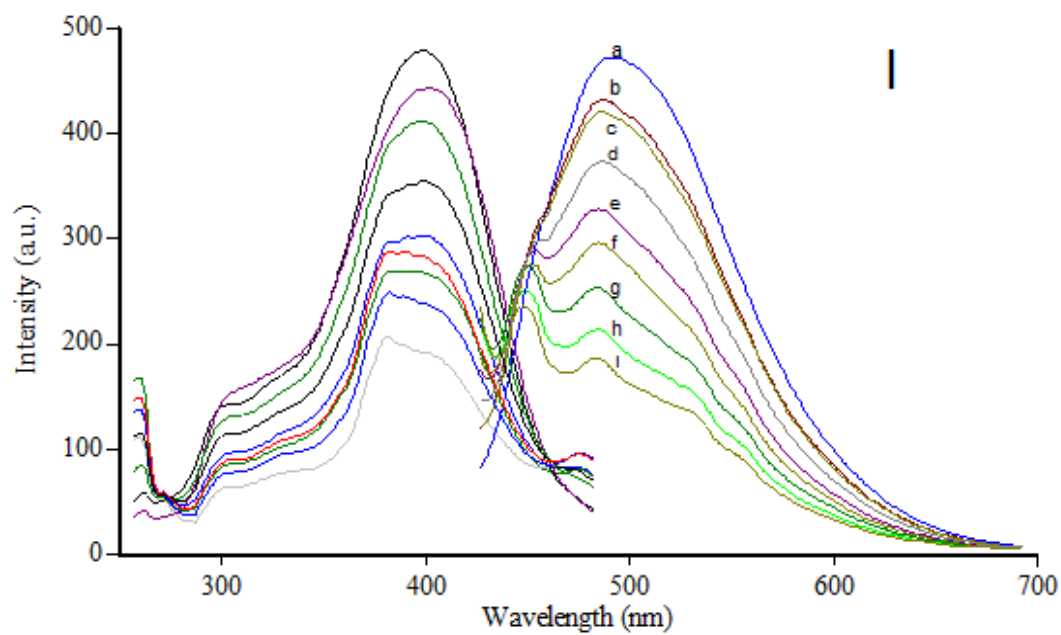Figure 6.13 pH induced emission based spectral response of the PMMA doped MY9 in the pH range of. 7.00 -4.00.
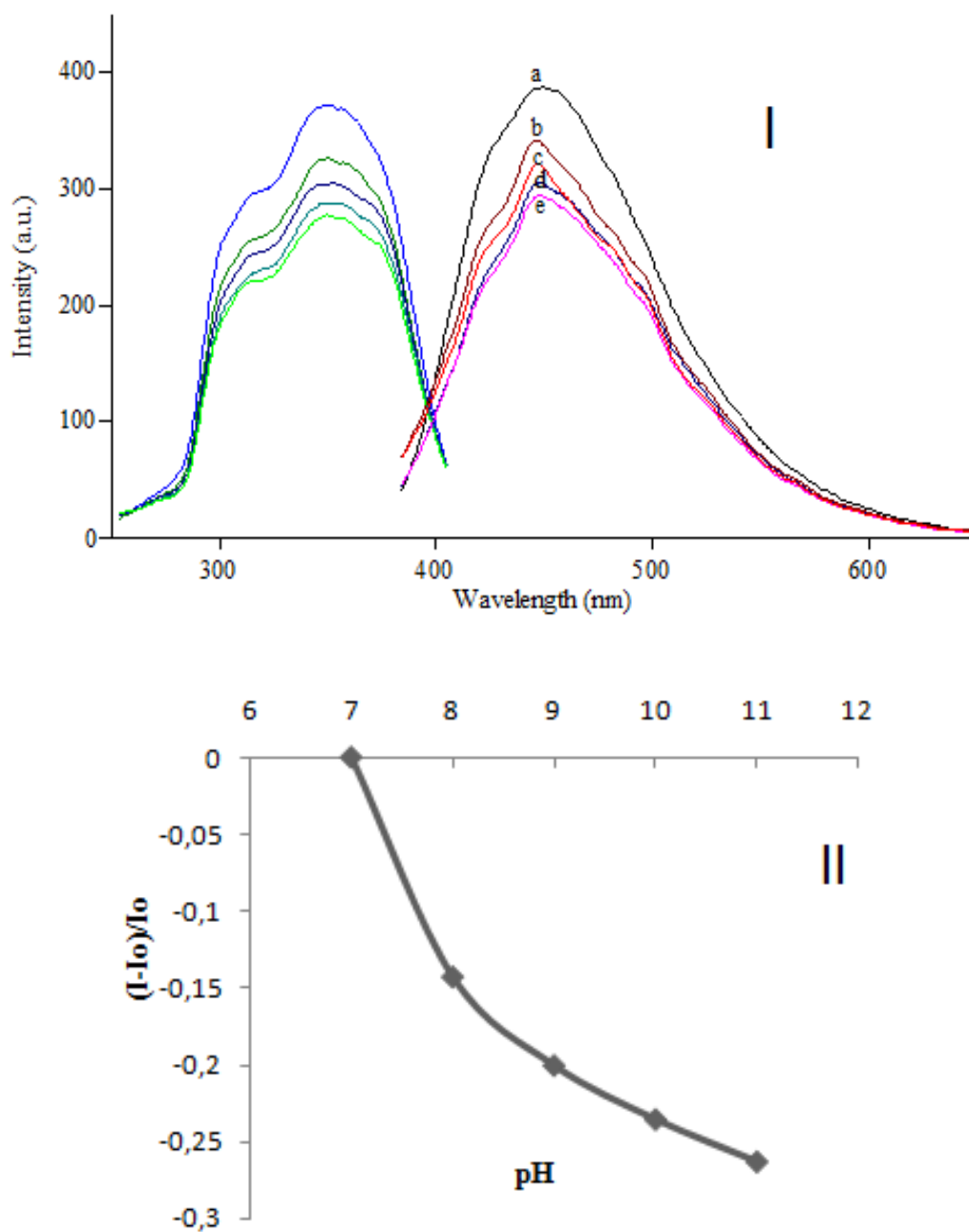
Figure 6.14 I: pH induced emission based spectral response of the PMMA doped MY9 in the pH range of. 7.00 -11.00. pH: a) 7.00 b) 8.00 c) 9.00 d) 10.00 e) 11.00.

II: Emission based response of MY9 to pH.

The MY9 dye exhibited 25 % and 10 % relative signal change in the basic and acidic regions of the pH scale, respectively.

Figure 6.15 and 6.16 show pH induced spectral response of the PMMA doped MY10 dye in the pH range of 3.00-7.00 and 7.00-11.00, respectively. Thin film form of MY10 dye shows decrease in signal intensity after exposure to different concentrations of acid solutions in the pH range of 3.00-7.00.
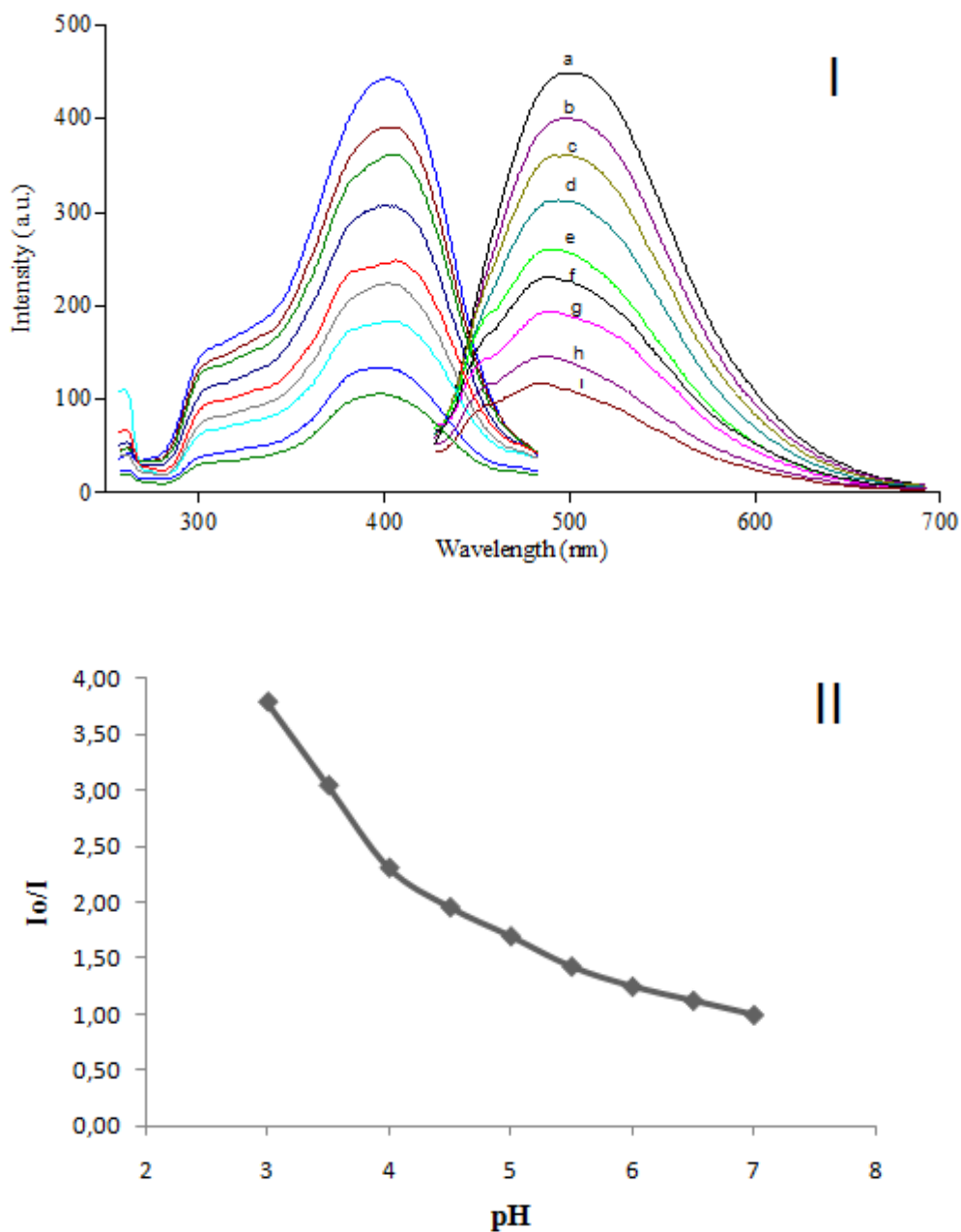
Figure 6.15 I: pH induced emission based spectral response of the PMMA doped MY10 in the pH range of. 7.00 -3.00. pH: a) 7.00 b) 6.50 c) 6.00 d) 5.50 e) 5.00 f) 4.50 g)4.00 h)3.50 j) 3.00.

II: Emission based sigmoidal response of MY10 to pH.

Figure 6.16 I: pH induced emission based spectral response of the PMMA doped MY10 in the pH range of. 7.00 -11.00. pH: a) 7.00 b) 7.50 c) 8.00 d) 8.50 e) 9.00 f) 9.50 g)10.00 h)10.50 j) 11.00.

II: Emission based sigmoidal response of MY10 to pH.

For all dyes, emission based pKa values were calculated via equation,

$$pKa = pH + \log [(Ix-Ib)/(Ia-Ix)]$$

where Ia and Ib are the fluorescence signal intensities of the dyes in their acid and conjugate base forms, respectively (Mills & Chang, 1992). pKa values of PMMA doped MY9 and MY10 were found to be 9.6 and 9.5 in thin film form, respectively.

6.3.5 Dissolved CO_2 Sensing Studies with MY9 and MY10 in Thin Film Form in EC and PMMA Matrix

Sensor performances of all of the employed dyes were also tested for dissolved CO_2. Standard solutions were prepared freshly from 1 mol L−1 $NaHCO_3$ stock solution prior to the measurements. CO_2-free standard solutions were prepared with doubly distilled water after boiling and bubbling with nitrogen; they were stored in closed containers. Certain concentrations of $NaHCO_3$ were added to the sensing agent-containing cuvette, mixed and the changes in fluorescence intensity caused by addition of different concentrations of dissolved CO_2 were measured. All the experiments were performed at room temperature (25°C).

The relative signal changes of emission spectra of the dyes were monitored. The emission based response of MY9 and MY10 dyes for dissolved CO_2 in EC matrix and linearized calibration curves of the dyes are shown in Figure 6.17 and 6.18. The observed working range is logarithmic and covers the concentration range of 4×10^{-8} to 4×10^{-4} mol L−1 for MY9 and 4×10^{-8} to 4×10^{-5} mol L−1 for MY10 in EC matrix, respectively.
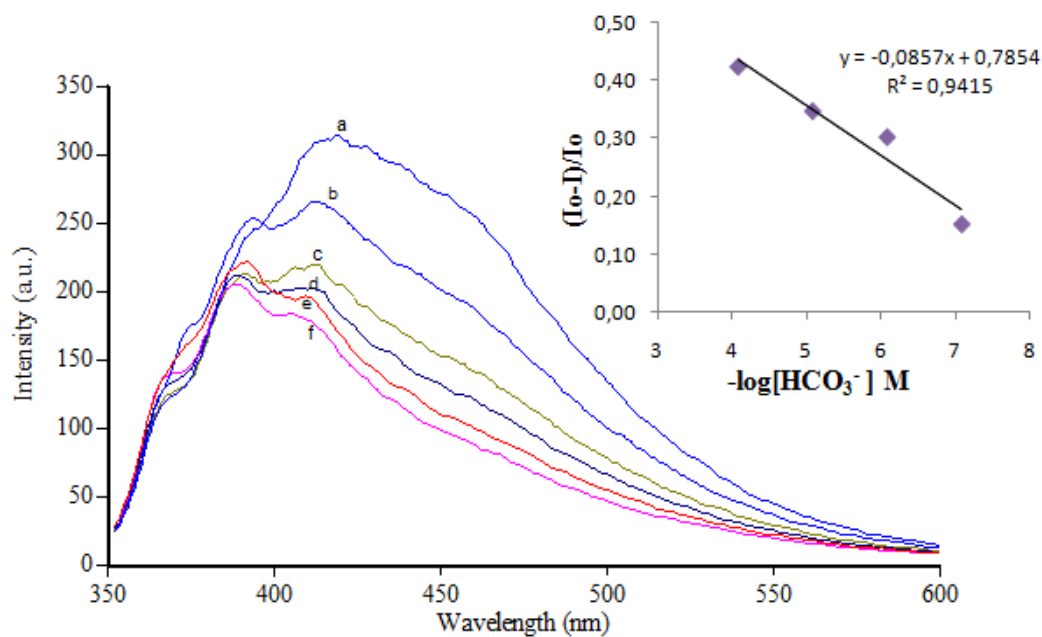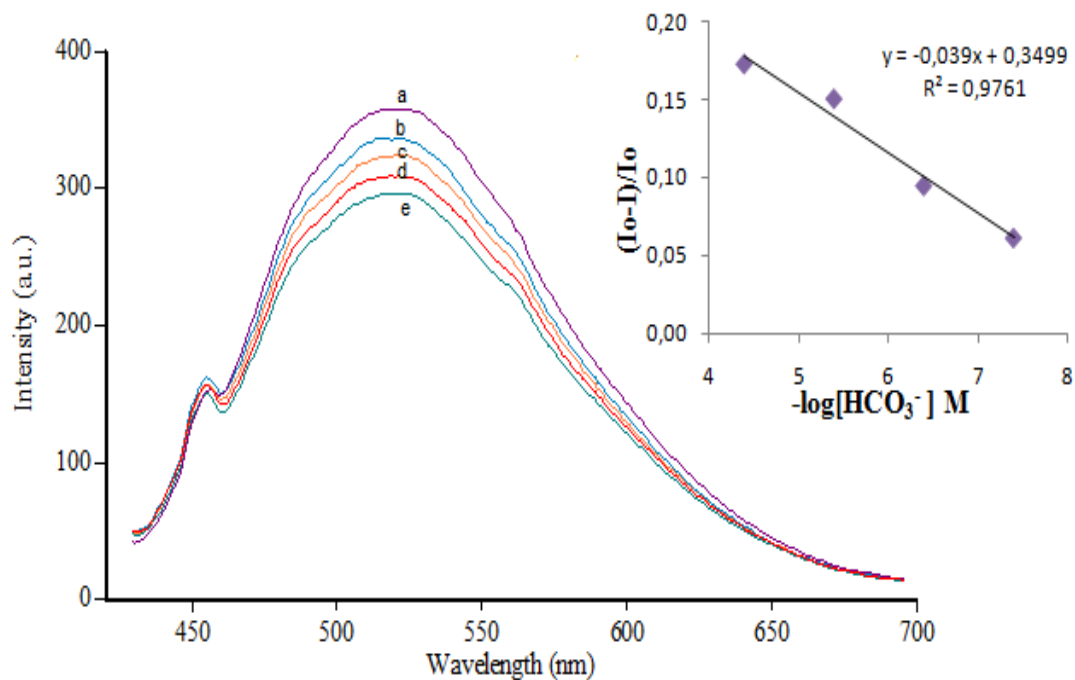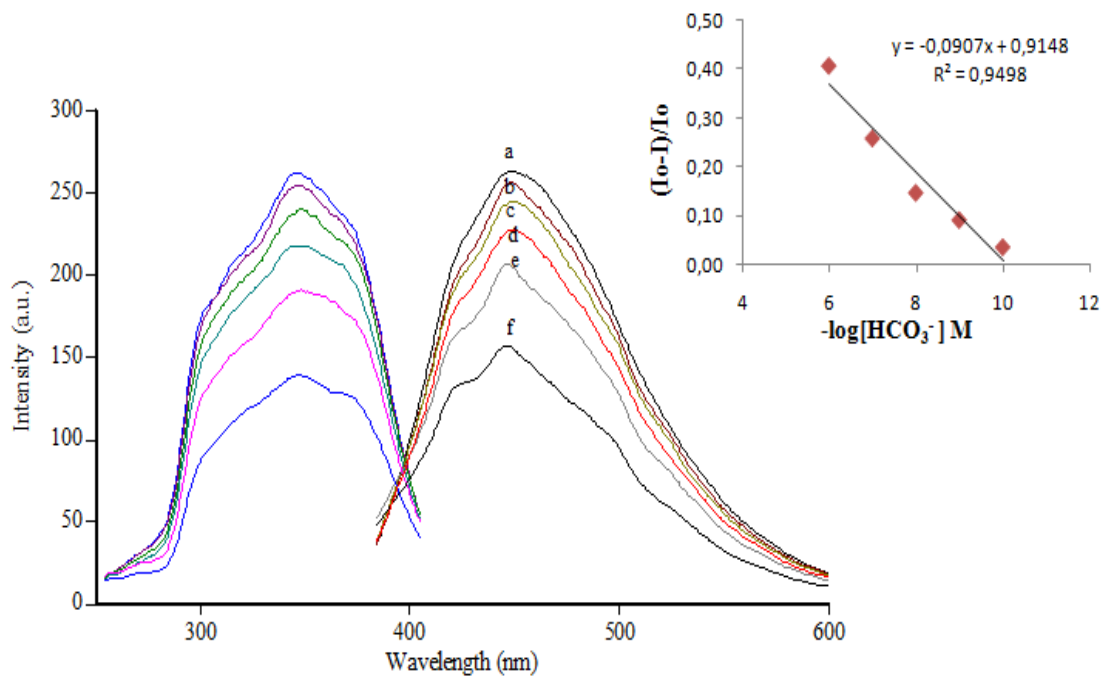
Figure 6.17 Emission spectra of immobilized MY9 in EC based thin film matrix after exposure to different HCO_3^- concentrations; (a) bicarbonate free water (b) 4.00×10^{-8} M (c) 4.00×10^{-7} M (d) 4.00×10^{-6} M (e) 4.00×10^{-5} M.
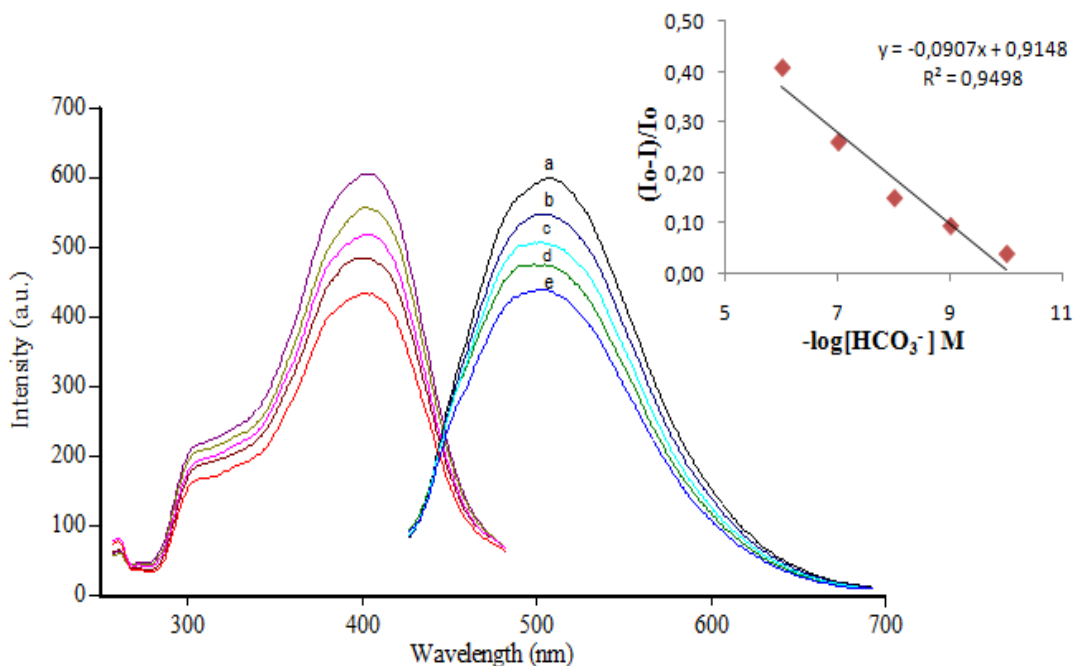

Figure 6.18 Emission spectra of immobilized MY10 in EC based thin film matrix after exposure to different HCO_3^- concentrations; (a) bicarbonate free water (b) 4.00×10^{-8} M (c) 4.00×10^{-7} M (d) 4.00×10^{-6} M (e) 4.00×10^{-5} M.

The fluorescence based response of MY9 and MY10 dyes for dissolved CO_2 in PMMA matrix and related linearized calibration curves of the dyes are shown in Fig. 6.19 and Fig. 6.20. The MY9 and MY10 dyes responded to dCO_2 in the concentration range of 1×10^{-10} to 1×10^{-6} and 1×10^{-8} to 1×10^{-5} mol L-1, respectively.

Figure 6.19 Emission spectra of immobilized MY9 in PMMA based thin film matrix after exposure to different HCO_3^- concentrations;   (a) bicarbonate free water   (b) 1.00×10^{-10} M   (c) 1.00×10^{-9} M (d) 1.00×10^{-8} M   (e) 1.00×10^{-7} M   (f) 1.00×10^{-6} M.

Figure 6.20 Emission spectra of immobilized MY10 in PMMA based thin film matrix after exposure to different HCO_3^- concentrations; (a) bicarbonate free water (b) 1.00×10^{-8} M (c) 1.00×10^{-7} M (d) 1.00×10^{-6} M (e) 1.00×10^{-5} M.

6.3.6 Linear Response for dCO₂ with MY9 and MY10 in Nanofiber Form in EC and PMMA Matrix

In this part of the study quenching-based optical chemical sensors were fabricated by the electrospinning technique utilizing the same compositions for thin film studies. Electrospinning fabrication, characterization, and dCO_2 sensing capability of these fibers were also discussed. SEM images of electrospun membranes of the EC and PMMA at various magnifications are shown in Fig 6.21, 6.22, 6.23 and 6.24. The SEM images reveal that the diameters of the EC based nanofibers were smaller than that of the PMMA based ones. Rather than type of the dye, the utilized matrix material has been effective on fiber diameters.
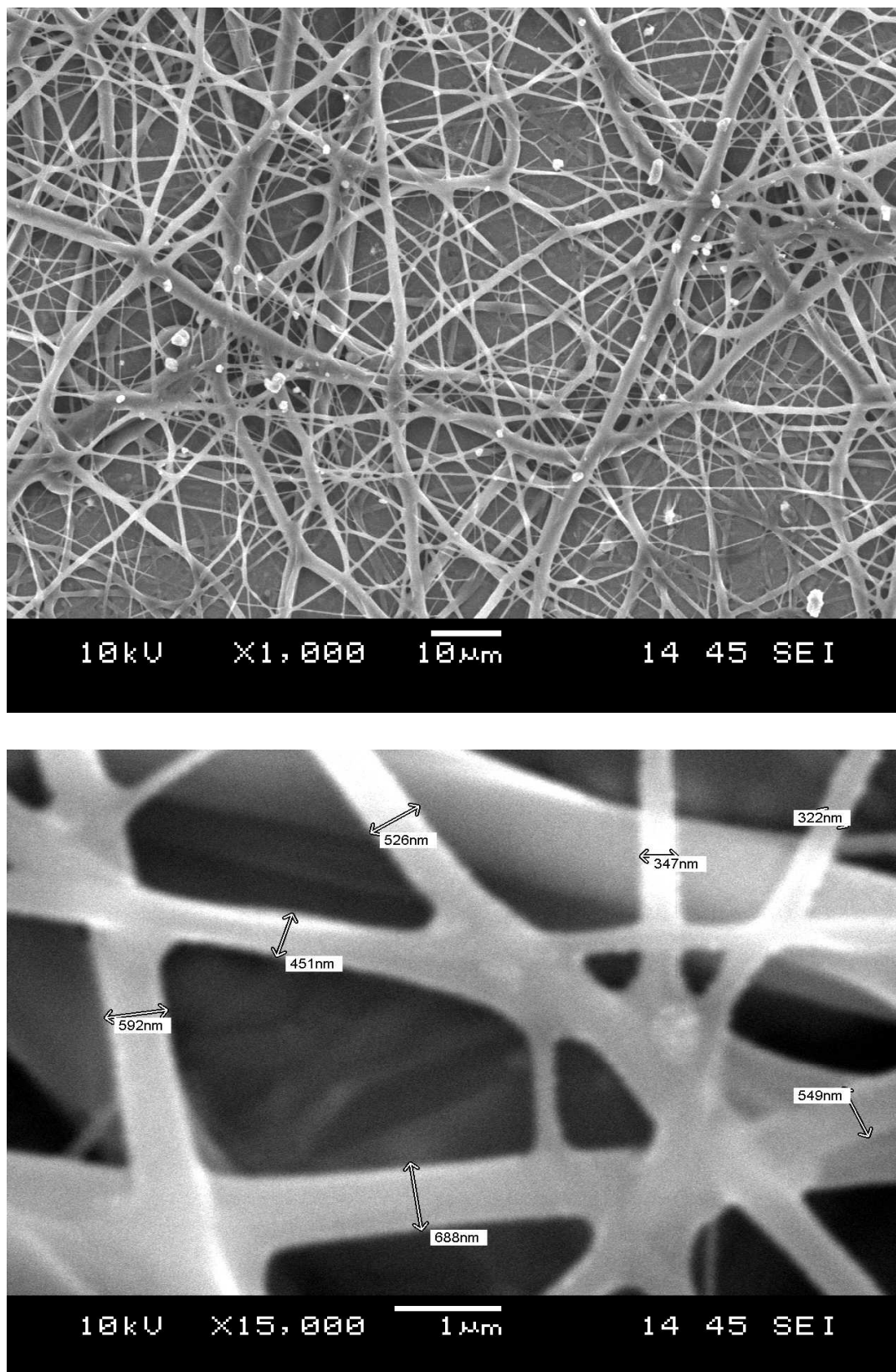
Figure 6.21 SEM images of EC based electrospun nanofibers for MY9 dye at different magnifications such as ×1 000 and ×15 000. Fiber diameters were between 322-688 nm.

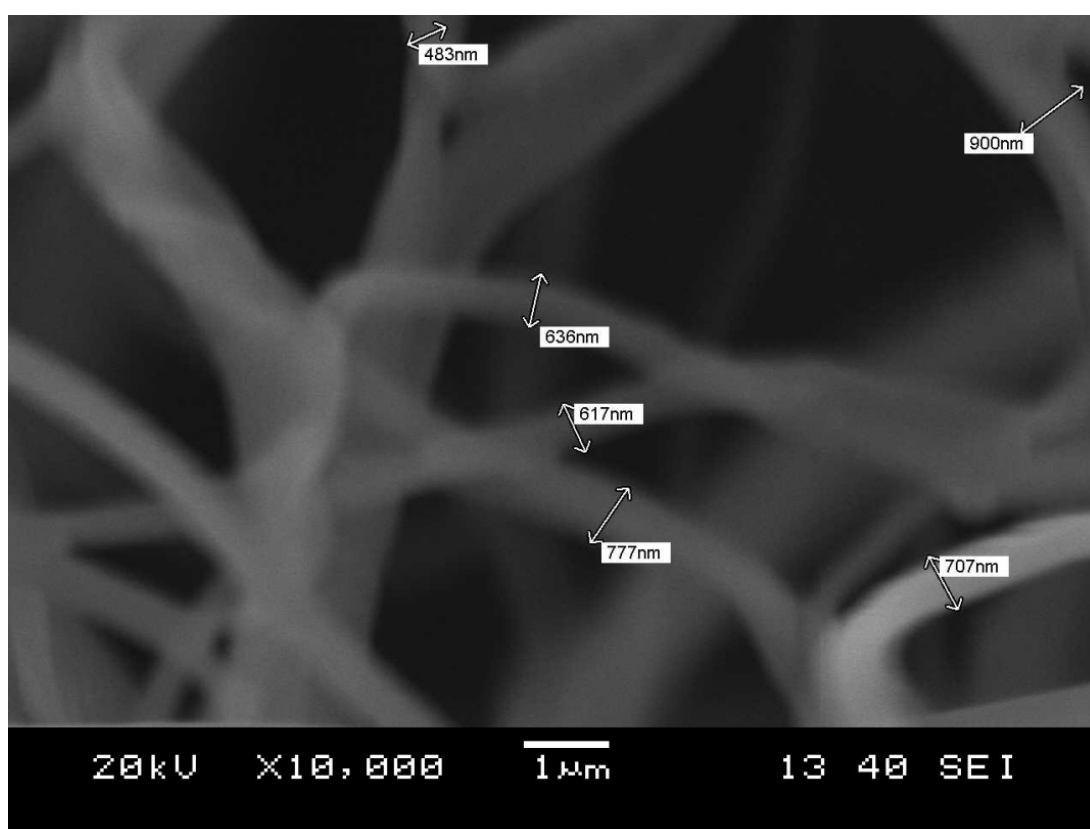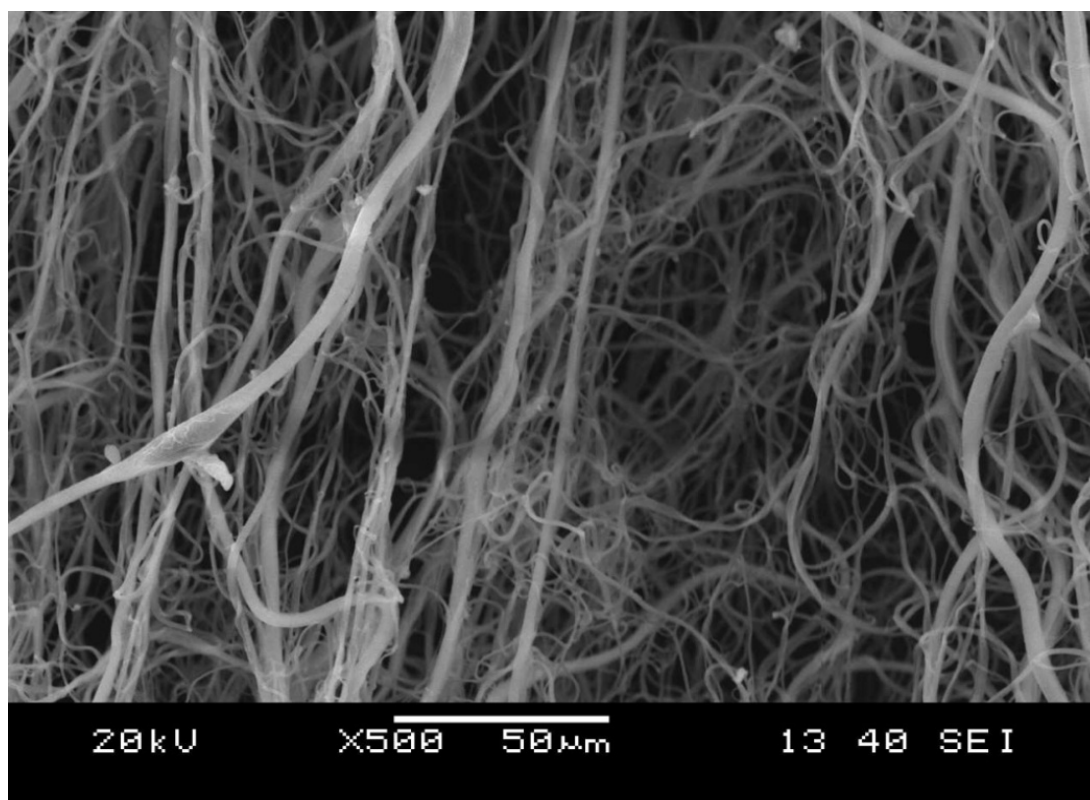Figure 6.22 SEM images of EC based electrospun nanofibers for MY10 dye at different magnifications such as ×500 and ×10 000. Fiber diameters were between 483-900 nm.

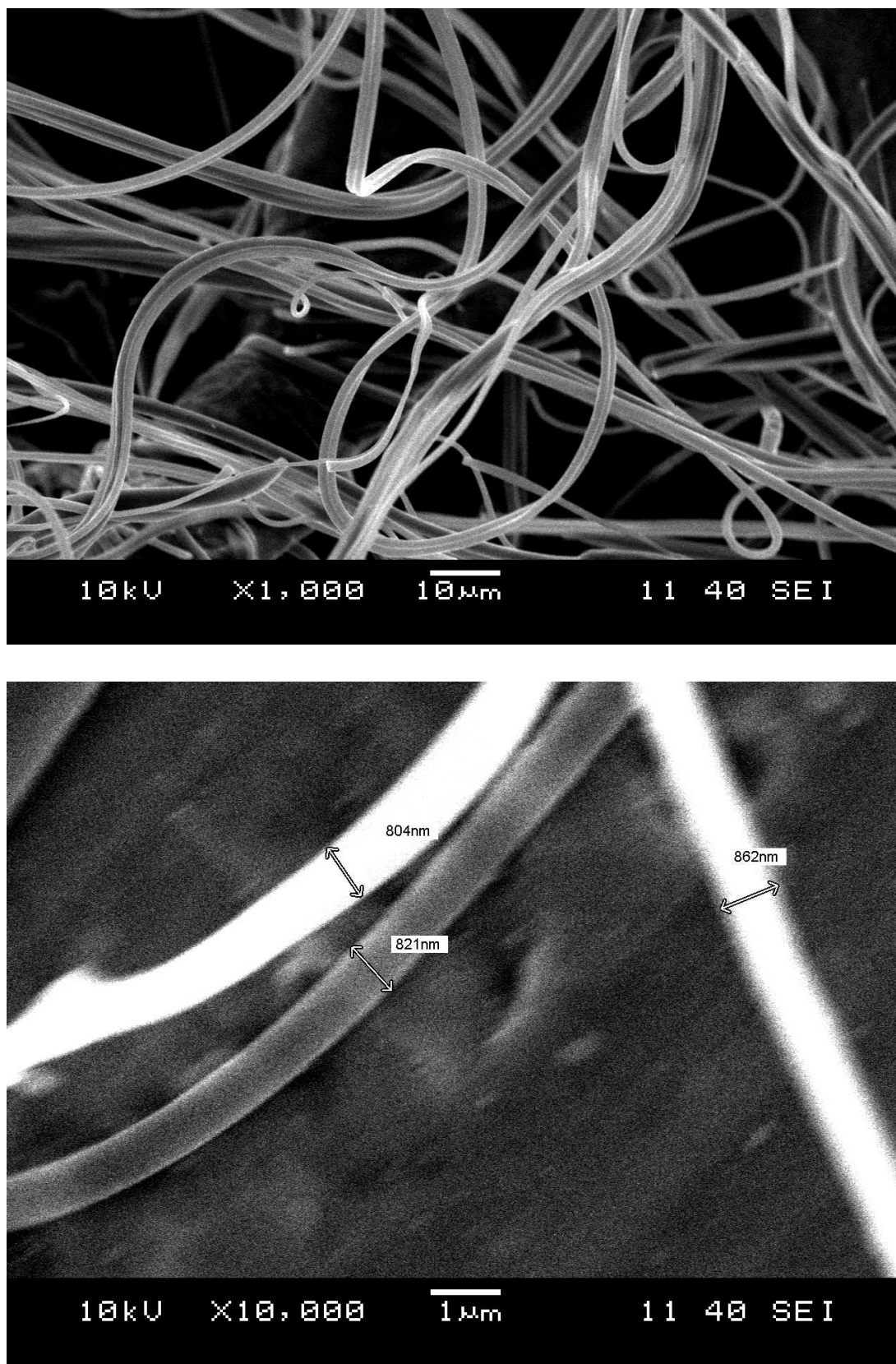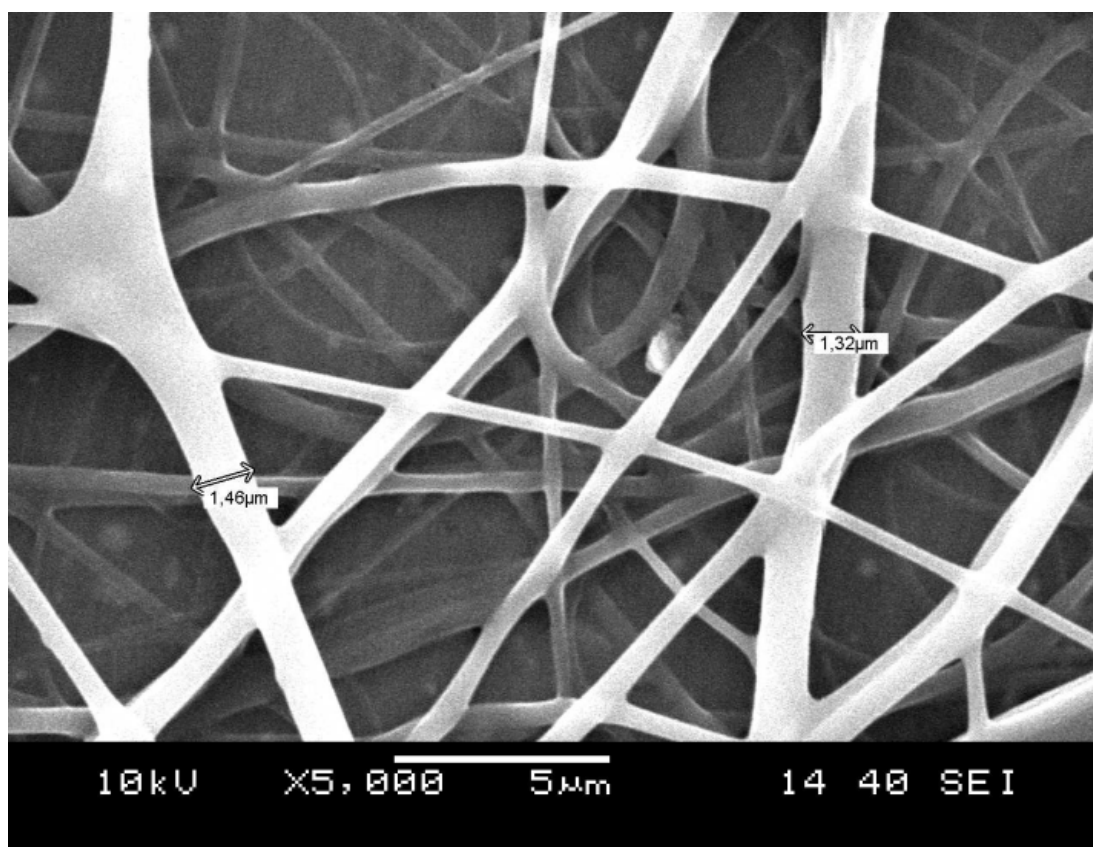Figure 6.23 SEM images of PMMA based electrospun nanofibers for MY9 dye at different magnifications such as ×1 000 and ×10 000. Fiber diameters were between 804-862 nm.
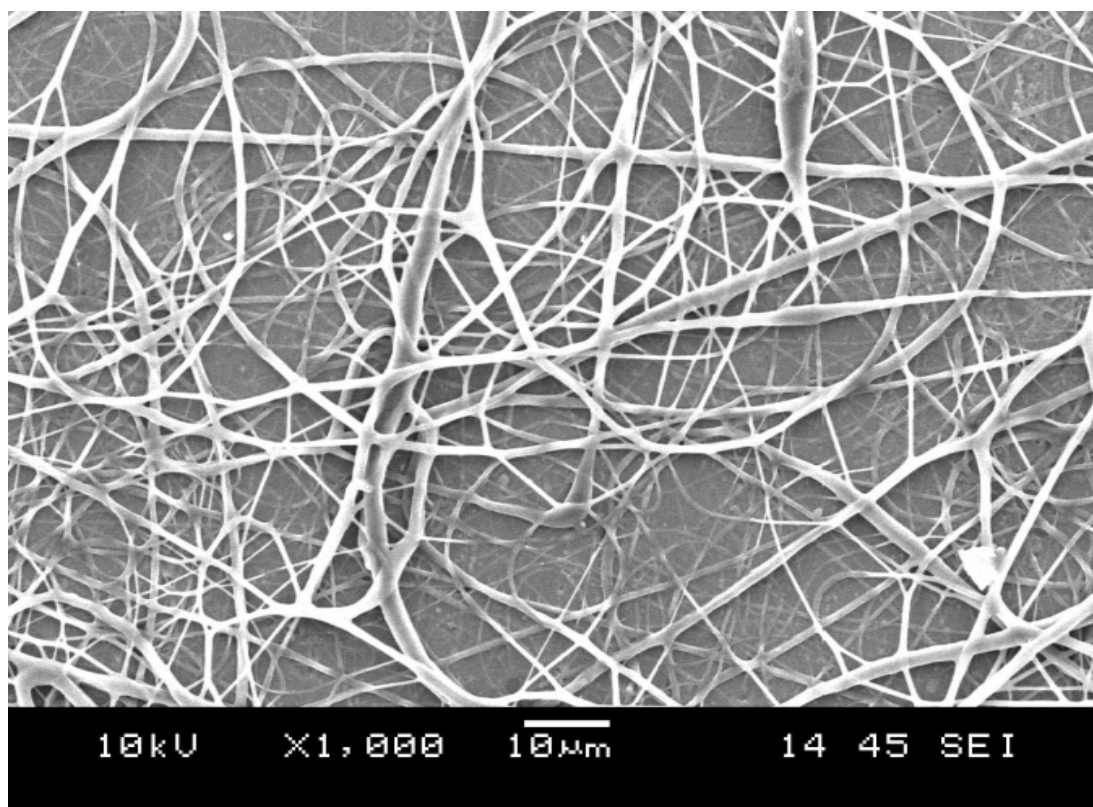
Figure 6.24 SEM images of PMMA based electrospun nanofibers for MY10 dye at different magnifications such as ×1 000 and ×5 000. Fiber diameters were between 1032-1046 nm.

Figure 6.25 and 6.26 show fluorescence quenching based response of nanofiber forms of MY9 and MY10 dyes in EC after exposure to certain concentrations of HCO_3^-. The electrospun fibers exhibited decreasing response for dCO_2 in the concentration range of 5.00×10^{-8} to 2.42×10^{-5} and 1.00×10^{-12} to 1.00×10^{-7} for MY9 and MY10 in EC matrix, respectively.
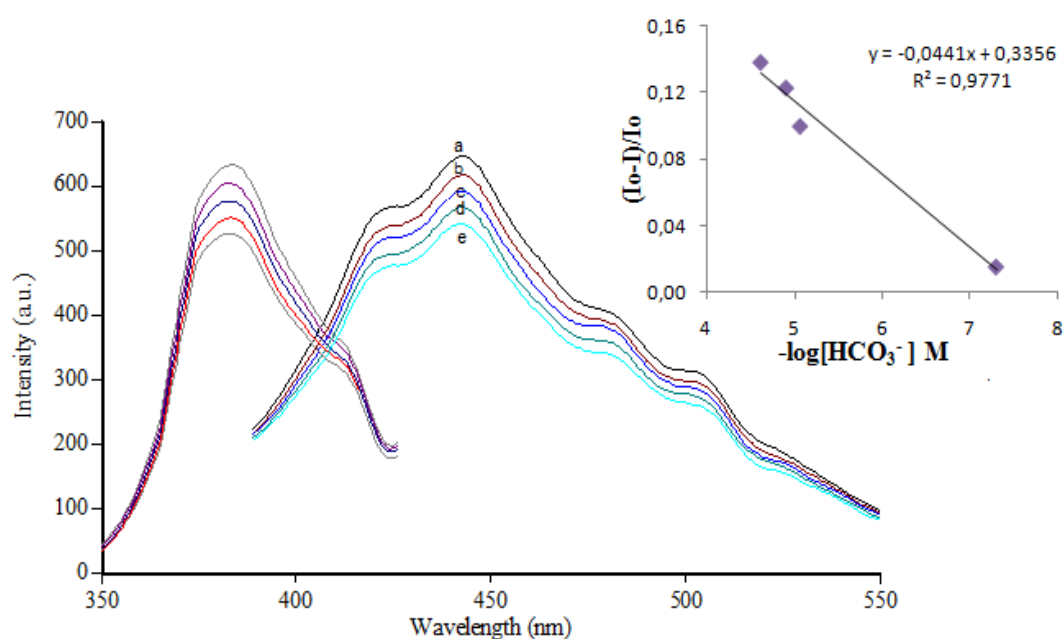

Figure 6.25 Emission spectra of immobilized MY9 in EC based nanofibers after exposure to different HCO_3^- concentrations; (a) bicarbonate free water (b) 5.00×10^{-8} M (c) 8.50×10^{-6} M (d) 1.24×10^{-5} M (e) 2.42×10^{-5} M.
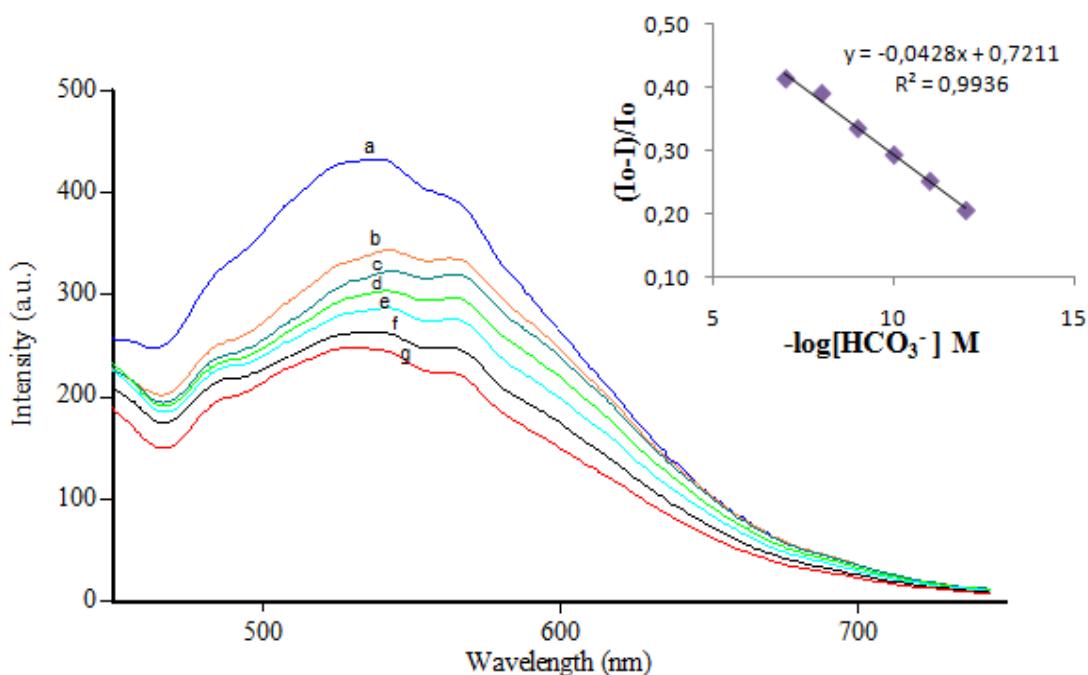
Figure 6.26 Emission spectra of immobilized MY10 in EC based nanofibers after exposure to different HCO_3^- concentrations; (a) bicarbonate free water   (b) 1.00×10^{-12} M   (c) 1.00×10^{-11} M (d) 1.00×10^{-10} M   (e) 1.00×10^{-9} M   (f) 1.00×10^{-8} M   (g) 1.00×10^{-7} M.

Nanofiber forms of the MY10 exhibited better sensitivity with respect to the thin film forms of same composition. In case of nanofiber form, for MY10, the working range was considerably expanded (from 4.00×10^{-8} - 4.00×10^{-5} to 1.00×10^{-12}-1.00×10^{-7}). Additionally, response was more lineer in case of nanofiber forms. The R^2 values of the calibration plots of thin film and nanofibers were 0.9558 and 0.9936, respectively (See insets of Fig 6.20 and Fig 6.26).

The dCO_2 response of the PMMA doped nanofiber forms of MY9 and MY10 were shown in Figure 6.27 and 6.28. They exhibited 45 % and 30 % relative signal change upon exposure to dCO_2 solutions.
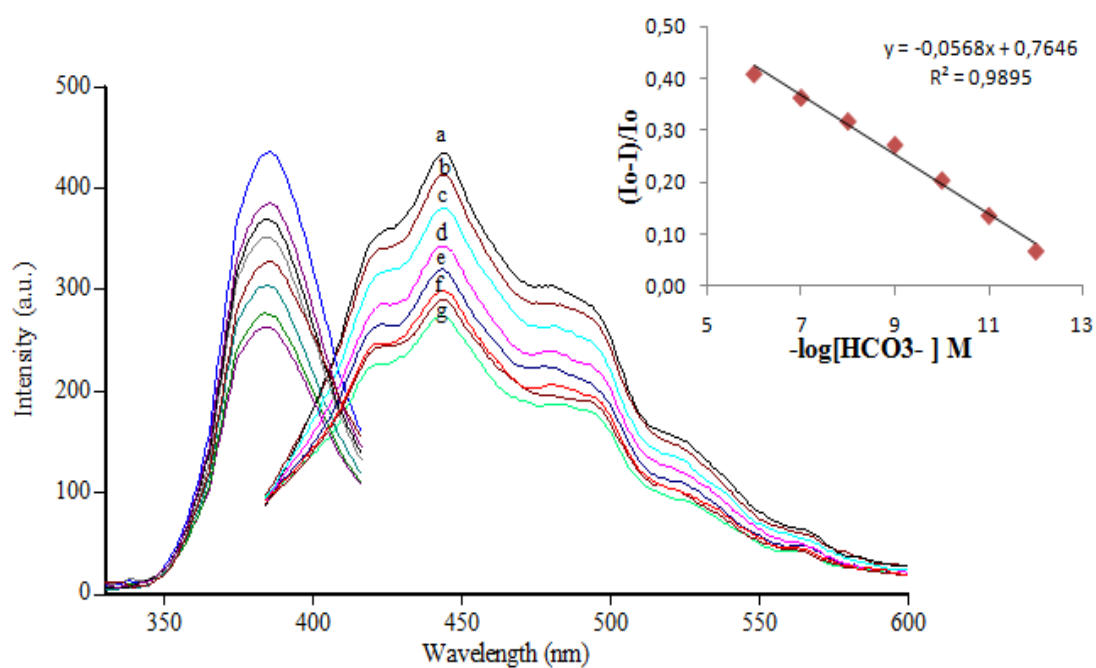
Figure 6.27 Emission spectra of immobilized MY9 in PMMA based nanofibers matrix after exposure to different HCO_3^- concentrations; (a) bicarbonate free water (b) 1.00×10^{-12} M (c) 1.00×10^{-11} M (d) 1.00×10^{-10} M (e) 1.00×10^{-9} M (f) 1.00×10^{-8} M (g) 1.00×10^{-7}; 1.00×10^{-6} M.
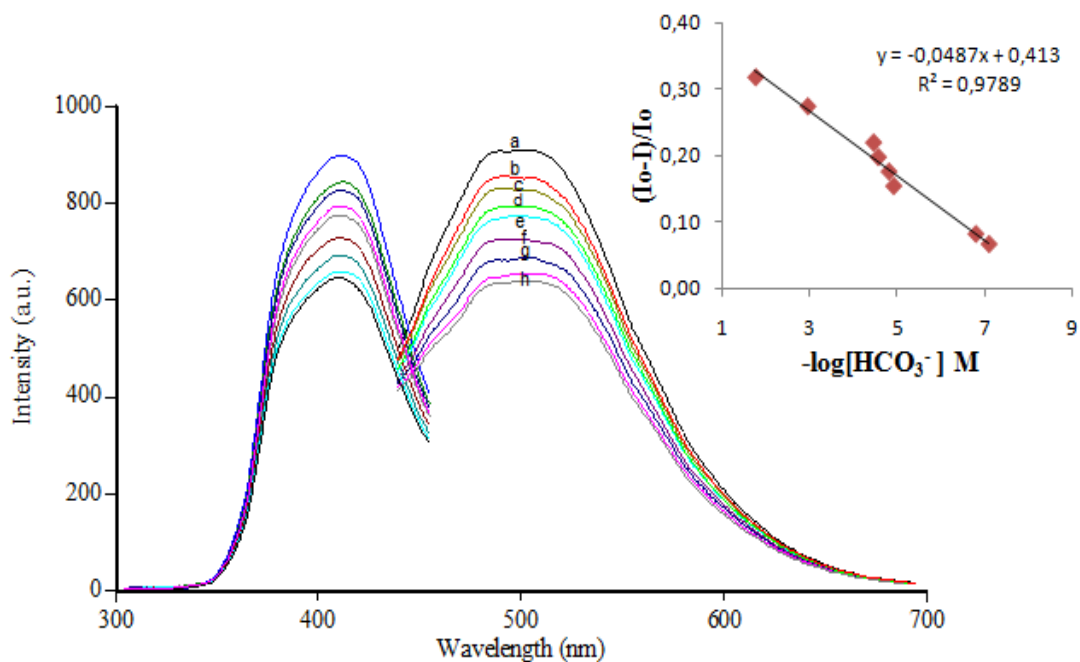

Figure 6.28 Emission spectra of immobilized MY10 in PMMA based nanofibers matrix after exposure to different HCO_3^- concentrations; (a) bicarbonate free water (b) 8.00×10^{-8} M (c) 1.60×10^{-7} M (d) 1.20×10^{-5} M (e) 1.57×10^{-5} M (f) 2.75×10^{-5} M (g) 3.50×10^{-5} M (h) 1.13×10^{-3}; 1.80×10^{-2} M.

When immobilized in PMMA the MY9 dye exhibited linear working ranges of 1.00×10^{-10}-1.00×10^{-6} mol L-1 and 5.00×10^{-8}-2.42×10^{-5} mol L-1 in nanofiber and thin film forms, respectively. The numerical values reveal that the same sensing agent works better when put into nanosize. This means enhanced sensitivity, larger working ranges and lower detectable concentrations.

The MY10 dye, when immobilized in PMMA, exhibited similar behavior to MY9 (See Figure 6.20 and 6.28).

6.3.7 Selectivity Studies

In this work we intended to study with real groundwater samples as analytical applications of the offered sensing designs. Therefore we investigated the interference possibility of large amout of anions and cations as well as pH. The pH of groundwater resources ranges from moderately alkaline (8.5) to moderately acid (5.5). The dissolved solids are usually composed mainly of sodium (Na^+), calcium (Ca^{2+}), potassium (K^+), chlorine (Cl^-), silica (SiO_2), sulfate (SO_4^{2-}), and bicarbonate (HCO_3^-) at considerably high concentrations. Minor constituents include a wide range of elements with mercury (Hg^{2+}), fluorine (F^-), boron (B) and arsenic (As) being toxic in high enough concentrations and therefore, are of environmental concern. Dissolved gases usually include carbon dioxide (CO_2), hydrogen sulfide (H_2S), ammonia (NH_3) and methane (CH_4) (Kacmaz, 2009). Determination of the dissolved CO_2 is our concern.

In order to examine the response of the MY9 and MY10 dyes to possible interfering cations, the sensing agents were treated with 5×10^{-3} M concentrations of Ag^+, Al^{3+}, Ba^{2+}, Ca^{2+}, Co^{2+}, Cr^{3+}, Cu^{2+}, Fe^{3+}, Fe^{2+}, Hg^{2+}, K^+, Li^+, Mg^{2+}, Mn^{2+}, Na^+, Ni^{2+}, Pb^{2+}, Sn^{2+} and Zn^{2+} ions in acetic acid/acetate buffer solutions at pH 5.5. The interference effects of the conventional anions; F^-, Cl^-, Br^-, NO_3^-, SO_4^{2-} and PO_4^{3-} were also tested.

Results were evaluated in terms of relative signal changes (RSC); $(I-I_o)/I_o$, where I was the fluorescence intensity of the sensing membrane after exposure to ion-containing solutions and Io is the fluorescence intensity of the sensing agent in ion-free buffer solution.

From Fig 6.29 I-II it can be concluded that, the MY9 is capable of determining bicarbonate ions (HCO_3^-). The fluorescence was dramatically quenched in the presence of HCO_3^-, exhibiting a relative signal change (RSC) ratio of 35 %. Except that of Ag^+, Ba^{2+}, Cu^{2+}, Fe^{3+} and Hg^{2+} ions the response to potential interferents cations was less than 5 %. The potential interference effects of alkaline and earth alkaline metals can be overcome adding a few drops of 0.01 M EDTA solution prior to tests.

The interference effects of the conventional anions; F^-, Cl^-, Br^-, NO_3^-, SO_4^{2-} and PO_4^{3-} were also tested. Relative signal changes of less than 1 % were observed for PMMA doped films at pH 5.5.

Figure 6.30 I-II reveals that the MY10 is capable of determining HCO_3^- ions. Only the HCO_3^-, induced fluorescence bands of MY10 dye exhibiting a RSC ratio of 58 %. The fluorescence was dramatically quenched in presence of Cu^{2+} and Fe^{2+} at 500 nm exhibiting a RSC ratio of 52 % and 40 %, respectively. Other alkali, alkaline earth, and transition metal ions produced insignificant responses where RSCs of less than 10 %. Similarly, the interference effects of Cu^{2+} and Fe^{2+} can be overcome adding masking agents and/or EDTA solutions prior to spectral analysis. Interference by iron and copper can be suppressed exploiting triethanolamine, thiourea, fluoride, acetylacetone or cyanide in the buffer as masking agents.
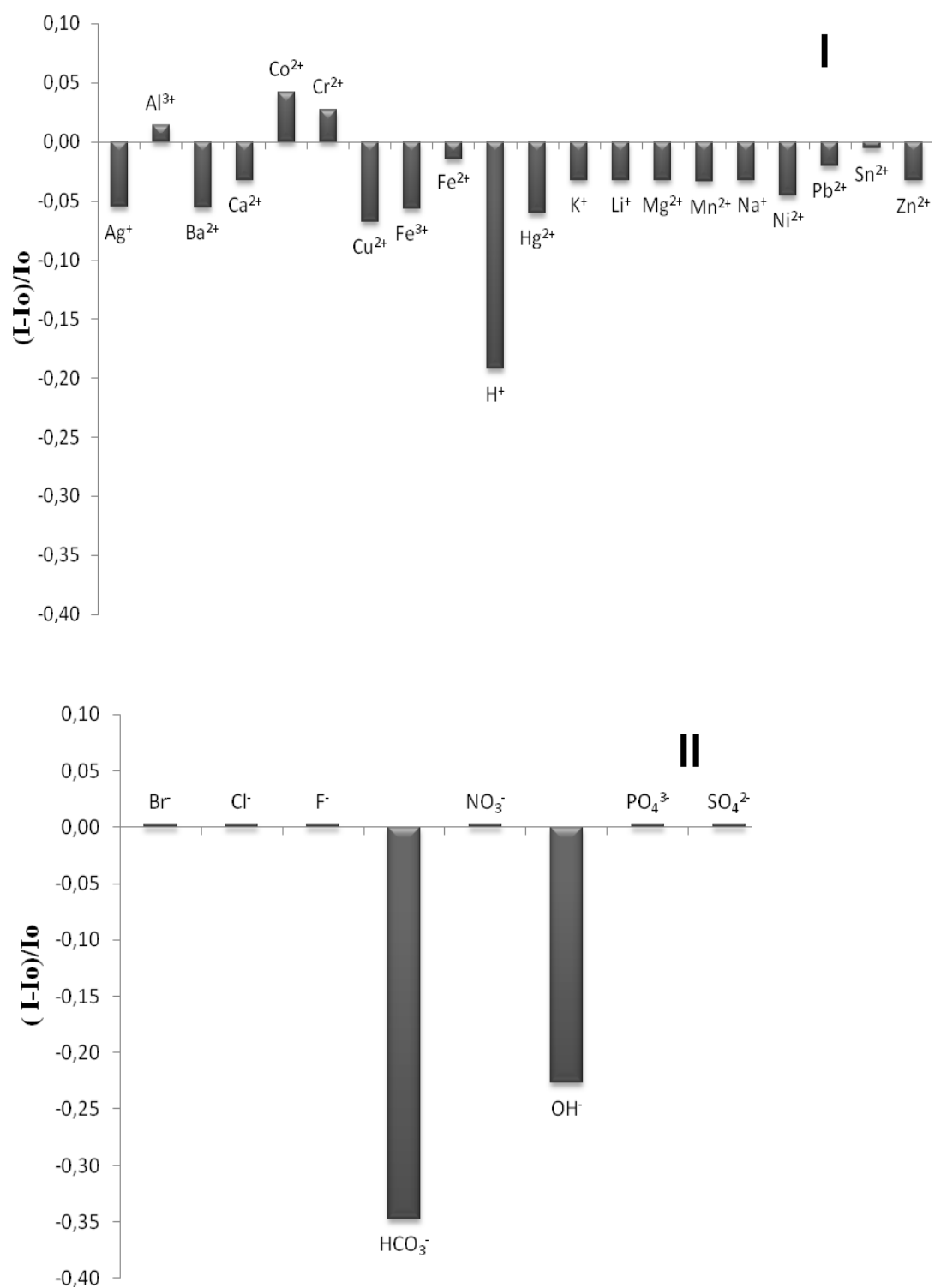
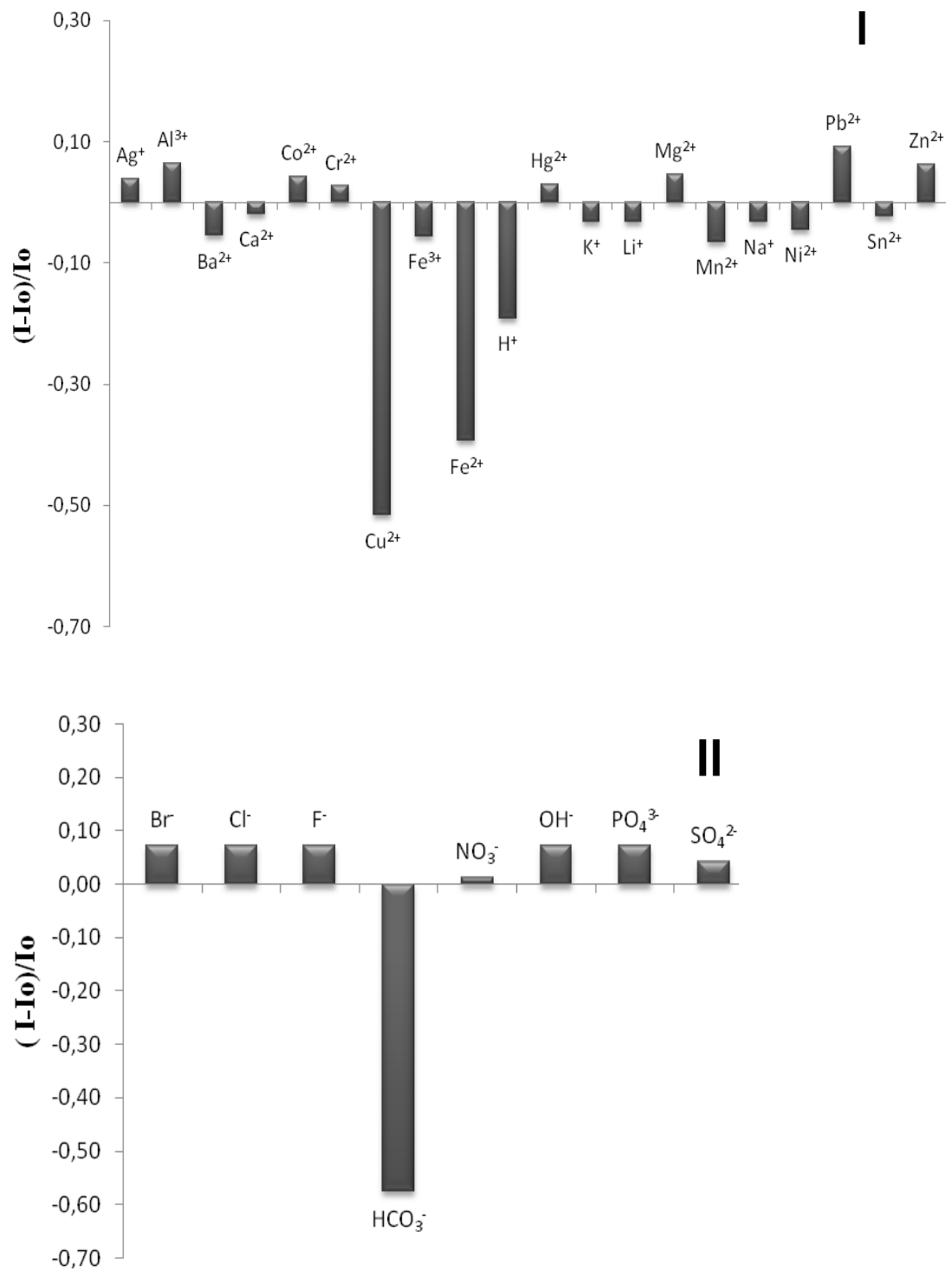Figure 6.29 Metal-ion (I) and anion (II) response test for MY9.

Figure 6.30 Metal-ion (I) and anion (II) response test for MY10.

6.3.8 Response to Groundwater Samples

Analytical applications of offerded sensing designs were tested with real groundwater samples. We collected the samples from location of Sarikiz, Manisa; Turkey; Latitude: 38.34125º N, Longitude: 28.52355º. The temperature of water from well was remarkably constant and 16.9ºC.

Prior to spectral tests, ion chromatographic (IC) analysis of groundwater samples was performed. Seven anions (Fluoride, Chloride, Nitrite, Bromide, Nitrate, Phosphate, and Sulfate) and six cations (Lithium, Sodium, Ammonium, Potassium, Magnesium, and Calcium) were analyzed with IC. Results of chromatographic measurements and heavy metal compositions were shown Table 6.5 and 6.6, respectively. The bicarbonate analysis was performed both with potentiometric method and exploiting indicators.

6.3.9 Chromatographic Measurements

6.3.9.1 Chromatographic System

The instrument for ionic analysis of anions was from Dionex. The hardware used for these analyses consisted of an ICS-1000 ion chromatograph equipped with an isocratic pump, a conductivity detector, a self regenerating suppressor (ASRS ultra II 4mm), an AS40 autosampler and a column heater. Eluent flow rates were set at 1 mL/min with an injection volume of 25μL. An IonPac AG9-HC (50mm×4mm I.D.) guard column and an IonPac AS9-HC (250mm×4mm I.D) analytical column were used to separate the anions. The current of the suppressor was set at 45 mA to give a background conductivity of 25.5-26.5 μS.

An Ion Pac® CG12A (50mm×4mm I.D.) guard column and an Ion Pac® CS12A (250mm×4mm I.D) analytical column were used to separate the cations. The current of the suppressor was set at 59 mA to give a background conductivity of 1.5-2 μs. The complete operating conditions and the composition of the eluent used by the ion

chromatography systems during the chromatographic runs were summarized in Table 6.3 and 6.4. All measurements were performed at 30°C. The pre-treated samples were filtered through 0.45 μm filters before injection, and kept in high density polyethylene containers at 25°C.

Table 6.3 Operating conditions for anion analysis (was taken from Zeyrek, 2008).

IC	
Ion-chromatographic unit	Dionex ICS-1000 IC
Pump	GP50 gradient pump
Guard column	IonPac® AG9-HC Guard, 50mm×4mm I.D
Column	IonPac® AS9-HC Analytical, 250mm×4mm I.D
Column temperature	30 ∘C
Suppressor	ASRS Ultra II 4mm
Suppressor current	45 mA
Eluent	9mM NaCO3
Eluent source	Dionex EluGen® EGC-KOH cartridge
Flow-rate	1 mL/min
Detector	Dionex CD20 conductance detector
Cell temperature	35 ∘C
Injection volume	25μL
Run time	30 min
Background conductance	≈25.5-26.5mS
Back pressure	≈2000 psi
Data management	Chromeleon® 6.5 chromatography workstation
Auto sampler	AS-40

Table 6.4 Operating Conditions for cation analysis (was taken from Kacmaz, 2009).

IC	
Ion-Chromatographic Unit	Dionex ICS-1000 IC
Pump	GP50 Gradient Pump
Guard Column	IonPac® CG12A Guard, 50mm×4mm I.D
Column	IonPac® CS12A Analytical, 250mm×4mm I.D
Column Temperature	30 ∘C
Suppressor	CSRS Ultra II 4mm
Suppressor Current	59 mA
Eluent	20mM Methanesulfonic acid
Eluent Source	Dionex EluGen® EGC Cartridge
Flow-Rate	1 mL/min
Detector	Dionex DS6 Heated Conductivity Cell
Cell Temperature	35 ∘C
Injection Volume	25μL
Run Time	12.5 min
Background Conductance	≈1.5-2 mS
Back Pressure	≈1050 psi
Data Management	Chromeleon® 6.5 Chromatography Workstation
Auto Sampler	AS-40

6.3.9.2 Reagents and Samples

Deionized water with a resistivity greater than 18.2 MΩcm generated by a Milli-Q deionized water unit was used for the preparation of all the solutions. Working standard solutions were prepared by serial dilution of Certified Reference anion standard solution of Dionex (Fluoride 20 mg/L, Chloride 30mg/L, Nitrite 100mg/L, Bromide 100 mg/L, Nitrate 100mg/L, Phosphate 150 mg/L, Sulfate 150mg/L) with deionized water in the ratio of 1:1, 3:4, 1:2, 1:3, 1:4, 1:8, 1:12 and 1:60. Calibration curves were obtained with standards using the concentrations 1:1, 3:4, 1:2, 1:4, 1:60. All reagents were of analytical reagent grade unless otherwise specified. Separations were performed with 9.0 mM sodium carbonate as the eluent. The experimental procedure involved choice of column type, eluent concentration and flow rate, reagent concentration and flow rate, dilution ratio and integration parameters. Most of these parameters were selected based upon literature references, personal experience and operators' manuals of Dionex (Zeyrek, 2008).

Certified reference cations standard (CRS) solution of Dionex were used throughout the study. Methansulfonic acid (1 M) was obtained from DIONEX and used for the mobile phase for seperation of cations. The mobile phase was prepared daily before use. For preparing 20 mM eluent, 20 mL methansulfonic acid added to the volumetric flask and finally diluted to 1000 mL by water.

Table 6.5 Results of ion chromatographic measurements for groundwater samples of Sarikiz.

Anion/Cation	Amount (ppm)
Fluoride	0,13
Chloride	13,32
Nitrite	<LOD
Bromide	<LOD
Nitrate	2,90
Phosphate	<LOD
Sulfate	92,68
Lithium	0,2
Sodium	56,00
Ammonium	<LOD
Potassium	5,87
Magnesium	67,00
Calcium	91,00

Table 6.6 Heavy metal composition of Sarikiz (taken from http://www.sarikiz.com.tr/esasanaliz.html).

Heavy Metal	ppm (mg/(L)
Antimony	0
Arsenic	0.001
Copper	0.018
Barium	0.069
Boron	0.01
Mercury	0
Cadmium	0
Chromium	0.015
Lead	0
Manganese	0.077
Nickel	0.005

6.3.10 Potentiometric Measurements

Potentiometric and indicator based measurements were performed in accordance with literature information given in page 15. pH and potential measurements were recorded with an Orion pH meter. The pH meter was calibrated with buffers prior to measurements. Potentiometric titration curve of 50 mL of bicarbonate containing groundwater sample (diluted 1:1000) with 0.1 M HCl was shown in Figure 6.31. A comparision of results of volumetric methods with proposed method was given in Table 6.6 the MY9 dye was choosen for comparision due to the more appropriate working range for concentrated groundwater samples. The inflection points were estimeated visually.
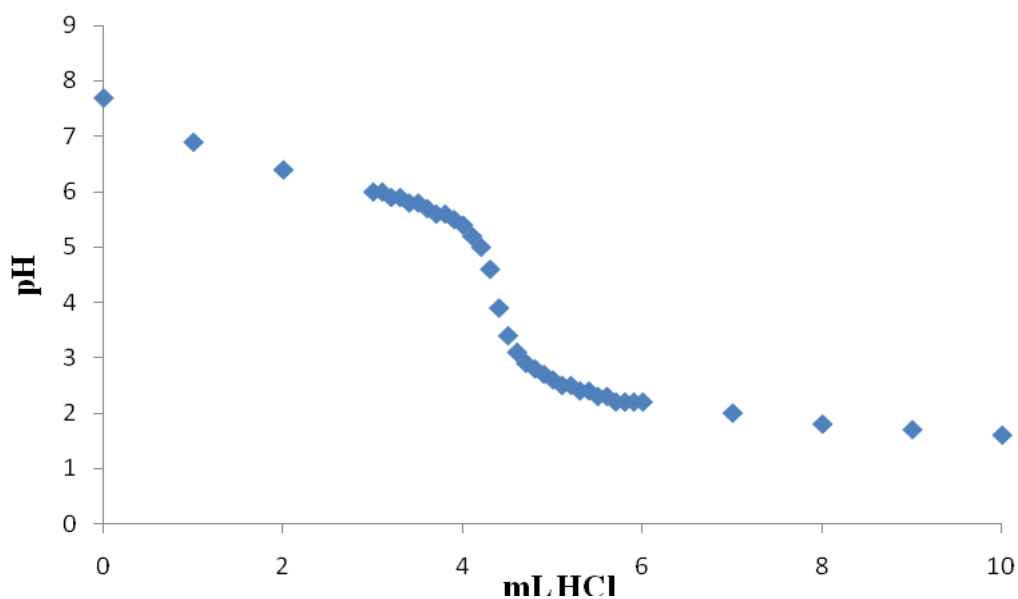
Figure 6.31 Potentiometric titration curve of groundwater sample with 0.1 M HCl.

Table 6.6 A comparision of results of volumetric methods with proposed method.

Method	Sarıkız
Potentiometric Method (mol/L) HCO_3^-	0.0122
Titration with indicator (phenolphatelyn and methyl orange) (mol/L) HCO_3^-	0.0125
Proposed Method with MY9 (mol/L) HCO_3^-	0.00122

6.4 Conclusions

In this chapter two newly synthesized indicator dyes N'-[(E)-(9-methyl-9H-carbazol-3-yl) methylidene] pyridine-4-carbohydrazide (MY9) and N'-{(1E, 2E)-3-[4-(dimethylamino) phenyl] prop-2-en-1-ylidene} pyridine-4-carbohydrazide (MY10) were investigated spectroscopically. The dyes were embedded in EC and PMMA matrices. Their thin film and nanofiber forms were fabricated, acidity constants were calculated and competibilities for dCO_2 sensing were evaluated.

The relative signal changes of emission spectra of the dyes were monitored both thin film and nanofiber forms after addition of certain concentrations of HCO_3^- solutions. For all dyes electrospun films offered enhanced sensitivity and reactivity with respect to continuous thin films. The MY9 and MY10 dyes are promising fiber optic compatible fluorescent indicators for dissolved CO_2 sensing.

CHAPTER SEVEN
EMISSION BASED BICARBONATE SENSING WITH ELECTROSPUN NANOFIBERS

In this chapter the newly synthesized dyes; MY2, MY4 and MY5; were characterized in different solvents and in polymer matrix of EC. We encoded the bicarbonate sensitive fluorescent dyes; *N'*-[(*E*)-(2-hydroxyphenyl) methylidene] pyridine-4-carbohydrazide as MY2, *N'*-[(*E*)-(3-hydroxyphenyl) methylidene] pyridine-4-carbohydrazide as MY4 and *N'*-[(*E*)-(4-nitrophenyl) methylidene] pyridine-4-carbohydrazide as MY5. Indicator dyes were synthesized in our laboratories according to the literature method and characterized with 1H NMR and IR based data (Manikandan, Viswanathamyrthi & Muthukumar, 2011; Thomas et al., 2011) by Prof.Dr. Yavuz Ergün. Schematic structures of the employed molecules are shown in Figure 7.1.

The first part of this study covers determination of the photophysical properties of indicator dyes, pH dependent response and ınterferenference effects. In the second part the performance of the sensor for dissolved carbon dioxide in thin film and nanofiber form is reported. In the third part of the study proposed optic sensors were used for HCO_3^- analysis in real groundwater sample. Obtained results were compared classical titrimetric method.

7.1 Structural Identification of MY2, MY4 and MY5 Dyes

The molecules MY2, MY4 and MY5 were characterized with 1H NMR and IR based data.

MY2: IR (KBr): 3179 (NH), 1678 (C=O), 1612 (C=N) cm^{-1}.

^{1}H-NMR (400 MHz, CDCl$_3$): δ 6.89-7.60 (m, 4H, ArH), 7.82-7.84 (d, 2H, pyridine H), 8.35 (s, N=CH), 8.77-8.79 (d, 2H, pyridine H), 9.98 (s, 1H, NH), 11.06 (s, 1H, OH), mp=229 ^{o}C.

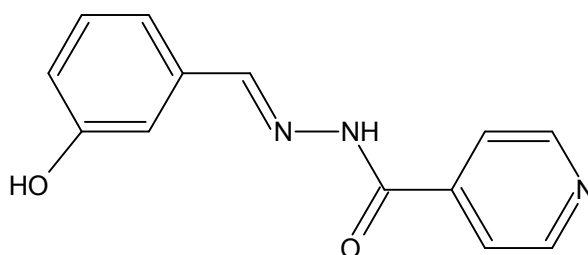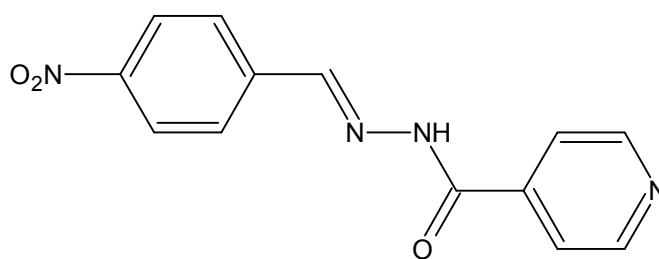**MY4**: IR (KBr): 3233 (NH), 1657 (C=O), 1610 (C=N) cm^{-1}.

^{1}H-NMR (400 MHz, CDCl$_3$): δ 6.80-7.54 (m, 4H, ArH), 7.80-7.82 (d, 2H, pyridine H), 8.33 (s, N=CH), 8.76-8.79 (d, 2H, pyridine H), 9.95 (s, 1H, NH), 11.20 (s, 1H, OH), mp=250 ^{o}C.

MY5: IR (KBr): 3220 (NH), 1684 (C=O), 1615 (C=N) cm^{-1}.

^{1}H-NMR (400 MHz, d$_6$-DMSO): δ 7.60-7.62 (d, 2H, ArH), 7.89-7.93 (d, 2H, ArH), 8.11 (s, 1H, NH), 8.34 (s, 1H, N=CH), 8.51-8.55 (d, 2H, pyridine H), 9.32-9.35 (d, 2H, pyridine H), mp=205 ^{o}C.
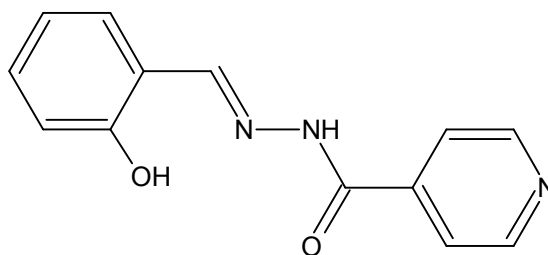
MY-2

MY-4

MY-5

Figure 7.1 Schematic structures of the employed molecules, MY2, MY4 and MY5.

7.2 Thin Film and Nanofiber Preparation Protocols

The optode membranes were prepared by mixing of 240 mg of polymer (EC), 192 mg of plasticizer (DOP), 48 mg of IL, 6 mg of dye and in 1.5 mL of THF in a glass vial. The solution was immediately shaken vigorously to provide homogeneity. The prepared mixture contained 50 % polymer and 50% additivies of plasticizer and ionic liquid. We referred these mixtures as cocktails. The resulting cocktails were spread onto a 125 μm polyester support (MylarTM type) by knife coating and located in a THF saturated dessicator.

In thin film form the employed polyester support was optically fully transparent, ion impermeable and exhibited good adhesion to EC. Each sensing film was cut to 1.2 cm width and fixed diagonally into the sample cuvette and the excitation and fluorescence emission spectra were recorded.

The nanofibers were prepared employing the same composition explained for the thin films. Electrospun nanofibers were produced by electrospinning technique. The solution flow rate was maintained at 1.0 mL/h using the syringe pump. An electric potential of 25 kV was applied between the needle of the syringe and the substrate. The nanofiber was collected on an aluminum substrate. The electrospun membranes exhibited good adhesion to the aluminum. The deposited nanofibers were cut into proper size, fixed in the flow cell and the excitation or emission spectra were recorded. For the flow system experiments, the films were cut to 1 cm width and 1 cm long and placed into the 300 μL black-Teflon flow cell and interfaced with the fiber tip (6mm diameter). Flow rate of the peristaltic pump was kept at 2.4 mL min-1. The electrospun nanofibers were characterized using scanning electron microscopy (SEM) and their average diameter was evaluated.

7.3 Results and Discussion

7.3.1 Absorption Based Spectral Characterization

Absorption spectra of the MY2, MY4 and MY5 dyes were recorded in solvents of EtOH, DCM, THF and EC matrix (see Figure 7.2, 7.3 and 7.4) for spectral characterization.
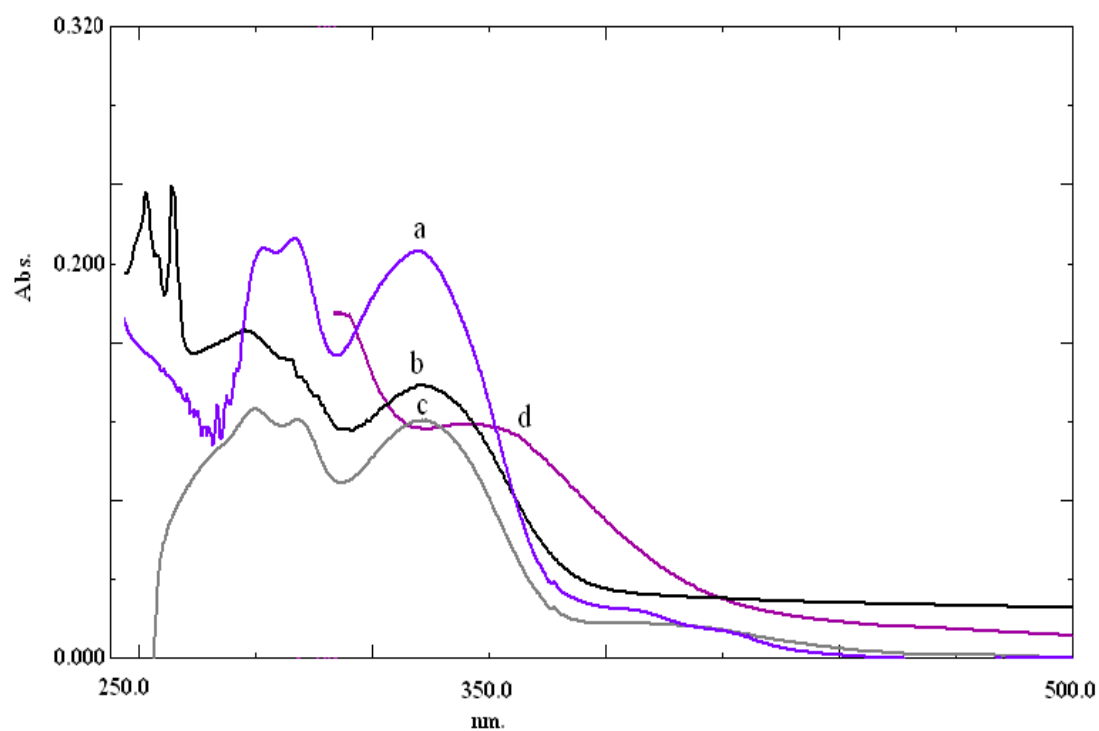

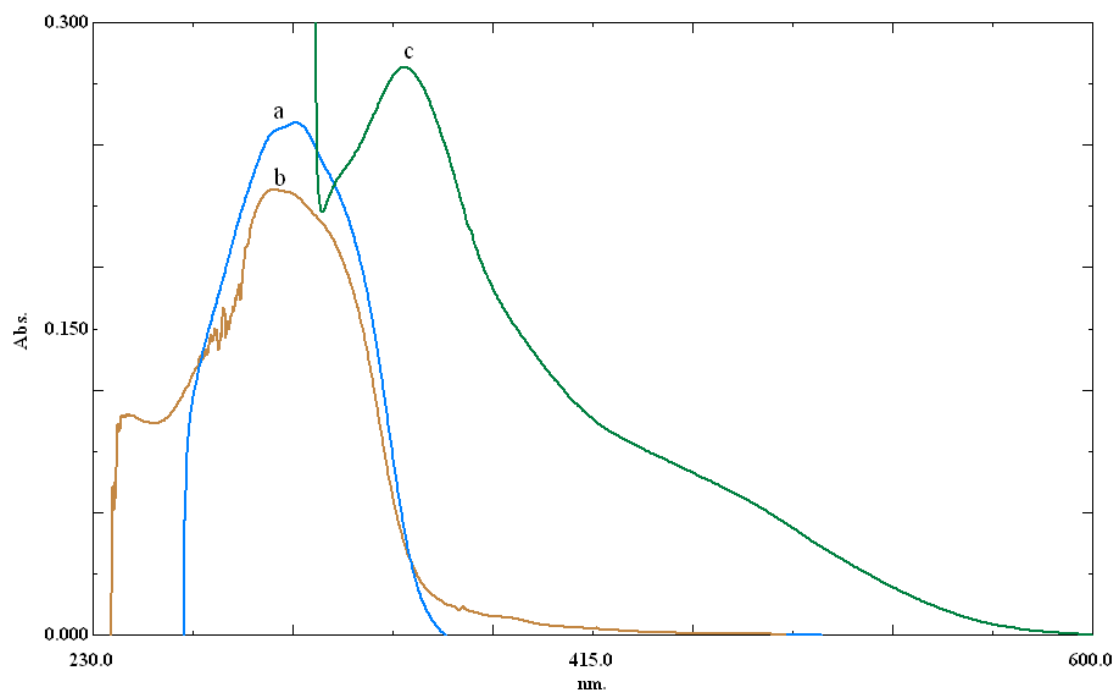Figure 7.2 Absorption spectra of the MY2 dye in a: THF   b: EtOH   c: DMF   d: EC.

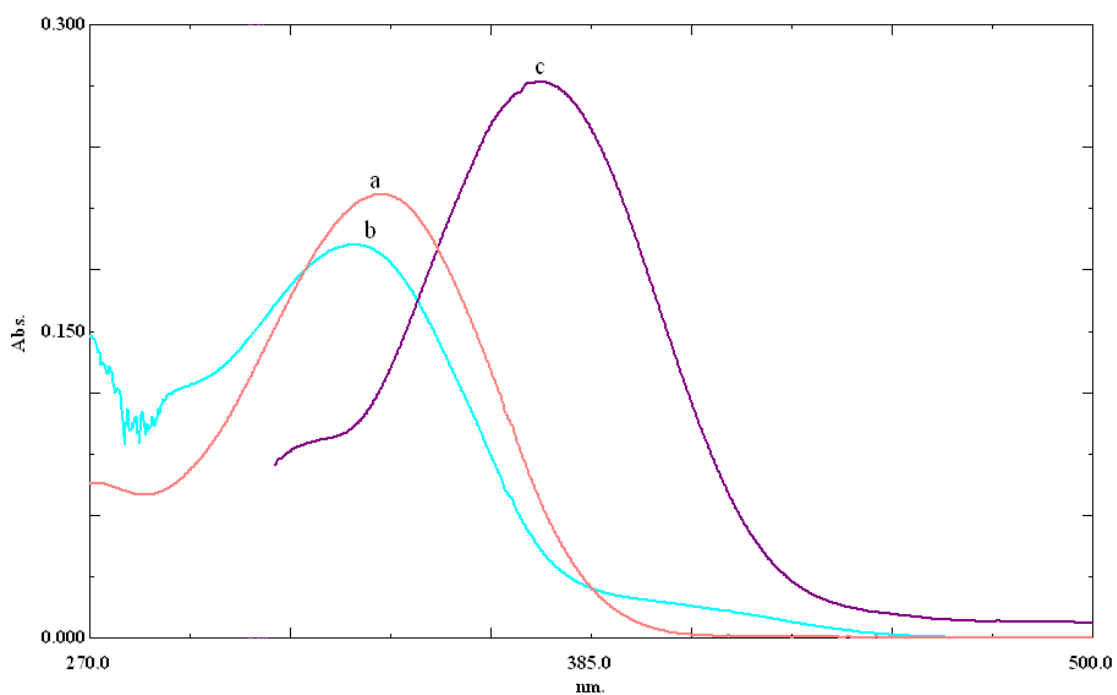Figure 7.3 Absorption spectra of the MY4 dye in a: DMF   b: THF   c: EC.

Figure 7.4 Absorption spectra of the MY5 dye in a: DMF b: THF   c: EC

Table 7.1 reveal UV-VIS spectra related characteristics (absorption maxima; λabs, and molar extinction coefficient; ε), of MY2, MY4 and MY5, respectively. Subjective dyes exhibited strong absorption bands around 330, 300 and 330 nm in

EtOH, THF and/or DMF. When immobilized in EC, the metioned absorption maxima of MY2, MY4 and MY5 were red shifted 22, 45 and 43 nm, respectively.

In agreement with literature (Ertekin and et.al, 2000) molar extinction coefficients (ε_{max}) of employed indicators were also increased in EC with respect to (ε_{max}) solution phase. These data can be taken as proofs that MY2, MY4 and MY5 molecules absorb better in plasticized EC matrices with respect to solution phase.

Table 7.1 UV-Vis spectra related data of MY2, MY4 and MY5 in the solvents of EtOH, THF and DMF and in solid matrices of EC.

Compound	Matrix	λ_{abs}^1 (nm)	λ_{abs}^2 (nm)	ε_{max} (L×mol-1× cm-1)	ε_{max} (L×mol-1× cm-1)
MY2	EtOH	334	289	49700	57800
MY2	THF	332	300	20800	21500
MY2	DMF	333	--	12300	--
MY2	EC	352	--	64200	--
MY4	DMF	305	--	25200	--
MY4	THF	297	--	21900	--
MY4	EC	345	--	60340	--
MY5	DMF	337	--	21800	--
MY5	THF	330	--	19300	--
MY5	EC	373	--	65700	--

7.3.2 Emission Spectra Related Characteristics and Assessment of Compatibility with Solid State Optics

Excitation and corrected emission spectra of employed molecules were recorded in solvent and solid matrices. The emission spectra were corrected using commercially available silica ground of the instrument. Figure 7.5, 7.6 and 7.7 and Table 7.2 reveal emission based spectral characteristics of the dyes. In all of the employed matrices the Stoke's shift values, $\Delta\lambda_{ST}$, calculated from the spectral data were quietly high.
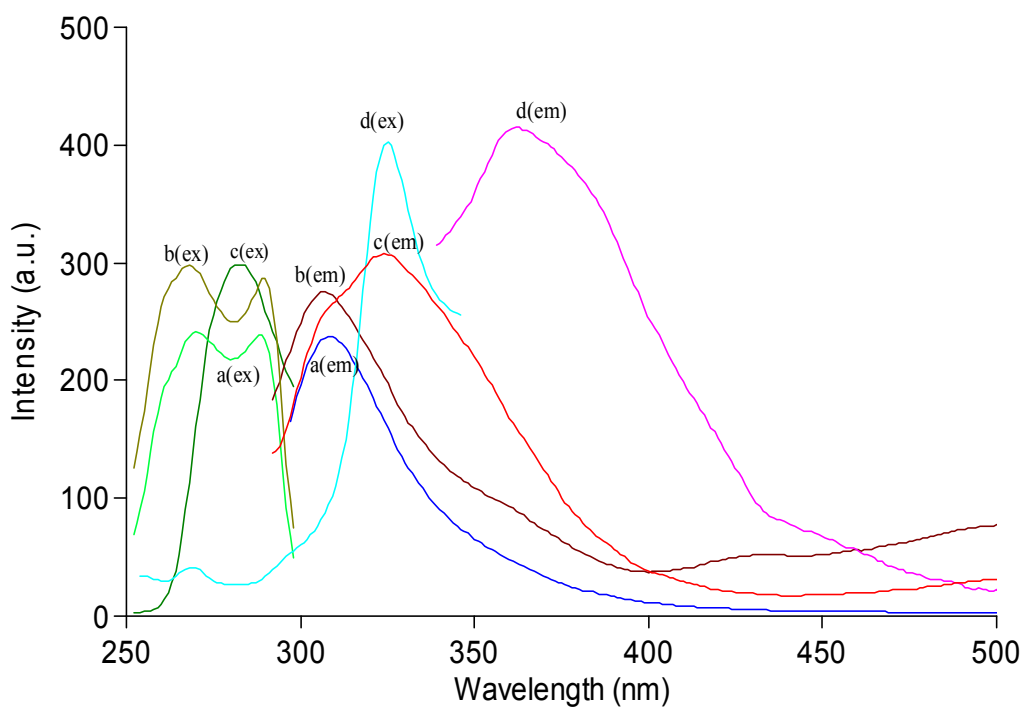
Figure 7.5 Excitation and corrected emission spectra of the MY2 dye in   a: THF   b: EtOH c: DMF d: EC.
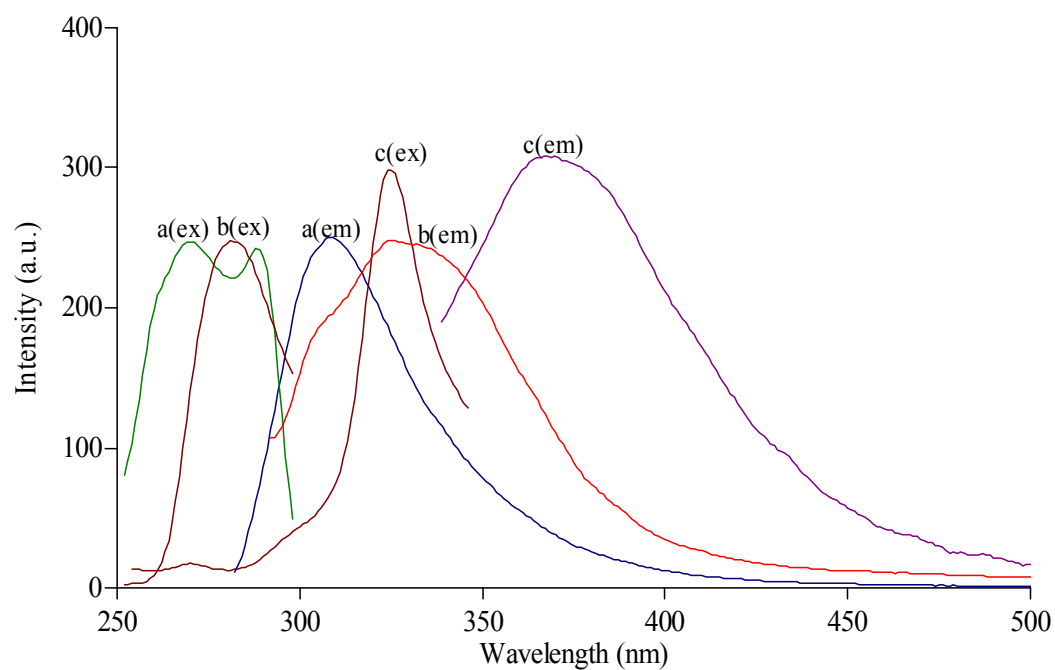
Figure 7.6 Excitation and corrected emission spectra of the MY4 dye in a: THF   b: DMF c: EC.
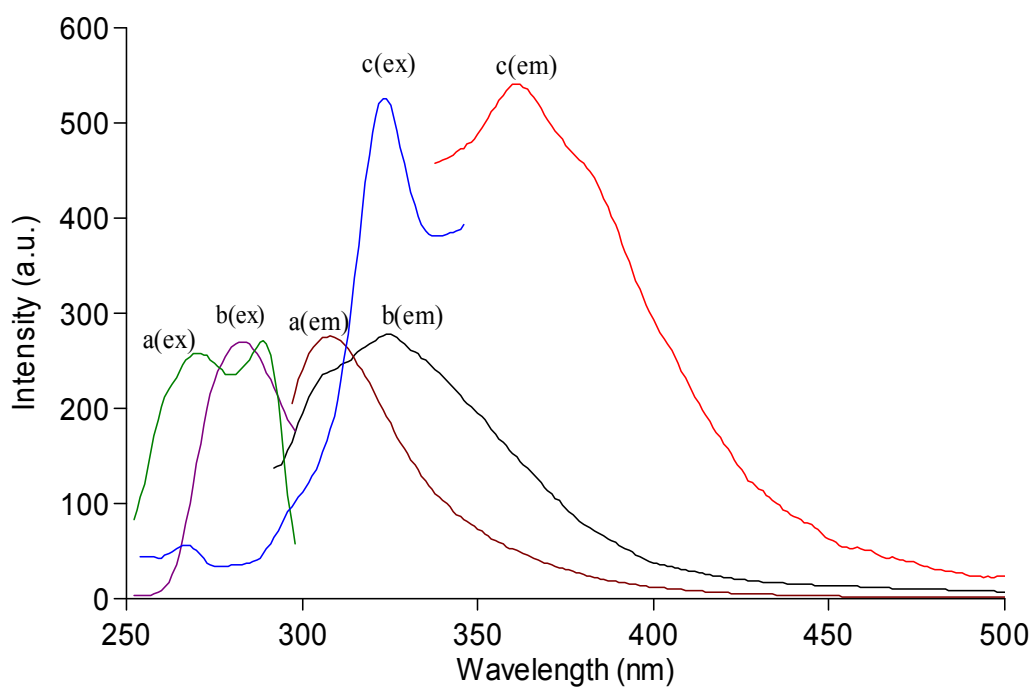
Figure 7.7 Excitation and corrected emission spectra of the MY5 dye in a: THF   b: DMF   c: EC.

Table 7.2 Spectral characterization of MY2, MY4 and MY5 dyes: $\lambda_{\max}^{em}$: maximum emission wavelength in nm; $\lambda_{\max}^{ex}$: maximum excitation wavelength in nm; $\Delta\lambda_{ST}$: Stoke's shift and Φ_F : Quantum yield.

Compound	Matrix	$\lambda_{\max}^{ex}$	$\lambda_{\max}^{em}$	$\Delta\lambda_{ST}$ (Stoke's shift)	Φ_F Quantum yield
MY2	THF	290	310	20	1.218×10^{-1} in THF
MY2	EtOH	290	310	20	
MY2	DMF	285	325	40	
MY2	EC	325	365	40	0.2586 in EC
MY4	THF	290	310	20	3.18×10^{-1} in THF
MY4	DMF	280	330	50	
MY4	EC	320	370	50	0.5709 in EC
MY5	THF	280	310	30	1.79×10^{-1} in THF
MY5	DMF	285	325	45	
MY5	EC	320	360	40	0.7609 in EC

In all of the employed matrices, Stoke's shift values were high enough and extended from 20 to 50 nm. In immobilized forms the dyes MY2, MY4 and MY5 exhibited Stoke's shift values of 40, 50 and 40 nm, respectively. A high Stoke's shift value of is a desirable characteristic for fluorescence and optical sensor studies because the high Stoke's shift value allows the emitted fluorescence photons to be easily distinguished from the excitation photons. Stoke's shift exceeding 30 nm is recommended for easy visualization and sensitive detection. The observed Stoke's

shift values permit the usage of these dyes in together with solid-state optic components such as bifurcated optical fibers and LEDs for UV region of electromagnetic spectrum.

7.3.3 Fluorescence Quantum Yield Calculations

Fluorescence quantum yield values (Φ_F) of the MY2, MY4 and MY5 were calculated employing the comparative William's method (Williams et al., 1983), which involves the use of well-characterized standards with known Φ_F values. For this purpose, the UV-Vis absorbance and corrected emission spectra of different concentrations of reference standard Quinine Sulphate (λ_{ex} = 350 nm, quantum yield (Φ_F) = 0.546 in H_2SO_4) and the employed molecules were recorded, and, the integrated fluorescence intensities were plotted versus corresponding absorbances (See Figure 7.8-10).
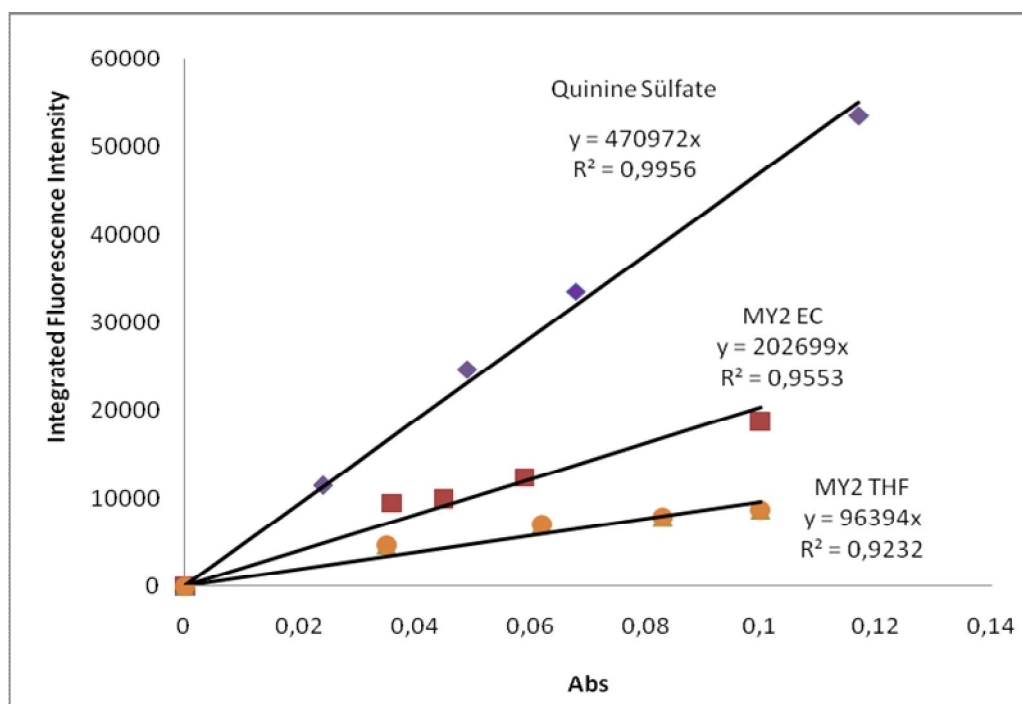
Figure 7.8 The integrated fluorescence intensities vs absorbance for the reference standard; quinine sulphate in H_2SO_4, MY2 dye in EC and THF matrices.
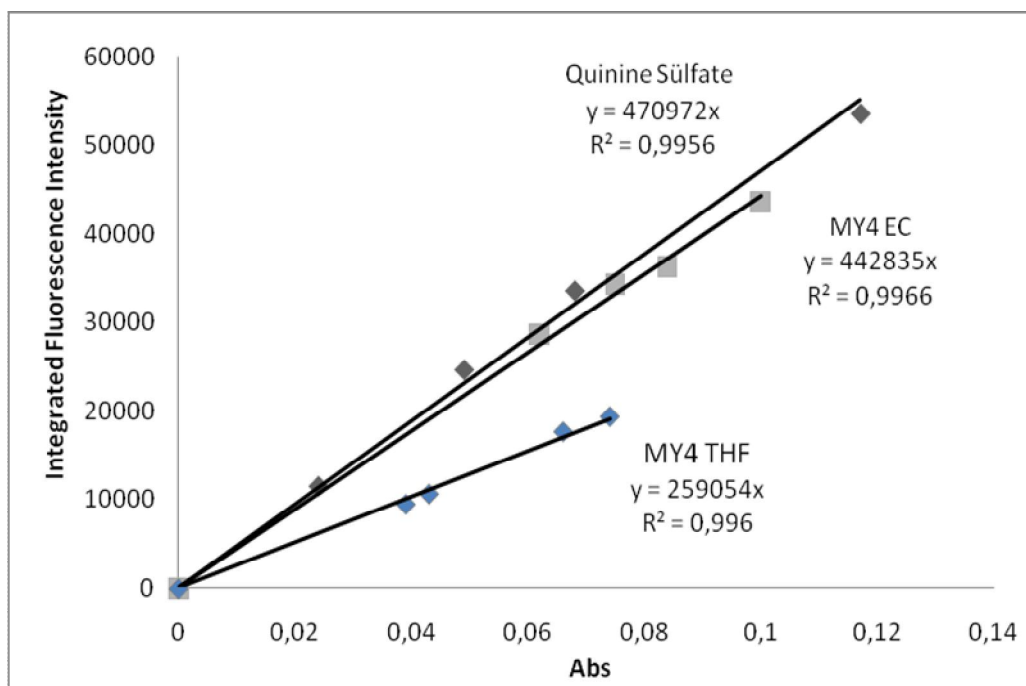
Figure 7.9 The integrated fluorescence intensities vs absorbance for the reference standard; quinine sulphate in H_2SO_4, MY4 dye in EC and THF matrices.
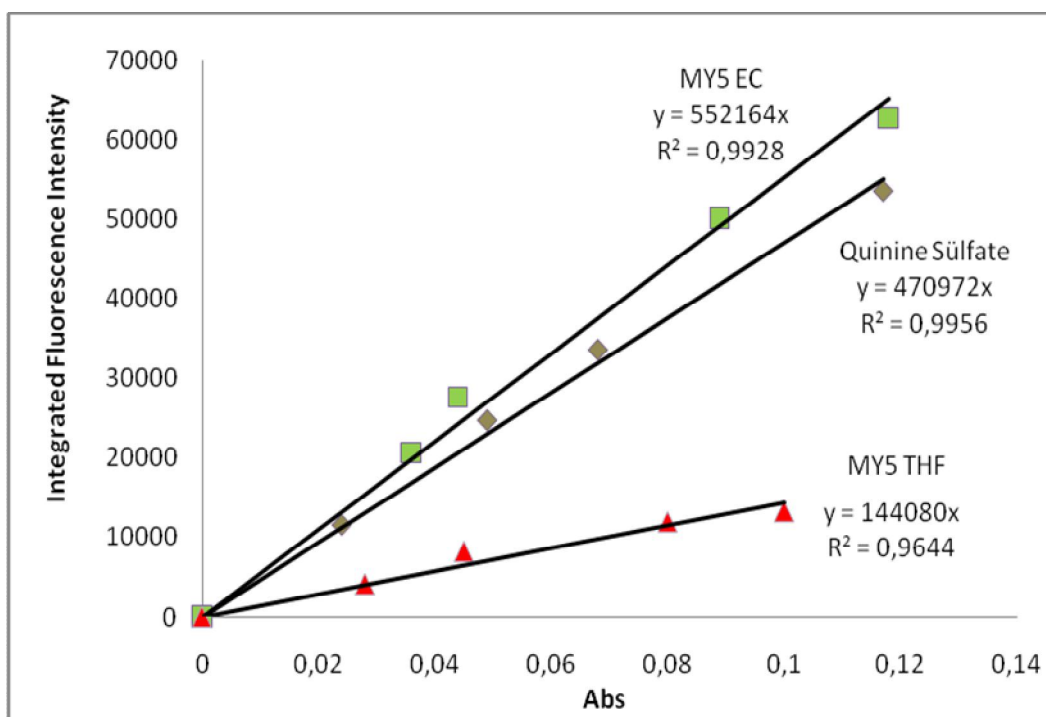

Figure 7.10 The integrated fluorescence intensities vs absorbance for the reference standard; quinine sulphate in H_2SO_4, MY5 dye in EC and THF matrices.

7.3.4 Acid–Base Behavior of the MY2, MY4 and MY5

In order to calculate acidity constant (pKa) of employed molecules, their acid-base behavior investigated in EtOH or DMF solvents. Dye solutions were titrated with 10^{-3} M solutions of nonaqueous $HClO_4$ or tetrabutylammonium hydroxide (TBAOH), and after each addition, pH values of the media and absorption spectra were recorded. pH-dependent absorption spectra of MY2, MY4 and MY5 were shown in Figure 7.11-16, respectively.

The MY2 dye did not exhibit significant relative signal change in EtOH both in acidic and basic region of the pH scale (See Figure 7.11 and 7.12).
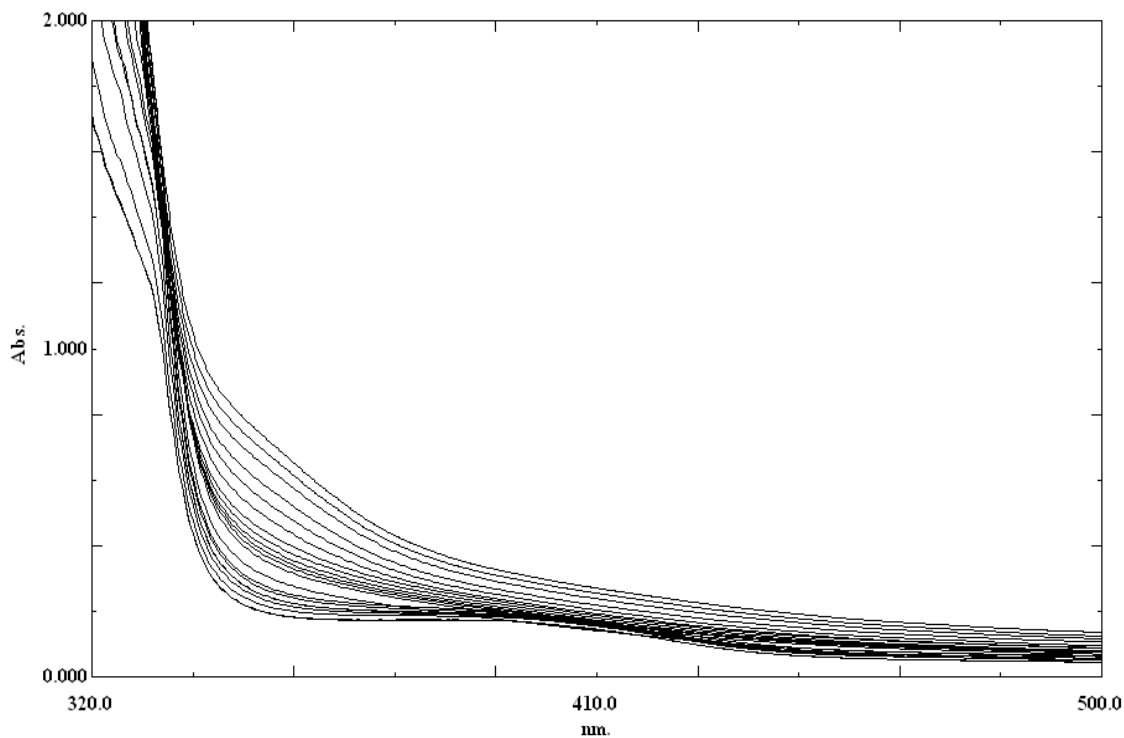
Figure 7.11 Absorption spectra of MY2 in EtOH after addition of base solutions in the pH range of 7.10-10.25.
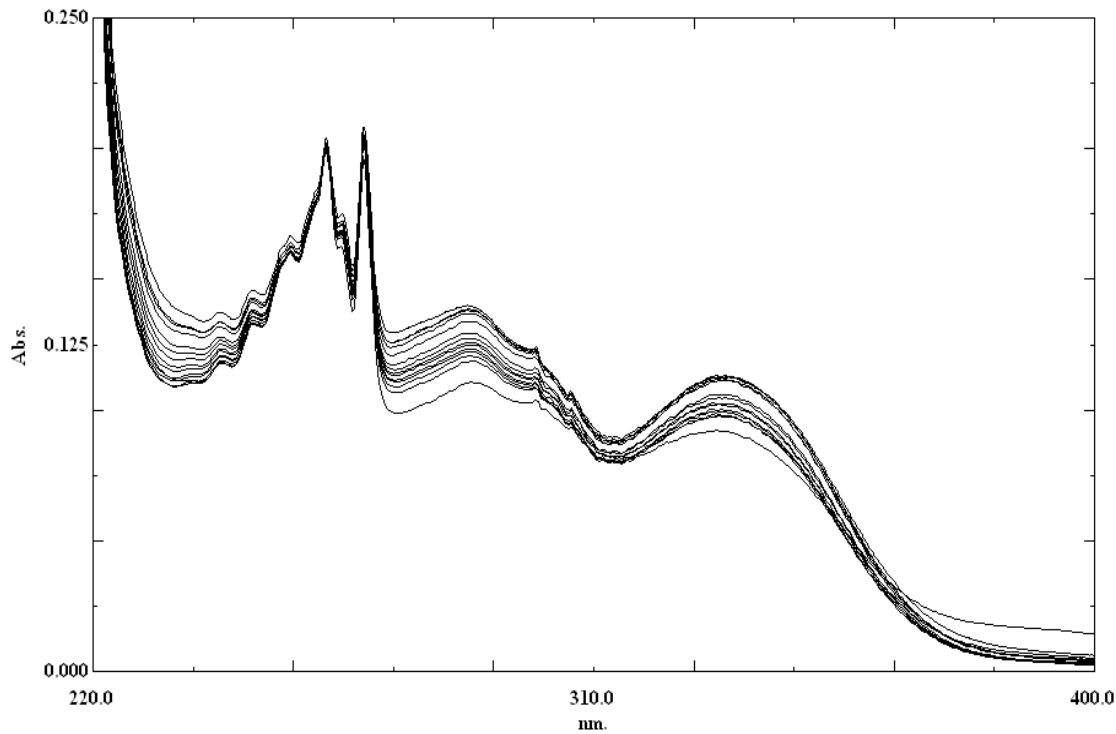
Figure 7.12 Absorption spectra of MY2 in EtOH after addition of acid solutions in the pH range of 7.39-2.72.

Similarly, the MY4 dye, upon exposure to the acid solutions (pH range 12.00–4.50, in DMF), did not exhibit significant spectral response (See Fig 7.13). However in the basic region (pH range 12.40 - 15.70, in DMF), MY4 exhibited a dramatic response to pH yielding 98 % relative signal change in direction of increase in absorbance intensity. Figure 7.14 shows the absorption spectrum of MY4 dye in DMF solvent and related absorbance based sigmoidal response (pH versus (I−Io)/Io).

The representative absorption spectra of MY5 in DMF between pH 12.50 - 14.80 and related absorption based sigmoidal response were shown in Figure 7.15. Here a relative signal change of approximately 97 % has been reached. However MY5 dye did not response to pH in the acidic region (See Fig 7.16).
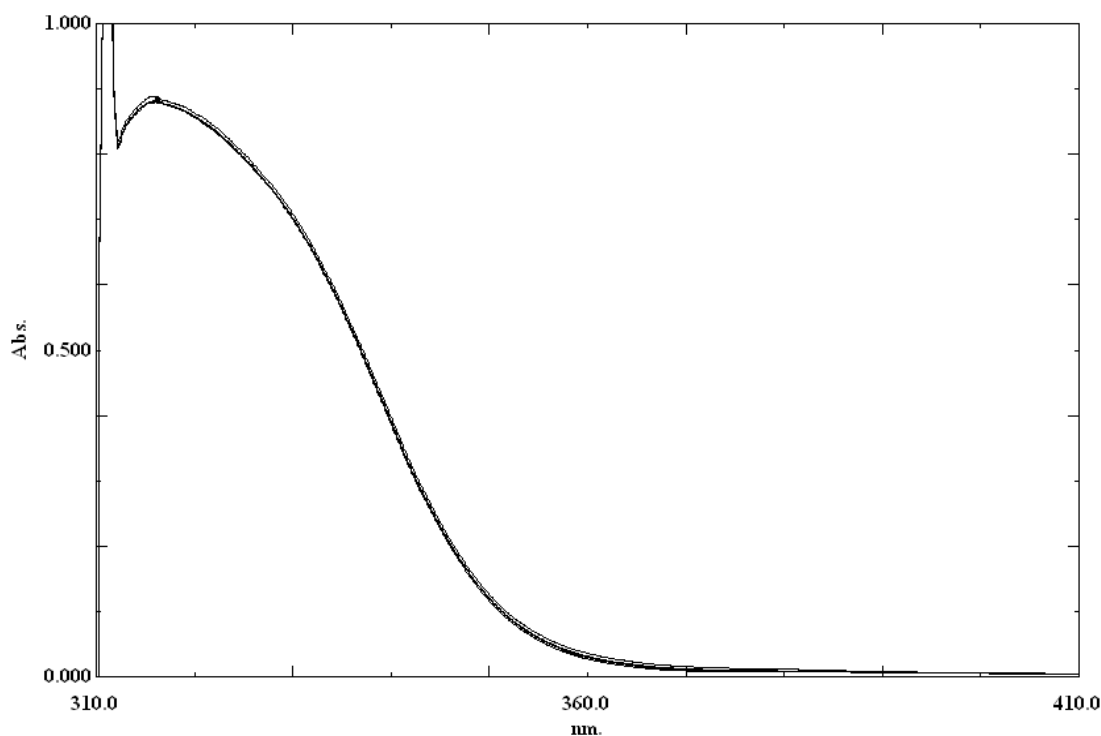

Figure 7.13 Absorption spectra of MY4 in DMF after addition of acid solutions in the pH range of 12.00 - 4.50.
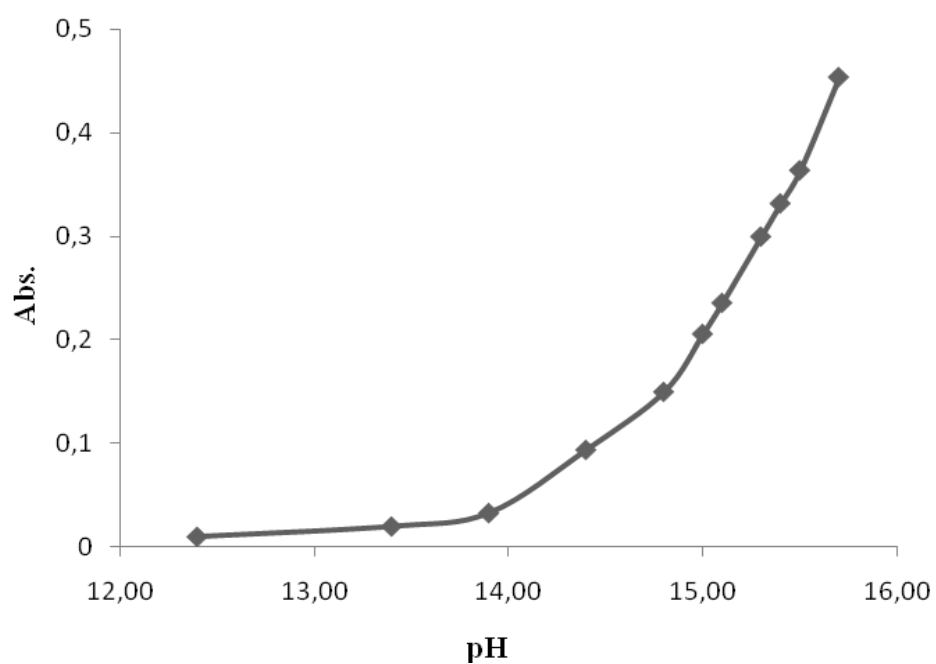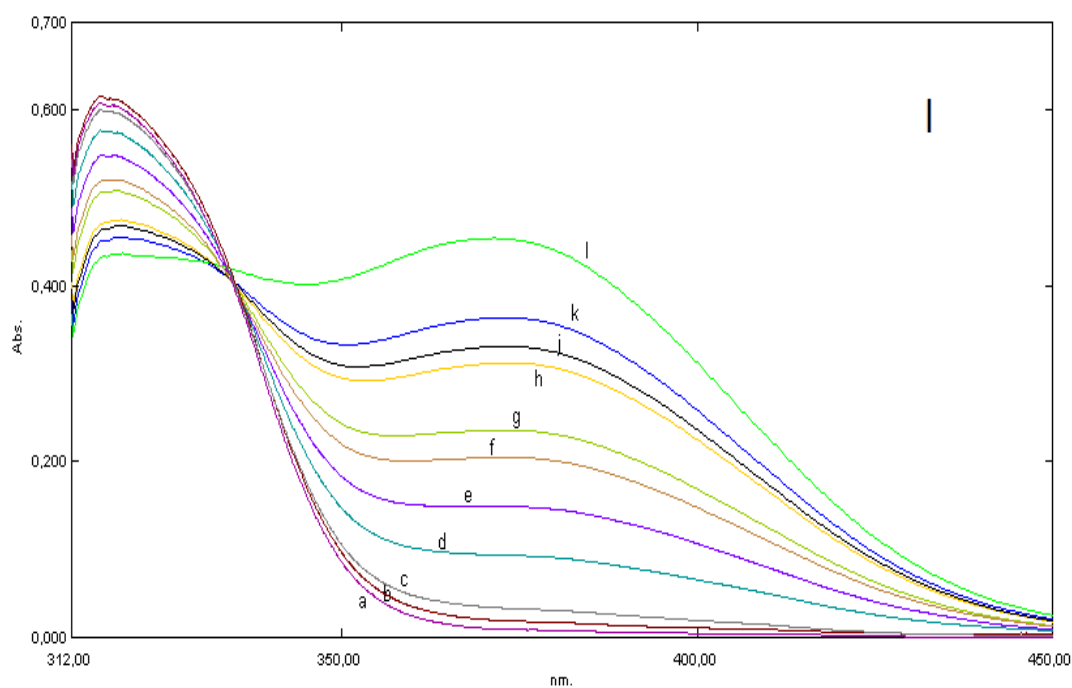
Figure 7.14 I:Absorption spectra of MY4 in DMF after addition of base solutions in the pH range of 12.40 - 15.70 pH: a) 12.40 b) 13.40 c) 13.90 d) 14.40 e) 14.80 f) 15.00 g) 15.10 h) 15.30 j) 15.40 k) 15.50 l) 15.70.

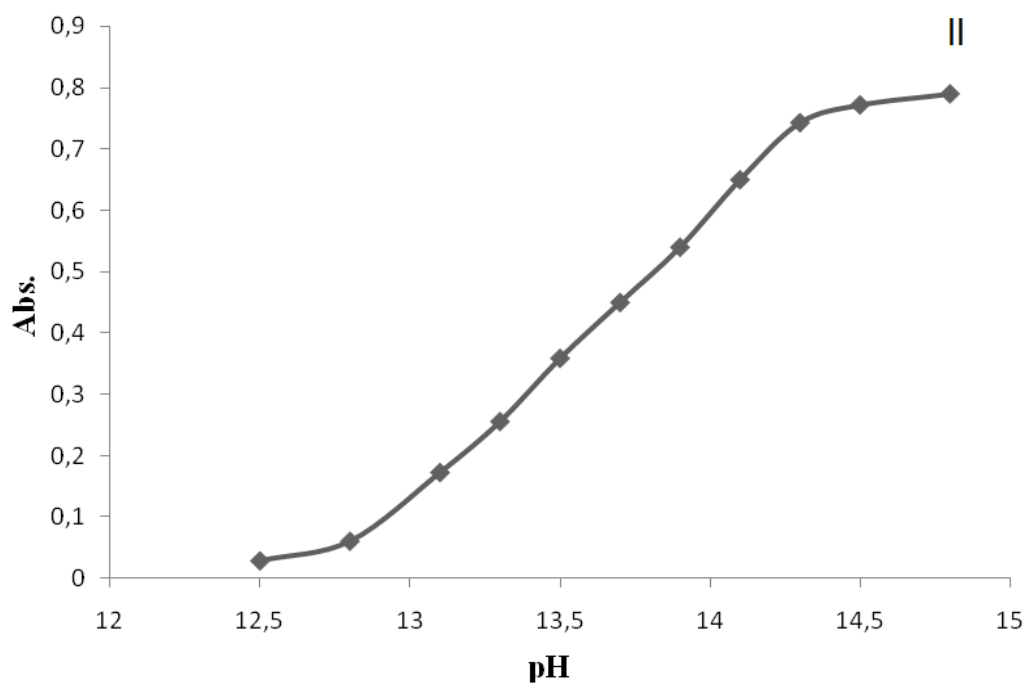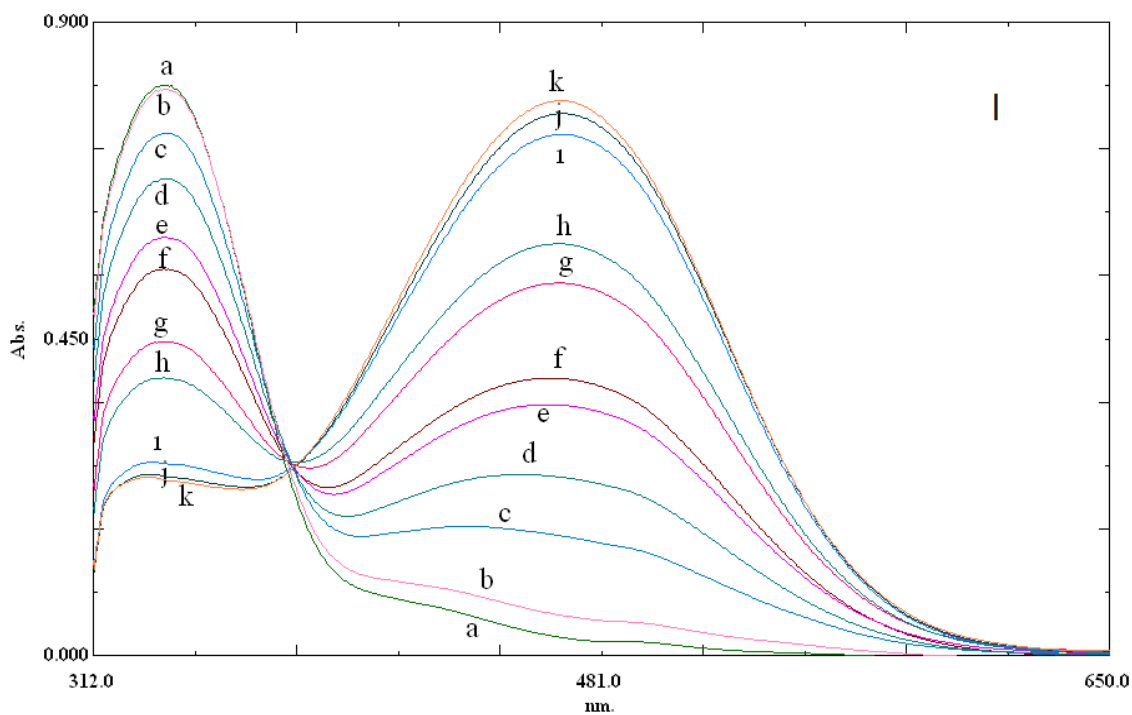II: Absorption based sigmoidal response of MY4 to pH.

Figure 7.15 I: Absorption spectra of MY5 in DMF after addition of base solutions in the pH range of 12.50 - 14.80. pH: a) 12.50   b) 12.80   c) 13.10   d) 13.30 e) 13.50 f) 13.70 g) 13.90 h) 14.10 ı) 14.30 j) 14.50 k) 14.80.

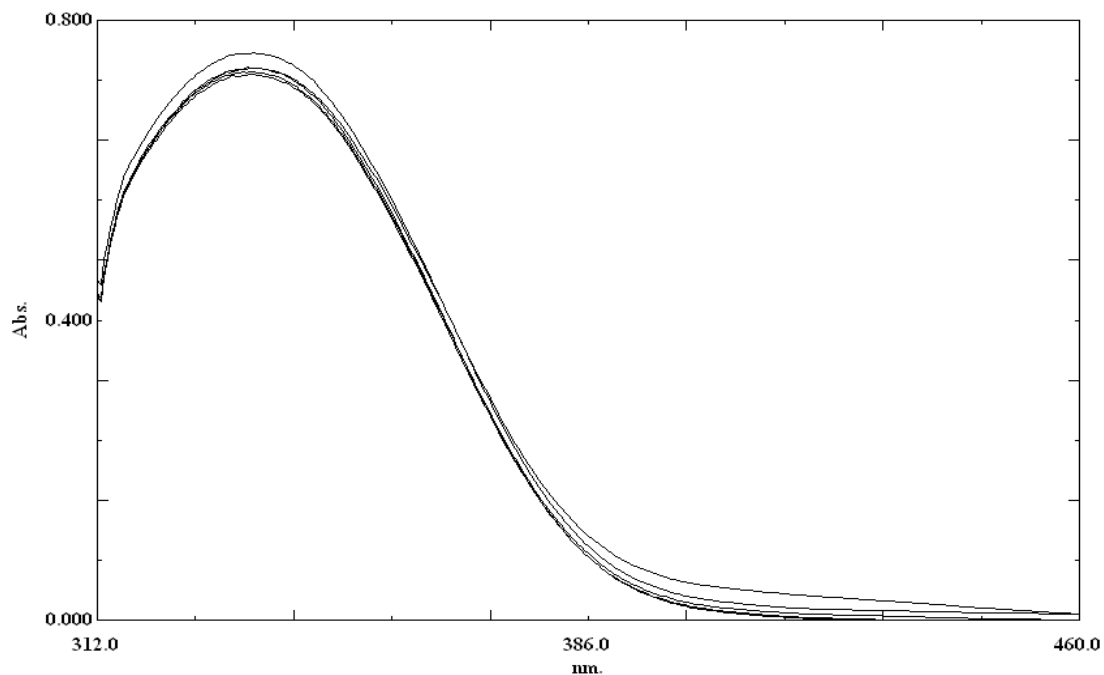II: Absorption based sigmoidal response of MY5 to pH.

Figure 7.16 Absorption spectra of MY5 in DMF after addition of base solutions in the pH range of 12.00-4.50.

Given pKa values were calculated by using non-linear fitting algorithm of Gauss–Newton–Marquardt method,

pKa = pH+log [(Ax -Ab)/(Aa-Ax)]

where Aa and Ab are the absorbance intensities of acidic and basic forms and Ax is the intensity at a pH near to the midpoint (Werner & Wolfbeis, 1993).   The calculated pKa values were found to be 15.20 and 13.60 for MY4 and MY5 in DMF, respectively. It is a well known fact that, the pH scale in nonaqueous media is governed by the autoprotolysis or autodissociation constant of the solvent.

7.3.5 pH Dependency of MY2, MY4 and MY5 Dye in Solid Matrix

As mentioned earlier indicators with pKa values between 6.8 and 10.0 in aqueous media are essential for sensitive pCO_2 optodes. To evaluate the availability of employed molecules for dCO_2 sensing, the acidity constant was calculated. pH-induced emission spectra of PMMA doped dyes were recorded. The relative signal change of emission spectra of the MY2, MY4 and MY5 was monitored after

addition of certain concentrations of buffered acid solutions at different pH ranges.

Upon exposure to the buffered solutions of different pH's the immobilized MY2 exhibited significant emission based spectral response near neutral region (See Figure 7.16 and 7.17).
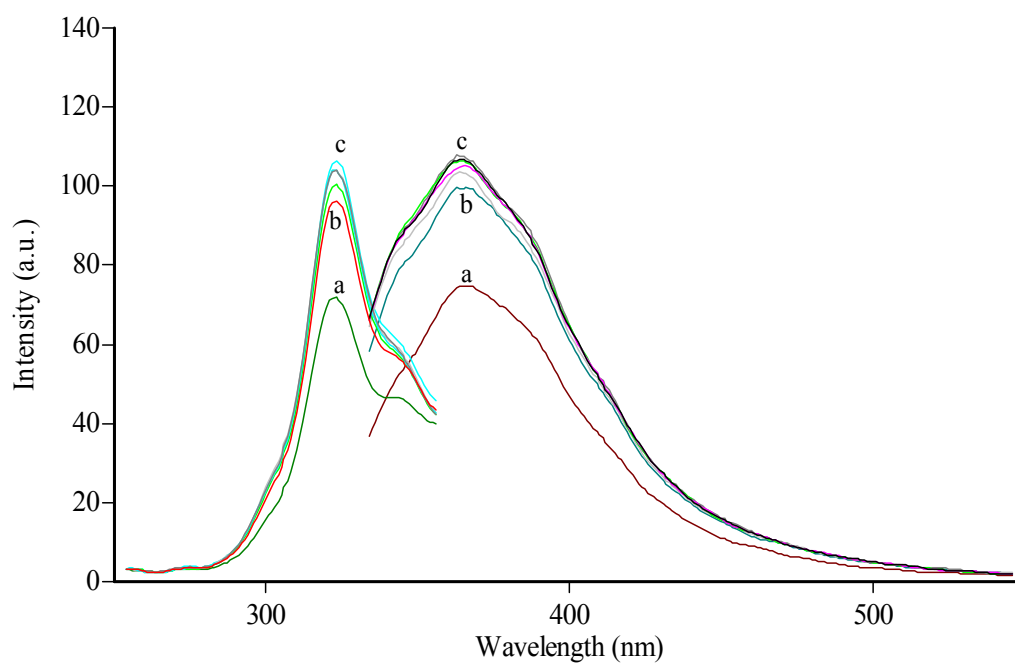

Figure 7.16 pH induced emission based spectral response of the EC doped MY2 in the pH range of 7.00-10.00.   pH: a) 7.00 b) 7.50 c) 8.00, 8.50, 9.00, 9.50, 10.00.
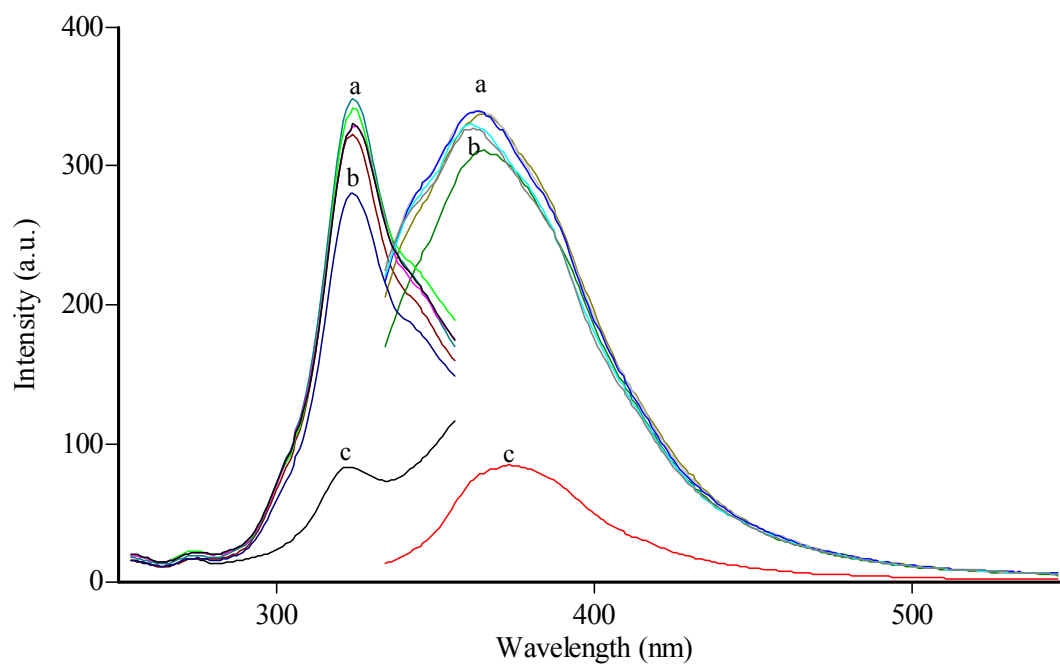
Figure 7.17 pH induced emission based spectral response of the EC doped MY2 in the pH range of 7.00-4.00. pH: a) 7.00, 6.50, 6.00, 5.50, 5.00 b) 4.50 c) 4.00.

The MY4 dye responded to pH near neutral region around pH 7.0. Figure 7.18 and 7.19 show pH dependent emission based spectral response of EC doped MY4 in acidic and basic region of the pH scale.

Figure 7.18 pH induced emission based spectral response of the EC doped MY4 in the pH range of 7.00-4.00. pH: a) 7.00, 6.50, 6.00, 5.50, 5.00, 4.50 b) 4.00.
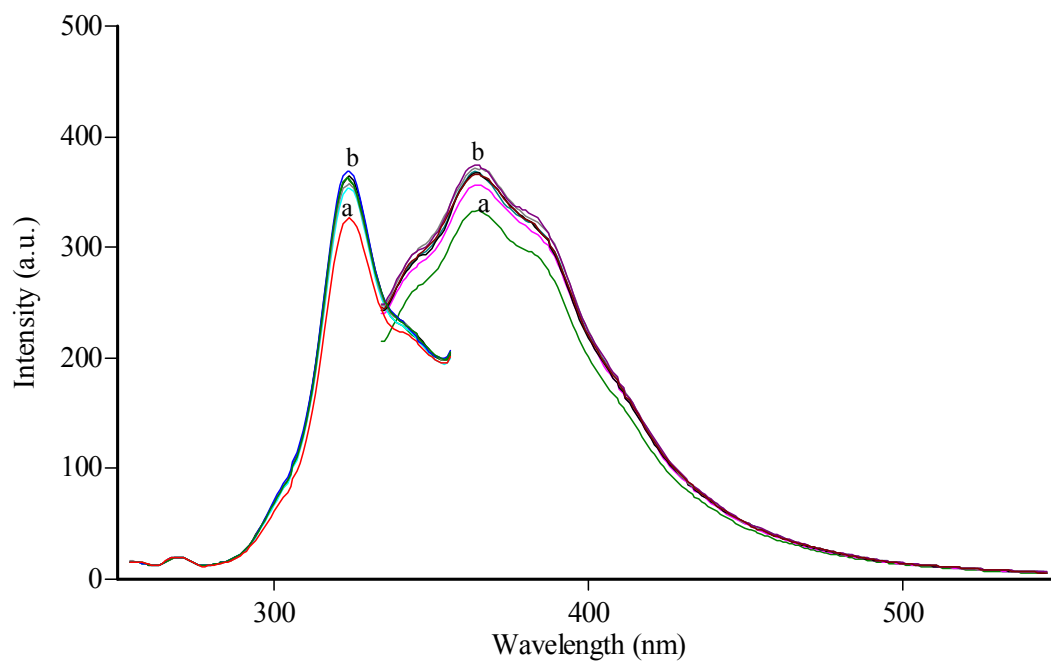
Figure 7.19 pH induced emission based spectral response of the EC doped MY4 in the pH range of 7.00-10.00. pH: a) 7.00 b) 7.50, 8.00, 8.50, 9.00, 9.50, 10.00.
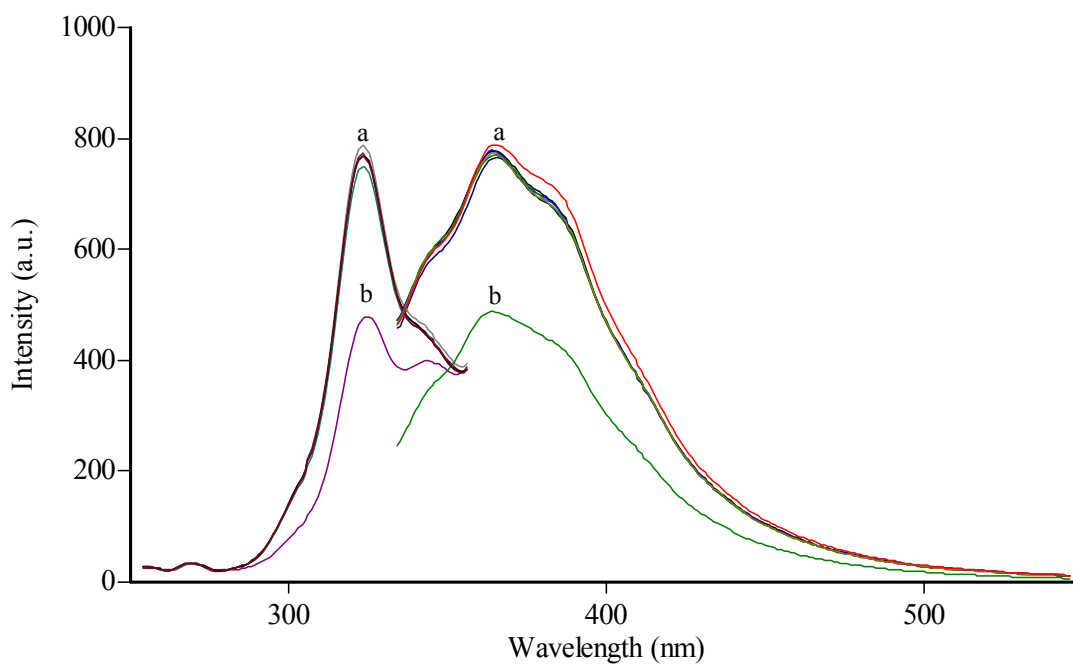
The MY5 dye responded significantly to pH between 7.00-7.50 in direction of increase in signal intensity (See Fig 7.20). The sensitivity to pH in this region is a promising response for bicarbonate detection. Emission based spectral response of the MY5 dye in the pH range of 7.00-4.00 was shown in Fig 7.21.

Figure 7.20 pH induced emission based spectral response of the EC doped MY5 in the pH range of 7.00-10.00. pH: a) 7.00 b) 7.50, c) 8.00, 8.50, 9.00, 9.50, 10.00.

Figure 7.21 pH induced emission based spectral response of the EC doped MY5 in the pH range of 7.00-4.00. pH: a) 7.00, 6.50, 6.00, 5.50, 5.00, 4.50 b) 4.00.
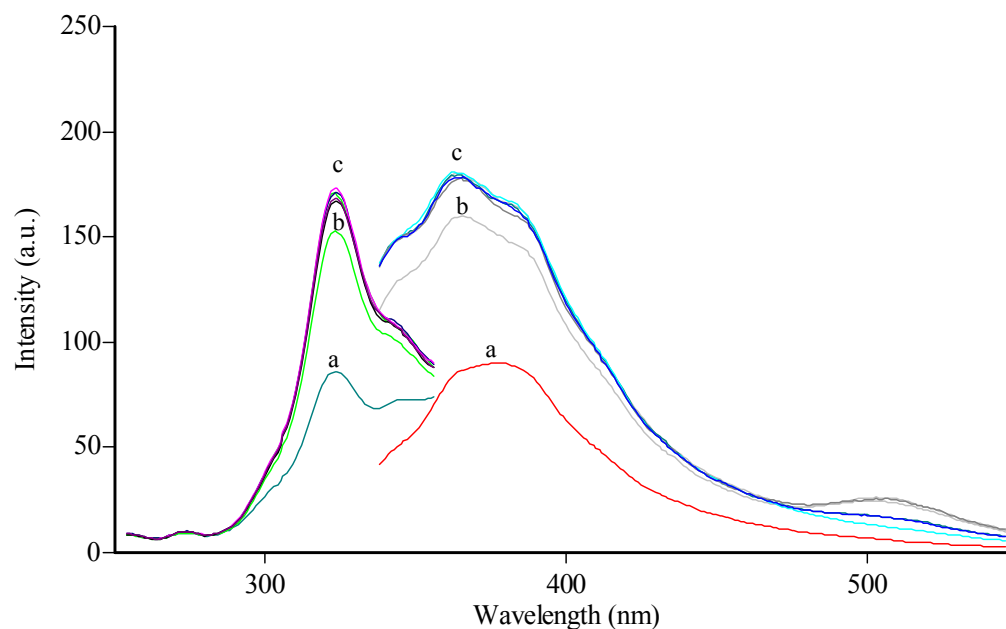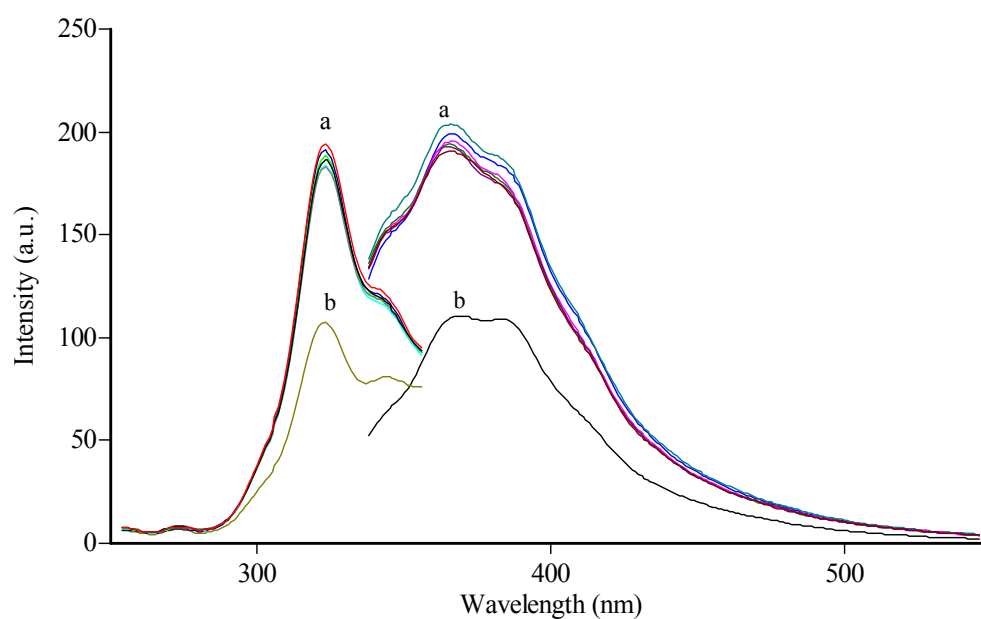
7.3.6 Dissolved CO₂ Sensing Studies with MY2, MY4 and MY5 in Thin Film and Nanofiber Form

Sensor performances of all of the employed dyes were tested for dissolved CO_2 both in thin film and nanofiber forms. Standard solutions were prepared freshly from 1 mol L−1 $NaHCO_3$ stock solution prior to the measurements. CO_2-free standard solutions were prepared with doubly distilled water after boiling and bubbling with nitrogen; they were stored in closed containers. Addition of certain concentrations of $NaHCO_3$ were added to the sensing agent-containing cuvette, mixed and the changes in fluorescence intensity were measured. All the experiments were performed at room temperature (25 ° C).

Figure 22, 23 and 24 show the emission and excitation spectra of MY2, MY4 and MY5 dyes after exposure to HCO_3^- ions in EC based thin film, respectively. Insets of the figures show linearized calibration plots of related spectral responses. Calibration plots were drawn normalized fluorescence intensity (I-Io/Io) versus bicarbonate concentration.

The working range for thin film forms of MY2 doped EC is between 1.00×10^{-4} and 5.00×10^{-3} mol L−1 HCO_3^-. After exposure to HCO_3^- a 45 % relative signal change is obtained (See Fig 7.22).

Thin film form of MY4 dye exhibited spectral response for dCO_2 in the same concentration range (1.00×10^{-4} - 5.00×10^{-3}M) as MY2 44 % relative signal change is obtained. The calibration plot of the sensor is shown in inset of Figure 7.23.

The working range and linearized calibration graph for MY5 in EC matrix was shown Figure 7.24. The MY5 dye responded to dCO_2 in a large concentration range (1.00×10^{-5} to 1.00×10^{-1}) with respect to MY2 and MY4. Relative signal change was 44 % in thin film form.
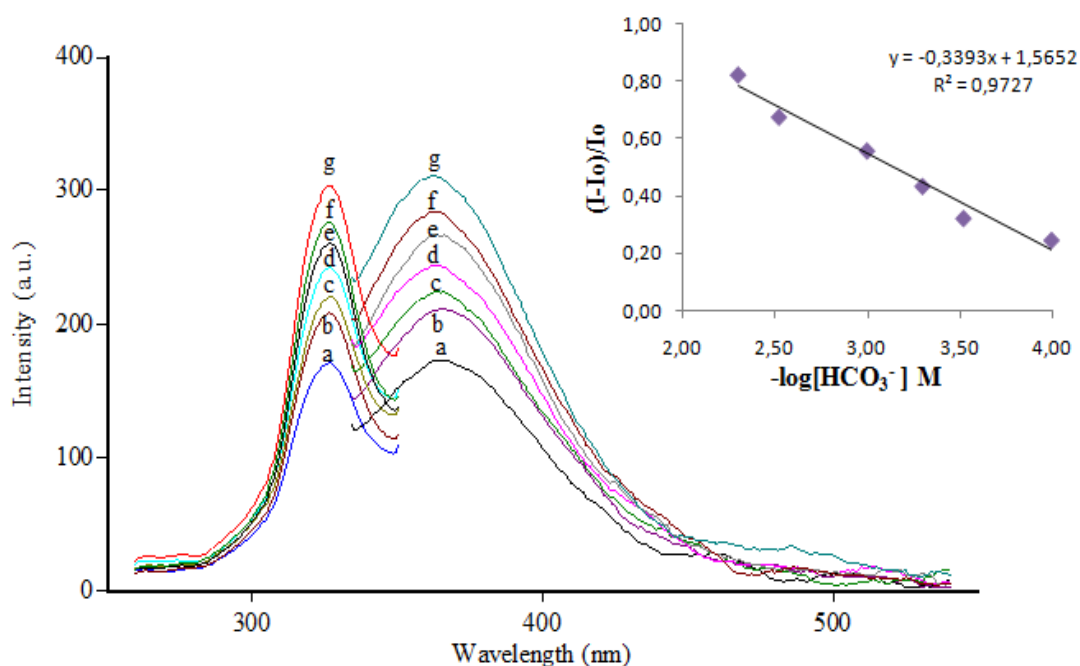
Figure 7.22 Excitation-emission based response of the MY2 dye-doped EC based thin film to HCO_3^- ions; (a) bicarbonate free water (b) 1.00×10^{-4} M (c) 3.00×10^{-4} M (d) 5.00×10^{-4} M (e) 1.00×10^{-3} M (f) 3.00×10^{-3} M (g) 5.00×10^{-3} M.

Figure 7.23 Emission spectra of immobilized MY4 in EC based thin film matrix after exposure to different HCO_3^- concentrations; (a) bicarbonate free water (b) 1.00×10^{-4} M (c) 3.00×10^{-4} M (d) 5.00×10^{-4} M (e) 3.00×10^{-3} M (f) 5.00×10^{-3} M.
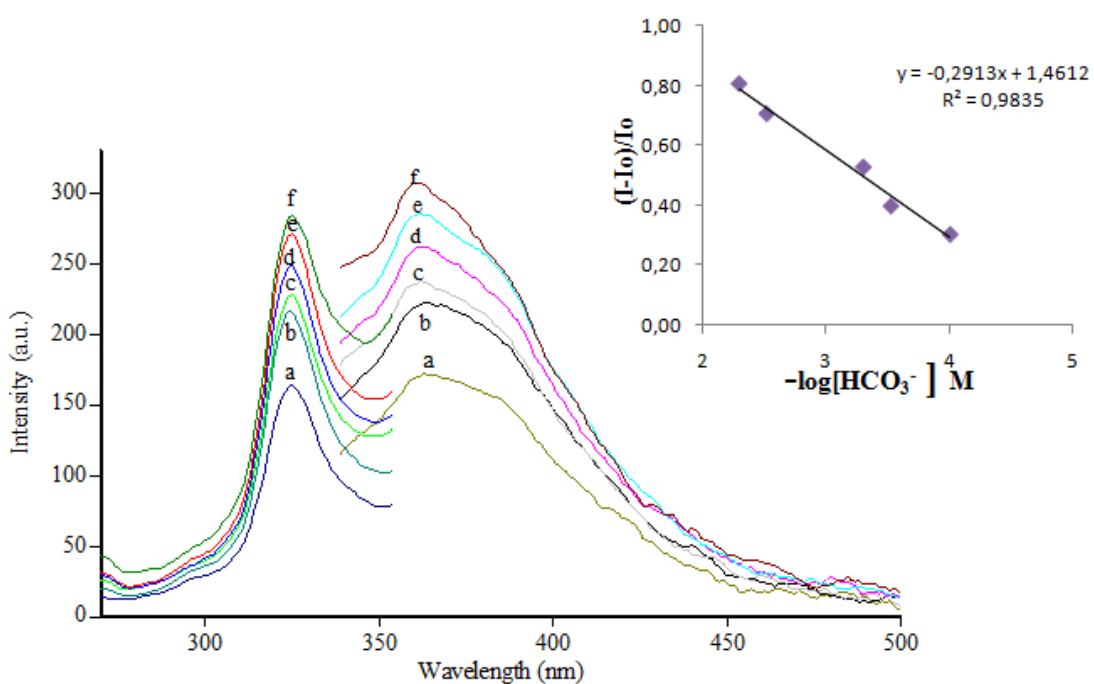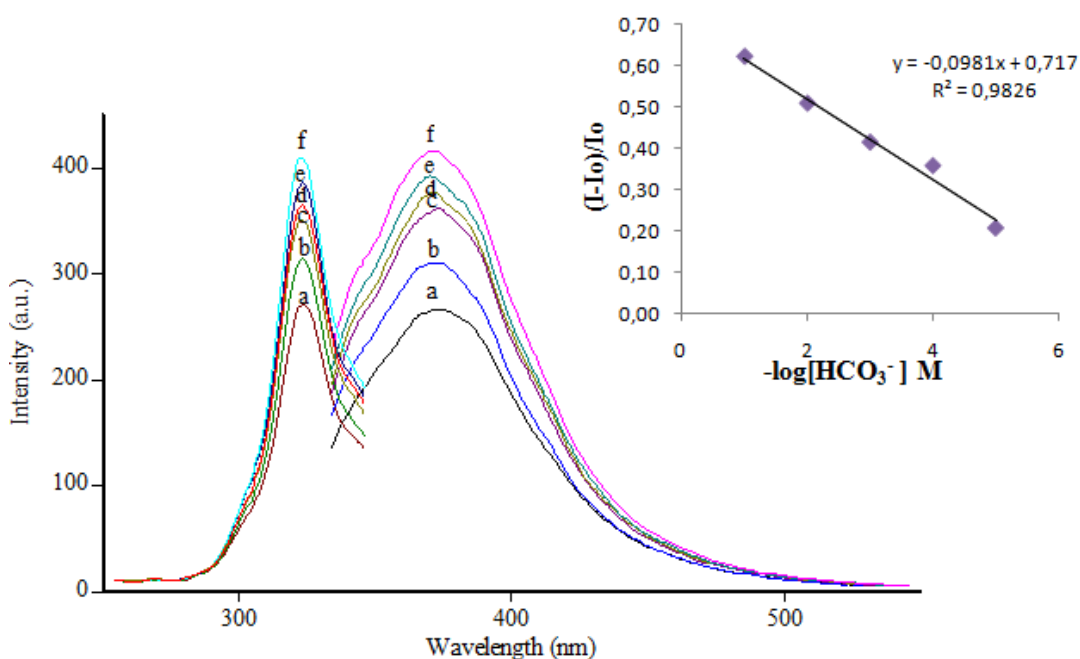
Figure 7.24 Emission spectra of immobilized MY5 in EC based thin film matrix after exposure to different HCO_3^- concentrations; (a) bicarbonate free water (b) 1.00×10^{-5} M (c) 1.00×10^{-4} M (d) 1.00×10^{-3} M (e) 1.00×10^{-2} M (f) 1.00×10^{-1} M.

Dissolved CO_2 sensing studies were also performed with nanofiber forms of the sensing agent. For this purpose sensing materials were then fabricated with electrospinning technique. The surface morphology of the fabricated nanofibers was studied using the scanning electron microscope (SEM) instrument. SEM images of electrospun membranes of the dyes at various magnifications are shown in Figure 7.25-27. The diameters were varying between 456 -927, 645-1026 and 553-860 nm for EC based electrospun fibers for MY2, MY4 and MY5 dyes, respectively.

Figure 7.25 SEM images of EC based electrospun nanofibers for MY2 dye at different magnifications such as ×1 000 and ×11 000.
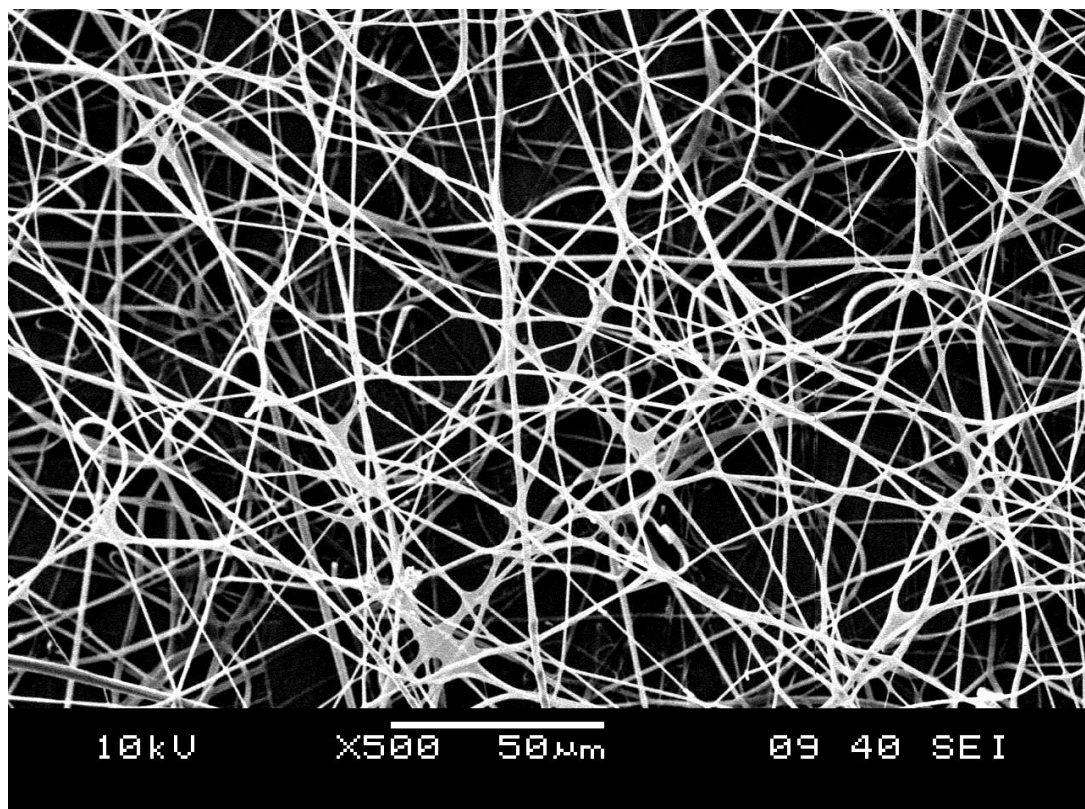
Figure 7.26 SEM images of EC based electrospun nanofibers for MY4 dye at different magnifications such as ×500 and ×10 000.
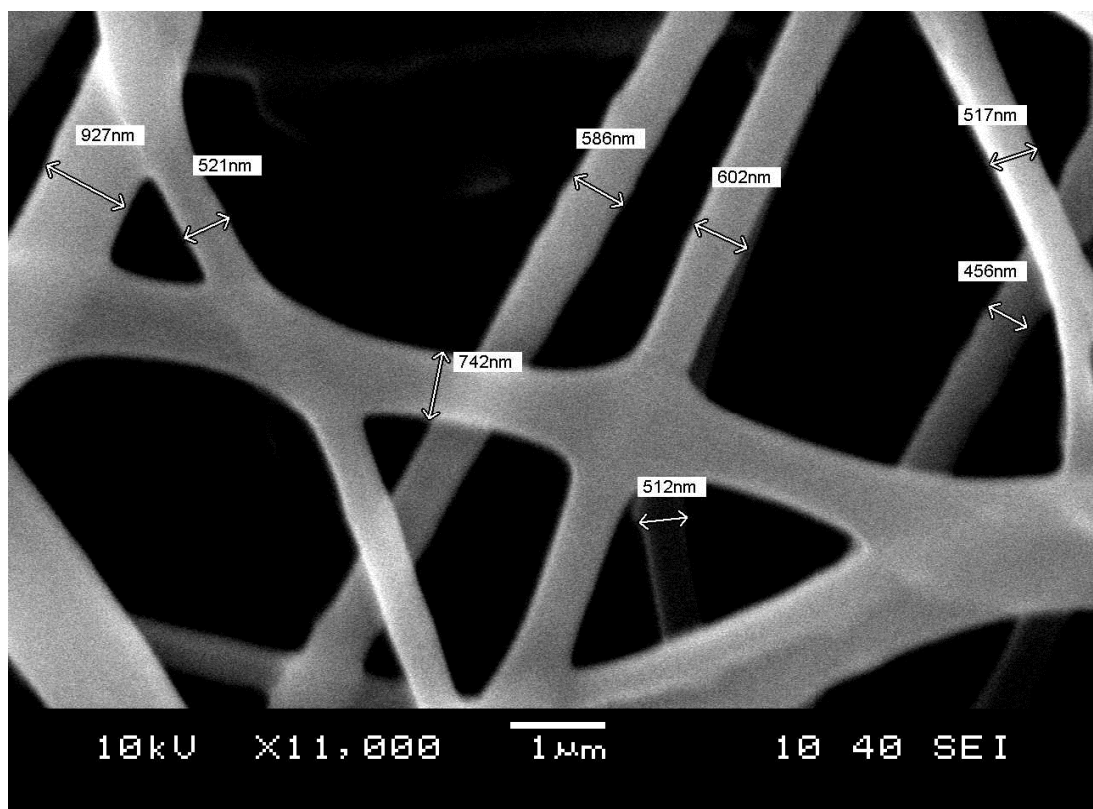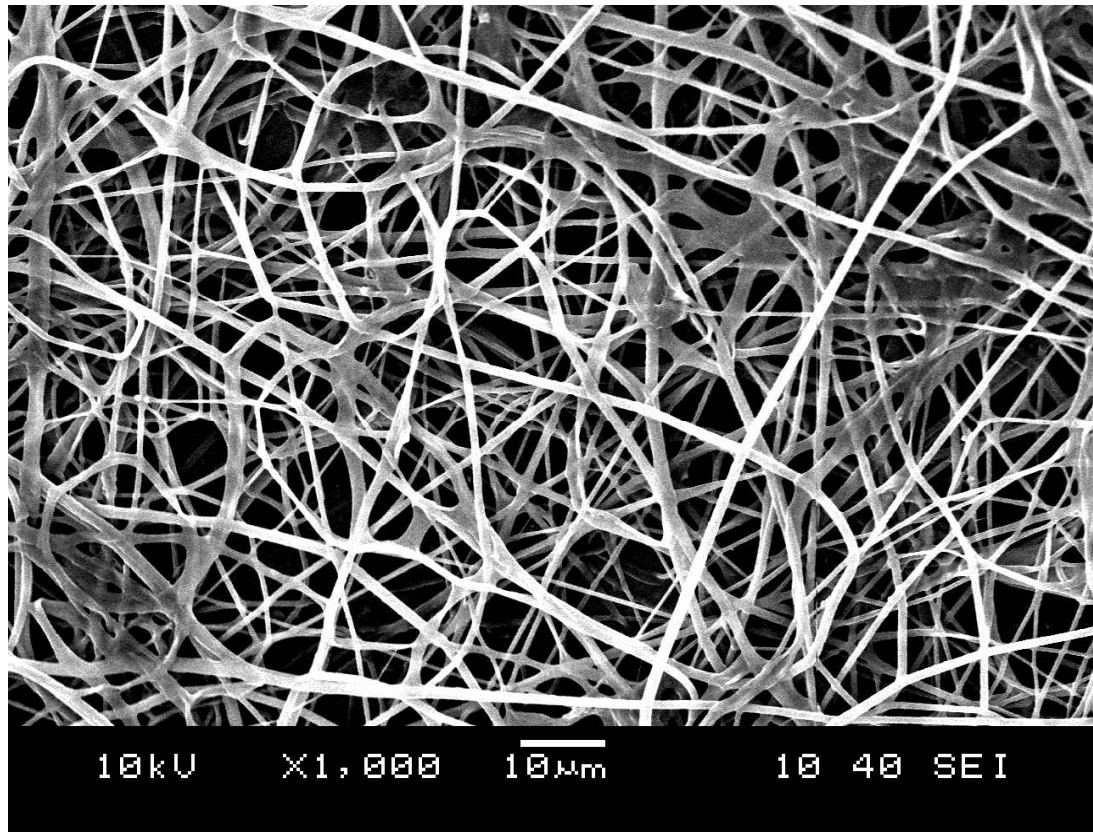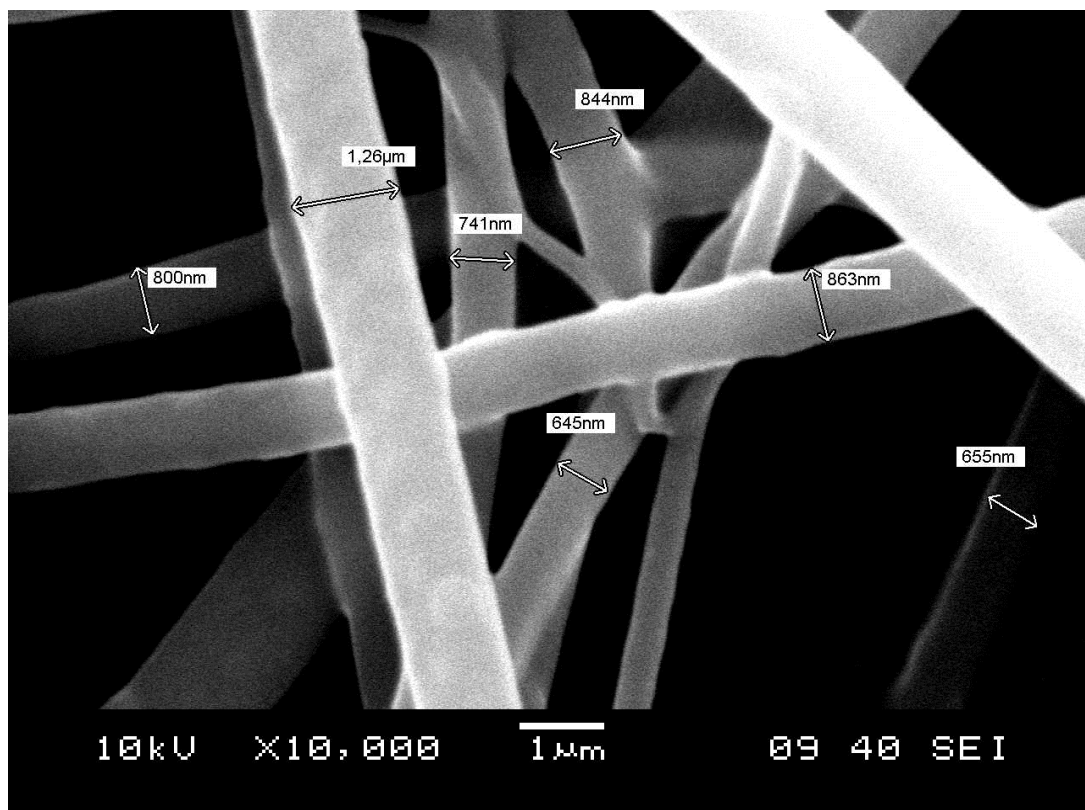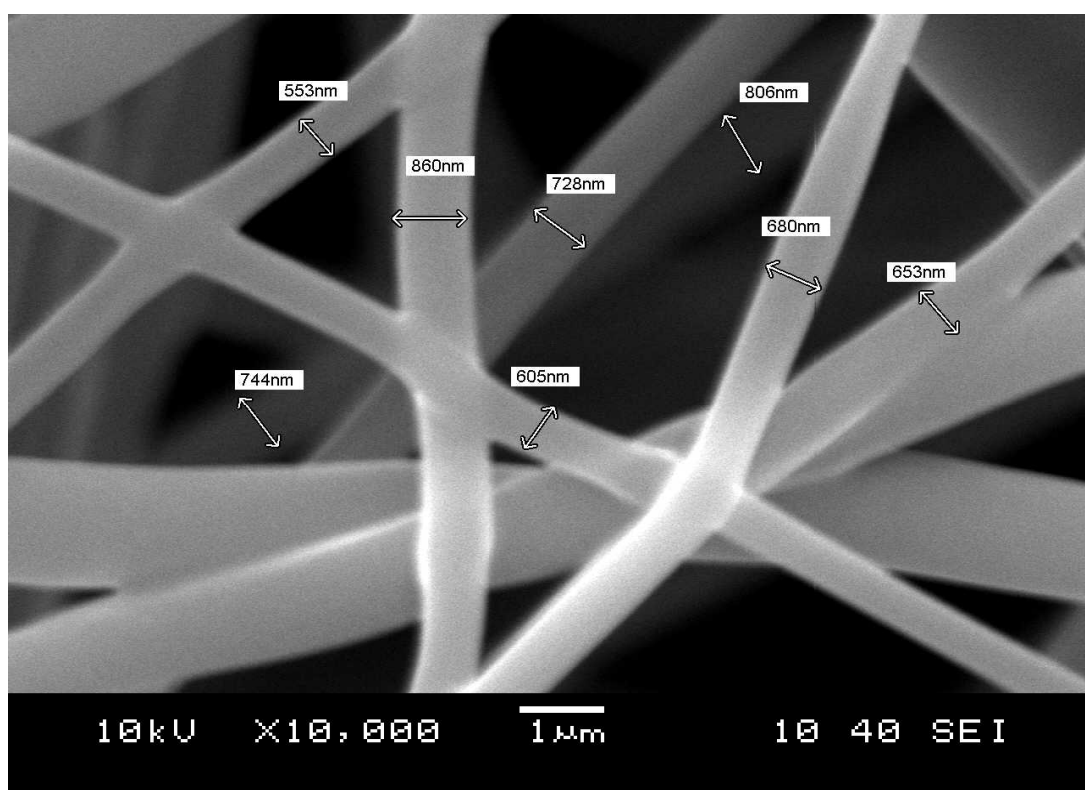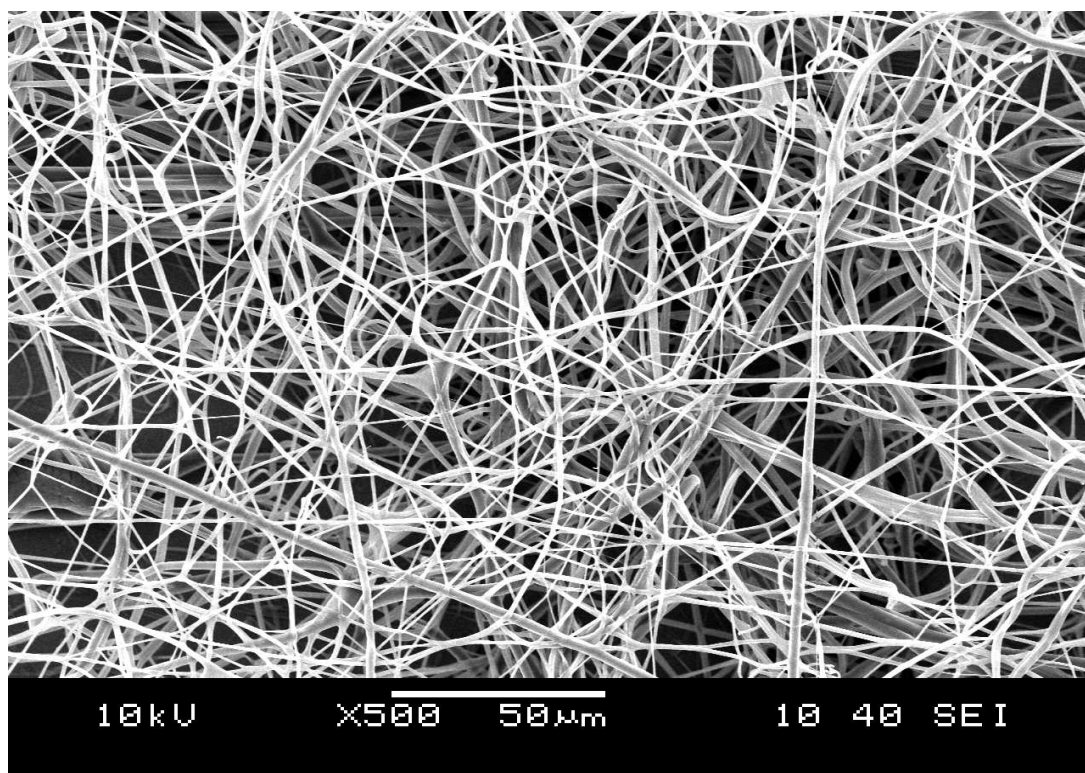
Figure 7.27 SEM images of EC based electrospun nanofibers for MY5 dye at different magnifications such as ×500 and ×10 000.

For all dyes the electrospun fibers exhibited enhanced response for dCO_2. The concentration range was between 1.00×10^{-9} to 1.00×10^{-4}, 1.00×10^{-9} to 1.00×10^{-2} and 1.00×10^{-9} to 1.00×10^{-4} for MY2, MY4 and MY5, respectively. The calculated relative signal changes were 63, 61 and 74 %, respectively.

Figure 7.28, 29 and 30 show emission based response of nanofiber forms of MY2, MY4 and MY5 dyes after exposure to certain concentrations of HCO_3^-.

For all of the exploited dyes, the nanofiber forms exhibited larger response ranges, better sensitivity and higher relative signal changes with respect to the thin film forms.

Figure 7.28 Emission spectra of immobilized MY2 in EC nano fibers after exposure to different HCO_3^- concentrations; (a) bicarbonate free water (b) 1.00×10^{-9} M (c) 1.00×10^{-8} M (d) 1.00×10^{-7} M (e) 1.00×10^{-6} M (f) 1.00×10^{-5} M (g) 1.00×10^{-4} M.

Figure 7.29 Emission spectra of immobilized MY4 in EC nano fibers after exposure to different HCO_3^- concentrations; (a) bicarbonate free water (b) 1.00×10^{-9} M (c) 1.00×10^{-8} M (d) 1.00×10^{-7} M (e) 1.00×10^{-6} M (f) 1.00×10^{-5} M (g) 1.00×10^{-4} M (h) 1.00×10^{-3} M (ı) 1.00×10^{-2} M.

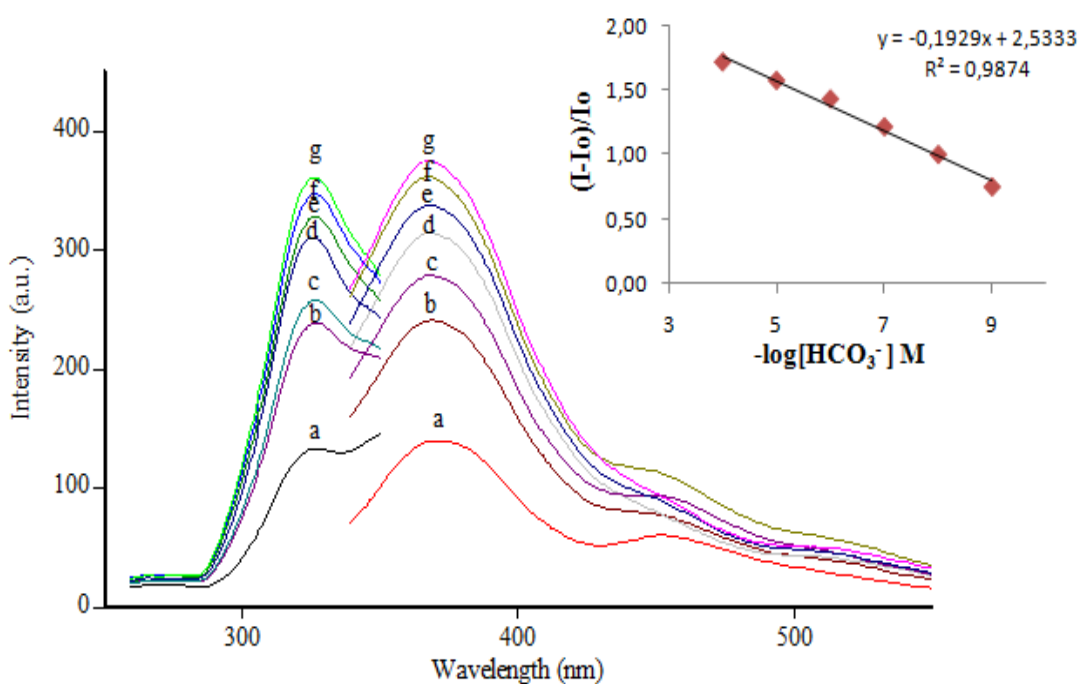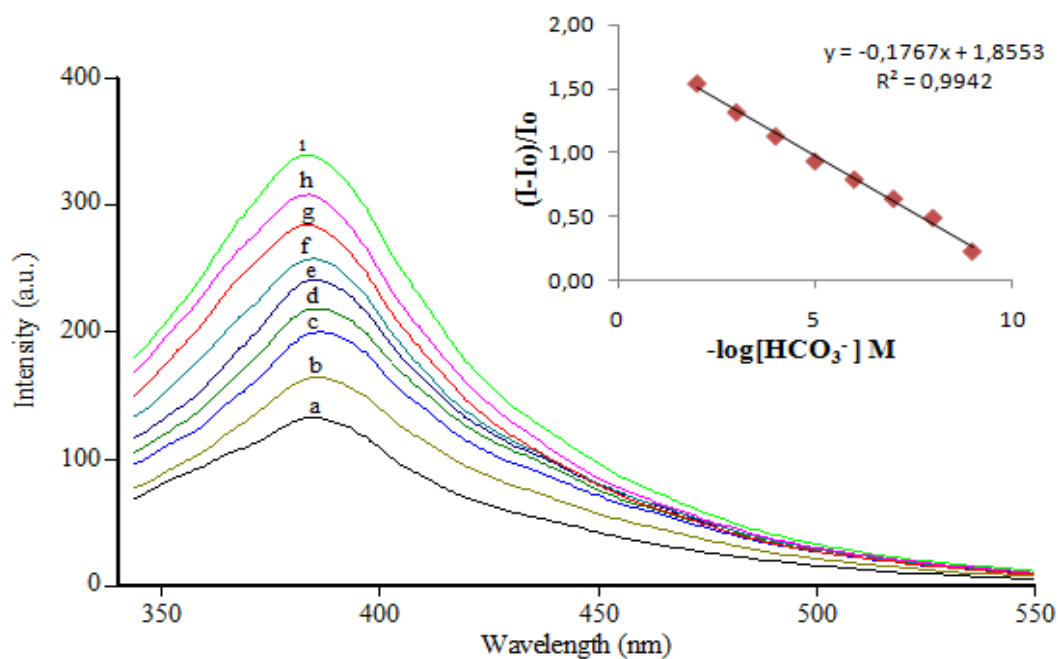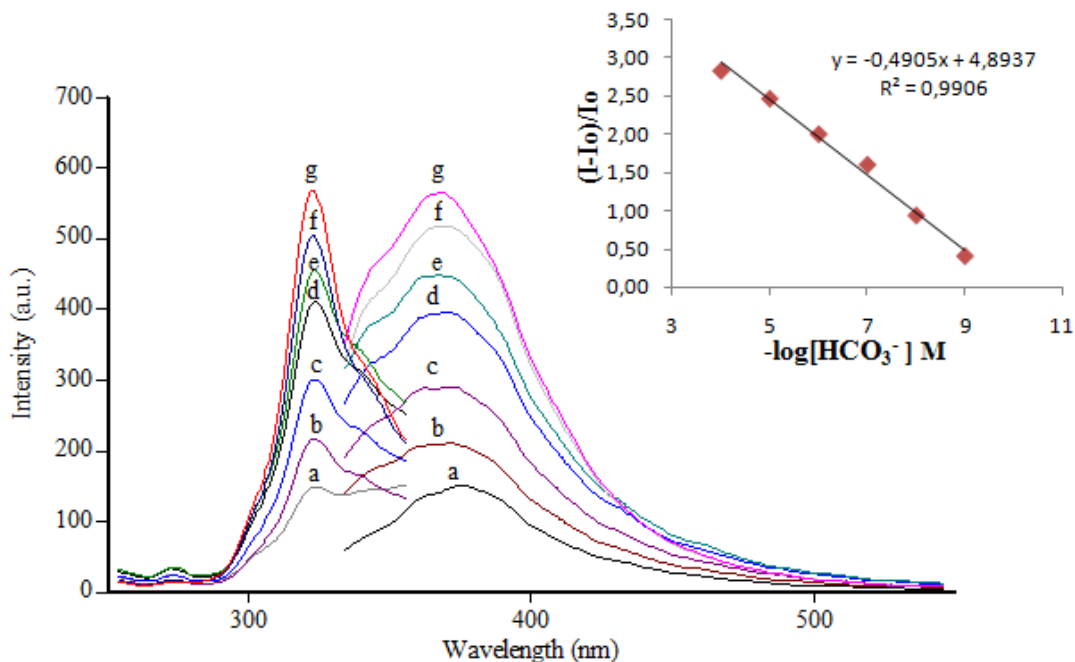Figure 7.30 Emission spectra of immobilized MY5 in EC based nanofibers after exposure to different HCO_3^- concentrations; (a) bicarbonate free water (b) 1.00×10^{-9} M (c) 1.00×10^{-8} (d) 1.00×10^{-7} M (e) 1.00×10^{-6} M (f) 1.00×10^{-5} M (g) 1.00×10^{-4} M.

7.3.7 Selectivity Studies

In order to examine the response of the MY2, MY4 and MY5 dyes to possible interfering cations, the sensing agents were treated with 5×10^{-3} M concentrations of Ag^+, Al^{3+}, Ba^{2+}, Ca^{2+}, Co^{2+}, Cr^{3+}, Cu^{2+}, Fe^{3+}, Fe^{2+}, Hg^{2+}, K^+, Li^+, Mg^{2+}, Mn^{2+}, Na^+, Ni^{2+}, Pb^{2+}, Sn^{2+} and Zn^{2+} ions in acetic acid/acetate buffer solutions at pH 5.5. The interference effects of the conventional anions; F^-, Cl^-, Br^-, NO_3^-, SO_4^{2-} and PO_4^{3-} were also tested.

Results were evaluated in terms of relative signal changes (RSC); $(I - Io)/Io$, where I was the fluorescence intensity of the sensing membrane after exposure to ion-containing solutions and Io is the fluorescence intensity of the sensing slide in ion-free buffer solution.

From Fig 7.31 I-II it can be concluded that, the MY2 is capable of determining bicarbonate ions (HCO_3^-) with a high selectivity over other ions. The fluorescence was significantly enhanced in the presence of HCO_3^- exhibiting a relative signal change (RSC) ratio of 36 %. The interference effects of the conventional anions; F^-, Cl^-, Br^-, NO_3^-, SO_4^{2-} and PO_4^{3-} were also tested. Relative signal changes of less than 10 % were observed for EC doped films.

Figure 7.32 and 7.33 I-II reveals that the MY4 and MY5 are capable of determining HCO_3^- ions. Only the HCO_3^-, induced fluorescence bands of MY4 and MY5 dye exhibiting a RSC ratio of 48 % and 47 %, respectively. Other alkali, alkaline earth, and transition metal ions produced insignificant responses where RSCs of less than 10 %.
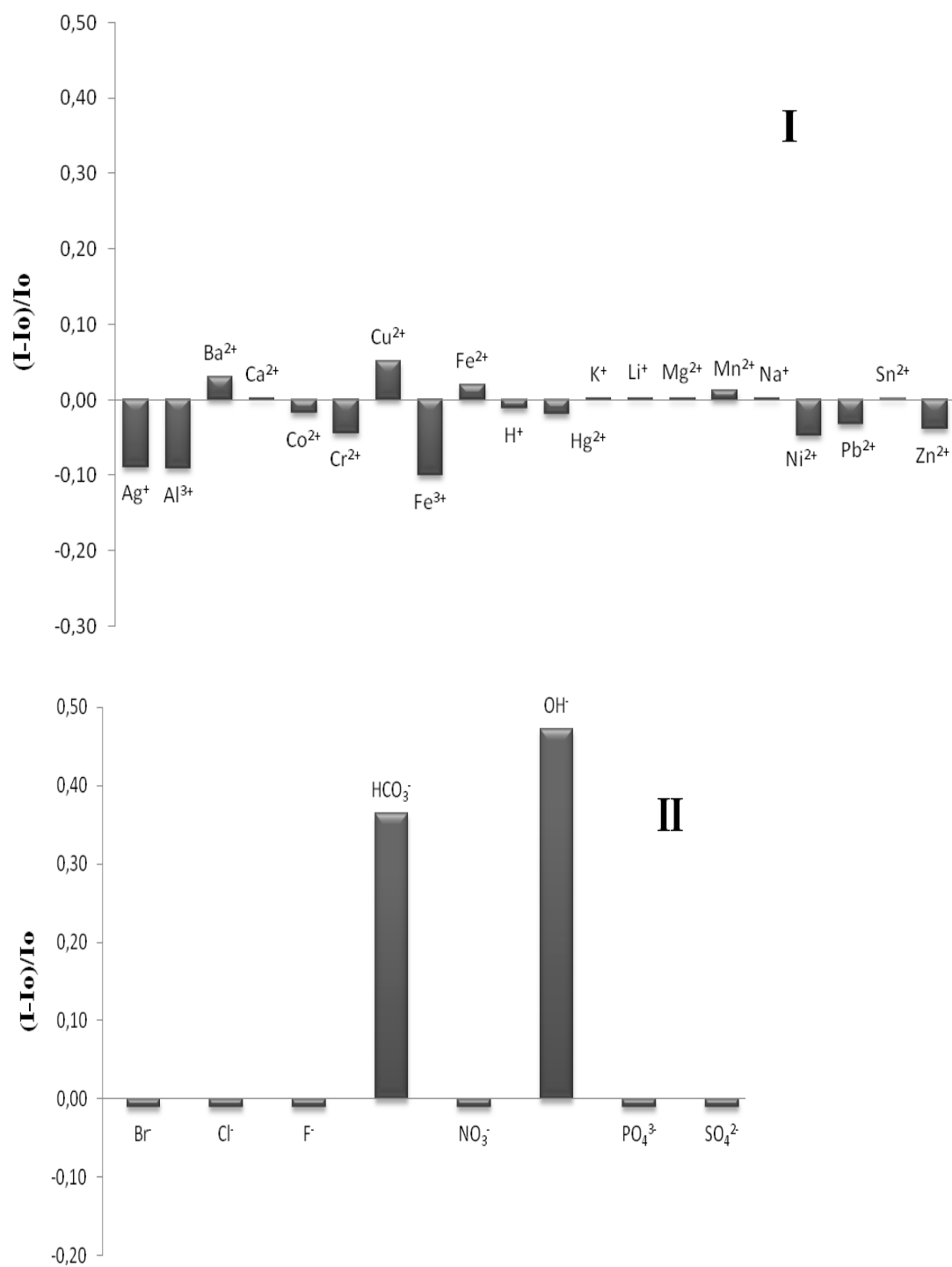
Figure 7.31 Metal-ion (I) and anion (II) response test for MY2.
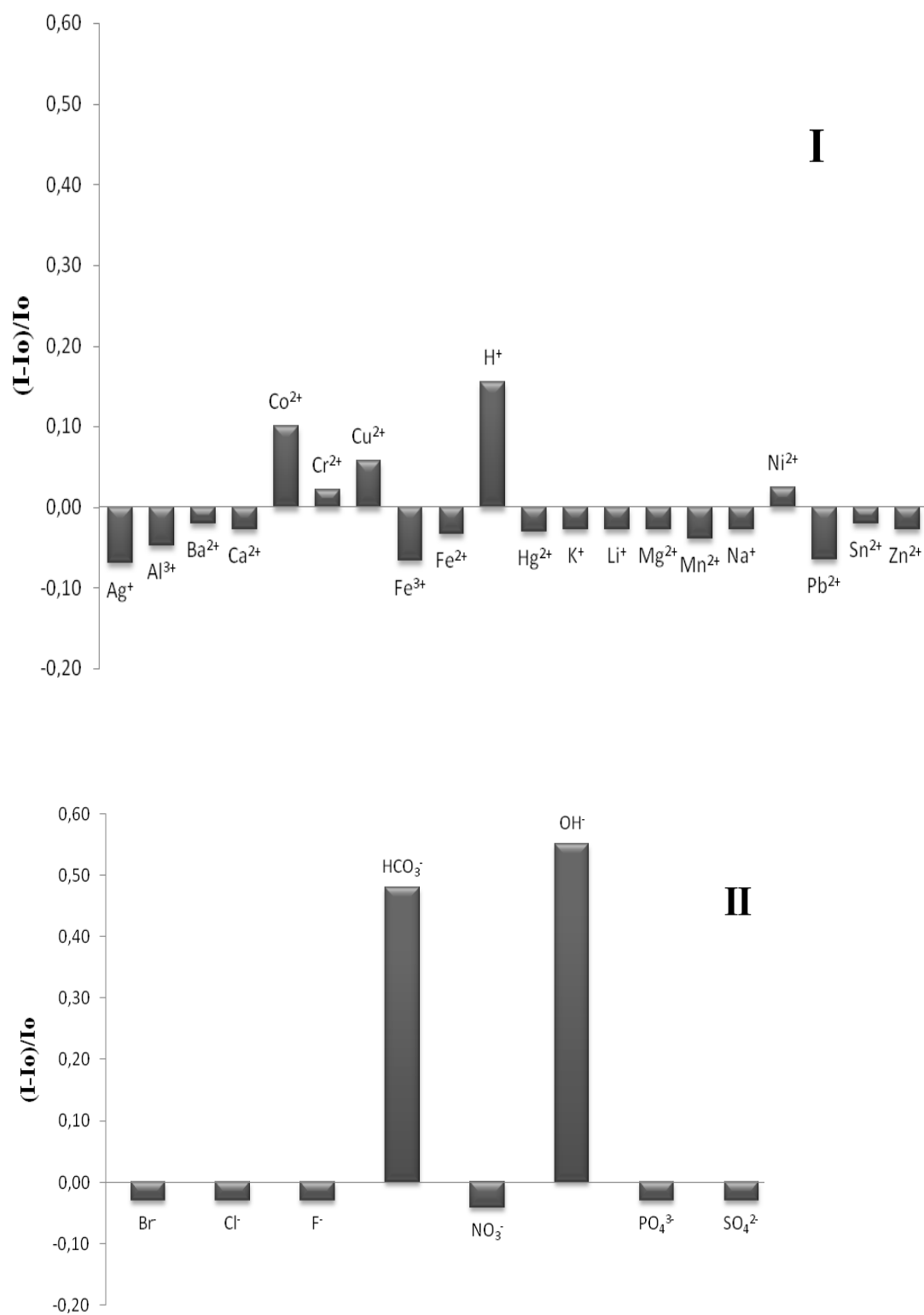
Figure 7.32 Metal-ion (I) and anion (II) response test for MY4.
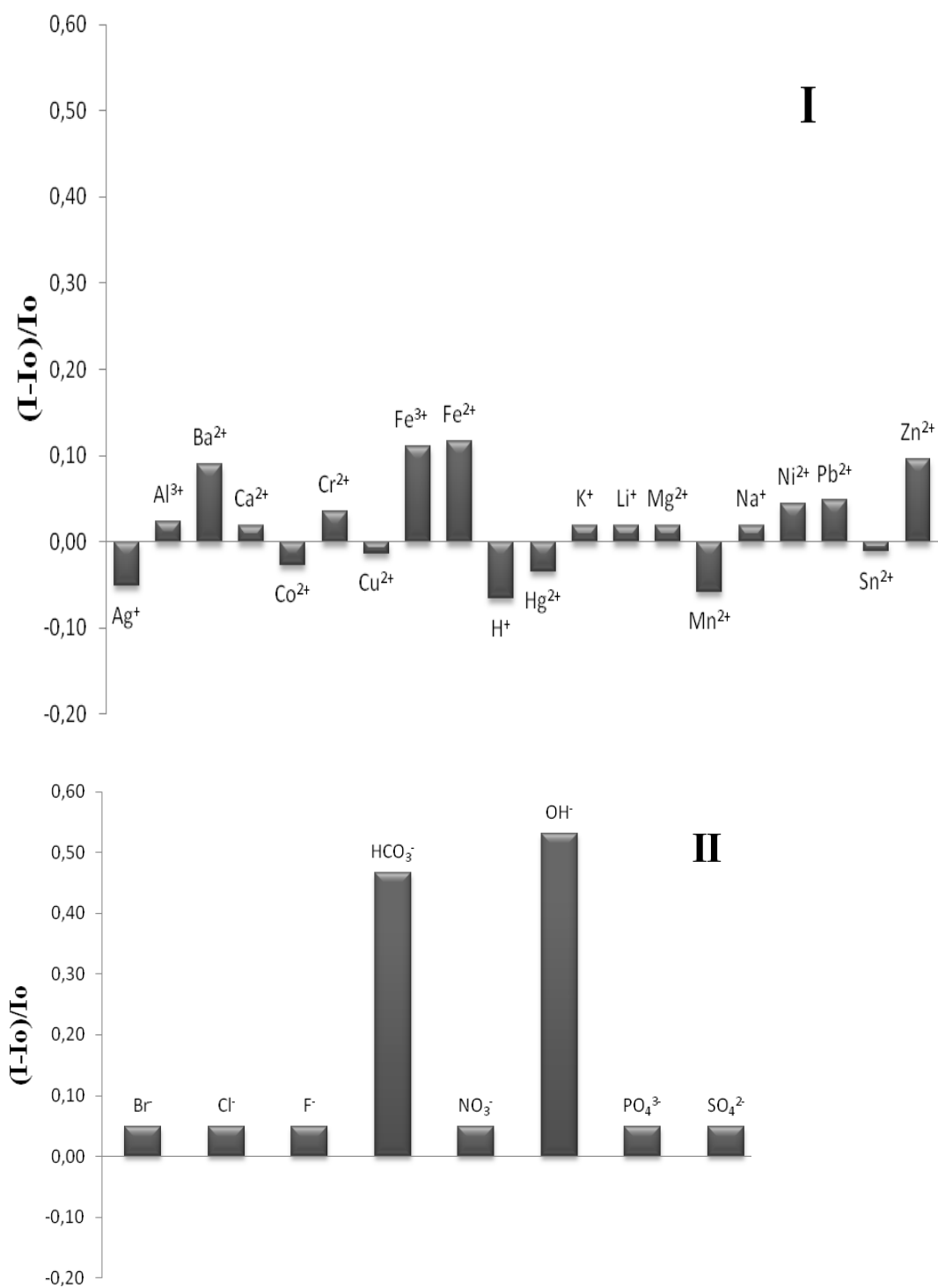
Figure 7.33 Metal-ion (I) and anion (II) response test for MY5.

7.3.8 Response to Real Sample

Analytical applications of offerded sensing designs were tested with real groundwater samples. We collected the samples from location of Sarikiz, Manisa; Turkey; Latitude: 38.34125º N, Longitude: 28.52355º. The bicarbonate analysis was performed potentiometric, indicator method and exploiting indicators.

7.3.9 Potentiometric Measurements

Potentiometric and indicator based measurements were performed in accordance with literature information given in page 15. pH and potential measurements were recorded with an Orion pH meter. The pH meter was calibrated with buffers prior to measurements. Potentiometric titration curve of 50 mL of bicarbonate containing groundwater sample with 0.1 M HCl was shown in Figure 7.34. A comparision of results of volumetric methods with proposed method was given in Table 6.6
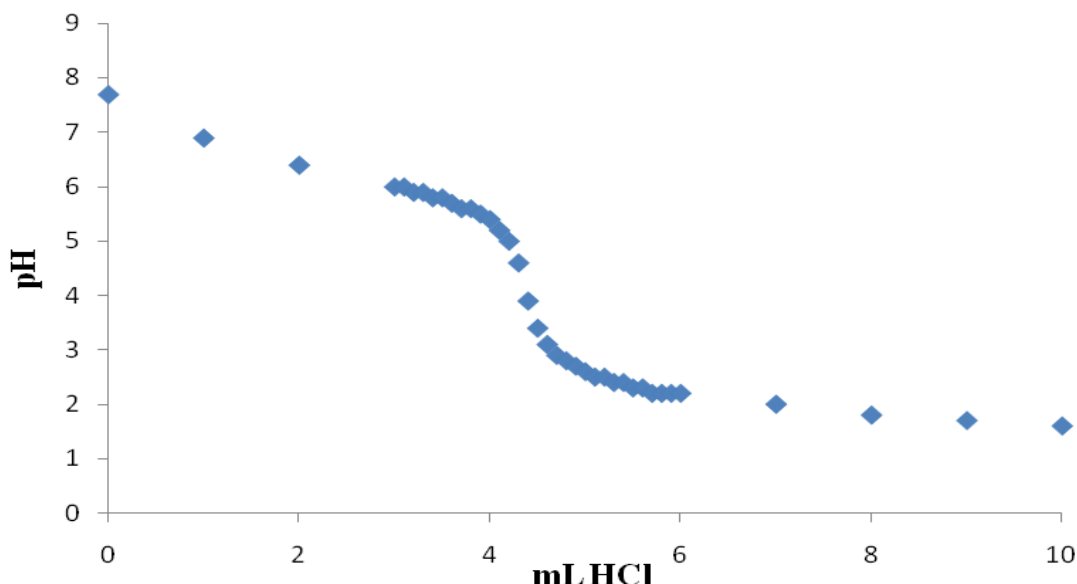
Figure 7.34 Potentiometric titration curve of groundwater sample with 0.1 M HCl.

Table 7.3 A comparision of results of volumetric methods with proposed method.

	MY2	MY4	MY5
Potentiometric Method (mol/L) HCO_3^-	0.0122	0.0122	0.0122
Titration with indicator (phenolphatelyn and methyl orange) (mol/L) HCO_3^-	0.0120	0.0120	0.0120
Proposed Method with employed dyes (mol/L) HCO_3^-	0.116	0.011	0.014

7.4 Conclusions

In this chapter three newly synthesized indicator dyes were N'-[(E)-(2-hydroxyphenyl) methylidene] pyridine-4-carbohydrazide (MY2), N'-[(E)-(3-hydroxyphenyl) methylidene] pyridine-4-carbohydrazide (MY4), N'-[(E)-(4-nitrophenyl) methylidene] pyridine-4-carbohydrazide (MY5) investigated spectroscopically. Their acidity constants were calculated and competibilities for dCO_2 sensing were evaluated.

The relative signal changes of emission spectra of the dyes were monitored both thin film and nanofiber forms after addition of certain concentrations of HCO_3^- solutions.

For all dyes electrospun films offered enhanced sensitivity and reactivity with respect to continuous thin films. The MY2, MY4 and MY5 dyes are promising fiber optic compatible fluorescent indicators for dissolved CO_2 sensing.

CHAPTER EIGHT
CONCLUSIONS

In the first part of the experimental studies (chapter 5), optical CO_2 sensor based on the change in the fluorescence signal intensity of 8-hydroxypyrene-1,3,6-trisulfonic acid trisodium salt (HPTS) were reported. Sensing slides were fabricated by electrospinning technique. With respect to continuous thin films, electrospun films can offer enhanced sensitivity and reactivity in optical chemical sensing.

The preliminary results of Stern-Volmer analysis show that the sensitivities of electrospun nanofibrous membranes to detect CO_2 are 24 to 120 fold higher than those of the thin film based sensors. The sensor slides showed high sensitivities due to the high surface area-to-volume ratio of the nanofibrous membrane structures. The response times of the sensing reagents were short and the signal changes were fully reversible. The stability of ion pair form of HPTS in the employed matrix materials was excellent and when stored in the ambient air of the laboratory there was no significant drift in signal intensity after 7 months.

In Chapter 6, two newly synthesized indicator dyes N'-[(E)-(9-methyl-9H-carbazol-3-yl) methylidene] pyridine-4-carbohydrazide (MY9) and N'-{(1E, 2E)-3-[4-(dimethylamino) phenyl] prop-2-en-1-ylidene} pyridine-4-carbohydrazide (MY10) were investigated spectroscopically. The dyes were embedded in EC and PMMA matrices. Their thin film and nanofiber forms were fabricated and compatibilities for dCO_2 sensing were evaluated. Acidity constants and cross sensitivities to other cations and anions was also tested and evaluated.

The relative signal changes of emission spectra of the dyes were monitored both thin film and nanofiber forms after addition of certain concentrations of HCO_3^- solutions. For all dyes electrospun films offered enhanced sensitivity and reactivity with respect to continuous thin films.

163

In Chapter 7, three newly synthesized indicator dyes were N'-[(E)-(2-hydroxyphenyl) methylidene] pyridine-4-carbohydrazide (MY2), N'-[(E)-(3-hydroxyphenyl) methylidene] pyridine-4-carbohydrazide (MY4), N'-[(E)-(4-nitrophenyl) methylidene] pyridine-4-carbohydrazide (MY5) were characterized spectroscopically. Their quantum yield, acidity constants were calculated and compatibilities for dCO_2 sensing were evaluated.

The relative signal changes of emission spectra of the dyes were monitored both thin film and nanofiber forms after addition of certain concentrations of HCO_3^- solutions. For all dyes electrospun films offered enhanced sensitivity and reactivity with respect to continuous thin films. The MY2, MY4 and MY5 dyes are promising fiber optic compatible fluorescent indicators for dissolved CO_2 sensing.

REFERENCES

Ali, R., Saleh, S. M., Meier, R. J., Azab, H. A., Abdelgawad, I. I., & Wolfbeis, O. S. (2010). Upconverting nanoparticle based optical sensor for carbon dioxide. *Sensors and Actuators B, 150*, 126–131.

Amao, Y., & Nakamura, N. (2004). Optical CO_2 sensor with the combination of colorimetric change of α-naphtholphthalein and internal reference fluorescent porphyrin dye. *Sensors and Actuators B, 100* (3), 347-351.

Amao, Y., Komori, T., & Nishide, H. (2005). Rapid responsible optical CO_2 sensor of the combination of colorimetric change of α–naphtholphthalein in poly (trimethylsiliylpropyne) layer and internal reference fluorescent porphyrin in polystyrene layer. *Reactive & Functional Polymers, 63*, 35–41.

Anthony, J. L., Maginn, E. J. & Brennecke, J. F. (2002). Solubilities and thermodynamic properties of gases in the ionic liquid 1- n-Butyl-3-methylimidazolium hexafluorophosphate. *J. Phys. Chem. B, 106* (29), 7315–7320.

Aydogdu, S., Ertekin, K., Suslu, A., Ozdemir, M., Celik, E., & Cocen, U. (2011). Optical CO_2 sensing with ionic liquid doped electrospun nanofibers. *Journal of fluorescence, 21* (2), 607-613.

Bacon, J. R., & Demas, J.N. (1987). Determination of oxygen concentrations by luminescence quenching of a polymer-immobilized transition-metal complex. *Anal. Chem., 59* (23), 2780 – 2785.

Baker, S. N., Baker, G. A., & Bright, F. V. (2002). Temperature-dependent microscopic solvent properties of dry and wet 1-butyl-3-methylimidazolium hexafluorophosphate: correlation with ET (30) and Kamlet-Taft polarity scales. *Green Chem., 4*, 165–169.

Baldini, F., Falai, A., De Gaudio, A. R., Landi, D., Lueger, A., & Mencaglia, A. (2003). Continuous monitoring of gastric carbon dioxide with optical fibres. *Sensors and Actuators B, B90* (1-3), 132-138.

Baldini, F., Chester, A.N., Homola, J., & Martellucci, S. (2006). *Optical Chemical Sensors.* Netherlands: Springer

Baltus, R. E., Culbertson, B. H., Dai, S., Luo, H., & DePaoli, D. W. (2004). Low - pressure solubility of carbon dioxide in room temperature ionic liquids measured with a quartz crystal microbalance. *J. Phys. Chem. B.*, *108*, 721-727.

Bates, E. D, Mayton, R. D., Ntai, I., & Davis, J. H. (2002). CO_2 capture by a task-specific ionic liquid. *J. Am. Chem. Soc.*, *124*, 926-927.

Blanchard, L. A., Hancu, D., Beckman, E., & J., Brennecke, J. F. (1999). Green processing using ionic liquids and CO_2. *Nature*, *399* (6731), 28–29.

Borisov, S. M., Ch, O. M., Klimant, I., Wolfbeis, O.S. (2007). Optical carbondioxide sensors based on silicone-encapsulated room-temperature ionic liquids. *Chem. Mat.*, *19*, 6187– 6194.

Brennecke, J. F., & Maginn, E. J. (2001). Ionic liquids: innovative fluids for chemical processing. *AICHE J.*, *47*, 2384–2389.

Bültzingslöwen, C., McEvoy, A. K., McDonagh, C., MacCraith, B. D., Klimant, I., Krause, C., et. al. (2002). Sol-Gel based optical carbon dioxide sensor employing dual luminophore referencing for application in food packaging technology. *Analyst*, *127* (11), 1478-1483.

Bultzingslowen, C. von., McEvoy, A. K., McDonagh, C., & MacCraith, B. D. (2003). Lifetime-based optical sensor for high-level pCO_2 detection employing fluorescence resonance energy transfer. *Anal. Chim. Acta*, *480* (2), 275–283.

Burke, C. S., Markey, A., Nooney, R. I., Byrne, P., & McDonagh, C. (2006). Development of an optical sensor probe for the detection of dissolved carbon dioxide. *Sensors and Actuators B*, *119*, 288–294.

Buzzeo, M. C., Hardacre, C., & Compton, R. G. (2004). Use of room temperature ionic liquids in gas sensor design. *Anal. Chem.*, *76* (15), 4583-4588.

Camara, C., Perez-Conde, C., Moreno-Bondi, M. C., & Rivas, C. (1995). Fiber optical sensors applied to field measurements. In P. Quevauviller, E. A. Maier, B. Griepink, (Ed.), *Quality assurance for environmental analysis* (165-193). Netherland: Elsevier.

Carmichael, A. J., & Seddon, K. R. (2000). Polarity study of some 1-alkyl-3-methylimidazolium ambient-temperature ionic liquids with the solvatochromic dye Nile red. *J. Phys. Org. Chem.*, *13*, 591–595.

Carraway, E. R., Demas, J. N., DeGraff, B. A., & Bacon, J. R. (1991). Photophysics and photochemistry of oxygen sensors based on luminescent transition-metal complexes. *Anal. Chem.*, *63* (4), 337–342.

Certificate of Analysis Sarikiz Groundwater. (n.d.) Retrieved February 2, 2012, from http://www.sarikiz.com.tr/esasanaliz.html.

Chang, Q., Randers-Eichhorn, L., Lakowicz, J. R., & Rao, G. (1998). Steam-sterilizable, fluorescence lifetime-based sensing film for dissolved carbon dioxide. *Biotechnol. Prog.*, *14*, 326−331.

Chu, C., & Lo, Y. (2008). Fiber-optic carbon dioxide sensor based on fluorinated xerogels doped with HPTS. *Sensors and Actuators B*, *129*, 120–125.

Chu, C. S., & Lo, L. (2009). Highly sensitive and linear optical fiber carbon dioxide sensor based on sol–gelmatrix doped with silica particles and HPTS. *Sensors and Actuators B, 143,* 205–210.

Compendium of chemical terminology gold book, (October 11, 2011). Retrieved January 2, 2012, from http://goldbook.iupac.org/PDF/goldbook.pdf

Deitzel, J. M., Kleinmeyer, J., Harris, D., & Tan, N. C. (2001). The effect of processing variables on the morphology of electrospun nanofibers and textiles. *Polymer, 42* (1), 261– 272.

Derinkuyu, S. (2010). Application of new matrix materials for dissolved and gaseous carbon dioxide sensing and fiber optic CO_2 sensor design, Ph.D. thesis.

Dhami, S., Mello, A. J., Rumbles, G., Bishop, S. M., Phillips, D., & Beeby, A. (1995). Phthalocyanine fluorescence at high concentration: dimers or reabsorption effect. *Photochem. Photobiol., 61* (4), 341-346.

Dieckmann, M., & Buchholz, R. (1999). Apparatus for measuring the partial pressure of gases dissolved in liquids. US Patent 60 03362.

Ertekin, K., Alp, S., Karapire, C., Yenigül, B., Henden, E., & Icli, S. (2000). Fluorescence emission studies of an azlactone derivative embedded in polymer films; an optical sensor for pH measurements. *J. Photochem. Photobiol. A, 137*, 155–161.

Ertekin, K., Klimant, I., Neurauter, G., & Wolfbeis, O. S. (2003a). Characterization of a reservoir-type capillary optical microsensor for pCO_2 measurements. *Talanta, 59* (2), 261-267.

Ertekin, K., Karapire, C., Alp, S., Yenigül, B., & Içli, S. (2003b). Photophysical and photochemical characteristics of an azlactone dye in sol-gel matrix; a new fluorescent pH indicator. *Dyes and Pigments, 56,* 125–133.

Ertekin, K., & Alp, S., (2006). Enhanced emission based optical carbon dioxide sensing in presence of perfluorochemicals (PFCs). *Sensors and Actuators, 115*, 672–677.

Fidanboylu, K., & Efendioğlu, H. S. (2009). *Fiber optic sensors and their applications*. Retrieved October, 9, 2001, from http://iats09.karabuk. edu.tr/press/pro/02_KeynoteAddress.pdf.

Galinski, M., Lewandowski, A., & Stepniak, I. (2006). Ionic liquids as electrolytes. *Electrochim Acta, 51* (26), 5567– 5580.

Ge, X. D., Kostov, Y., Rao, G. (2003). High-stability non-invasive autoclavable naked optical CO_2 sensor. *Biosens. Bioelectron., 18* (7), 857–865.

Gibson, P., Schreuder-Gibson, H., & Rivin, D. (2001). Transport properties of porous membranes based on electrospun nanofibers. *Colloids Surf. A,* 187–188.

Göpel, W., Hesse, J., & Zemel, J. N. (Ed.). (1991-1993). *Sensors -A Comprehensive Survey*. Weinheim: VCH.

Hulanicki, A., Geab, S., & Ingman, F. (1991). *Chemical sensors definitions and classification.* Pure&App/. Chem., 63(9), 1247-1250. Retrieved September 12, 2001, from http://www.iupac.org/publications/pac/1991/pdf/6309x1247.pdf.

Infrared Spectroscopy. (n. d.). Retrieved January 2, 2012, from http://www.wag.caltech.edu/home/jang/genchem/infrared.htm

Jacquemin, J., Gomes, M. F. C., Husson, P. & Majer, V. (2006). Solubility of carbon dioxide, ethane, methane, oxygen, nitrogen, hydrogen, argon, and carbon monoxide in 1-butyl-3-methylimidazolium tetrafluoroborate between temperatures 283 K and 343 K and at pressures close to atmospheric. *J. Chem. Thermodyn., 38* (4), 490–502.

Jaffe, M. B. (2008). Infrared measurement of carbon dioxide in the human breath: "Breathe-Through" devices from Tyndall to the present day. *Anesthesia & Analgesia, 107* (3), 890-904.

Janata, J. (1989). *Principles of chemical sensors*, New York: Plenum Press.

Janata J. (1990). Anal. Chem., 62:33R

Jenny, R. (2000). *Fundemantals of fiber optics: An introduction for beginners.* New York: Volpi Manufacturing USA Co.

Jones, D., (1998). *Introduction to fiber optics*. Pensacola: Naval Education and Training Professional Develeopment and Technology Center.

Kacmaz, S. (2009). Cation analysis of geothermal water samples with ion chromatography and spectroscopic methods. M.Sc thesis.

Kacmaz, S., Ertekin, K., Suslu, A., Ozdemir, M., Ergun, Y., Celik, E. et. al. (2011). Emission based sub-nanomolar silver sensing with electrospun nanofibers. *Sensors & Actuators: B. Chemical, 153* (1), 205–213.

Lakowicz, J. R. (1993). *Principles of Fluorescence Spectrocopy*. New York and London: Plenum Press.

Lakowicz, J. R. (1999). *Principles of Fluorescence Spectroscopy*, (2nd ed.). New York: Kluwer Academic/Plenum Publishers.

Lev, O., Tsionsky, M., Rabinovich, L., Glezer, V., Sampath, S., Pankratov, I., & Gun, J. (1995). Organically modified sol-gel sensors. *J. Anal Chem, 67*, 22A-30A.

Liang, C., Yuan, C. Y., Warmack, R. J., Barnes, C. E., & Dai, S. (2002). Ionic liquids: a new class of sensing materials for detection of organic vapors based on the use of a quartz crystal microbalance. *Anal. Chem., 74* (9), 2172-2176.

Lobnik, A. (2006). Absorption-based sensors. In F. Baldini, A.N. Chester, J. Homola, & S. Martellucci, (Ed.), *Optical Chemical Sensors* (77-98). Netherlands: Springer.

Lu, Z., Daia, M., Xua, K., Chen, J., & Liao, Y. (2008). A high precision, fast response, and low power consumption in situ optical fiber chemical pCO_2 sensor. *Talanta, 76*, 353–359.

MacCraith, B. D., O'Keeffe, G., McEvoy, A. K., McDonagh, C. M., McGilp, J. F., O'Kelly B., et. al. (1994). LED-based oxygen sensing using evanescent wave excitation of a dye-doped sol-gel coating. *Journal of Optical Engineering, 33*, 3861-3866.

Mackenzie, J. D. (1994). Structures and properties of Ormosils. *J Sol-Gel Sci Tech., 2,* 81-86.

Maleki, M., Latifi, M., & Amani-Tehran, M. (2010). Optimizing electrospinning parameters for finest diameter of nano fibers. *World Academy of Science, Engineering and Technology, 64,* 389-392.

Manikandan, R., Viswanathamurthi, P., & Muthukumar, M. (2011). Ruthenium(II) hydrazone Schiff base complexes: Synthesis, spectral study and catalytic applications. *Spectrochimica Acta Part A: Molecular and Biomolecular Spectroscopy, 83,* 297–303.

Mayr, T. (1999). Neutral carrier based fluorosensor for silver (I) ions. Diploma Thesis, Graz.

McKiernan, J. M., Yamanaka, S. A., Dunn, B., & Zink, J. I. (1990). Spectroscopy and laser action of Rhodamine 6G doped aluminosilicate xerogels. *J. Phys Chem., 94* (15), 5652 –5654

McNaught, A. D. and Andrew Wilkinson (Royal Society of Chemistry, Cambridge, UK). Towards the end of 2003, http://old.iupac.org/goldbook/S06031.pdf

Mills, A., Chang, Q., & McMurray, N. (1992). Equilibrium study on colorimetric plastic film sensors for carbon dioxide. *Anal. Chem., 64,* 1383-1389.

Mills, A., & Chang, Q. (1993). Fluorescence plastic thin-film sensor for carbondioxide, *Analyst, 118* (7), 839–843.

Mills, A., & Chang, Q. (1994). Colorimetric polymer film sensors for dissolved carbon-dioxide. *Sens. Actuator B: Chem., 21* (2), 83–89.

Mills, A., Lepre, A., & Wild, L. (1997). Breath-by-breath measurement of carbon dioxide using a plastic film optical sensor. *Sens. Actuator B: Chem., 39* (1–3), 419–425.

Mohr, G. J. (2002). *Materials and Polymers in Optical Sensing.* Retrieved October 10, 2011, from http://www2.uni-jena.de/~c1moge/Mohr/ASCOS2002.pdf.

Mohr, G. J. (2006). Polymers for optical sensors. In F. Baldini, A.N. Chester, J. Homola, & S. Martellucci, (Ed.), *Optical Chemical Sensors* (297-321) Netherlands: Springer.

Moore, E. W., & Dye, J. F. (1980). CO_2. A.E. Greenberg, J. J. Connors, D. Jenkins, (Eds.), *Standard Methods for the Examination of Water and Wastewater* (15.th edition). 262-269. USA: American Public Health Association.

Müller, B., & Hauser, P.C. (1996). Fluorescence optical sensor for low concentrations of dissolved carbon dioxide. *Analyst, 121*, 339-343.

Nakamura, M., Nasu, H., & Kamiya, K. J. (1991). Preparation of organic dye-doped SiO_2 gels by the sol-gel process and evaluation of their optical non-linearity. *Non-Cryst Solids, 135,* 1-7.

Neurauter, G., Klimant, I., & Wolfbeis, O. S. (1999). Microsecond lifetime-based optical carbon dioxide sensor using luminescence resonance energy transfer. *Anal. Chim. Acta, 382* (1/2), 67-75.

Neurauter, G., Klimant, I., & Wolfbeis, O. S. (2000). Fiber-optic microsensor for high resolution pCO_2 sensing in marine environment. *Fresenius J Anal Chem., 366,* 481–487.

Nivens, D. A., Schiza, M. V., & Angel, S. M. (2002). Multilayer sol–gel membranes for optical sensing applications: single layer pH and dual layer CO_2 and NH_3 sensors. *Talanta, 58* (3), 543–550.

Numerical Aperture (NA). (n. d.). Retrieved January 2, 2012, from http://www.ofsoptics.com/resources/Understanding-Fiber-Optics-Numerical-Aperture.pdf.

Oter, O., Ertekin, K., Topkaya, D., & Alp, S. (2006a). Room temperature ionic liquids as optical sensor matrix materials for gaseous and dissolved CO_2. *Sensors and Actuators B: Chemical, 117* (1), 295-301.

Oter, O., Ertekin, K., Topkaya, D., & Alp, S. (2006b). Emission based optical carbon dioxide sensing with HPTS in green chemistry reagents: room temperature ionic liquids. *Analytical and Bioanalytical Chemistry, 386*, 1225-1234.

Oter, O., Ertekin, K., & Derinkuyu, S. (2008). Ratiometric sensing of CO_2 in ionic liquid modified ethyl cellulose matrix. *Talanta, 76,* 557 – 563

Park, S., & Kazlauskas, R. (2003). Biocatalysis in ionic liquids—advantages beyond green technology. *Curr. Opin. Biotechnol., 14*, 432–437.

Parker, C. A. (1968). *Photoluminescence of Solutions*. Amsterdam: Elsevier.

Podbielska, H., Ulatowska-Jarza, A., Müller, G., & Eichler, H. J. (2006). Sol-gels for optical sensors. In F. Baldini, A.N. Chester, J. Homola, & S. Martellucci, (Ed.), *Optical Chemical Sensors* (353–385). Netherlands: Springer.

Rantwijk, F., Lau, R. M., & Sheldon, R. A. (2003). Biocatalytic transformations in ionic liquids. *Trends Biotechnol., 21*, 131–138.

Reichardt, C. (1988). *Solvents and solvent effects in organic chemistry*. (6th ed.). Weinheim: VCH.

Reneker, D. H., & Chun, I. (1996). Nanometre diameter fibres of polymer produced by electrospinning. *Nanotechnology, 7,* 216-223.

Sakka, S. (1994). The current state of sol-gel technology. *J Sol-Gel Sci Tech., 3*, 69-81.

Schaden, S., Haberkorn, M., Frank, J., Baena, J.R., & Lendl, B. (2004). Direct determination of carbon dioxide in aqueous solution using mid-infrared quantum cascade lasers. *Appl. Spectrosc., 58* (6), 667–670.

Schmidt, W. (1994). *Optische Spektroskopie*. Weinheim: VCH.

Schröder, C. R. & Klimant, I. (2005). The influence of the lipophilic base in solid state optical pCO_2 sensors. *Sensors and Actuators B, 107*, 572–579.

Seddon, K. R., Stark, A., & Torres, M. J. (2000). Influence of chloride, water, and organic solvents on the physical properties of ionic liquids. *Pure Appl. Chem., 72*, 2275–2287.

Seitz, W. R. (1991). *Optical ion sensing, in: Fiber optic chemical sensors and biosensors II* (Wolfbeis O.S., ed.), CRC Press, Boca Raton, Florida.

Sill, T. J. & Von Recum, H. A. (2008). Electrospinning: Applications in drug delivery and tissue engineering. *Biomaterials, 29*, 1989-2006.

Skoog, D. A., West, D. M., & Holler, F. J. (1994). *Analytical Chemistry* (6th edition), Philadelphia: Saunders College Publishing.

Smith, K. C. (2011). *Basic photochemistry*. Retrieved September 8, 2011, from http://www.photobiology.info/Photochem.html

Thomas, A. B., Sharma, A. P., Tupe, N. P., Badhe, R. V., Nanda, K. R., Kothapalli, L. P., Paradkar, O. D., Banerjee, A. G., & Deshpande, A. D. (2011). Green route synthesis of 4-thiazolidinone analogs of isonicotinic acid hydrazide, *Green Chemistry Letters and Reviews, 4* (3), 211-217.

Vargas-Sansalvador, I. M., Carvajal, P. M. A., Roldán-Munoz, O. M., Banqueri, J., Fernández-Ramos, M. D., Capitán-Vallvey, L.F. (2009). Phosphorescent sensing of carbon dioxide based on secondaryinner-filter quenching. *Analytica Chimica Acta, 655*, 66–74.

Varlan, A. R., & Sansen, W. (1997). Micromachined conductometric p(CO_2) sensor. *Sensors and Actuators B, 44*, 309-315.

Wang, R., Okajima, T., Kitamura, F., & Ohsaka, T. (2004). A Novel O_2 Gas Sensor Based on Supported Room Temperature Ionic Liquid Membrane-Coated Electrodes. *Electroanalysis, 16* (1-2), 66-72.

Weigl, B. H., & Wolfbeis, O. S. (1995). New hydrophobic materials for optical carbon dioxide sensors based on ion pairing. *Anal. Chim Acta, 302* (2-3), 249–254.

Wencel, D., Moore, J. P., Stevenson, N., & McDonagh, C. (2010). Ratiometric fluorescence-based dissolved carbon dioxide sensor for use in environmental monitoring applications. *Anal Bioanal Chem, 398*, 1899– 1907.

Werner, T., & Wolfbeis, O. S. (1993). Optical sensor for the pH 10–13 range using a new support material. *Anal. Chem., 346*, 564-568.

Williams, A. T. R., Winfield, S. A., & Miller, J. N. (1983). Relative fluorescence quantum yields using a computer co ntrolled luminescence spectrometer. *Analyst, 108,* 1067-1071.

Winter, J. A., Midgett, M. R., Brown, E., Skoug, M. W. & Fishman, M. J. (1980). Acidity. A.E. Greenberg, J. J. Connors, D. Jenkins, (Eds.), *Standard Methods for the Examination of Water and Wastewater* (15.th edition). 249-253. USA: American Public Health Association.

Wolfbeis, O.S. (1991). *Fiber optic chemical sensors and biosensors.* Boca Raton, Florida: CRC.

Wolfbeis, O. S., Kovács, B., Goswami, K., & Klainer, S. M. (1998). Fiber-optic fluorescence carbon dioxide sensor for environmental monitoring. *Mikrochim. Acta, 129,* 181-188.

Wong, J., & Angell, C. A. (1977). *Glass structure by spectroscopy.* New York: Marcel Dekker Inc.

Yang, Z., & Pan, W. (2005). Ionic liquids: Green solvents for nonaqueos biocatalysis. *Enzyme and Microbial Technology, 37*, 19–28.

Yu, F. T. S., & Shizhuo, Y. (2002). *Fiber optic sensors.* Newyork: Marcel Decker Inc.

Zeyrek, M. (2008). Anion analysis of geothermal water samples with ion chromatography and spectroscopic methods. M.sc thesis.

Zhang, G., Li, Y., & Li, Q. (2010). A miniaturized carbon dioxide gas sensor based on infrared absorption**.** *Optics and Lasers in Engineering, 48*, 1206–1212.